CLEAN WATER **WATER POLLUTION CONTROL RESEARCH SERIES** • 16070ENS06/71

W72-10146

PB 210 406

# AIRPHOTO ANALYSIS OF OCEAN OUTFALL DISPERSION

**Details of illustrations in this document may be better studied on microfiche**

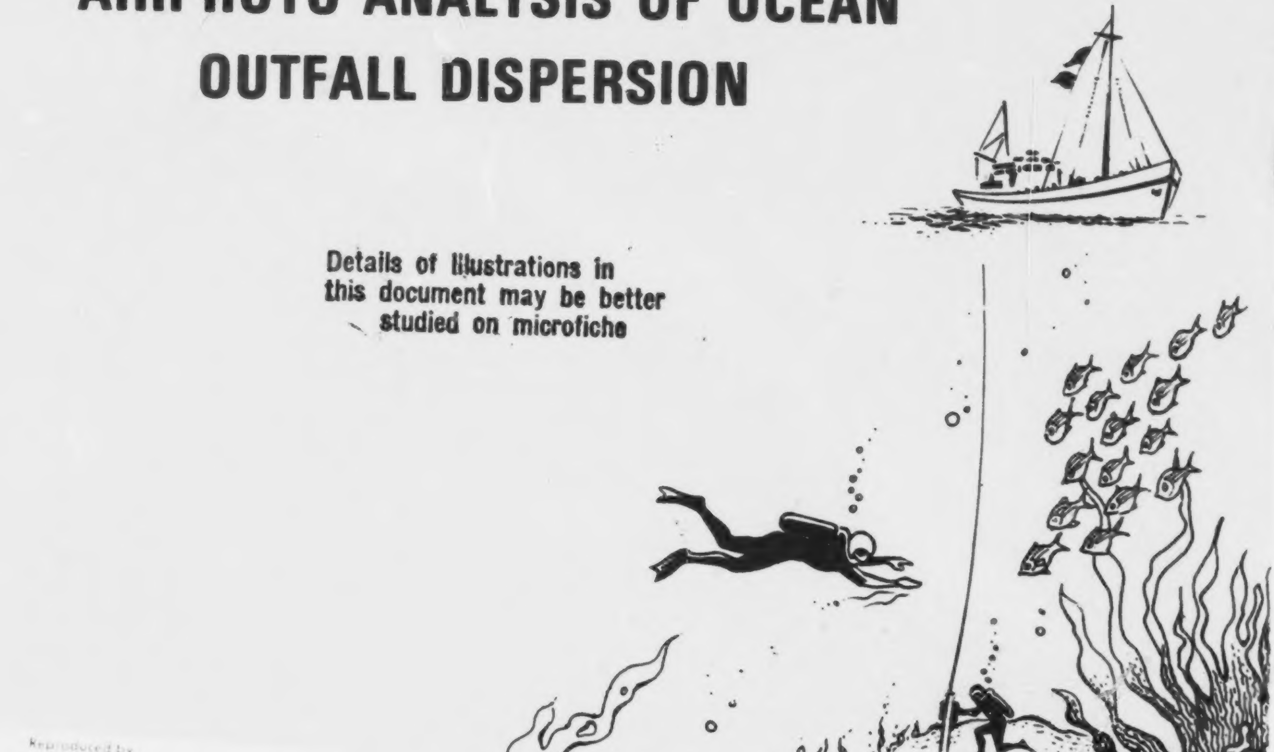

Reproduced by
NATIONAL TECHNICAL INFORMATION SERVICE
U S Department of Commerce
Springfield VA 22151

U.S. ENVIRONMENTAL PROTECTION AGENCY

292

## WATER POLLUTION CONTROL RESEARCH SERIES

The Water Pollution Control Research Series describes the results and progress in the control and abatement of pollution in our Nation's waters. They provide a central source of information on the research, development and demonstration activities in the Environmental Protection Agency, through inhouse research and grants and contracts with Federal, State, and local agencies, research institutions, and industrial organizations.

Inquiries pertaining to Water Pollution Control Research Reports should be directed to the Chief, Publications Branch (Water), Research Information Division, R&M, Environmental Protection Agency, Washington, D.C. 20460.

***SELECTED WATER***
***RESOURCES ABSTRACTS***
**INPUT TRANSACTION FORM**

*1. Report No.* *2.*

**W** 72-10146

# AIRPHOTO ANALYSIS OF OCEAN OUTFALL DISPERSION,

*5. Report Date*
*6.*
*8. Performing Organization Report No.*

Burgess, F. J., and James, W. P.

EPA Program
16070 ENS 06/71

Oregon State University, Corvallis, ~~Oregon~~,
School of Engineering.

*13. Type of Report and Period Covered*

*12. Sponsoring Organization*

Environmental Protection Agency

✓Water Pollution Control Research Series, ~~16070 ENS 06/71~~, June 1971.
297 p, 102 fig, 12 tab, 52 ref, 5 append.

During the summers of 1968, 1969 and September 1970 to May 1971 aerial photographs were taken of the ocean outfall waste plume at Newport, Oregon. The principles of photogrammetry and photo interpretation were combined to analyze the photos. Waste concentrations, water currents and diffusion coefficients were yielded by this remote sensing system using multispectral photography. Concurrent boat sampling was conducted. Results of the two methods were compared and the correlation coefficient ranged from 0.85 to 0.95. Discrepancies between these figures stemmed from shifting of the waste field during the 2 hour boat sampling period. Dye drops from an airplane were used to evaluate proposed ocean outfall sites. Diffusion coefficients, current velocity, wind velocity, sea state and wave height were determined from the aerial photographs. Airphoto pattern elements are given for visual interpretation of the photography. (Ensign-PAI)

*Oregon, *Aerial photography, *Remote sensing, *Photogrammetry, *Outlets, *Waste disposal, Currents (water), Diffusion, Waves (water), Wind velocity, Sampling, Boats, Correlation analysis.

*17b. Identifiers*

*Newport, Photo interpretations.

*17c. COWRR Field & Group* 05A, 05B

Copy available from GPO Sup Doc
as , $2.25; microfiche
from NTIS as PB 210 406, $0.95.

*18. Availability* ✓

| | | |
|---|---|---|
| *19. Security Class. (Report)* | *21. No. of Pages* | ***Send To:*** |
| *20. Security Class. (Page)* | *22. Price* | WATER RESOURCES SCIENTIFIC INFORMATION CENTER<br>U.S. DEPARTMENT OF THE INTERIOR<br>WASHINGTON, D. C. 20240 |

Barbara A. Ensign | Pollution Abstracts, Inc.

# AIRPHOTO ANALYSIS
# OF
# OCEAN OUTFALL DISPERSION

by

Oregon State University
Fred J. Burgess, Principal Investigator
Dean, School of Engineering
Wesley P. James, Research Associate
Corvallis, Oregon 97331

for the

ENVIRONMENTAL PROTECTION AGENCY

Program No. 16070 ENS
June, 1971

## EPA Review Notice

This report has been reviewed by the Water Quality Office, EPA, and approved for publication. Approval does not signify that the contents necessarily reflect the views and policies of this office, nor does mention of commercial products constitute endorsement for use.

For sale by the Superintendent of Documents, U.S. Government Printing Office, Washington, D.C., 20402 - Price $2.25

# ABSTRACT

Aerial photography was taken of the ocean outfall waste plume at Newport, Oregon, during the summers of 1968, 1969, and the period extending from September 1970 through May 1971. Computerized techniques to analyze the photos were developed by combining the principles of photogrammetry and photo interpretation. This remote sensing system involving multispectral photography was utilized to yield waste concentrations, water currents and diffusion coefficients.

Conventional boat sampling of the waste field was conducted concurrently with the photography during the 1968 and 1969 field seasons. The waste concentrations determined by the two methods were compared by matching ground coordinates. The correlation coefficient for the comparison ranged from 0.85 to 0.95. The photographic technique is more comprehensive than conventional boat sampling and permits waste concentrations to be measured throughout the plume in one instant. Discrepancies between concentrations determined by boat sampling and concentrations determined from aerial photography appear to be due primarily to changing and shifting of the waste field during the two hour boat sampling period.

Procedures were developed to evaluate proposed ocean outfall sites by using dye drops from an airplane. Diffusion coefficients and water current velocities were determined from aerial photography. A minimum of two photographic flights over the area were required to show the transport and spread of the dye patches.

When the hydrography of the receiving water allowed the formation of a surface plume, the water current velocity was found to be the dominant factor in the resulting plume pattern. The steady state form of the Fickian diffusion equation with a unidirectional transport velocity was not applicable to the majority of the observations. The equation for a line source in a uniform stream provided the x and y velocity components for a two-dimensional diffusion model with the losses to the lower layers being considered by including a decay coefficient. The second model was found to be more applicable to the diffusion process.

Characteristic airphoto pattern elements are given for visual interpretation of the photography. Wind velocity, sea state, current velocity, wave height and diffusion coefficients can be estimated from the aerial photography.

Key Words: Ocean outfall, aerial photography, remote sensing, marine disposal, diffusion, water currents.

# CONTENTS

| Section | | Page |
|---|---|---|
| I | Conclusions | 1 |
| II | Recommendations | 3 |
| III | Introduction | 5 |
| IV | Background | 7 |
| V | Rationale | 13 |
| VI | Diffusion Studies | 43 |
| VII | Sampling Procedures | 47 |
| VIII | Dye Patch Studies | 55 |
| IX | Data Processing | 59 |
| X | Sampling Results | 77 |
| XI | Discussion of the Results | 153 |
| XII | Summary | 175 |
| XIII | Acknowledgments | 179 |
| XIV | References | 181 |
| XV | Publications | 185 |
| XVI | Appendices | 187 |

## FIGURES

Page

1. Camera filtered to absorption band of rhodamine WT dye. 8
2. Camera filtered to fluorescence band of rhodamine WT dye. 8
3. Infrared black and white photo of algal bloom in a lake. 11
4. Infrared black and white photo of a waste plume. 11
5. Spectral distribution of radiant energy. 14
6. Direct sunlight and skylight on a horizontal plane. 17
7. Sunlight reflection from a sloping water surface. 18
8. Light penetration into the sea. 19
9. Typical attenuation coefficients. 21
10. Volume scattering function. 22
11. Variation in the scattering angle. 23
12. Effect of contaminant on the scattering function. 24
13. Light from the sea. 26
14. Depth of light return from the sea. 28
15. Typical spectral signature. 31
16. Geometry of exposure calculation. 32
17. Typical characteristic curve of an aerial positive film. 34
18. Spectral response curves. 37
19. Aerial view of Newport area. 48
20. Sketch of the Newport outfall. 49
21. Multiple camera unit. 53
22. Dye patch on July 7, 1969. 56
23. Data processing flow diagram. 60

Page

24. Waste concentrations from boat sampling on August 12, 1969. 61

25. Surface water temperature on August 12, 1969. 61

26. Water temperature profiles on August 12, 1969. 62

27. Flow diagram for photographic processing. 64

28. Symbolic plots from two flights August 16, 1968. 67

29. Isoconcentration plot, flight on August 16, 1968. 67

30. Digitizing aerial film. 73

31. Scanning densitometer. 73

32. Infrared black and white photo on July 7, 1969. 79

33. Plume on July 8, 1969 at 15:21 from 4000 feet. 79

34. Temperature profiles July 7 and 8, 1969. 80

35. Plume July 8, 1969 at 15:56 from 4000 feet. 81

36. Plot of residuals - 1968. 86

37. Plot of residuals - 1969. 87

38. Comparison of boat and photo values on August 8, 1968. 88

39. Comparison of boat and photo values on August 16, 1968. 89

40. Comparison of boat and photo values July 8, 1969. 90

41. Comparison of boat and photo values August 12, 1969. 91

42. Chart of the outfall area at Newport, Oregon. 99

43. Aerial photo of outfall area on September 9, 1970 from 8000 feet at 14:30. 100

44. Data for September 9, 1970. 101

45. Aerial photo of outfall area on September 23, 1970 from 8000 feet at 15:30. 102

46. Data for September 23, 1970. 103

Page

47. Aerial photo of outfall area on September 30, 1970 from 5000 feet at 14:54. 104

48. Data for September 30, 1970. 105

49. Aerial photo of outfall area on October 7, 1970 from 3000 feet at 14:32. 106

50. Data for October 7, 1970. 107

51. Aerial photo of outfall area on October 12, 1970 from 4000 feet at 14:10. 108

52. Data for October 12, 1970. 109

53. Aerial photo of outfall area December 21, 1970 from 6000 feet at 13:15. 110

54. Data for December 21, 1970. 111

55. Aerial photo of outfall area on December 23, 1970 from 3000 feet at 11:25. 112

56. Data for December 23, 1970. 113

57. Aerial photo of outfall area on December 31, 1970 from 3000 feet at 12:10. 114

58. Data for December 31, 1970. 115

59. Aerial photo of outfall area on January 2, 1971 from 4000 feet at 11:40. 116

60. Data for January 2, 1971. 117

61. Aerial photo of outfall area on February 6, 1971 from 6000 feet at 11:55. 118

62. Data for February 6, 1971 AM. 119

63. Aerial photo of outfall area on February 6, 1971 from 4000 feet at 14:18. 120

64. Data for February 6, 1971 PM. 121

65. Aerial photo of outfall area on March 16, 1971 from 4250 feet at 12:20. 122

Page

66. Data for March 16, 1971. 123

67. Aerial photo of outfall area on March 17, 1971 from 4000 feet at 14:25. 124

68. Data for March 17, 1971. 125

69. Aerial photo of outfall area on March 18, 19.1 from 8000 feet at 11:42. 126

70. Data for March 18, 1971. 127

71. Aerial photo of outfall area on March 19, 1971 from 8000 feet at 11:27. 128

72. Data for March 19, 1971 AM. 129

73. Aerial photo of outfall area on March 19, 1971 from 6000 feet at 13:50. 130

74. Data for March 19, 1971 PM. 131

75. Aerial photo of outfall area on March 24, 1971 from 6000 feet at 16:00. 132

76. Data for March 24, 1971. 133

77. Aerial photo of outfall area on April 12, 1971 from 6000 feet at 14:45. 134

78. Data for April 12, 1971. 135

79. Aerial photo of outfall area on April 15, 1971 from 4000 feet at 14:07. 136

80. Data for April 15, 1971. 137

81. Aerial photo of outfall area on April 21, 1971 from 4000 feet at 13:46. 138

82. Data for April 21, 1971. 139

83. Aerial photo of outfall area on April 26, 1971 from 6000 feet at 14:20 140

84. Data for April 26, 1971. 141

85. Aerial photo of outfall area on May 7, 1971 from 4000 feet at 15:13. 142

Page

86. Data for May 7, 1971. 143

87. Aerial photo of outfall area on May 10, 1971 from 4000 feet at 16:10. 144

88. Data for May 10, 1971. 145

89. Aerial photo of outfall area on May 13, 1971 from 6000 feet at 14:10. 146

90. Data for May 13, 1971. 147

91. Aerial photo of outfall area on May 14, 1971 from 4000 feet at 14:48. 148

92. Data for May 14, 1971. 149

93. Photos of sea conditions. 150

94. Plume patterns for a unidirectional transport velocity. 154

95. Isoconcentration plot, August 8, 1968. 155

96. Geometry for a line source in a uniform stream. 158

97. Plots of a source in a uniform stream. 160

98. Potential flow solutions for a line source. 161

99. Isoconcentration plots from diffusion model. 163

100. Typical diurnal thermoclines. 165

101. Development of current velocity profile. 166

102. Mottled photo pattern from surface waves. 173

## TABLES

| No. | | Page |
|---|---|---|
| 1 | Preliminary diffusion coefficients, flight 1, August 16, 1968. | 70 |
| 2 | Nonsteady-state diffusion coefficients, August 16, 1968. | 71 |
| 3. | 1968-1969 sampling summary for Newport. | 78 |
| 4. | Summary of the 1968 vertical aerial photography. | 83 |
| 5. | Summary of the 1969 oblique aerial photography. | 84 |
| 6. | Wind scales and sea descriptions. | 151 |
| 7. | Summary of the 1970-71 data. | 152 |
| 8. | Preliminary diffusion coefficients, flight 2, August 8, 1968. | 157 |
| 9. | Sea state due primarily to wind. | 168 |
| 10. | Sea state due primarily to swell. | 169 |
| 11. | Sea state due to wind and swell. | 170 |
| 12. | Conditions in fully developed seas. | 172 |

# SECTION I

## CONCLUSIONS

1. Aerial photography provides an effective method for a comprehensive analysis of the dispersion of wastes that are discharged into the ocean.

2. Aerial photographs showing the transport and spread of dye patches will provide detailed design information for evaluating proposed ocean outfall sites throughout the year.

3. Characteristic airphoto pattern elements can be utilized to estimate wind velocity, sea state, water current velocities and diffusion coefficients in the nearshore areas.

4. In addition to being technically feasible, aerial photography has been shown to be an economically feasible method for acquiring ocean outfall design data prior to discharge.

5. The surface water current is a dominant factor in the resulting plume pattern. The currents were primarily generated by the wind with tide playing a minor role.

6. A two dimensional Fickian diffusion model was usually adequate to explain the resulting plume pattern. The surface spreading of the waste field was considered in the model by including the equations for a line source in a uniform stream while vertical diffusion was considered by including a decay coefficient.

7. There was no indication that the diffusion coefficients varied to the 4/3 power of the scale.

## SECTION II

## RECOMMENDATIONS

1. It is recommended that aerial photography be used to obtain information for evaluation of requests for waste discharge permits that involve ocean outfalls.

2. It is recommended that aerial photography be used in establishing surveillance programs and in conducting surveillance programs on operating waste discharge outfalls.

3. It is recommended that future studies be conducted to establish the importance of both the vertical diffusion coefficient and the vertical stability on the waste disposal process. Such a study should include continuous recording of wind, water current profiles for several locations, and wave profiles in order to better understand the response of the sea to the wind forces. The effect of the scale of the turbulence on the rate of diffusion needs additional study.

4. It is also recommended that a critical analysis of actual field conditions versus the original design predictions be made for the several ocean outfalls in Oregon and at Eureka, California. Such a study will indicate areas of design deficiencies and will improve the technology of ocean outfall disposal.

Preceding page blank

# SECTION III

## INTRODUCTION

The objective of this research is to develop a remote sensing tool for the evaluation of dispersion of wastes from existing or proposed ocean outfalls. Photogrammetric and photo interpretation methods are used to determine dispersion patterns, diffusion coefficients, waste concentrations and nearshore currents. This study is unique in that the aerial photography is not only used to determine the position of points and the size of objects as in normal photogrammetry, but the photograph is also used as an energy sensor. The amount of light reflected from an object is recorded by the photograph as the film density of the image. The light scattered from within the sea is measured from the film with a photo densitometer and can be related to certain water quality parameters.

An ocean outfall is a pipeline that is used for discharging waste into the ocean. The pipeline extends into the receiving body of water and usually terminates with a diffuser section where the flow is divided into a number of small jets.

The discharging jets of waste are subjected to momentum forces and to a buoyant force which is proportional to the density difference between the effluent and the receiving water. As the jet of liquid rises towards the surface, it mixes with the ambient fluid and both its momentum and buoyance per unit volume decrease. The mixing causes a waste field to be formed either at the surface or submerged below the sea surface depending on the hydrography of the site and initial dilution.

If there is little density stratification in the receiving water, the effluent, being less dense than sea water, will rise to the surface to form a surface waste field. After the initial dilution due to jet diffusion, the waste is transported from the site by current action and continues to mix and spread by natural turbulence in the receiving body.

The conventional method of studying the waste field from an outfall has been by boat sampling with the tracer technique. The use of this method for water quality studies has been enhanced by the development of highly sensitive instruments and new dye tracers during the past several years.

The use of radioactive tracers has been limited by handling problems and misunderstanding by the public. The use of fluorescent dyes as tracers avoids these objections and gives satisfactory results in most quality studies. Fluorescein dye has been used for the past 50 years but has the disadvantage of a high photochemical decay rate (Wilson, 1968). Rhodamine B has a low decay rate but tends to adhere to suspended particles. This may result in a low recovery of the dye.

**Preceding page blank**

Rhodamine WT and pontacyl pink dyes both have low sorptive tendency, but the pontacyl pink is about four times as expensive as the rhodamine WT solution.

The general procedure for tracing waste discharged from an existing outfall is to meter the dye tracer into the pipeline. Complete mixing of the tracer and waste is required. By knowing the tracer injection rate and the waste discharge rate, the tracer concentration within the pipeline can be determined. This mixture passes through the diffusers and forms the waste field. Tracer concentrations in the waste plume are measured by sampling from a boat. The waste concentration at any point in the waste field can then be computed from the samples on the basis of the dye concentration.

Ocean outfall sewers for the disposal of waste along the Pacific Northwest coastline are, in general, located on the relatively shallow coastal shelf which is subjected to heavy seas. Sampling from a boat in these areas is dangerous at all times and impossible much of the time due to rough water. The use of aerial photography and photogrammetric methods presents a possible method for overcoming this difficulty. From two to eight hours of continuous sampling from a boat is required to adequately define the waste field in the vicinity of an ocean outfall. The waste field is usually shifting thus making a comprehensive study nearly impossible by conventional methods. The aerial photographic technique presents a method where concentrations throughout the waste field can be measured in one instant. Consideration of these factors suggest that photogrammetry can be a most useful tool for water quality investigations. Prior to this time the use of aerial photography for water quality studies has been limited to identifying pollution sources, but has not been used for making quantitative measurements from the photographs.

The field work was conducted at the Georgia-Pacific Kraft pulp mill outfall at Newport because of its convenient location. This site provided an additional advantage since the natural color of the waste effluent was visible on aerial photography. However, the results of this study are not limited to Kraft pulp mill outfalls. If the effluent from an outfall has the same light scattering and light absorption properties as the receiving water, dye can be added to the effluent to distinguish the waste field from the receiving body of water. The natural color characteristics of the Kraft pulp waste will vary with time while the addition of dye to a colorless waste will give greater control over the test.

In order to obtain design information at proposed outfall locations, aerial photography is taken of dye patches. The dye markers are dropped from the aircraft at selected locations in the waste disposal area. Current velocities and diffusion coefficients are determined from the change in position and size of the dye patches between two photographic flights over the proposed site.

## SECTION IV

## BACKGROUND

Both the color of the waste and the amount of light scattered from below the water surface can be recorded on aerial photography. Most black and white film used today for aerial photography is panchromatic film which is sensitive to the 400-700[1] nm region of the spectrum. By using lens filters on the camera, the exposure can be limited to a selected region of the spectrum. Generally the film-filter combination is sketched to give maximum contrast between the object and background. For example, when aerial photography is taken of a rhodamine WT dye patch in the ocean, high contrast can be obtained by either filtering the camera to the band of maximum light absorption of the dye or filtering the camera to the maximum fluorescence of the dye as shown in figures 1 and 2. For the first case, on a positive black and white print, the sea would appear light in tone while the dye patch would appear dark. However, if the camera is filtered to maximum fluorescence, the dye patch would be light in tone while the sea would appear dark.

Blue light with a wave length of about 480 nm has the greatest penetration in the deep ocean waters. In the turbid coastal waters the greatest penetration occurs at about 530 nm (Jerlov, 1968). As the composition, size or concentration of particles in the water vary, the band of greatest penetration and color of the sea may also change. Photography can, under certain conditions, be used to distinguish water masses, to delineate current patterns, to identify upwelled water along the coast and to track river plumes in the ocean.

Color photography divides the visible spectrum into three bands. The composition of the light is recorded as blue, green, and red colors on a positive transparency or print. For many applications of aerial photography the three bands are adequate. However, the color film has been designed to reproduce a natural land scene which is visually similar to the original view. The film may not give the best results possible if it is used for other than its designed purpose. Strandberg (1966, 1967) of Itek Data Analysis Center has published numerous examples of color photographs for water quality analysis. In these examples it was possible to detect the sources of pollution; however, no attempt was made to measure pollution concentration.

Color infrared film is sometimes called false color film. The blue, green and red colors on the photograph result from exposures to the green, red and infrared bands of the spectrum, respectively (Fritz, 1967). Besides military uses, the film has been used extensively in the detection of disease and insect pests in forest and agriculture

---

[1] Nanometers, $10^{-9}$ meters

Figure 1. Camera filtered to absorption band of rhodamine WT dye.

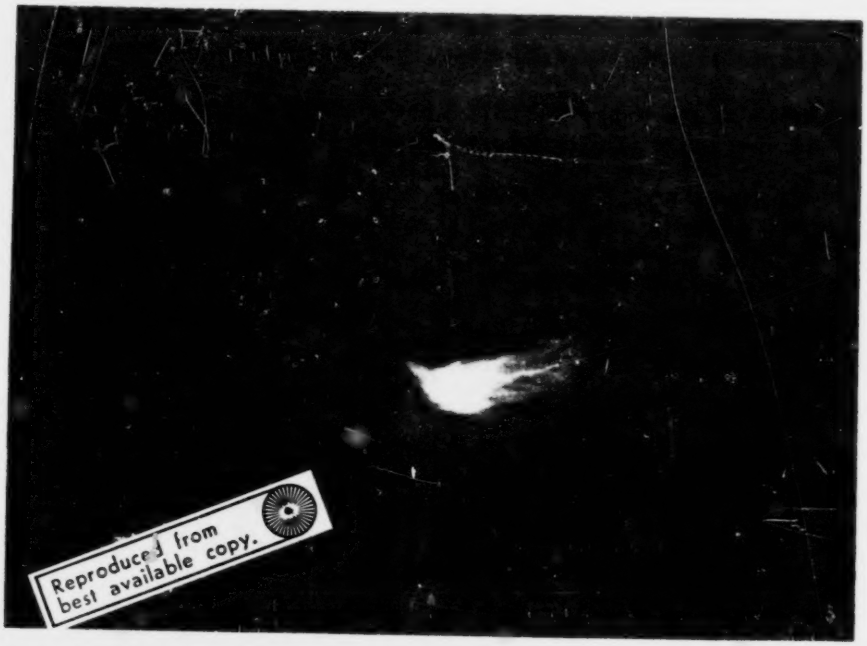

Reproduced from best available copy.

Figure 2. Camera filtered to fluorescence band of rhodamine WT dye.

crops (American. . ., 1960). It also has been used advantageously in geological and soils interpretation. When using this film a yellow filter is needed to eliminate the blue light, thereby reducing the degrading effect of haze. As skylight reflection on the water surface is also predominantly blue, infrared color photography of underwater details will appear clearer than with ordinary color photography. Generally, the infrared layer on the film is underexposed when photographing a water body.

Narrow band filters permit the selection of the region of the spectrum that has minimum interference and maximum subject contrast. Interference filters have several advantages over absorption filters including high peak transmittance and sharp cutoffs. However, the peak wave length of an interference filter is a function of the angle of incidence of the radiation impinging on the filter. If it is desired to record essentially the same band or region of the spectrum on the edges of the frame as in the center of the picture, interference filters can only be used with cameras having a narrow angle field of view. The color characteristics of waste from the Kraft pulp process vary causing the optimum film-filter combinations required to study the effluent plume to change. The same film-narrow band filter combinations used to study one waste can probably not be used to study a plume of a different waste or to study fluorescent dye concentrations in a dye patch.

Multiband camera systems have been developed by several organizations (Yost and Wenderoth, 1967; Molineux, 1965). This system has a number of film-filter combinations to take simultaneous photographs in several regions in the spectrum. This method not only allows the selection of several film-filter combinations for optimum results, but permits the proper exposure of each spectral band. For an example, on a normal color photograph of the sea, the blue sensitive layer is generally over exposed while the red sensitive is generally under exposed. A multiband camera system would allow the proper exposure of each band.

In research at the Allen Hancock Foundation it was found that high optical absorbance of millipore-filtered water to light at a wavelength of 230 nm is related to the concentration of sewage. In their study (Allen. . ., 1964), the ultraviolet absorbance was suggested as a possible method of tracing the sewage field by direct sampling without using a tracer. A film sensitive to the ultraviolet region of the spectrum might be used to trace the sewage field. However, the ultraviolet is also the region of maximum atmospheric interference.

Infrared film is sensitive to both the blue and infrared regions of the spectrum. It is, therefore, necessary to use lens filters in order to limit the exposure to the infrared region. Infrared photography will record energy in the 700-900 nm region. At normal temperatures the energy in this region is predominantly reflected energy, not emitted energy, and is not related to temperature. Due to the high attenuation of water in the infrared band, water surfaces on an infrared black and white photograph will normally appear black. The high contrast between the water and land is used to advantage when mapping the water line of a body of water. Algae have high reflectance in this band and infrared photography is used to monitor blooms. The photo in figure 3 shows the aerial distribution of the algal bloom in the lake. Concentration and total mass can be estimated from the photography. An infrared photo of the waste field from an ocean outfall is shown in figure 4. When taking black and white photographs of water, the exposure is about two stops greater than ordinary land detail. As a result, the shore in figure 3 and the four boats in figure 4 are overexposed.

Objects at normal temperature radiate thermal infrared rays at a wave length greater than can be recorded on ordinary infrared film. Suitable equipment is now available for measuring surface water temperatures by remote sensing. Infrared scanning of 4.5 - 5.5 micron wavelength has been used successfully by the U.S. Geological Survey to locate fresh water springs in Hawaii (Fisher, Davis, and Sousa, 1966). In this study the sea water temperature averaged 73.5 degrees F while the fresh water temperature was between 60 and 70 degrees F. Scanning in the 8-14 micron wavelength would be most suitable for water surface temperatures as this is the region of maximum radiation and the region relatively free of reflected sunlight interference. It is expected that temperature differences of 0.2 degrees C can be detected by scanning in this region (Ory, 1965). The temperature of the waste may provide a suitable tracer for a thermal effluent discharge. For cooler industrial wastes the use of heat as a tracer is unlikely since the thermal resolution of the scanning equipment is about the same magnitude as the expected maximum difference in temperature within the waste field. In the ocean, vertical thermal stratification will exist under certain conditions. Warm wastes discharged from the diffuser of an ocean outfall will mix with the colder subsurface water and by the time the mixture reaches the surface, the resulting plume temperature may be greater than, less than, or equal to the surrounding ocean temperature.

Surface currents have been measured successfully with aerial photography by a number of investigators. The Coast and Geodetic Survey has been using aerial photography to measure surface tidal currents for more than ten years (Keller, 1963). Waldichuk (1966) found long strips of buoyant paper provided an economical target for surface current measurement as long as the sea was not so rough that the paper would buckle and twist. A study by the Water Pollution Research Board of England (1964) indicated that drift cards released over the outlet of an ocean outfall did not in general follow the sewage field but were deflected by the wind; however, drift poles and surface floats with drogues at about five feet did follow the waste plume.

Romanousky (1966), from the Center for Oceanographic Research and Studies in Paris, has studied diffusion of wastewaters by photographing

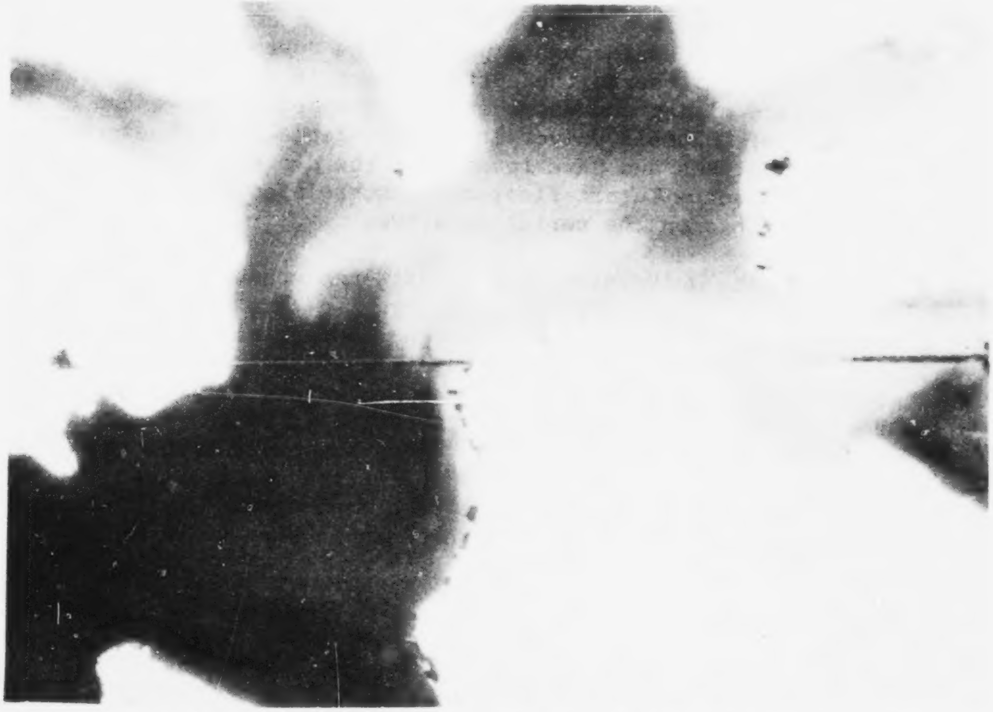

Figure 3. Infrared black and white photo of algal bloom in a lake.

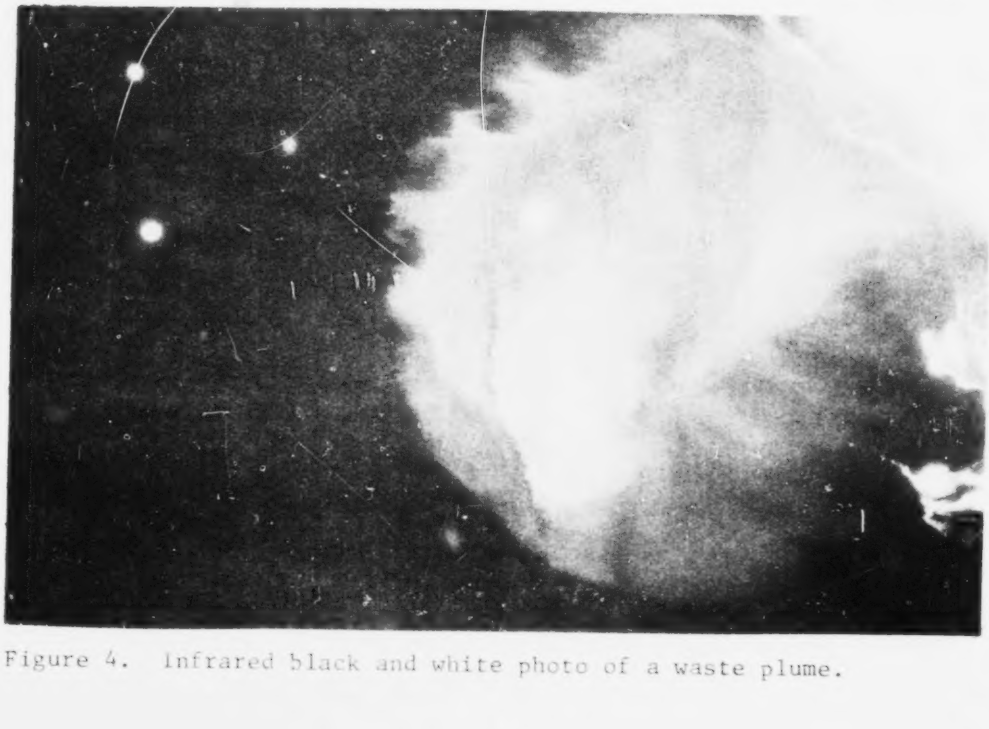

Figure 4. Infrared black and white photo of a waste plume.

dye releases from a balloon. Fresh water with rhodamine B or fluorescein dye added was pumped through a pipe to the bottom of the sea. The fresh water discharge rose to the surface where it spread under the influence of surface mixing and was then photographed. Ichiye and Plutchak (1966) of Columbia University have taken aerial photographs of rhodamine B dye patches and have found that the dye concentrations measured by a shipborne Turner fluorometer correlated very well with densitometer readings on the aerial negative.

Scherz (1967) at the University of Wisconsin has conducted work on pollution detection with aerial photography. In this work, aerial photographs were taken of various pollution sources using different film-filter combinations and the optimum film-filter was selected by visual observation. Cornell Aeronautical Laboratory (Neumaier et al., 1967) under project Aqua-Map has conducted studies on the reflectance of various polluted waters using test panels submerged below the water surface. Both laboratory studies with reflection spectrometer and field surveys with aerial cameras have been conducted. Their study indicated that industrial waste effluents can in some cases be identified photographically.

## SECTION V

## RATIONALE

Photographic films used in aerial photography are sensitive to the visible and near visible light. The main source of this light is the sun. Both the amount and composition of the light scattered from within the water are utilized in the study to determine the waste concentration in the effluent plume. The amount of light is recorded as the film density of the photographic image while the composition of the scattered light is determined from the film-filter combinations used for the photography. If the light scattering or light absorption properties of a waste are a function of the wave length of light, the ratio of the light return in the band of maximum absorption is a sensitive indicator of the waste concentration. However, if the waste is either black or white, the difference in the light returned in two bands divided by the sum will provide a sensitive indicator of the waste concentration. By using the ratio of light returned, the relationship between the film densities and the waste or dye concentration will be simplified as shown in the following sections.

### Sun Energy

Energy from the sun passes through the atmosphere to the sea. Upon reaching the water surface, the radiation is either reflected or transmitted through this interface. The refracted light is transmitted, scattered, or absorbed in the sea. Some of the scattered light is directed upwards and passes through the sea-air interface. A part of the light emerging from the sea reaches the aerial camera and exposes the photographic film.

The upper limit of the atmosphere receives energy at an average rate of about 0.135 watts per square cm perpendicular to the radiation. This value fluctuates about ±5% during a yearly period due to the eccentricity of the earth's orbit about the sun. The extraterrestrial energy spectrum of the sun's radiation is shown in figure 5 (Hutchinson, 1957).

The normal spectrum of solar radiation that reaches the sea surface is also shown in figure 5. Solar radiation, when passing through the atmosphere, is reduced by scattering and absorption. The amount of radiation received at the earth's surface (H)[2] can be estimated by

$$H = H_o \exp(-KL) \qquad (1)$$

where K is the attenuation coefficient which varies with wave length, $H_o$ is the incoming radiation at the outer atmosphere and L is the

---

[2] Terms in this chapter are defined where first used. Definition of these terms are also listed in Appendix A.

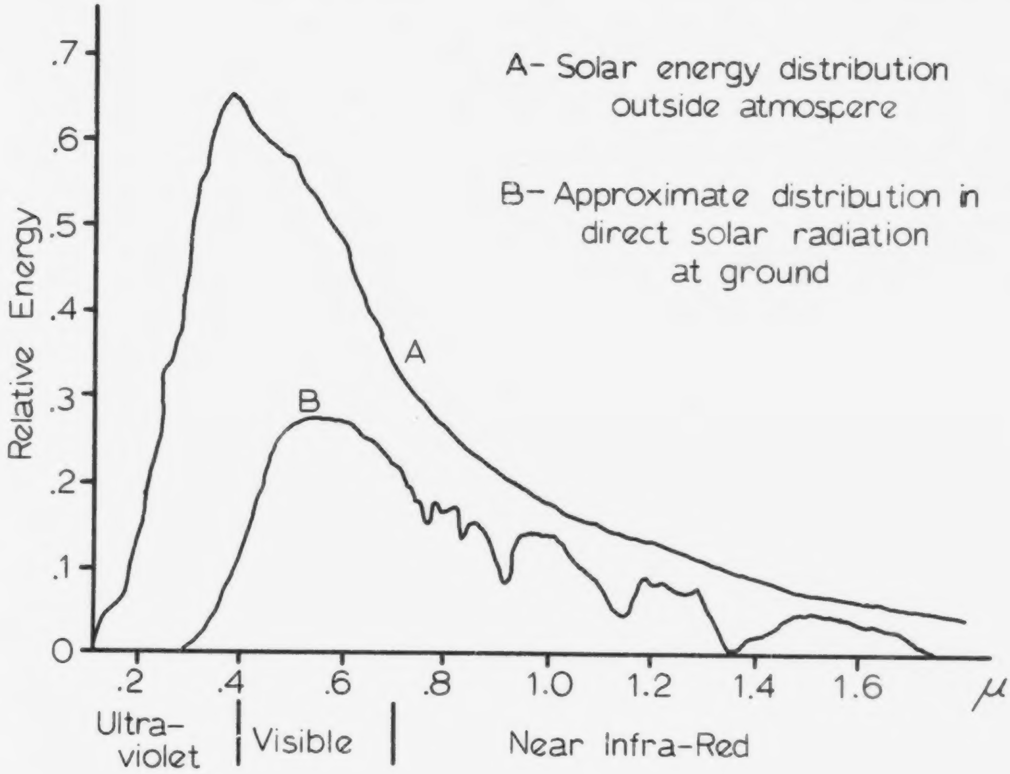

Figure 5. Spectral distribution of radiant energy.

light path length (Elterman and Toolin, 1965).

Absorption of light depends on the composition of the air, mainly water vapor, carbon dioxide and ozone, and the wave length of light. It can be seen in figure 5, that there are several zones of selective absorption. The ultraviolet part of the sun's radiation with a wave length of 290 nm or less is completely cut off by the atmospheric ozone layer and oxygen before it reaches the earth's surface. In the near infrared region (0.7 to 5 microns), the selective absorption is primarily due to water vapor and carbon dioxide (Holter, 1967).

The attenuation depends not only on the turbidity in the atmosphere but also on the length of path through the atmosphere. The length of the light path varies approximately as the secant of the zenith angle (i). Hence, the zenith angle (i) is involved in reducing illumination in two ways. First, the intensity on a horizontal surface is cos(i) times the intensity on a plane normal to the radiation. Second, the path traversed by radiation through the atmosphere is greater for large angles than for the small angles. The irradiance on a horizontal plane at sea surface is

$$H_s = H_o \cos(i) \exp(-A\sec(i)) \qquad (2)$$

where A is the extinction optical thickness and includes Rayleigh attenuation, aerosol attenuation, and ozone absorption for a standard atmosphere (Elterman and Toolin, 1965).

In clean, dry, air, molecular scattering is of primary importance. The scattering of very small particles of molecular dimensions is inversely proportional to the fourth power of the wavelength (Jensen, 1968) and, therefore, affects the shorter wavelengths more than the longer wavelengths. This is the reason most black and white aerial photography is taken with the minus-blue filter. As the particle sizes in the atmosphere increase, the wavelength of maximum scatter becomes less selective and extends into the green, yellow, etc., regions of the spectrum. Hence, the color of the sky changes toward cloud white as the particles increase from molecular to aerosol size. As a result, aerial photography taken under turbid atmospheric conditions requires filtering out of more of the spectrum, including green and possibly yellow light to produce a noticeable effect (Tarkington, 1966). Photographs taken in the near infrared wavelengths are better able to penetrate haze.

## Light Reflection

Since the reflected light from the water surface will not contribute information on the material in the water, it should be reduced to a minimum. The incident light includes both direct sunlight and diffused skylight. The reflection of direct sunlight will be partially polarized and can be reduced from exposing the film by the proper orientation of a polarized filter. On a cloudless day, the skylight will be predominantly blue and the surface reflection of diffused light can be reduced with a minus blue filter. Figure 6 shows the effect of the sun's altitude on the irradiance of skylight and direct sunlight (Jones and Condit, 1948).

The height of the sun above the horizon is critical for vertical aerial photography of a water surface. The maximum height determines the amount of reflected light reaching the film while the minimum height determines light penetration into the sea. If the sea surface were calm, a single mirror-like reflection of the sun would appear. As the sea surface is generally not smooth, the zenith angle of the sun must be greater than half the angular coverage of the camera to avoid photographing the sun spot glare. The width of the glitter pattern about the sun's reflection is an indication of the maximum slope of the sea surface. Cox and Munk (1955) have studied roughness of the sea surface by analyzing photographs of the sun's glitter. As shown in figure 7, a sloping water surface will require that the minimum zenith angle of the sun be at least half the angular coverage of the aerial camera plus twice the water surface slope if vertical photography is to be free of sun's glare. The slope of waves can vary from 0° to over 90° for breaking waves. It is, therefore, necessary to select a reasonable value of slope which will eliminate most of the sun spot glare for the expected sea conditions during photography. Studies (Cox and Munk, 1954) have indicated that for a 3-knot wind the maximum slope is about 15° and about 25° for an 18-knot wind. For photographing underwater objects Faas (1960) suggests that the slope 18.5° be used. This would indicate that the sun's zenith angle at the time of photography be at least 37° plus half the angular coverage of the aerial camera, if the sun's glitter is to be avoided on vertical photography. An alternate solution is to mount the camera to take oblique photography.

The light reaching the water surface is either reflected from or refracted through the air-sea interface. As shown in figure 8, the incident light ($H_s$) is divided into that which penetrates the sea ($H_w$) and that which is reflected from the interface. If i is the angle of incidence of the incoming radiation and j is the angle of refraction, then sin(i)/sin(j) is equal to the index of refraction for water or about 4/3. The reflectivity of an optically flat water surface is theoretically obtained for unpolarized light from Fresnel's law (Jerlov, 1968) which gives the ratio ($p_a$) of reflected energy to incoming radiation and is

$$P_a = \frac{1}{2}\left[\frac{\tan^2(i-j)}{\tan^2(i+j)} + \frac{\sin^2(i-j)}{\sin^2(i+j)}\right] \qquad (3)$$

where the terms inside the brackets are for the components of light parallels and perpendicular to the plane of incidence. A plot of the percent reflectivity for angles of incidence from 0 to 90 degrees is

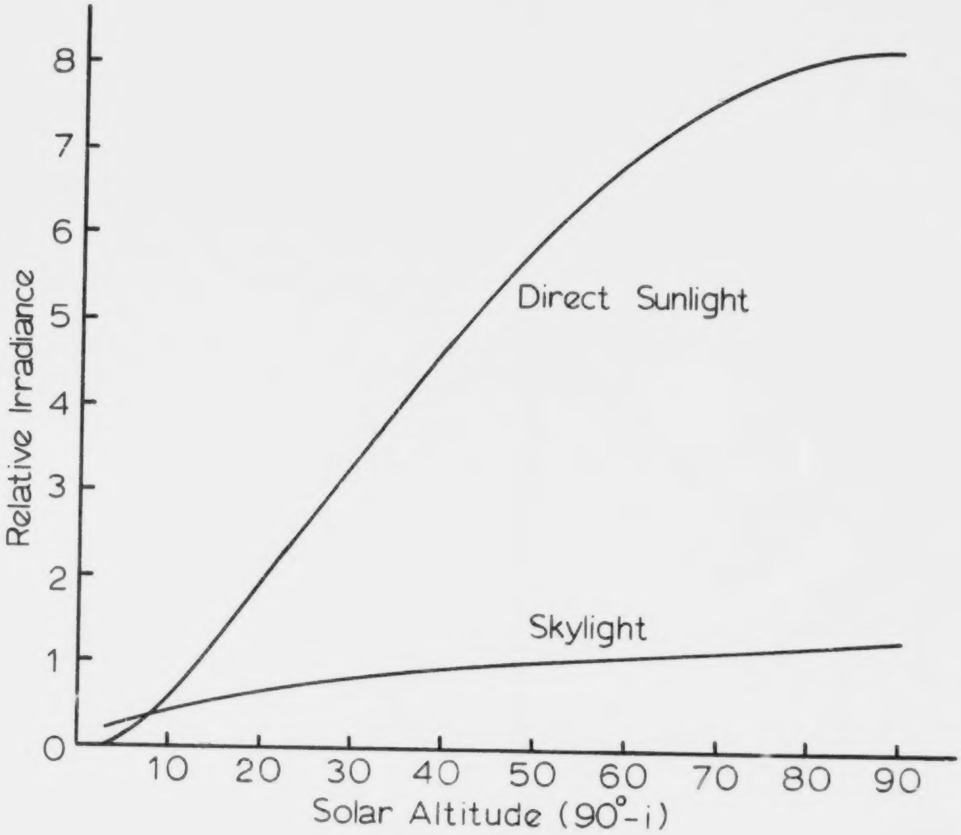

Figure 6. Direct sunlight and skylight on a horizontal plane.

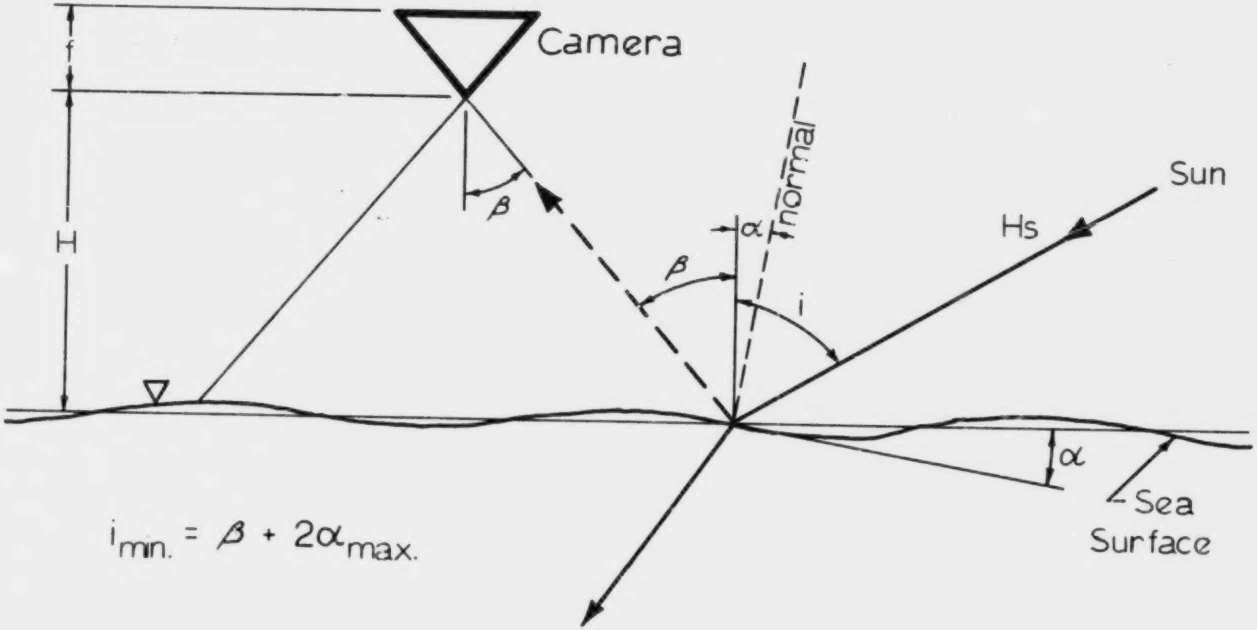

Figure 7. Sunlight reflection from a sloping water surface.

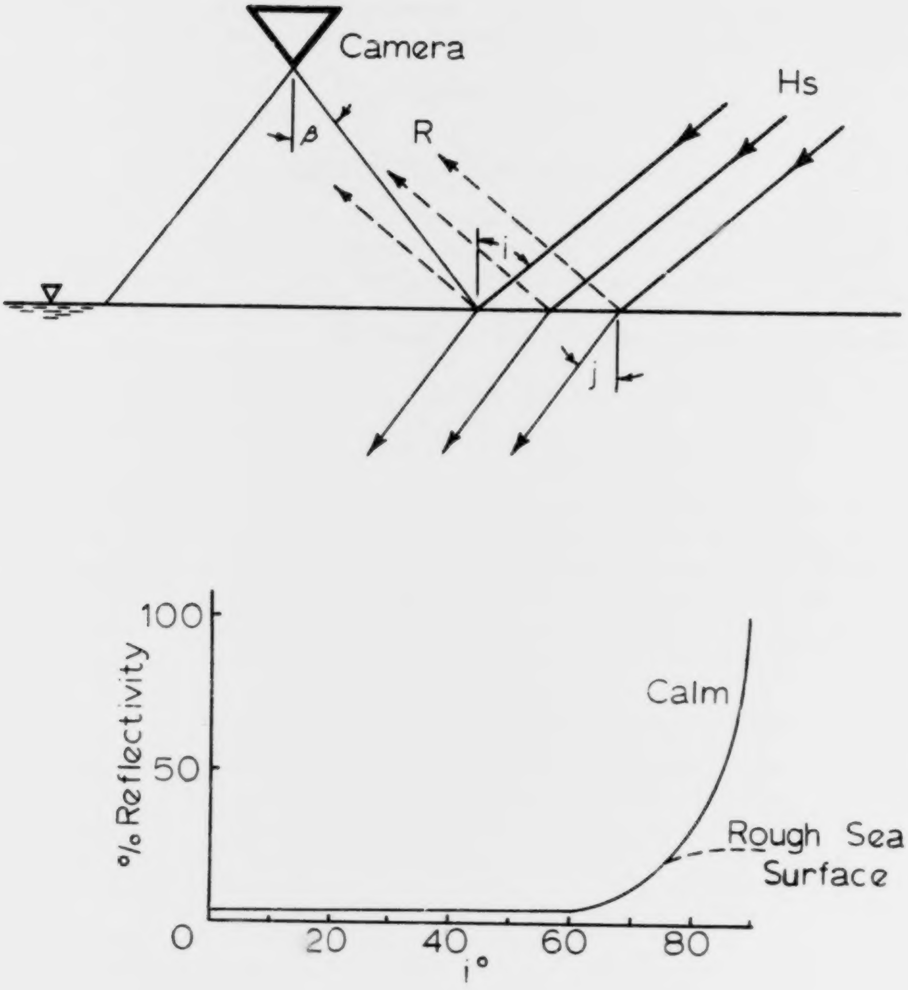

Figure 8. Light penetration into the sea.

shown in figure 8. It can be seen that the reflectivity increases rapidly when the angle of incidence exceeds 60 degrees. The irradiance ($H_w$) below the sea surface and normal to the beam is

$$H_w = (1 - p_a)\, H_s \sec(j) \tag{4}$$

## Light Attenuation in the Sea

The radiation that penetrates the surface of the sea is progressively diminished by extinction as it travels through the water. The attenuation of light is caused by scattering and absorption. By applying Lambert's and Beer's laws for monochromatic light the intensity $H_z$ at some depth z below the sea surface is given by

$$H_z = H_w \exp(-Cz \sec(j)) \tag{5}$$

$$C = a + bW \tag{6}$$

where C is the attenuation coefficient for sea water and waste, 'a' is the sea water attenuation coefficient, b is the waste absorption coefficient and W is the waste concentration. The attenuation coefficients for sea water and Kraft pulp waste are shown in figure 9. Minimum attenuation of sea water occurs at about 540 nm while the minimum for the waste is about 700 nm.

## Light Scattering in the Sea

The attenuation coefficients of both sea water and the waste can be divided into attenuation due to absorption and attenuation due to scattering. The scattering of light in a turbid medium is caused by reflection and diffraction light rays by small particles of suspended matter and colloidal solutions. As in the atmosphere, if the size of the particles is small compared to the wavelength of light, then the intensity of the scattering light is inversely proportional to the wavelength to the $n^{th}$ power. The exponent n decreases with increasing particle size from the value of four for pure water to approaching zero for coarse suspended matter (Jensen, 1968). Thus for solutions with small particles, the blue light has the maximum scatter, while for solutions with larger particles all colors are scattered about the same amount.

By definition of the volume scattering function $\beta(\alpha)$, the scattered light intensity (dJ) from an incremental volume dV is

$$dJ = H_z \beta(\alpha) dV \tag{7}$$

where $\alpha$ is the angle between the incident beam and the scattered light.

Figure 10 shows the variation in the volume scattering function for both sea water and pure water (Jerlov, 1964). It can be seen that the curve

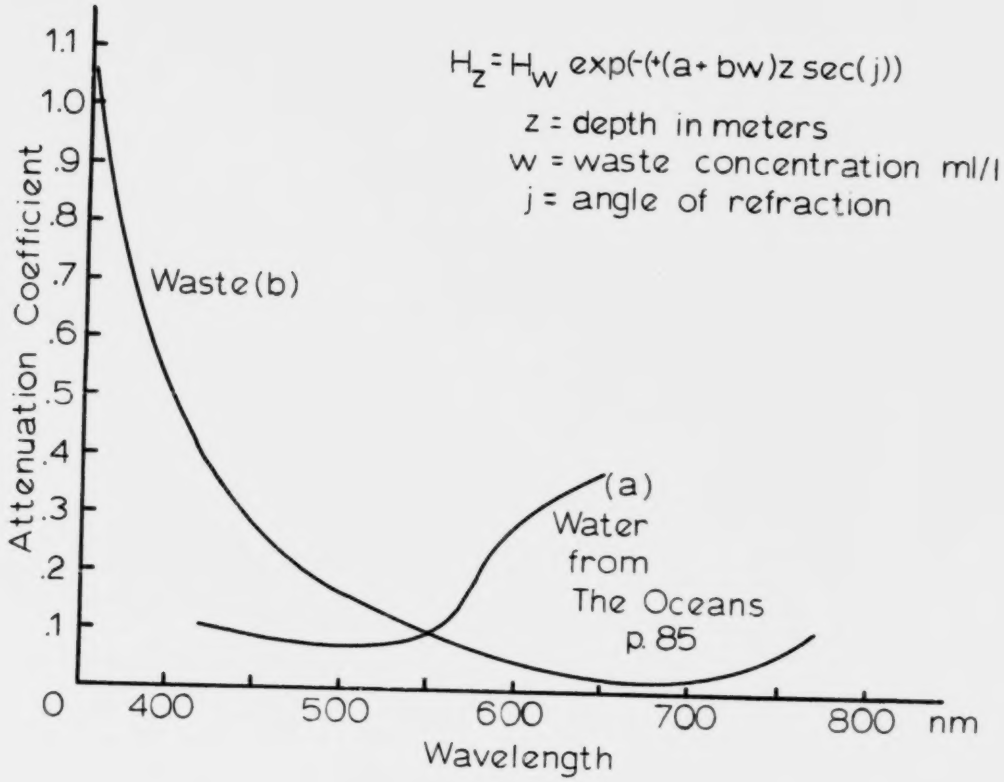

Figure 9. Typical attenuation coefficients.

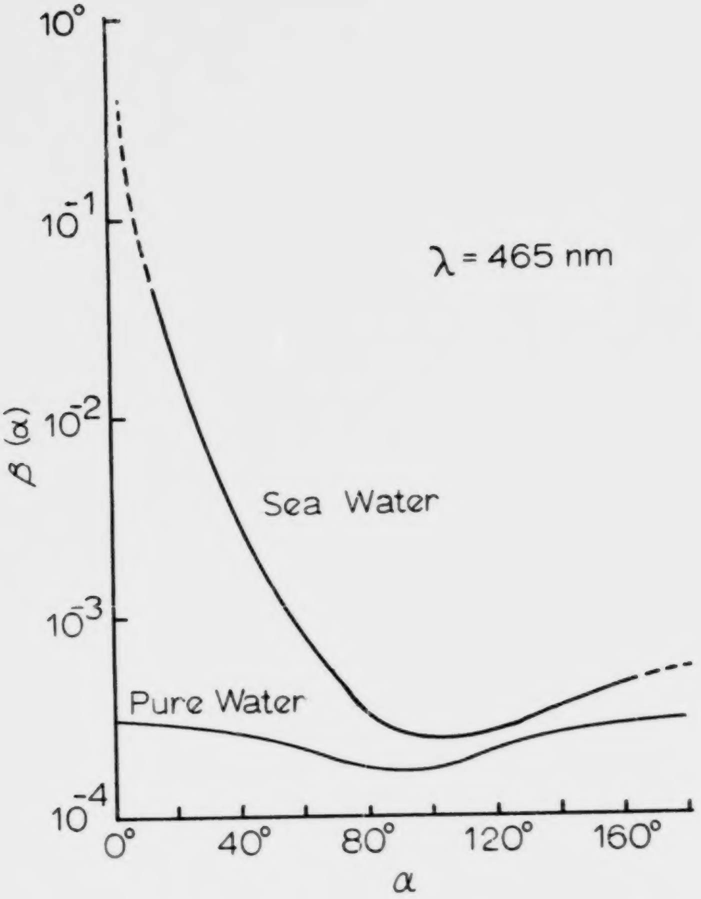

Figure 10. Volume scattering function.

for pure water is symmetrical with a minimum at α equal to 90 degrees. The scattering function for sea water varies greatly with α.

The variation of the scattering angle (α) on an aerial photograph is shown in figure 11. The angle between the incoming direct light in the sea and the scattered light reaching the camera changes with position; hence, the intensity of scattered light from below the sea surface will also vary. For a vertical photograph taken with a 6-inch aerial camera when the sun's zenith angle is 55 degrees, the angle "α" would vary from about 110 degrees to 170 degrees.

Figure 12 is a plot of data taken from work by Tyler and Richardson (1958). In this study a nephelometer was used to measure the radiant intensity scattered from a volume for various scattering angles (α). A

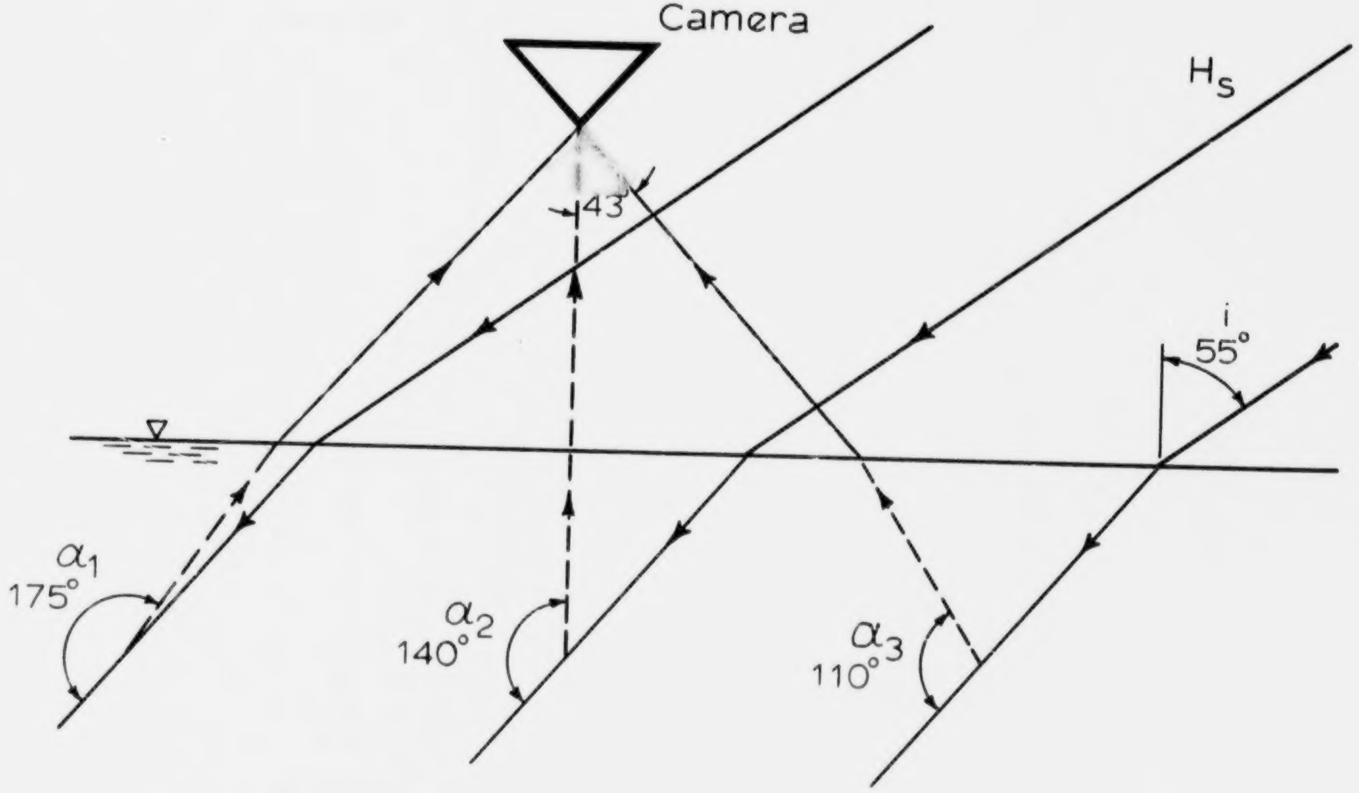

Figure 11. Variation in the scattering angle.

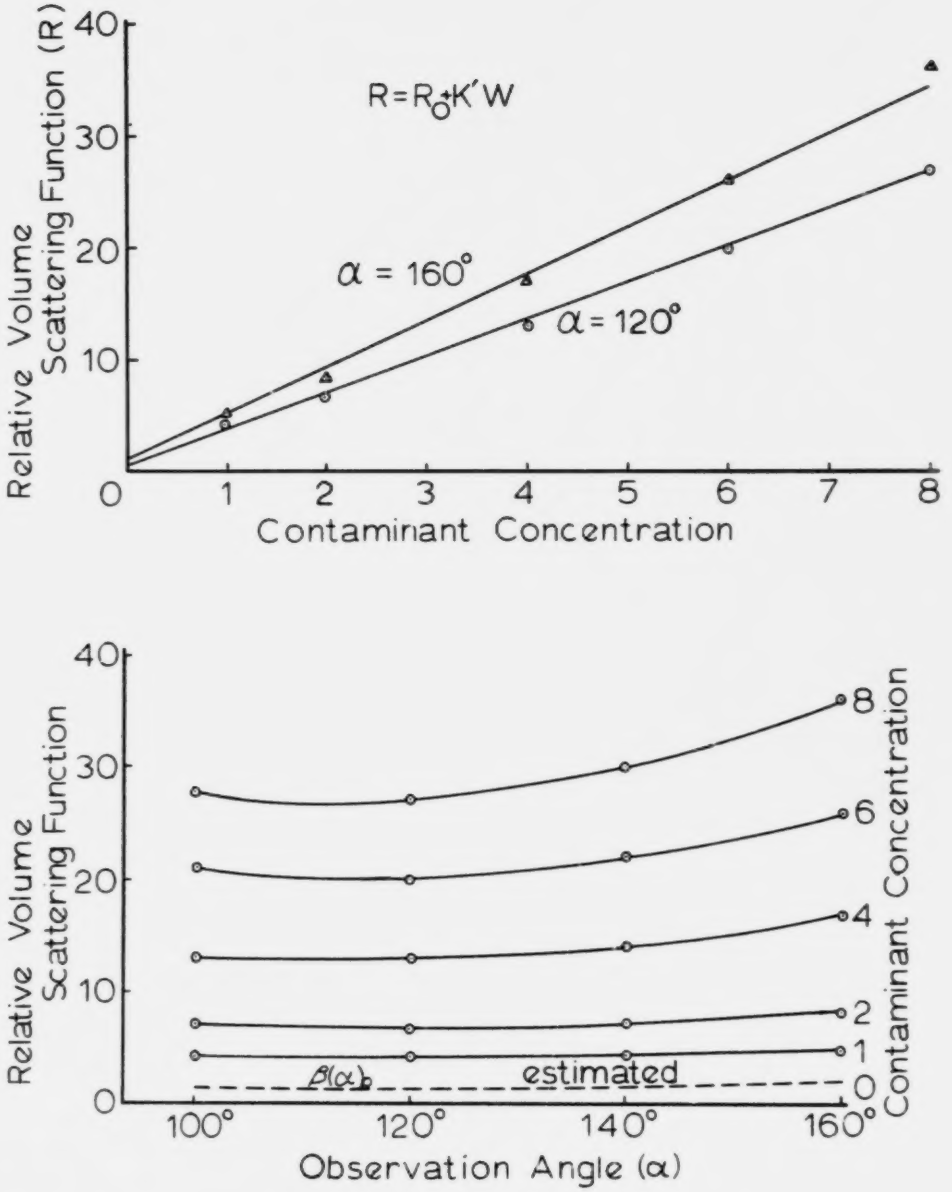

Figure 12. Effect of contaminant on the scattering function.

contaminant of skim milk was added at various concentrations. The light scattering for the various solutions is directly related to concentration of the contaminant.

For scattering by large particles, the intensity of the scattered light is proportional to the particle surface area that is exposed to the incident beam (Jerlov, 1968). If the particle size is uniform, then the intensity of the scattered light is proportional to the waste concentration. In the upper plot in figure 12 the volume scattering function is shown as a linear function of the waste concentration. From the lower plot in figure 12, it can be seen that the function $\beta(\alpha)$ can be approximated by

$$\beta(\alpha) = \beta_o(\alpha)(1 + K'W) \tag{8}$$

where $\beta_o(\alpha)$ is the volume scattering function of the sea water, $K'$ is a constant for a particular waste and $W$ is the waste concentration.

As shown in figure 13, if $R$ is the distance from the volume element ($dV$) to the point where the scattered light strikes the surface and $d\Omega$ is the solid angle formed at the surface by $dV$, then

$$dV = R^2 \, d\Omega dR \tag{9}$$

In addition, the emerging ray of scattered light from the incremental volume will be augmented by diffused light of almost uniform intensity in all directions. As the intensity of the light which is scattered for the second time, will be approximately three orders of magnitude less than that of the direct lighting, the addition of the rescattered light to the emerging ray will not be considered. The intensity of the emerging ray $dJ$ will be reduced by the absorption and scattering of the water and particles. From the inverse square law, the irradiance from the scattering volume incident on a normal plane to the beam at the surface is

$$dH_a = \frac{dJ}{R^2} \exp(-CR) \tag{10}$$

By combining equations and integrating, the irradiance at the surface is

$$H_a = \frac{H_o \beta_o(\alpha) \cos(i) \; (1 - pa) \; \exp(-A \sec(i)) d\Omega}{\cos(i_2) \; \cos(j)} \int (1 + K'W) \exp(-(a+bW)(\sec(j) + \sec(i_2))z) \; dz \tag{11}$$

If the waste concentration is a known function of the depth ($z$), then equation 11 can be integrated numerically. However, if the waste field forms a relatively stable layer at the surface and the waste concentra-

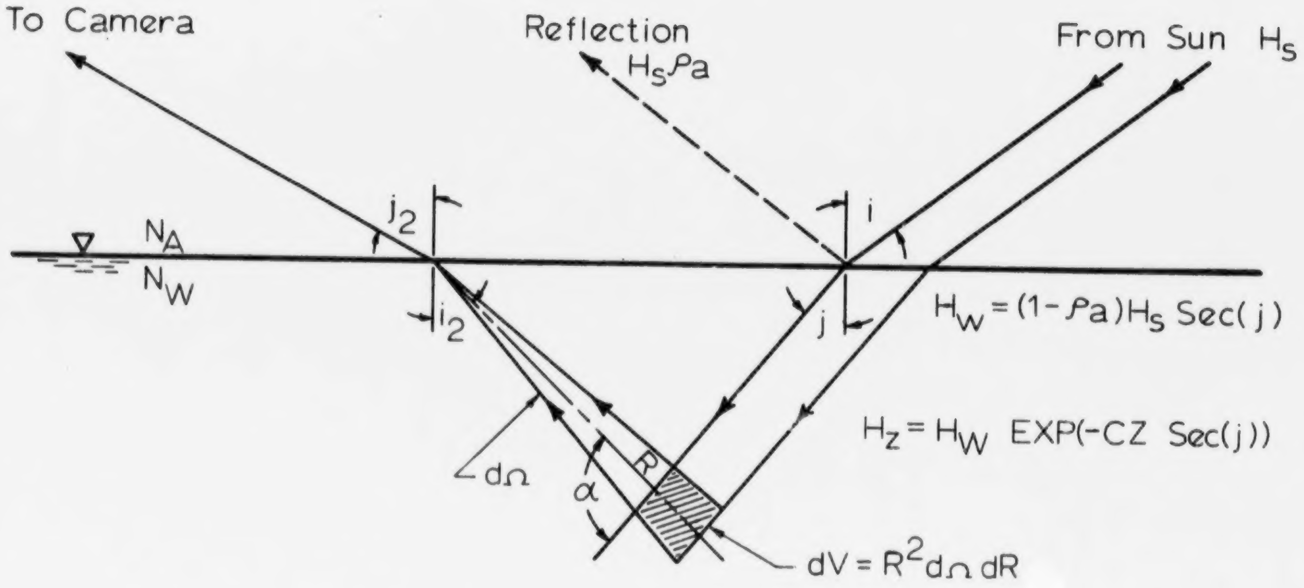

Figure 13. Light from the sea.

tion is approximately uniform throughout the depth of this layer, then equation 11 can be integrated directly.

If the waste concentration is not a function of depth and $\exp(-(a + bW)\ z(\sec(j) + \sec(i_2))$ approaches zero, equation 11 reduces to

$$H_a = \frac{(1 + K'W)\ Ho\beta_o(\alpha)\ \cos(i)(1 - pa)\ \exp(-A\ \sec(i))\ d\Omega}{(a+bW)\ \cos(i_2)\ \cos(j)(\sec(i_2) + \sec(j))} \qquad (12)$$

Evaluation of $\exp(-Cz(\sec(j) + \sec(i_2)))$ is shown in figure 12 for the green, red, and infrared regions of the spectrum. The expression was evaluated for values of the angles j and $i_2$ other than those listed in figure 14; however, the expression was relatively insensitive to changes in these angles. Average values of attenuation coefficients were selected from figure 9. It can be seen from the upper plot in figure 14 that 90% of the light returned in the infrared region is from the upper half meter of water. In the red and green bands the depth above which 90% of the light is returned is a function of the waste concentration. From the lower plot in figure 14, it can be seen that in the open sea 50% of the light in the red and green bands is returned from the upper two and four meters, respectively.

## Radiance from the Sea

From equation 12 the radiance (Nw) from the scattering volume below the sea surface is

$$Nw = \frac{H_a}{d\Omega} \qquad (13)$$

The light spreads into a larger solid angle when passing through the sea-air interface (Jerlov, 1968) and the radiance in air is

$$Na = \frac{Nw}{n^2}\ (1 - pw) \qquad (14)$$

where n is the refractive index of water and pw is the reflectivity of light at the interface.

In addition to the upward radiance from the sea, the light reaching the photographic sensor includes skylight reflection, direct sunlight reflection and path radiance intensity. Reflectance of skylight from a rough sea surface can be approximated by a Lambert reflector while the direct sunlight is reflected specularly. Skylight radiance reflected from the surface is given by

$$N\ sky = ps\frac{H\ sky}{\pi} \qquad (15)$$

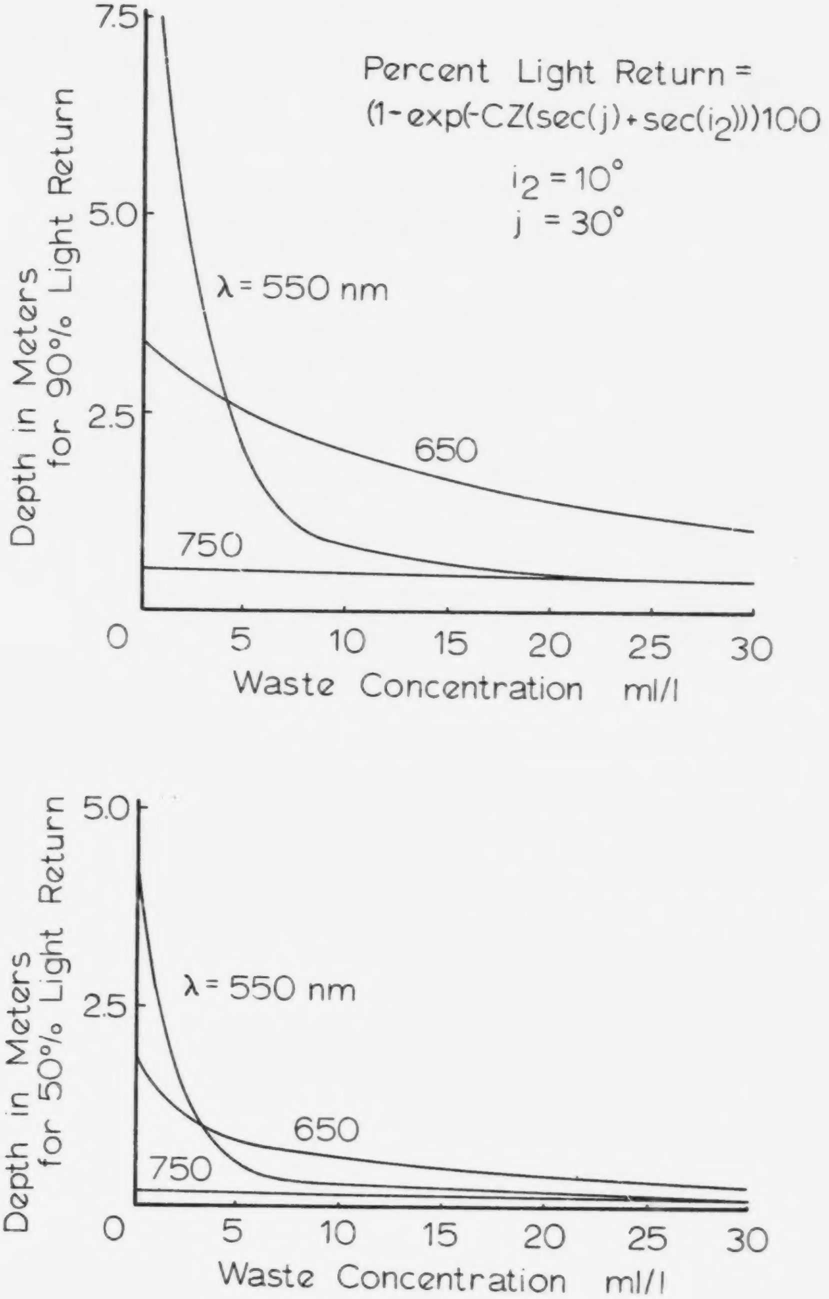

Figure 14. Depth of light return from the sea.

where ps is reflectivity of the skylight and was found by Burt (1953) to be approximately 0.066. The skylight irradiance (Hsky) is a function of solar altitude, atmospheric scattering and wave length of light. Path radiance intensity is a function of the length of sight ray, angle between sight and sun rays, atmospheric condition and wave length. For a clear atmosphere, skylight irradiance will be due predominantly to Rayleigh scattering and will have greatest influence on the shorter wave lengths. The reflection of direct sunlight is mathematically easier to estimate in magnitude by Fresnel's equations but its direction is difficult to predict without knowing the surface configuration of the sea. Since the Fresnel's equations are nearly independent of wave length, the magnitude of direct sunlight reflection will be proportional to each other in spectral bands of the sensor.

If N is the radiance from the sea surface and the path radiance is neglected then the radiance at the sensor is

$$Nc = N \exp(-E \sec(j_2)) \tag{16}$$

where E is the extinction optical thickness for the attenuation by the atmosphere from the sea to the camera. E is, therefore, a function of flying height and wave length. N includes the skylight reflection (N sky), direct sunlight reflection (Nd), and upward radiance from the sea and the waste (Na) or

$$N = Nsky + Nd + Na \tag{17}$$

By combining equations 12, 13, 14, 15, and 17 the radiance N is equal to

$$N = ps\frac{Hsky}{\pi} + Nd + \frac{(1 - pw)(1 + K'W)\beta_o(\alpha)\ Ho \exp(-A \sec(i)) \cos(i)(1 - pa)}{n^2\ (a + bW) \cos(j) \cos(i_2)(\sec(i_2) + \sec(j))} \tag{18}$$

The first term on the right is the skylight reflection, the second term is direct sunlight reflection and the last term is the uplighting from the sea (Na).

Equation 18 can be expanded by writing the equation for each of the spectral bands. The subscripts g and r refer to the bands of maximum absorption and scatter, respectively.

$$N_g = K_4 p_s \frac{H\ sky}{\pi} + K_5 N_d + K_6 Y\ (\exp(-A_g\ \sec(i)))\frac{(1 + K_g'W)}{a_g + b_g W}\ \beta_o(\alpha) \tag{19}$$

$$N_r = K_7 p_s \frac{Hsky}{\pi} + K_8 N_d + K_9 Y \left(\exp(-A_r \sec(i))\right) \frac{(1 + K'_r W)}{a_r + b_r W} \beta_o(\alpha) \qquad (20)$$

A typical spectral signature of both the open sea and the waste field is shown in figure 15. The effect of skylight, direct sunlight, and waste on the spectral signature is shown in the figure. Whenever possible direct sunlight reflection from the water surface should be avoided as it will cause interference with the data processing. Hence, the second term on the right of the three equations is zero. As skylight is predominantly blue

$$K_4 \sim 0, \quad K_7 \sim 0$$

Rewriting equations 19 and 20

$$N_g = K_6 Y \frac{(1 + K'_g W)}{a_g + b_g W} \exp(-A_g \sec(i)) \qquad (21)$$

$$N_r = K_9 Y \frac{(1 + K'_r W)}{a_r + b_r W} \exp(-A_r \sec(i)) \qquad (22)$$

Where Y is a constant for the two bands at a point on the photograph and is equal to

$$Y = \frac{H_o(1 - pw)(1 - pa) \cos(i) \beta_o(\alpha)}{n^2 \cos(j) \cos(i_2)(\sec(i_2) + \sec(j))} \qquad (23)$$

The Y term can be eliminated by taking the ratio (Rp) of the radiance in the two bands

$$R_p = K_{10} \frac{1 + K'_r W}{1 + K'_g W} \frac{a_g + b_g W}{a_r + b_r W} \exp(-(A_r - A_g) \sec(i)) \qquad (24)$$

where $K_{10}$ is a constant.

$\frac{1 + K'_r W}{1 + K'_g W}$ is the scattering coefficient ratio and shows the effect of scattering on the composition of the scattered light. As the particle size is relatively large compared to the wavelength of light, the scattered light is of nearly the same composition as the incident light. Therefore, this term is approximately equal to one.

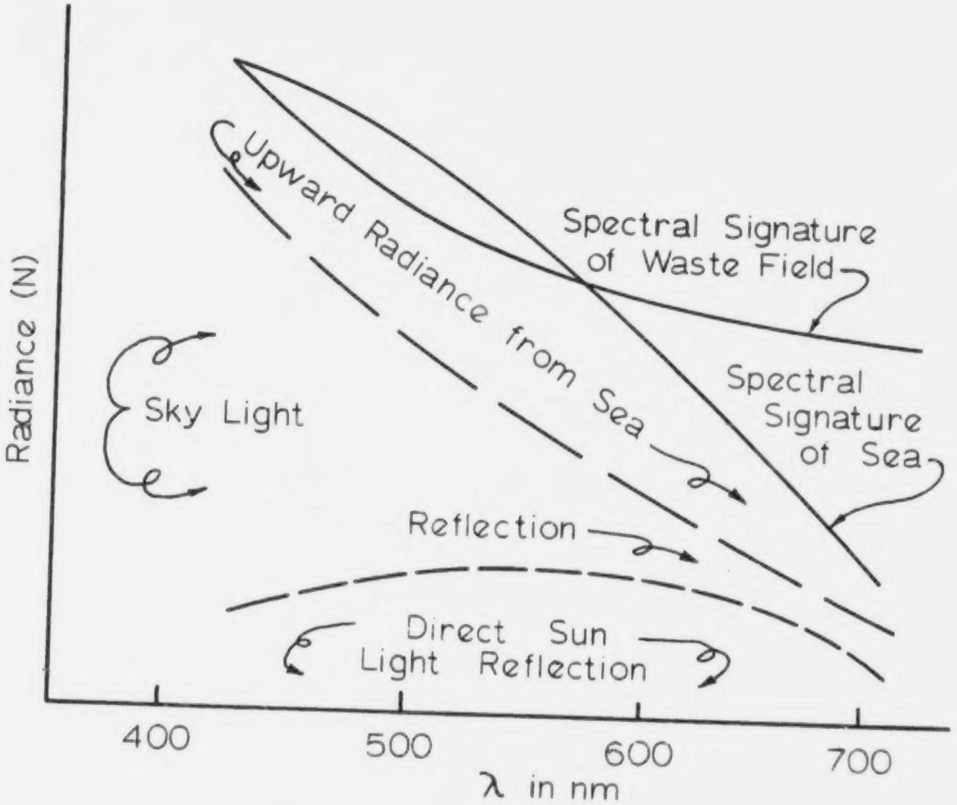

Figure 15. Typical spectral signature.

The term $\frac{a_g + b_g W}{a_r + b_r W}$ represents the change in light composition due to the selective absorption of the waste and the sea water.

$\exp(-(A_r - A_g)\sec(i))$ is the atmospheric attenuation ratio and shows the effect of the sun's altitude on the incident light composition.

From equation 24, the ratio at the sea surface (Rph) is

$$Rph = Rp \exp((A_r - A_g)\sec(i)) = K_{10} \frac{a_g + b_g W}{a_r + b_r W} \qquad (25)$$

## Photographic Measurement of Light

The aerial photograph is a light detector and can be used to measure the light return from objects. As shown in figure 16, $j_2$ is the angle between the ray to the camera and the vertical. If the angle between

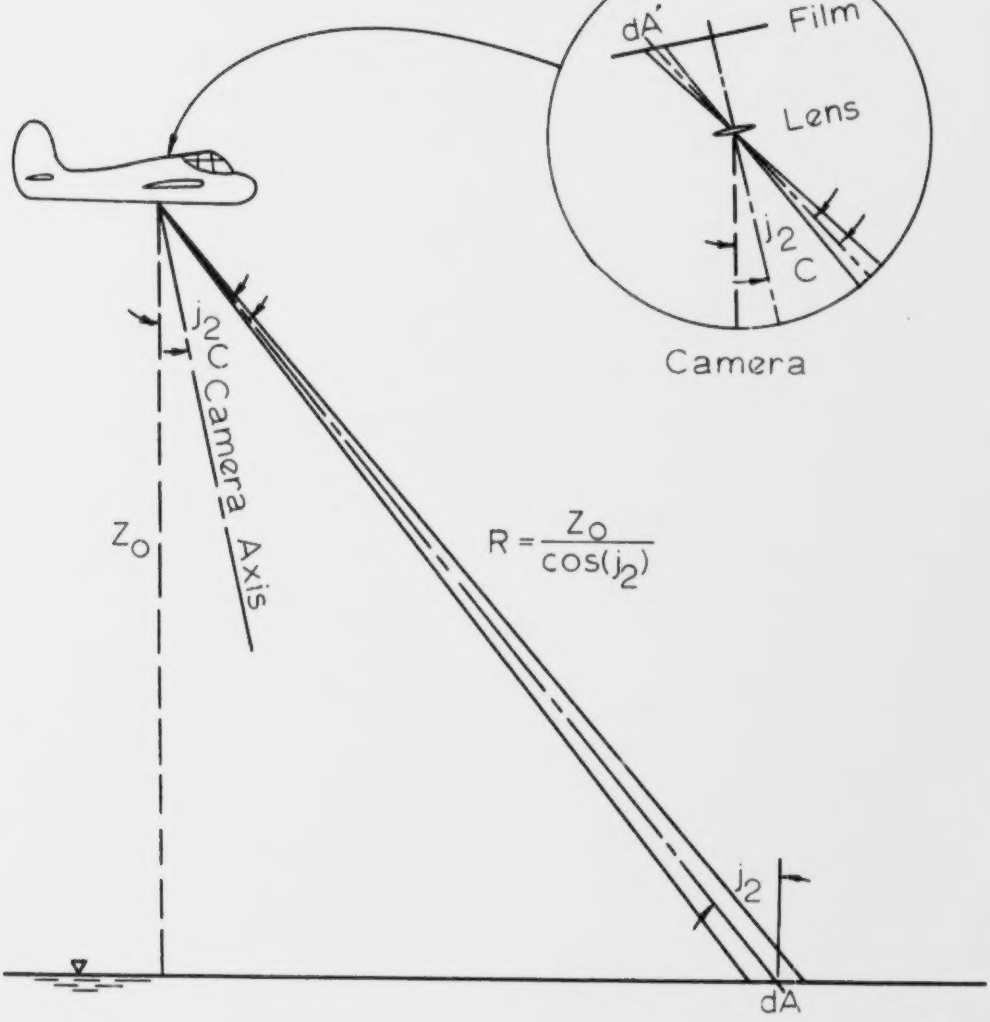

Figure 16. Geometry of exposure calculation.

the ray and the camera axis is represented by c, then by geometry

$$dA = dA' \left[\frac{Zo}{f}\right]^2 \left[\frac{\cos(c)}{\cos(j_2)}\right]^3 \tag{26}$$

where dA is the area on the sea surface included in the densitometer aperture area dA' on the photographic film, Zo is the flying height and f is the focal length of the camera. The solid angle subtended by the lens of diameter D is

$$d\Omega = \frac{\pi}{4}\left[\frac{D\cos(j_2)}{Zo}\right]^2 \cos(c) \tag{27}$$

The radiant flux (dp') collected by the camera lens is

$$dp' = N_c \; dA \cos(j_2) \; d\Omega \tag{28}$$

The irradiance of the film image is

$$H' = \frac{dp'}{dA'} = K_{12} \frac{TR \; N_c \cos^4(c)}{(FNO)^2} \tag{29}$$

where $K_{12}$ is a constant, FNO is the relative aperture of the lens (f/D), TR is the lens transmittance and $N_c$ is the object radiance at the camera.

The photographic exposure (EX) is the product of image irradiance (H') or the rate at which energy is incident upon a unit area of the film and the time (TIM) during which it acts. The equation

$$EX = H' \times TIM \tag{30}$$

indicates that there are many combinations of H' and TIM that will give the same exposure. This is known as the Reciprocity Law and is correct for normal aerial photography where extremes in exposure times are not employed.

The density of a film is defined as the common logarithm of the reciprocal of the transmittance or the logarithm of the ratio of incident light on the film and the transmitted light through the film. The relationship between film density and exposure is shown by the characteristic curves of a film. The curve is a plot of log exposure against film density for a particular development. A typical characteristic curve is shown in figure 17 (American..., 1968).

The characteristic curve can be divided in three parts; the lower part of the curve AB which is concaved upward is known as the toe, the

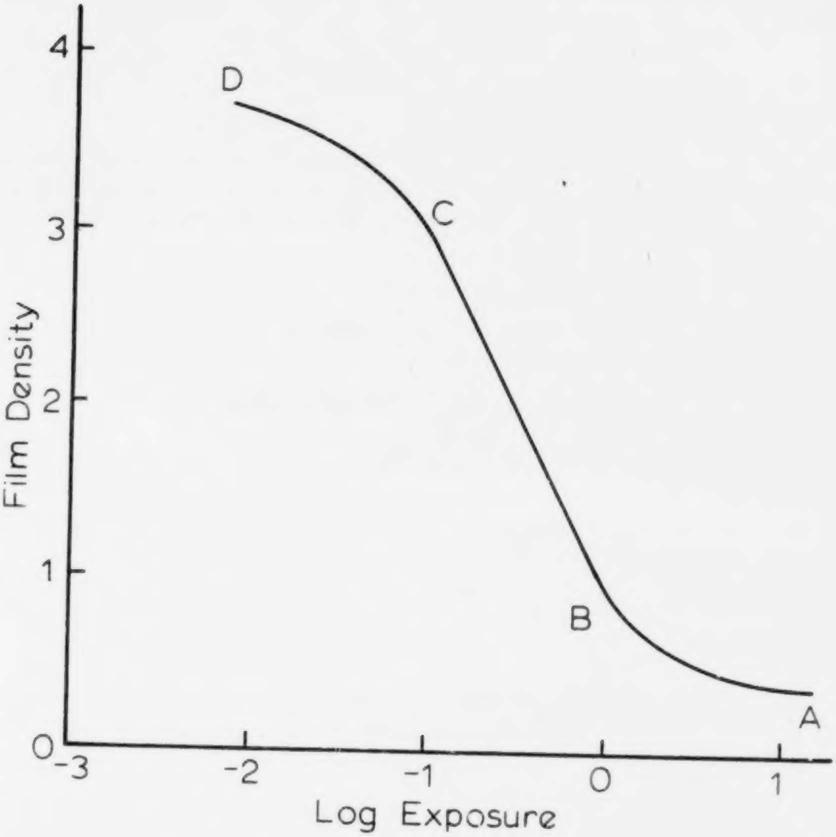

Figure 17. Typical characteristic curve of an aerial positive film.

the straight line portion of the curve BC, and the top part of the curve CD which is concaved downward and is known as the shoulder region. The toe of the characteristic curve approaches a horizontal line at some value of density greater than zero. This value represents the density of the base of the film.

The slope of the straight line portion of the characteristic curve is known as the film gamma. The greater the gamma the greater the contrast or the greater the difference in densities on a given photograph. The gamma is a characteristic of the film but varies within limits with different development time. The speed or exposure index of the film is indicated by the horizontal position of the characteristic curve along the exposure axis.

If the exposure of the film is on the straight line portion of the D or E curve, then the film density can be expressed by

$$D(x, y) = M + G \ln (EX) \tag{31}$$

D(x, y) is the film density at the point on the photo with film coordinates x and y, M is a constant representing the film speed, G is the gamma or contrast of the film and EX is the exposure.

Combining equations 30 and 31 and solving for the image irradiance

$$H' = \frac{K_{13}}{TIM} \exp((D(x,y) - M)/G) \tag{32}$$

The radiance from the sea as measured at the camera station is determined from equations 29 and 32

$$N_c = \frac{K_{14}\ (FNO)^2 \exp((D(x,\ y) - M)/G)}{(TIM)(TR)\ \cos^4(c)} \tag{33}$$

By including the atmospheric attenuation, but neglecting light path radiance in the atmosphere, the radiance at the sea surface (N) is equal to

$$N = \frac{K_{15}\ (FNO)^2}{(TIM)(TR)\ \cos^4(c)} \exp(D(x,y)/G + E \sec(j_2)) \tag{34}$$

where the term exp(-M/G) has been included in the constant ($K_{15}$). The factor $\exp(E \sec(j_2))$ compensates for the atmospheric attenuation of the light from the sea surface to the camera. Writing equation 34 for two spectral bands:

$$N_g = \frac{K_{17}(FNO)^2 \exp(D_g(x,y)/G_g + E_g \sec(j_2))}{(TIM)(TR_g)\ \cos^4(c)} \tag{35}$$

$$N_r = \frac{K_{18}(FNO)^2 \exp(D_r(x,y)/G_r + E_r \sec(j_2))}{(TIM)(TR_r)\ \cos^4(c)} \tag{36}$$

The ratio (R) of the radiance in the two bands is obtained by dividing equation 36 by 35

$$R_p = \frac{N_r}{N_g} = K_{19} \exp((D_r(x,y)/G_r - D_g(x,y))/G_g + (E_r - E_g) \sec(j_2)) \tag{37}$$

For the color films used on this project the gamma (G) was nearly the same in the spectral bands. As in equation 25, the value of Rph is defined as

$$
\begin{aligned}
Rph &= R_p \exp(A_r - A_g)\sec(i) \\
&= K_{19} \exp((D_r(x,y)/G_r - D_g(x,y))/G_g + (E_r - E_g) \sec(j_2) \\
&\quad + (A_r - A_g) \sec(i)) \qquad (38)
\end{aligned}
$$

where angle i is the angle of incidence for the direct sunlight and $A_r$ and $A_g$ are the extinction optical thickness of a standard atmosphere for the maximum absorption and scatter bands respectively.

If Rpho is the ratio of the radiance from the sea for the two bands where no waste is present and this value is adjusted for the atmospheric attenuation as in equation 38, Rpho can be estimated by the following regression model for any point on the photograph.

$$Rpho = B_0 + B_1 \text{ SUNR} + \varepsilon \qquad (39)$$

In this equation $B_0$ and $B_1$ are regression coefficients to be determined by a least squares fit of the model to the data points outside the waste field. SUNR is the angle between the ray from the sea to the camera station and the direct sunlight reflected from a horizontal surface.

The ratio anomaly (RA) is defined as

$$RA = Rph - Rpho \qquad (40)$$

and is the variation in the ratio of two bands of light returned from within the sea due to the presence of waste. The value of the ratio anomaly is determined from equations 38 and 39.

## Waste Concentrations from Aerial Photography

The relationship between the photographic value RA and the concentration W can be developed from equation 25 as

$$RA = K_{10} \left[ \frac{(a_r b_g - a_g b_r)W}{a_r(a_r + b_r W)} \right] \qquad (41)$$

Evaluation of the term in the brackets of equation 41 is shown in figure 18. The relationship between the photographic value RA and the waste concentration is a function of the sea water attenuation coefficients and the waste absorption coefficients. Average values of these coefficients were selected from figure 9. The upper curve in figure 18 is for the ratio of red to green radiance. For comparison

$$f(a,b) = \frac{(a_r b_g - a_g b_r)W}{a_r^2 + a_r b_r W}$$

| Curve No. | Band Subscripts | | Evaluated For |
|---|---|---|---|
| | $r$ | $g$ | green at 550nm |
| 1 | red | green | red at 650nm |
| 2 | infrared | green | infrared at 750nm |
| 3 | infrared | red | |

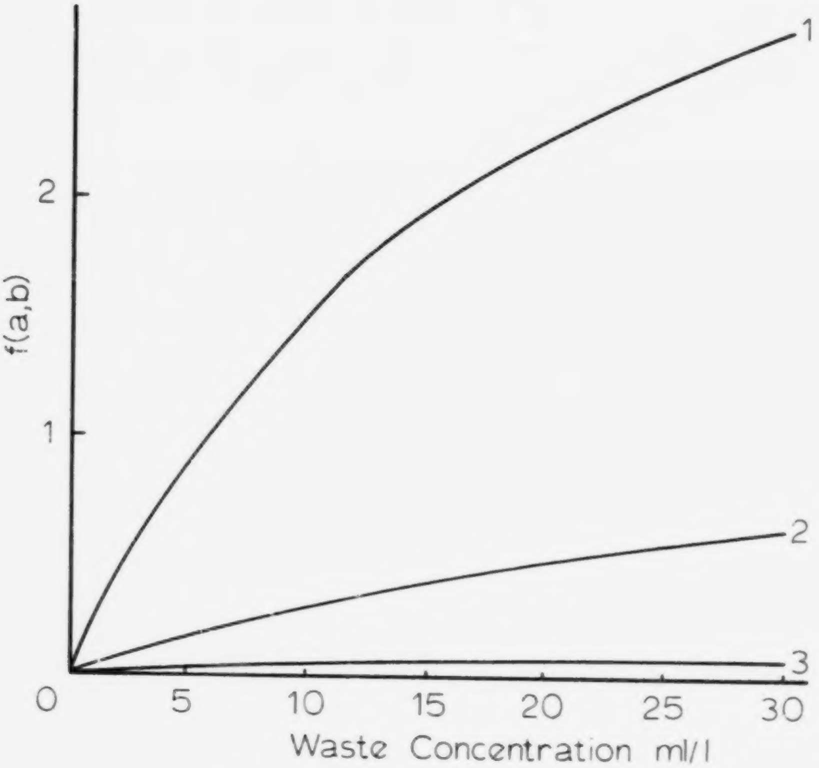

Figure 18. Spectral response curves.

two other curves were included. The lower curve is for the ratio of infrared to red and the center curve is for the ratio of infrared to green. While the ratio of red to green radiance is the most sensitive to changes in waste concentration, it is also the ratio with the greatest interference to skylight reflection and light path radiance.

Curves such as those shown in figure 18 are useful in predicting the response of different film-filter combinations for measuring waste concentrations; however, interference must be considered. If the two regions of the spectrum are measured with two cameras, the camera settings can be adjusted for optimum exposure in each band. By using high contrast developer and/or film, the sensitivity of the film density to the waste concentration can be increased.

From equation 41 the waste concentration can be expressed as

$$W = C_1 \, (RA) + C_2(RA)^2 + \dots \tag{42}$$

where $C_1$ and $C_2$ are coefficients. A stepwise regression analysis of this model has shown that only the first two terms are significant.

The F level to enter the first term ranges between 500 to 1000 while the F level to enter the second term generally ranges from 1 to 5.

## Photographic Orientation

Photographic orientation is accomplished by a non-linear solution to the collinearity condition equations (Keller and Tewinkel, 1966). Corrections are generally not required for atmospheric refraction, earth curvature, film shrinkage or lens distortion. The relationship between photo coordinates and ground coordinates is

$$\begin{bmatrix} x_p - x_0 \\ y_p - y_0 \\ -f \end{bmatrix} = K[RM] \begin{bmatrix} X_p - Y_c \\ Y_p - Y_c \\ Z_p - Z_c \end{bmatrix} \tag{43}$$

where $x_p$ and $y_p$ are photo coordinates of image point p, f is the camera focal length, $x_o$ and $y_o$ are photo coordinates of the principal point, K is a scale factor, the X, Y, and Z subscripted p and c refer to ground coordinates of the object and camera station respectively, RM is the rotational matrix. The matrix is defined as

$$[RM] = \begin{bmatrix} m11 & m12 & m13 \\ m21 & m22 & m23 \\ m31 & m32 & m33 \end{bmatrix} \tag{44}$$

where

$$m11 = \cos(\phi)\ \cos(K_a)$$

$$m12 = \cos(W_o)\ \sin(K_a) + \sin(W_o)\ \sin(\phi)\ \cos(K_a)$$

$$m13 = \sin(W_o)\ \sin(K_a) - \cos(W_o)\ \sin(\phi)\ \cos(K_a)$$

$$m21 = -\cos(\phi)\ \sin(K_o)$$

$$m22 = \cos(W_o)\ \cos(K_a) - \sin(W_o)\ \sin(\phi)\ \sin(K_a)$$

$$m23 = \sin(W_o)\ \cos(K_a) + \cos(W_o)\ \sin(\phi)\ \sin(K_a)$$

$$m31 = \sin(\phi)$$

$$m32 = \sin(W_o)\ \cos(\phi)$$

$$m33 = \cos(W_o)\ \cos(\phi)$$

The three parameters $W_o$, $\phi$ and $K_a$ are the photographic rotations about the X, Y and Z axis, respectively.

The collinearity equations are obtained by dividing the first and second rows of equation 43 by the third row hereby eliminating the scale factor.

$$\frac{x_p - x_o}{-f} = \frac{m11\ (X_p - X_c) + m12\ (Y_p - Y_c) + m13\ (Z_p - Z_c)}{m31\ (X_p - X_c) + m32\ (Y_p - Y_c) + m33\ (Z_p - Z_c)} \qquad (45)$$

$$\frac{y_p - y_o}{-f} = \frac{m21\ (X_p - X_c) + m22\ (Y_p - Y_c) + m23\ (Z_p - Z_c)}{m31\ (X_p - X_c) + m32\ (Y_p - Y_c) + m33\ (Z_p - Z_c)} \qquad (46)$$

These equations insure that the camera station, image and object lie on a straight line. For each point two collinearity equations can be written. As there are six unknowns ($X_c, Y_c, Z_c, W_o, \phi$ and $K_a$) a minimum of three noncollinear control points are required for their solution. However, a least squares solution permits the use of an unlimited number of control points.

Solution to the equations is obtained based on a set of initial approximations which are adjusted iteratively until the adjustments become small. The collinearity equations are linearized by the Taylor series with the expansion terminated at the first derivative.

When the initial approximations of $B_j$ are close to the actual parameters values (B)

$$f(B) = F(B_j) + \sum_{i=1}^{6} \frac{\partial f(B)}{\partial B_i} \Delta B_i \qquad (47)$$

Letting

$$Y = f(B) - f(B_j) \qquad (48)$$

$$Z_i = \frac{\partial f(B)}{\partial B_i} \quad \text{for} \quad B = B_j \qquad (49)$$

then

$$Y = \sum_{i=1}^{6} Z_i \Delta B_i + \varepsilon$$

which is a linear form of the collinearity equations. The least squares solution in matrix notation is

$$B = [Z^T Z]^{-1} Z^T Y \qquad (50)$$

The initial approximations of the parameters ($B_j$) are replaced by

$$B_{j+1} = B_j + \Delta B_j \qquad (51)$$

This iterative process is continued until the solution converges, that is, until all ΔB's are less than some prespecified amount. In this space resection problem no test is made on the linear adjustments but solution is terminated when the angular adjustments are less than about two seconds of arc.

By knowing the photo orientation, it is possible to determine the position vectors for any point on the photograph. The position vector ($\bar{X}$) based on the state plane coordinate system axis is related to the photographic vector ($\bar{X}_p$) by the equation

$$\bar{X} = [RM]^{-1} \bar{X}_p \qquad (52)$$

The ground coordinate of any point on the photograph can be computed from the unit position vector and the camera station coordinate determined from the photographic orientation.

In order to compute the required angle between this position vector and the light rays, the sun's position must be determined. The altitude (h) and azimuth (Az) from true north of the sun are determined from

$$\sin(h) = \sin(L)\sin(D) + \cos(L)\cos(D)\cos(t) \qquad (53)$$

$$\mathrm{Tan}(Az) = \sin(t)/(\cos(L)\ \tan(D) - \sin(L)\ \cos(t)) \qquad (54)$$

where
L = latitude
D = declination of the sun
t = hour angle of the sun

The vector representation of the light ray from the sun is

$$\bar{X}_s = \cos(h)\ \sin(AZ)\,i + \cos(h)\ \cos(AZ)\ j - \sin(h)\ k \qquad (55)$$

AZ represents the azimuth of the sun from grid north and differs from the azimuth from true north by the state plane coordinate mapping angle. The position vector as defined by equation 52 and the sun ray vector as defined by equation 55 are based on the same coordinate system.

## SECTION VI

## DIFFUSION STUDIES

Numerous investigators have employed solutions to the diffusion equations for the estimation of waste concentrations in the waste plume that occurs at an outfall location. If the scale of the current eddies is much smaller than the dimensions of the waste field, then the Fickian form of diffusion equation can be applied. The basic equation is:

$$\frac{\partial W}{\partial T} = \frac{\partial}{\partial Y}\left(D_y \frac{\partial W}{\partial Y}\right) + \frac{\partial}{\partial X}\left(D_x \frac{\partial W}{\partial X}\right) + \frac{\partial}{\partial Z}\left(D_z \frac{\partial W}{\partial Z}\right) - \left[ \frac{\partial}{\partial Y}(V_y W) + \frac{\partial}{\partial X}(V_x W) + \frac{\partial}{\partial Z}(V_z W)\right] + S \tag{56}$$

where V is velocity, W is waste concentration, D is eddy diffusivity. The first three terms on the right are the diffusion terms, the next three are convection terms and S represents the sources and sinks.

Solutions to the equations have required various assumptions such as steady state condition, no vertical or longitudinal mixing and unidirectional transport velocity in the x direction. With these assumptions, the equation becomes:

$$V_x \frac{\partial W}{\partial X} = \frac{\partial}{\partial Y}\left(D_y \frac{\partial W}{\partial Y}\right) + aW \tag{57}$$

Where "a" is a first order decay constant and "aW" represents a sink or loss in the system.

Investigators such as Pearson (1955-1967), Brooks (1960) and others have reported solutions to the diffusion equation for various conditions. Pearson points out that for point and line sources, steady unidirectional current, uniform mixing of the waste over a depth, d and continuous uniform flow from the source, solutions to the diffusion equation in terms of the minimum dilution, $S_{om}$, along the centerline axis of the waste sea water plume are as follows:

Point Source

$$S_{om} = \frac{2.35\ d \sqrt{D_y V_x X}}{Q} \tag{58}$$

where $S_{om}$ is the minimum dilution along axis of waste plume at distance X from source; $D_y$ is the assumed diffusivity, $ft^2/sec$; X is the distance from source, feet; $V_x$ is the average velocity of water mass, ft/sec; Q is the waste discharge, MGD; and d is the assumed mixing depth, ft.

Preceding page blank

Including the decay function for bacterial dieaway for disappearance, and expressing the waste concentration in terms of coliform concentration, the above expression becomes:

$$MPN = \frac{0.425\ QC_o}{d\sqrt{D_y V_x X}\ \exp(aXV_x)} \tag{59}$$

where MPN is the most probable number of organisms per ml on plume centerline at X; $C_o$ is the concentration of organisms in waste, MPN/ml; and a is the bacterial dieaway (decay) constant, $sec^{-1}$.

Line Source

$$S_{om} = \frac{0.622\ V_x bd}{Q\ \text{erf}\ [(b/4)\ \sqrt{V_x/D_y X}\ ]} \tag{60}$$

where b is equal to the width of diffuser source, feet and

$$MPN = \frac{1.55\ Q\ C_o\ \text{erf}\ [(b/4)\ \sqrt{V_x/D_y X}\ ]}{b\ d\ V_x\ \exp\ (aX/V_x)} \tag{61}$$

Pearson (1967) further points out that: "The above equations assume a constant eddy diffusivity; correspondingly, the value of $D_y$ employed must be representative of the overall or average scale of the diffusion phenomenon.

Brooks has reported a solution to the diffusion equation with a variable coefficient of diffusivity. It is assumed that the diffusivity coefficient, $D_y$, varies as the four-thirds power of the scale of the diffusion phenomenon, $D_y \cong \alpha\ l^{4/3}$, where $\alpha$ is a constant. Brooks' equation for a line source is as follows:

$$C_m = C_o e^{-at}\ \text{erf} \left[ \frac{3/2}{(1 + 2BX/(3b))^3 - 1} \right]^{1/2} \tag{62}$$

Where:

$C_o$ = initial coliform concentration

$C_m$ = maximum coliform concentration at time, t

t = time of travel = $\frac{X}{V_x}$

$B = \frac{12D_y}{V_x b}$

$a$ = decay constant

$D_y$ = eddy diffusivity at source ($X = 0$)

$b$ = initial width of sewage field

Considering the foregoing solutions to the diffusion equation, the four characteristics of the receiving waters which have the major effect on waste concentration are the following:

1. $V_x$, average current speed
2. $D_y$, eddy diffusivity
3. d, average mixing depth
4. a, decay or dieaway constant of pollutant

The Allen Hancock Foundation conducted an investigation on the dilution and dispersion of a waste field in the sea (1965). In their study rhodamine B dye was introduced as slugs from a point source, continuous plume from a point source and continuous plume from a volume source. Dye concentration was measured with a Turner fluorometer. The mathematical models used for analysis of data were statistical models based on Gaussian distribution. The basic three-dimensional model for the dye slug was

$$W(x,y,z,t) = \frac{M}{\pi\sqrt{2\pi}\,[\bar{\sigma}_x^{\,2}\bar{\sigma}_y^{\,2}\bar{\sigma}_z^{\,2}]^{1/2}} \exp -\left[\frac{X^2}{2\bar{\sigma}_x^{\,2}} + \frac{Y^2}{2\bar{\sigma}_y^{\,2}} + \frac{Z^2}{2\bar{\sigma}_z^{\,2}}\right] \qquad (63)$$

where W is the average concentration of a point X, Y, Z, and time t, M is the amount of dye initially discharged from an instantaneous point source and $\bar{\sigma}_x^{\,2}$, $\bar{\sigma}_y^{\,2}$, $\bar{\sigma}_z^{\,2}$ are the average values of the variances of the concentration distribution.

One of the two dimensional models used describe a continuous plume from point source neglecting diffusion in the direction of motion was

$$W(x,y,z) = \frac{Q}{\pi(\bar{\sigma}_y^{\,2}\bar{\sigma}_z^{\,2})^{1/2}\,V_x} \exp -\left[\frac{Y^2}{2\bar{\sigma}_y^{\,2}} + \frac{Z^2}{2\bar{\sigma}_z^{\,2}}\right] \qquad (64)$$

where Q is the continuous steady rate of discharge of material, $V_x$ is the mean current velocity. The variances are a function of diffusion time or distance from the source, i.e., by making the substitution $t = X/V_x$ the variances can be expressed approximately as functions of distance.

For volume source the basic equation was

$$W(x,y,z) = \frac{2Q}{\pi V_x \left[2\bar{\sigma}_y^{\,2} + \bar{\sigma}_y^{\,2}(0)\right]^{1/2} \left[2\bar{\sigma}_z^{\,2} + \bar{\sigma}_z^{\,2}(0)\right]^{1/2}}$$

$$\exp - \left[\frac{Y^2}{2\bar{\sigma}_y^{\,2} + \bar{\sigma}_y^{\,2}\,(0)} + \frac{Z^2}{2\bar{\sigma}_z^{\,2} + \bar{\sigma}_z^{\,2}\,(0)}\right] \qquad (65)$$

where $\bar{\sigma}^2$ (0) is the variance of the initial waste concentration distribution.

Several of the conclusions of this investigation are listed below.

1. The rate of vertical diffusion can contribute significantly to the overall diffusion process at wind speeds greater than eight knots and/or low water column stability.
2. The rate of longitudinal and lateral diffusion appeared to be influenced by wind speed but not by water column stability.
3. The "4/3 law" relating the lateral coefficient of eddy diffusion as a function of average eddy scale did not hold in the particular oceanic areas studied.

Vertical mixing does occur in the waste field as well as horizontal mixing. As indicated by Wiegel (1964), vertical mixing is difficult to study in the laboratory because of limitations of tank size. In these studies the wind drags the surface water to the down wind end of the tank producing a hydraulic head which causes a flow in the opposite direction.

Laboratory studies have indicated that wind drag on the water surface produces very little mixing. However, when wind generated waves appear, extremely rapid mixing occurs as wind waves are rotational in the generating area. On the other hand, there is some indication that swell is not important to the mixing process as it is apparently nearly irrotational (Wiegel, 1964).

Masch (1961) conducted a wave study in a wave tank and developed the following relationship for the coefficient of eddy diffusivity:

$$D_y = 0.0038\ (Vs + Qw)^{3.2}$$

where Vs is the surface current and Qw is the water particle orbit speed (Qw = H/T, H = significant wave height and T = average wave period.

# SECTION VII

## SAMPLING PROCEDURES

In order to achieve the goals of this research project, the Kraft pulp mill outfall at Newport, Oregon was selected as the study site. The Georgia-Pacific pulp and paper plant at Toledo produces about 900 tons of pulp per day. Waste from the process is pumped through an eight-mile pipeline to the outfall at Newport. Flow rates vary from six to twelve million gallons per day. The aerial photograph of the Newport-Toledo area shown in figure 19 was taken looking east with the ocean in the foreground. The location of the outfall in this figure was sketched on the photo and is shown in white. The 21-inch diameter outfall was rebuilt and extended to 3500 ft. offshore in 1965. The outfall terminates with a wye diffuser in about 40 feet of water at low tide. A sketch of the outfall is shown in figure 20. Thirteen outlet ports are located at 20-foot intervals on each leg of the wye section. The three-inch diameter ports discharge horizontally into the sea. The ports are oriented so that they discharge alternately on opposite sides of the header.

Three different field procedures were used on the project. During the 1968 and 1969 field seasons, work was carried out by conducting simultaneous studies of the waste plumes by aerial photographic methods and by conventional boat sampling. Concentrations in the plume were determined by metering rhodamine WT tracer into the pipeline and measuring the tracer concentration in the waste field with a fluorometer aboard the survey boat.

During the first field season, two fluorometers were used to sample from one foot and five feet below the water surface. Since there was no significant difference in the concentration at these two depths, only one fluorometer was used during the following field season. A ten-foot sampling probe for the fluorometer intake was constructed for the 1969 field season. Sample intake ports were located along the length of a sampling probe mounted on the side of the boat. The probe was designed to hang vertically at five knots. By a sliding valve arrangement in the body of the probe, the sampling depth could be selected from one to ten feet below the water surface. Boat sampling was discontinued during the 1970-71 field season and field work continued throughout the fall, winter, and spring when boat operations were impossible due to rough sea conditions most of the time.

Vertical aerial photography was taken with a single camera by a commercial aerial photography firm during the 1968 field season. As the firm was located approximately 100 miles from the study area, scheduling of the photography was difficult. After the 1968 field season, the project purchased three aerial cameras and the photography was taken with the cameras mounted obliquely in a rented four-passenger aircraft.

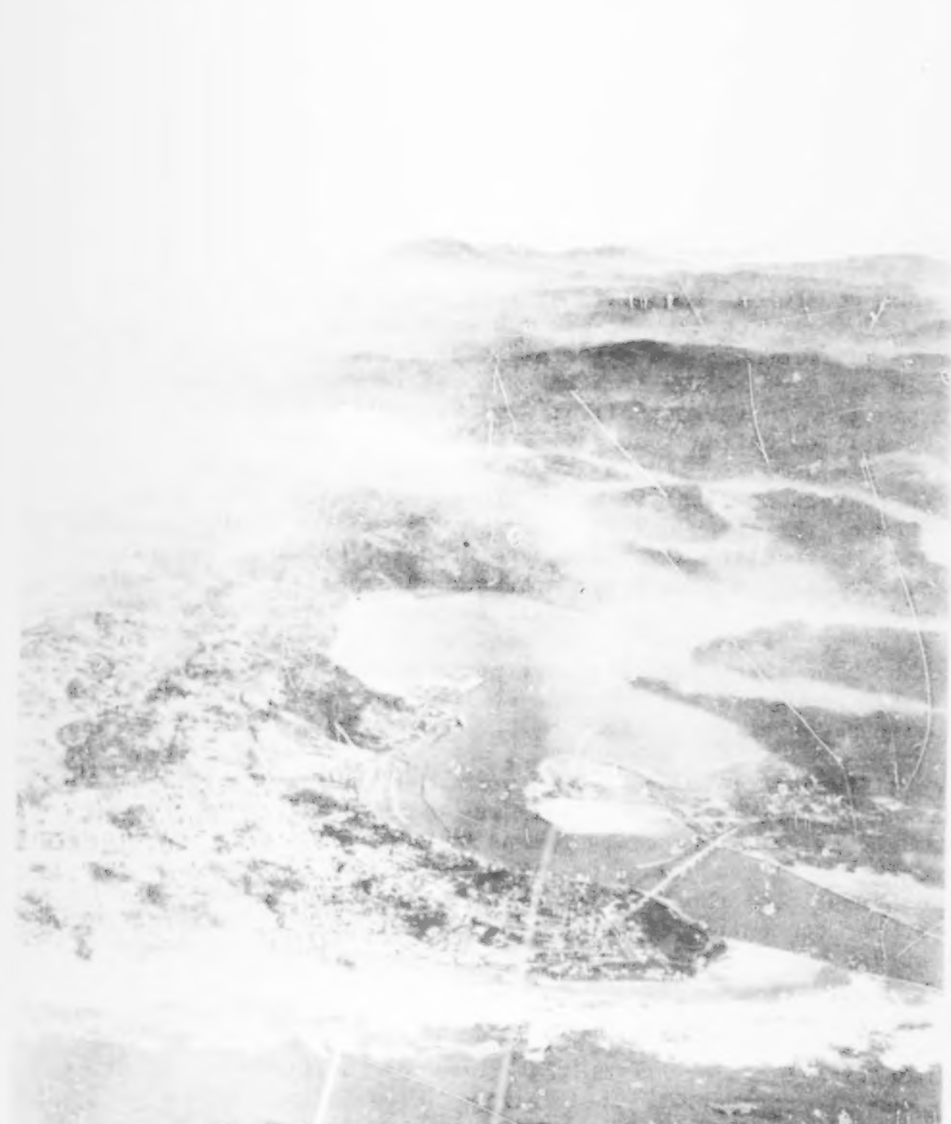

Reproduced from best available copy.

Figure 19. Aerial view of Newport area.

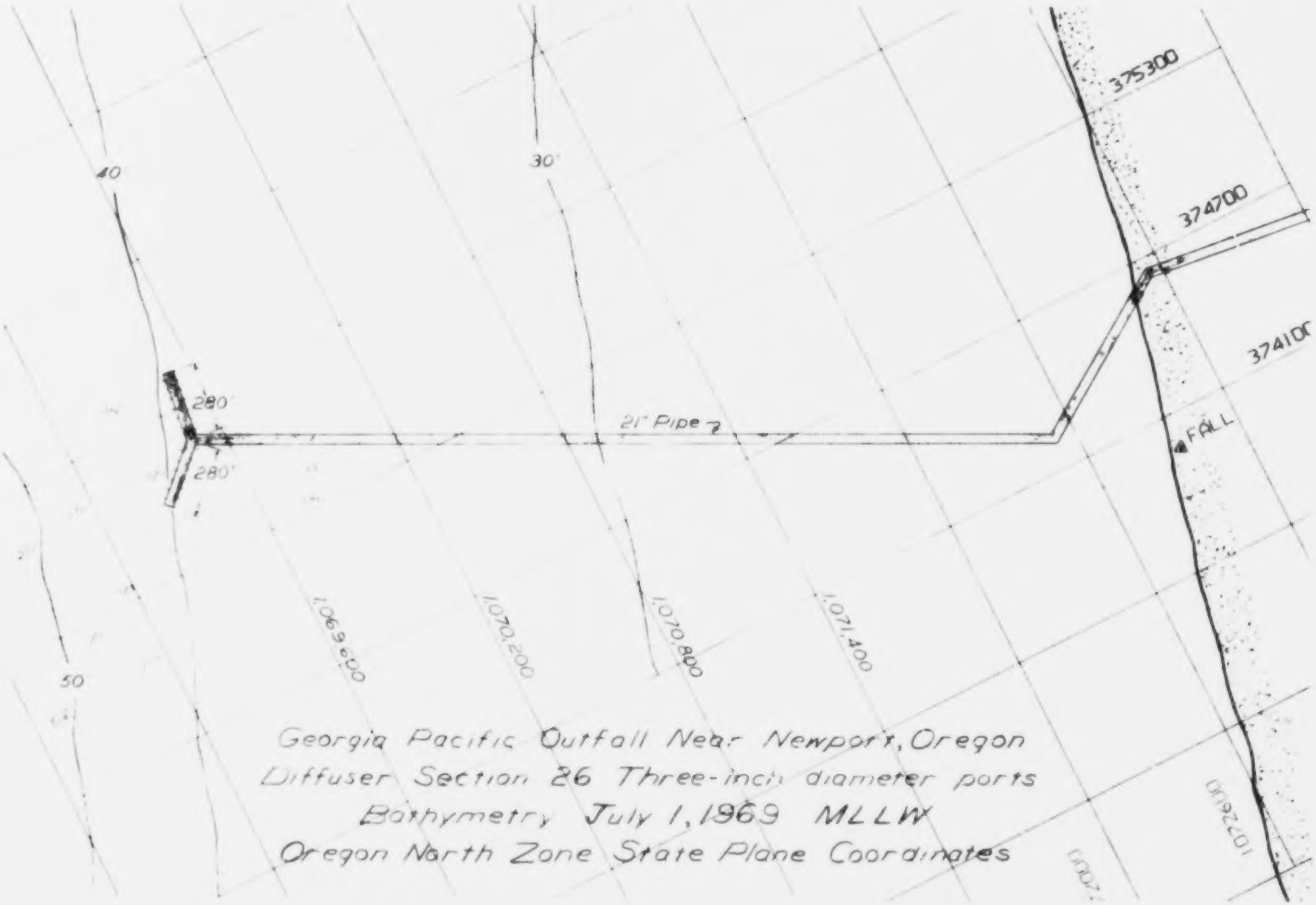
375300
374700
374100
FALL
21" Pipe
280'
280'
30'
40'
50
1,069,600
1,070,200
1,070,800
1,071,400
1072600
Georgia Pacific Outfall Near Newport, Oregon
Diffuser Section 26 Three-inch diameter ports
Bathymetry July 1, 1969 MLLW
Oregon North Zone State Plane Coordinates

Figure 20. Sketch of the Newport outfall.

## Shore Control

Accurate control for positioning the boat and orientation of the photography was essential. Concentrations computed from the photographs are compared to those measured by sampling from the boat. Since the comparison requires matching of ground coordinates, an accurate control network was established, thus eliminating the possibility of discrepancies in concentration being due to error in positioning.

Shore control for boat location and photograph orientation was provided by a ten-mile tellurometer traverse between two USC & GS triangulation stations. The traverse extended from a triangulation station on the south to station Yaquina Head Lighthouse on the North. Six traverse stations were established and marked with three quarter-inch steel rods 30 inches long. Horizontal angles were measured with a Wild T-3 theodolite. Initially the distances were to be measured with a geodimeter but due to poor visibility, a tellurometer was used. As the tellurometer measures slope distance, the station elevations were determined by reciprocal vertical angles. The established stations were marked with white cloth for photo identification.

## Buoy Control

During the 1968 field season vertical, color photography was taken by a commercial aerial mapping firm. Photography was taken at scales of 1:6,000 and 1:12,000 using precise mapping cameras. In addition to the shore control, control buoys were required in the water for photographic orientation of the low altitude photography. The buoys were positioned so that each photo would contain a minimum of three control points for photographic orientation. Control buoys were four-foot square plywood floats three inches deep attached to 500 lb concrete anchors. The floats were constructed of a two-inch thick sheet of polyurthene between two sheets of half-inch plywood. To hold the float together a metal flashing was fastened around the edge and an eye bolt was placed through the center of the float. The mooring line was attached to the eye bolt. This line consisted of a ten-foot length of half-inch chain attached to each end of a half-inch polyprophylene rope. A swivel was placed between the top section of chain and the rope. The weight of the chain added stability to the anchoring system. In addition, the top 10-foot section of chain prevented vandalism by boaters. The scope of the mooring line was made as short as possible to minimize movement of the float about the anchor yet long enough to prevent movement of the anchor during normal summer months. The mooring line was made equal to the depth of water at MLLW plus 20 feet. Summer storms did take out three of the near-shore buoys which were set in less than 20 feet of water.

The small scale photography taken during the 1968 field season was intended to be used for buoy location by analytical strip bridging. However, it was found more convenient to triangulate the position of the buoys from the shore stations.

The oblique camera mounting used after the first field season reduced the requirement for horizontal control in the water. The large camera photographs included the horizon and two horizontal control points could be identified on shore. In addition, one buoy was desired near the outfall to provide a strong fix for the photographic orientation. During the 1969 field season, two temporary buoys were set near the outfall on each day that field work was conducted. The buoy floats were four feet square, two inches thick polyurthene board which were fiberglassed and painted orange. The 60-lb anchors were adequate to hold the floats in position for the sea conditions encountered during the field work. Since boat operations were stopped during the 1970-71 field season, control buoys were not used during this period and photo control was provided by identification of at least three shore stations on the photography.

## Water Currents

During the 1968 field season, the survey boat would set two four foot square floats with drogues attached to measure the water currents. The drogues extended from one half foot below the water surface to five feet and were constructed of herculite material fitted over a conduit frame to form a cross banner 4-1/2 ft in length and in width. A ten pound weight was attached to the lower end of the drogue. The positions of the current floats were determined from the aerial photography. In addition, during the 1969 field season 500 ml of 20% rhodamine WT dye in a plastic bag were dropped from the aircraft. The change in location and size of the resulting dye patch provided information on both the current velocity and the diffusion coefficients. When boat sampling was discontinued after the 1969 field season, floats with drogues attached were no longer used but dye markers were used to determine water currents and diffusion coefficients.

## Continuous Boat Sampling

Cooperative arrangements were made with Georgia-Pacific Corporation to maintain a nearly constant waste discharge rate while field work was in progress. In addition, they provided the project with a dye tracer injection station installed on their outfall line near the beach. The station was equipped with a tap to the pipeline for injecting the tracer. A positive displacement pump was employed for continuous tracer injection into the pipeline. Pressure in the pipeline at the station varied from zero at low tide to about five psi at high tide for the pipeline flow rates encountered during the study.

Measurement of waste concentrations in the ocean was accomplished by metering a dye tracer, rhodamine WT 20% solution, into the outfall pipeline on shore to produce a dye concentration of about one part per million in the effluent at the point of discharge. Dye concentrations in the waste plume were measured with a Turner III Fluorometer aboard the survey boat. The fluorometer was equipped with a flow through sample cell and continuous readings were recorded with a chart recorder. The sample was drawn through the instrument with a pump on the discharge side of the fluorometer. By knowing the tracer injection rate and the effluent flow rate, the waste concentration was calculated from the measured tracer concentration. In order to eliminate the effect of temperature on the tracer fluorescence the instruments were standardized in the field.

While continuous sampling was underway, the fluorometer operator would mark each position, record position number, indicate any fluorometer scale change and any sampling depth change on the chart record. The boat's position was determined at one-minute intervals by triangulation. Simultaneous horizontal angles were measured from two shore stations with Wild T-2 Theodolites. The radio operator aboard the boat would signal the theodolite operators when the position was to be taken.

## Aerial Photography

One of the primary problems encountered in processing the 1968 vertical photography was the direct sunlight reflection from the water surface. Photography after 1968 was taken with an oblique camera mounting to avoid the sun spot. Prior to the 1969 field season, three cameras were purchased and mounted in the baggage compartment of a small high wing aircraft. This eliminated the need for advance scheduling of commercial aerial photography and allowed flexible planning of the changing weather and sea conditions. The camera package shown in figure 21 consisted of a K-17 mapping camera and two 70 mm cameras. Multiple cameras allowed the selection of optimum film, filter and exposure combinations for several photographic bands. The mapping camera, because of its large angular coverage, permitted photographic orientation of the two smaller cameras. Films from the two 70 mm cameras were used for detailed analyses and measurements of the waste field. Polarizing filters on the 70 mm cameras reduced the skylight reflection from the water surface.

The cameras were synchronized to take simultaneous pictures with a timing device consisting of a capacitor in parallel with a variable resistor. The cameras were lined up end to end without their magazines and the variable resistor was adjusted until a light could be seen through the cameras when the shutters were activated at 1/100 of a second.

When the aerial photography was taken with a single vertical mapping camera, normal color film was used. Both Ektachrome 8442 film and Anscochrome D200 film were tested. There was no significant difference in the results of the two films. When aerial photography was taken with the three camera unit, generally the K-17 was loaded with black and white film, type 2402, with a Wratten 25A filter, while one 70 mm

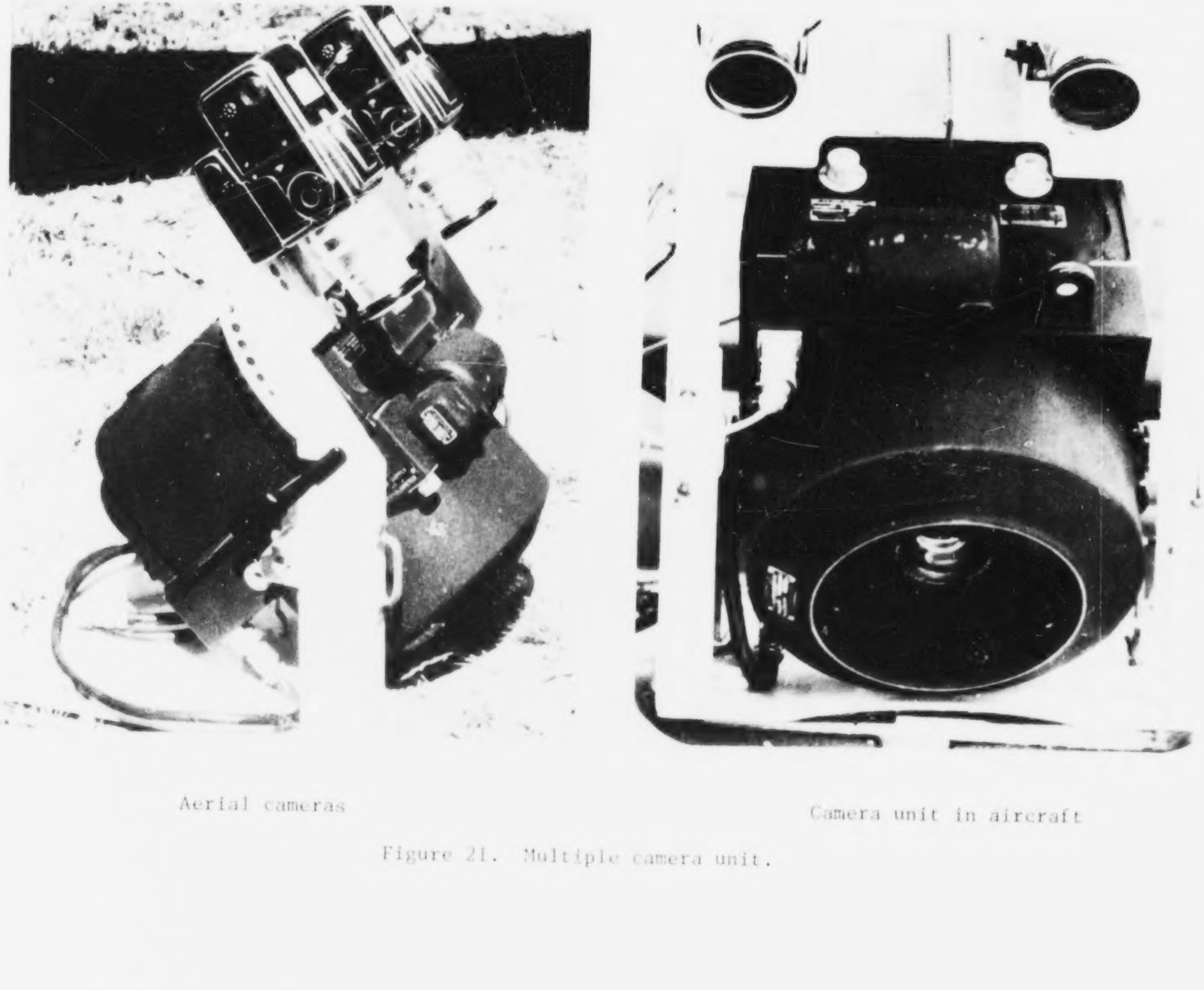

Aerial cameras

Camera unit in aircraft

Figure 21. Multiple camera unit.

Hasselblad camera was loaded with normal color film, type 2448, and the second Hasselblad camera was loaded with infrared black and white film, type 5424. Because of the variable light scattering and absorbing characteristics of the pulp mill effluent, a broad band photographic system was used.

The photographic film was developed by project personnel in accordance with the film manufacturer's directions. The aerial film from the mapping camera was 9-1/2 inches wide and 100 ft long, and was processed with a Morse B-5 rewind processor while the 70 mm film was processed with a Nikor reel and tank processor.

# SECTION VIII

## DYE PATCH STUDIES

During the 1969 field season, several dye drops were made from the aircraft. The three pictures shown in figure 22 were taken July 7, 1969 using panchromatic film type 8401 with a Wratten 25A filter. While this is not the best film-filter combination for observing the dye patch, the change in shape of the dye patch can be seen. The dye was dropped at 12:19 and the first photo was taken at 12:25 from 3000 ft at which time the size of the dye field was 160 ft by 40 ft. The photo in figure 22b was taken at 13:13 from 4000 ft. After 54 minutes from the time the dye was dropped, the dye patch had grown to approximately 70 ft wide and an overall curved length of 1000 ft. The light reflection in 22b could have been reduced with a polarizing filter. The photo in figure 22c was taken an hour and a half later at 14:43 from 5000 ft. The dye field at this time is 2100 ft long and 1300 ft wide.

The example given in figure 22 was an extreme example of elongation, curvature and striation of a dye patch. The wind was downward and to the right in the pictures at 5 to 12 knots with a swell height of 4 to 6 ft and a water current velocity of 0.4 ft/sec. Most dye patches observed have been elongated in a direction nearly parallel to that of the water flow. Striations and curvature of the dye patch are common. However, in most experiments the overall shape of the patch resembles an ellipse.

The elongation of the dye patch in the direction of flow suggests dispersion due to a vertical velocity gradient can, at times, be an important consideration. The upper layers of water are first influenced by a change in wind velocity or direction and vertical velocity gradients would be expected. Wind waves and swell both have specific orientation that suggest diffusion will occur at different rates in a horizontal plane.

The basic diffusion equation given as equation 56 is reduced to a two dimensional model.

$$\frac{\partial W}{\partial t} = D_y \frac{\partial^2 W}{\partial Y^2} + D_x \frac{\partial^2 W}{\partial X^2} + aW \tag{67}$$

A solution is

$$W(x, y, t) = W_{max} \exp - \left[ \frac{X^2}{2\sigma_x^2} + \frac{Y^2}{2\sigma_y^2} \right] \tag{68}$$

where the coordinate axis is assumed to move with the dye patch. In

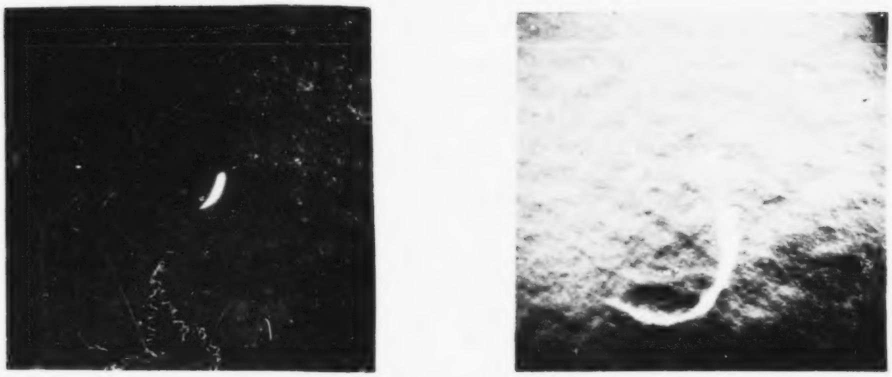

a
At 12:25 from 3000 ft

b
At 13:13 from 4000 ft

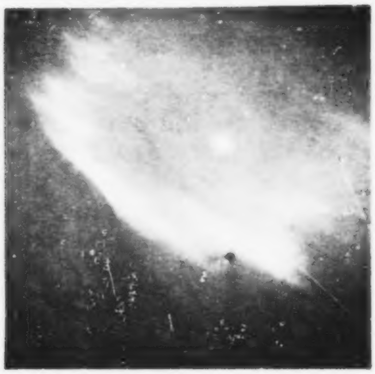

c
At 14:43 from 5000 ft

Figure 22. Dye patch on July 7, 1969.

the equation W represents the dye concentration, X and Y are the coordinates from the centroid of the dye patch parallel and transverse to the direction of flow, $D_x$ and $D_y$ are the longitudinal and lateral diffusion coefficients, "a" is a first order decay coefficient which includes the loss to the lower layers due to vertical diffusion and $\sigma_x^2$ and $\sigma_y^2$ represent the variances in the X and Y directions. The relationship between the change in variance and the diffusion coefficient is given by

$$D = \frac{1}{2} \frac{\Delta\sigma^2}{\Delta t} \tag{69}$$

The diffusion coefficient is equal to one half the change in variance ($\Delta\sigma^2$) divided by the time interval ($\Delta t$).

Dividing equation 68 by the maximum concentration at the centroid ($W_{max}$), taking the log of each side and multiplying by 2 the equation becomes

$$\frac{X^2}{\sigma_x^2} + \frac{Y^2}{\sigma_x^2} = 2 \ln \left[\frac{W_{max}}{W}\right] \tag{70}$$

by letting

$$a^2 = 2\sigma_x^2 \ln \left[\frac{W_{max}}{W}\right] \tag{71}$$

$$b^2 = 2\sigma_x^2 \ln \left[\frac{W_{max}}{W}\right] \tag{72}$$

equation 70 reduces to that of an ellipse

$$\frac{X^2}{a^2} + \frac{Y^2}{b^2} = 1 \tag{73}$$

where a and b are the major and minor semi axis of an ellipse fitted to a line of equal concentration about the dye patch. Since the edge of the dye patch is generally characterized by relatively steep concentration gradients, the visible boundary of the patch was assumed to have a concentration of W max/2. With this assumption equations 71 and 72 reduce to

$$\sigma_x^2 = 0.72 a_e^2 \tag{74}$$

$$\sigma_y^2 = 0.72\, b_e^2 \tag{75}$$

By using equation 69, 74 and 75 the diffusion coefficients are related to the change in size of the dye patch between photographic flights over the area. Since the dye patches seldom form a perfect ellipse, the major and minor semi axes of the edge of the patch ($a_e$ and $b_e$) can not be measured directly from the aerial photography. The procedures employed in determining diffusion coefficients from the aerial photography are given in Section IX on Data Processing.

## SECTION IX

## DATA PROCESSING

The general scheme for processing the boat and photographic data during both the 1968 and 1969 field seasons is shown in figure 23. Data processing included reduction of shore angles to state plane coordinates, conversion of fluorometer strip chart records to waste concentrations and reduction of photographic information. A comparison was made between the waste concentrations determined by boat sampling with those determined from aerial photography by matching ground coordinates.

During the 1970-71 field season only aerial photography required processing. Aerial film taken during this period was not digitized using the densitometer. The processing techniques were modified to achieve the research objective of the original proposal, which was to develop a remote sensing tool for the evaluation of dispersion of wastes from existing or proposed ocean outfalls. Since the 1968 and 1969 field seasons were concerned with existing outfall sites, the final year of the project was concerned with the development of simplified procedures for proposed outfall sites.

### 1968-1969 Boat Data

Angles from the shore stations to the photo control buoys and the boat were reduced to state plane coordinates. Boat positions were indexed by time for matching with waste concentration. Since theodolite sightings were made on the boat's mast, a correction was applied to determine the position of the fluorometer intake ports.

The fluorometer records were processed by 1) a least squares fit to the standardization data, 2) a shift of the index on the fluorometer reading to account for the time delay for the sample to pass from the intake port to the fluorometer, 3) reduction of the fluorometer reading to concentration of tracer and concentration of effluent, and 4) interpolating the ground coordinates from the processed shore control data.

Waste concentrations determined by boat sampling were displayed on a three dimensional plot. Figure 24 is a typical display of the boat sampling data where the grid represents the X and Y state plane coordinates and the Z axis represents the waste concentration in milliliters/liter. The waste concentration is represented by the length of a line drawn parallel to the z-axis. The state plane coordinate position of any sample point can be scaled from the grid to the base of the vertical line. The solid line on the plot is the boat's track. The plume in the plot extends upward and to the right.

The surface water temperature was also recorded along the boat's track and displayed on a three dimensional plot as shown in figure 25.

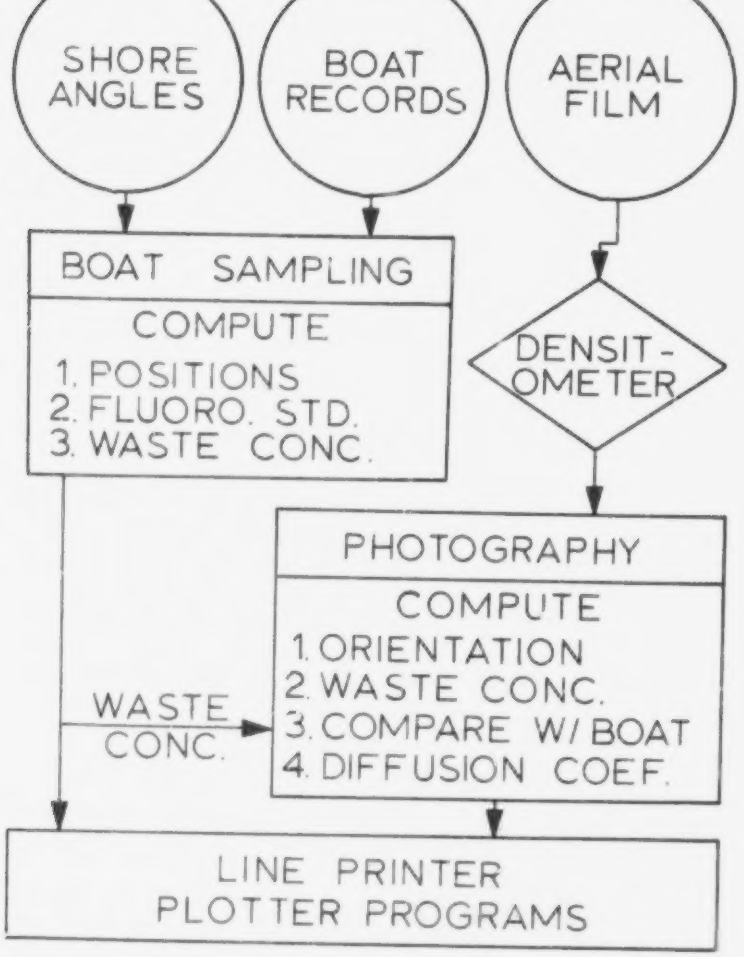

Figure 23. Data processing flow diagram.

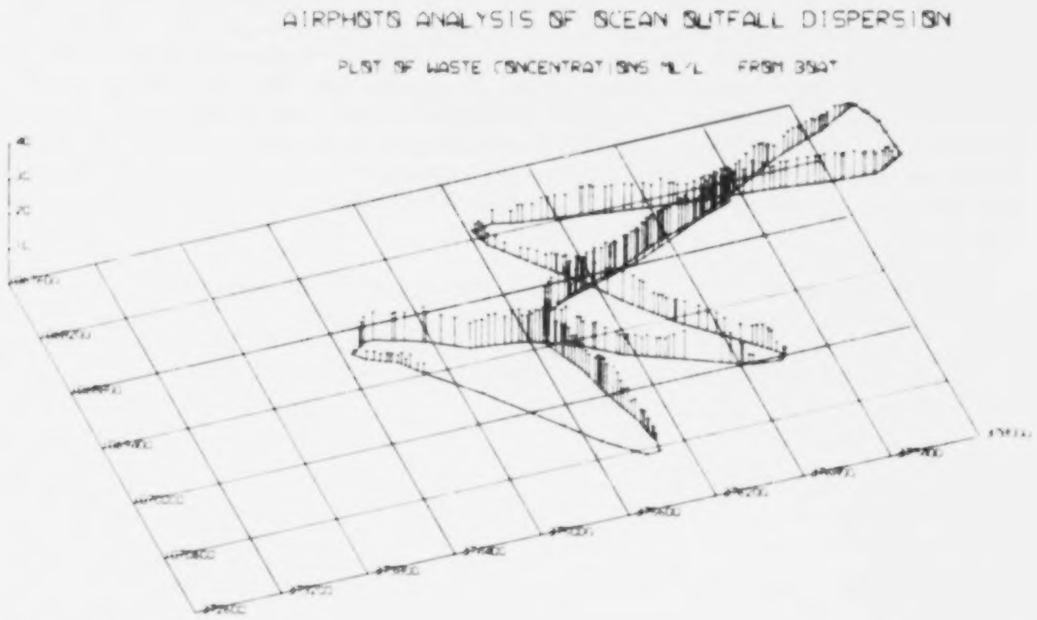

Figure 24. Waste concentrations from boat sampling on August 12, 1969.

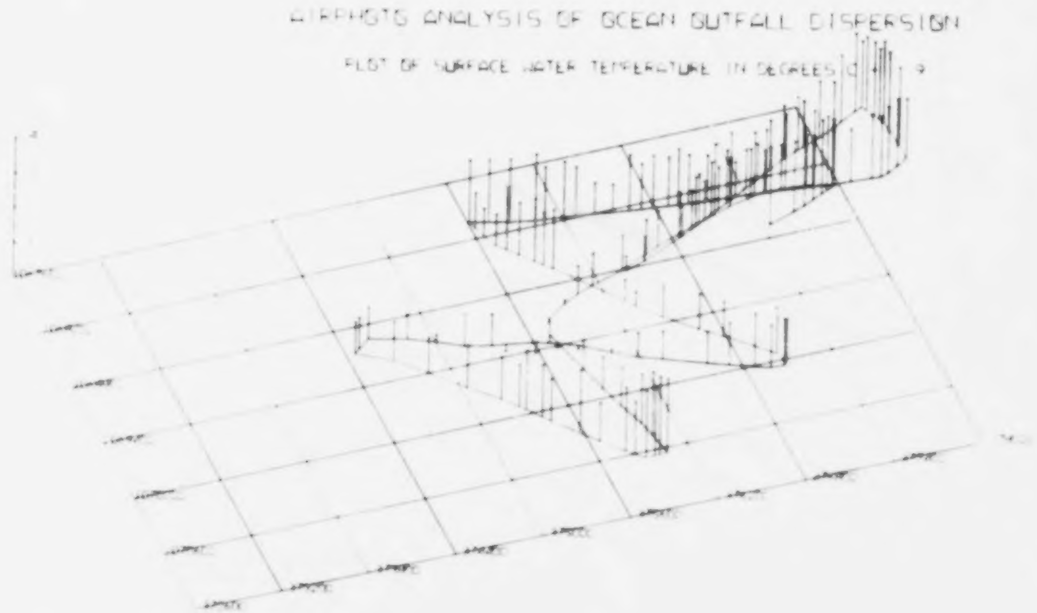

Figure 25. Surface water temperature on August 12, 1969.

In order to be able to show a smaller temperature variation, the values plotted in figure 25 were the surface temperatures minus nine degrees. The outfall in figures 24 and 25 is located near coordinates 1069400E, 375600N where the waste concentration is a maximum and the surface water temperature is a minimum. The temperature of the waste while in the pipeline is about 40°C. The waste discharged from the outfall ports mixes by jet diffusion with the colder subsurface water and the resulting mixture at the surface in this case was colder than the surrounding sea water.

A temperature profile taken over the outfall and one taken north of the waste field on August 12, 1969 are shown in figure 26. The temperature of the water near the bottom is 7.5°C while that near the surface over the outfall is 8.4°C and north of the waste field is 10°C.

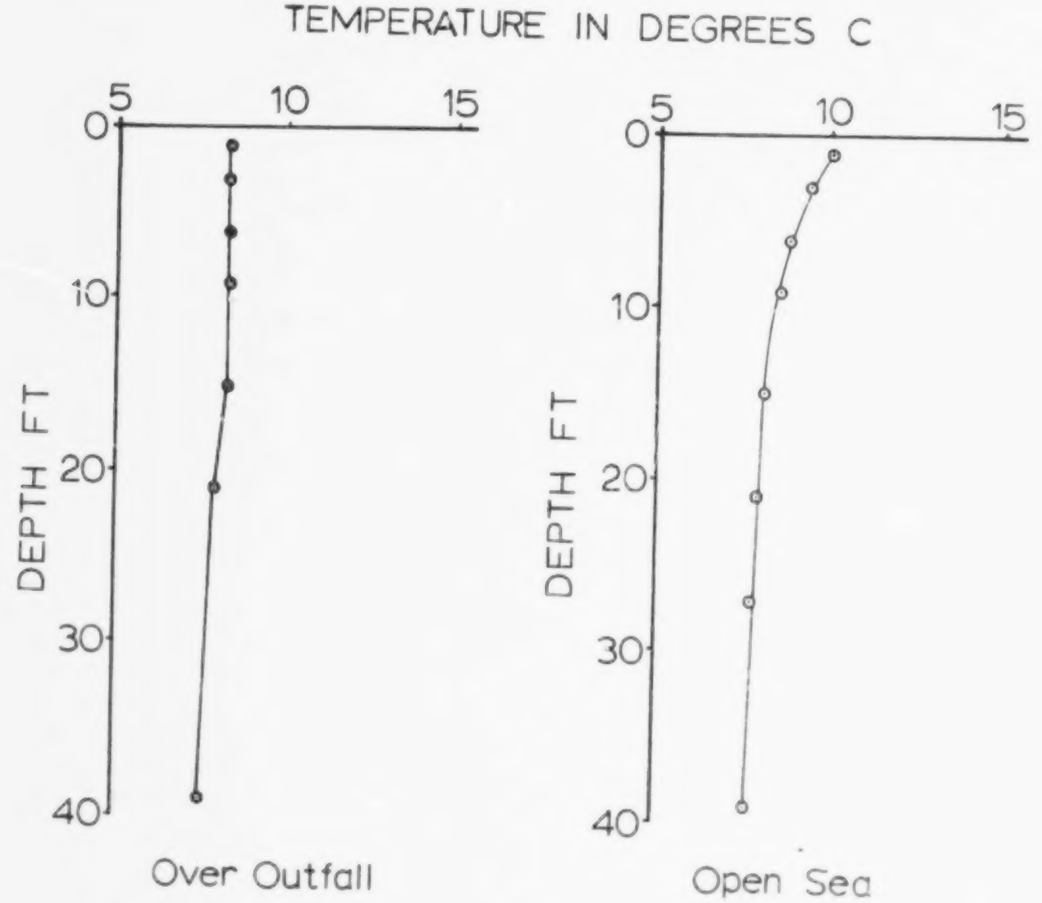

Figure 26. Water temperature profiles on August 12, 1969.

A detailed description including the computer program for processing the boat sampling data is given in Appendix C of the Water Pollution Control Research Series, 12040EBY on "Aerial Photographic Tracing of Pulp Mill Effluent in Marine Waters" by Burgess and James. Detailed description of the three dimensional plotting program was given in Appendix D of the "First Annual Progress Report" on this project (Burgess and James, 1969).

## 1968 Photographic Data

During the 1968 field season, color aerial photography was taken with a single vertical aerial mapping camera. The photographic film was converted to digital data with a McBeth model TD-102 photo densitometer. The densitometer can measure the density of the three layers of the color photo. Wratten filters numbers 92, 93, and 94 are utilized to measure the red, green and blue film densities, respectively. The aerial film holder was attached to an x - y coordinatograph which measured the photo coordinates to ± 0.001 inches. At the same time, the film densities were measured with a digital voltmeter. Both the voltmeter and coordinatograph were connected to a digitizer which in turn was connected to a card punch. One card was required for each point and contained the photo identification number, point number, x and y coordinates and the film densities for the three spectral bands of the color photo. The position of each data point was selected manually. The three film densities on each card were measured at the same point on the photograph.

A generalized flow diagram of the photographic data processing is shown in figure 27. The photographic analysis phase of the data processing began with the photographic orientation which was accomplished by a non-linear least square solution to the collinearity condition equations. After the last photograph has been oriented, the water currents are computed. The sun altitude and azimuth are computed for the first photograph of each flight.

The photographic variable that was the most sensitive to changes in waste concentration was the ratio of red to green light reflected from the waste field. This ratio, adjusted for atmospheric attenuation and for light scattered from the sea water, was related to the waste concentration by a least squares fit of the boat sampling data. The comparison was made by matching ground coordinates at 60-foot intervals along the boat's path. Utilizing this regression equation waste concentrations were computed throughout the waste field.

Film densities and photo coordinates were measured with the photo densitometer for points outside both the waste field and the area of direct sunlight reflections. The data from these points were used to determine the regression coefficients for the model

$$ATR = A_0 + A_1 (j_2) + A_2 (j_2)^2 + \varepsilon \qquad (76)$$

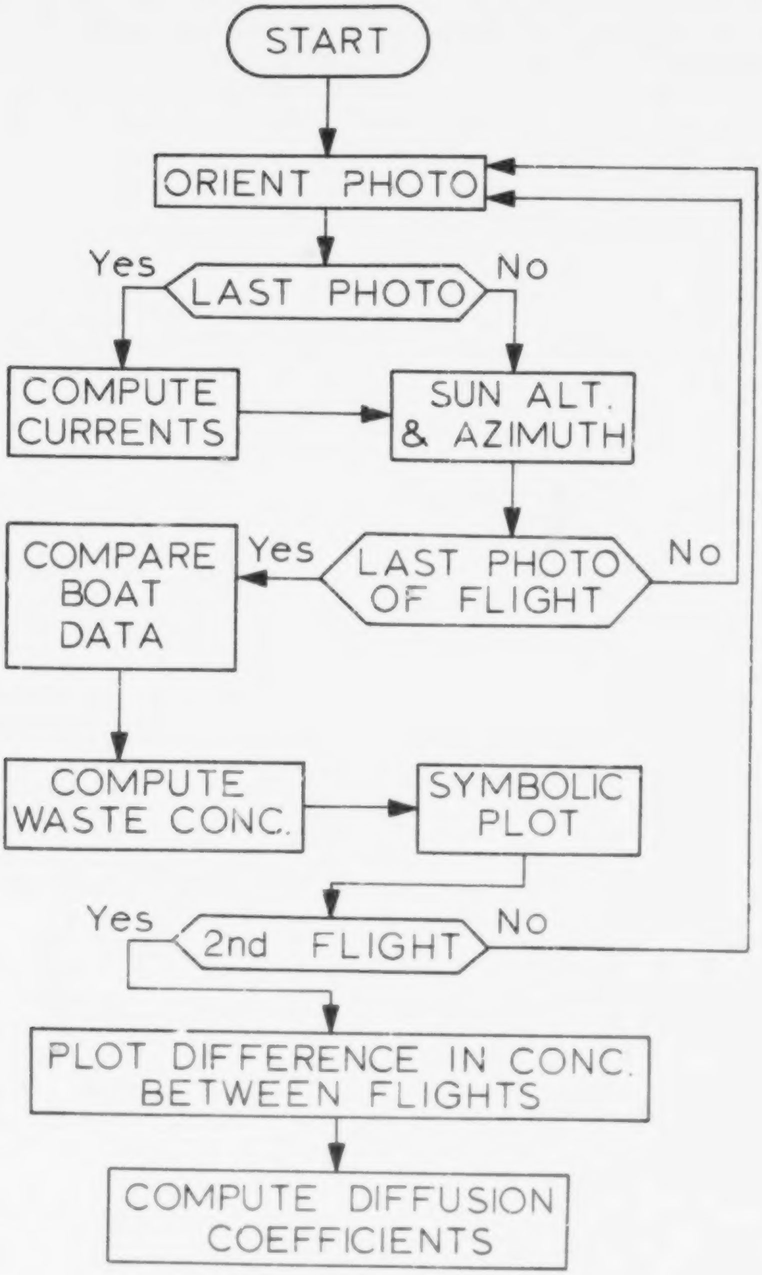

Figure 27. Flow diagram for photographic processing.

where $\varepsilon$ is the error term, $j_2$ is the angle between the ray to the camera and the vertical, and the A's are the regression coefficients. ATR is determined for each point from

$$ATR = \frac{(TIM)\ \cos^4(c)}{(FNO)^2\ \exp(D_b(x,y)/G)} \tag{77}$$

TIM is the photographic exposure time, c is the angle between the camera axis and the ray, FNO is the f-number setting on the camera, $D_b(x,y)$ is the blue film density as measured with the densitometer and G is the film gamma. The film gamma for the three spectral bands of the color photo was determined from sensometric curves made by Kodak and GAF for the film used on the project. The gamma to the base 10 was taken as -3.0 for the Ektachrome 8442 film and -2.4 for the anscochrome D200 film.

In the expression for the ratio ($R_{pho}$), the values of the coefficients were determined from the following method in place of that given by equation 39

$$R_{pho} = B_0 + B_1\ (SUNR) + B_2\ (N_b) + \varepsilon \tag{78}$$

The regression coefficients were determined by a least squares fit of data from selected points outside the waste field. $N_b$ is the radiance in the blue band as determined from

$$N_b = \frac{ATR\ (FNO)^2\ \exp(D_b(x,y)/G)}{(TIM)\ \cos^4\ (c)} \tag{79}$$

SUNR is the angle between the ray to the camera and the reflected direct sunlight. For the model 78 the value of $R_{pho}$ was determined from

$$R_{pho} = \exp[(D_r(x,y)-D_g(x,y))/G + (E_r-E_g)\sec(j_2) + (A_r-A_g)\sec(i)\ ] \tag{80}$$

where D(x,y) is the film density, E is the atmospheric attenuation from the sea surface to the camera, $j_2$ is the angle between the ray to the camera and the vertical axis, A is the atmospheric attenuation for a standard atmosphere and i is the angle of incidence for the direct sunlight. The subscripts r and g refer to the red and green bands, respectively. Atmospheric attenuation coefficients were determined from the Handbook of Geophysics and Space Environments for a standard atmosphere. The following coefficients and equations were used

$$A_r = 0.252$$

$$A_g = 0.331$$

$$E_r - E_g = 0.024 \ln (H + 1) \qquad (81)$$

where H is the camera station altitude in kilometers. After the coefficients in model 78 were computed, the ratio anomaly (RA) for any point on the photograph, excluding kelp and shallow nearshore areas, was determined from

$$RA = R_{ph} - R_{pho} \qquad (82)$$

where $R_{pho}$ was estimated from the regression equation

$$R_{pho} = \hat{B}_0 + \hat{B}_1 \text{ (SUNR)} + \hat{B}_2(N_b) \qquad (83)$$

and $R_{ph}$ was determined from

$$R_{ph} = \exp[ (D_r(x,y)-D_g(x,y))/G + (E_r-E_g)\sec(\theta_2)$$

$$+ (A_r-A_g)\sec(i) ] \qquad (84)$$

The ratio anomaly (RA) was computed for each data point on the aerial photo. The values were stored in a 120 by 60 array. The index on the array indicated the ground coordinates for each element of the array. Each element represented a 60-foot square area on the sea. After all the film density measurements were converted to RA values and stored in the array, missing values were interpolated from adjacent points.

Concentrations determined from the fluorometers aboard the boat were read into the computer program. Boat concentrations were interpolated at 60-foot intervals along the fluorometer track line. These values were matched by ground coordinates with the RA values in the array. A least square regression analysis was made on the data with the model

$$W = C_1(RA) + C_2(RA)^2 + \varepsilon \qquad (85)$$

where W is the waste concentration in milliliters per liter and $C_1$ and $C_2$ are regression coefficients.

The array was oriented so that the x-axis was along the center line of plume. Values of the waste concentration were computed from the above equation and stored in the array in place of the RA values. Waste concentrations were displayed as a symbolic plot on the line printer. In figure 28 are two plots from photographs taken August 16. The symbols on the plot represent different ranges in concentration and were selected so that the density of the plot increases with the concentration. The movement or change in shape of the waste field can be seen during the 22-minute period between the flights. The area of the waste field within each concentration range is determined by continuing the number of times each symbol is used to make the symbolic

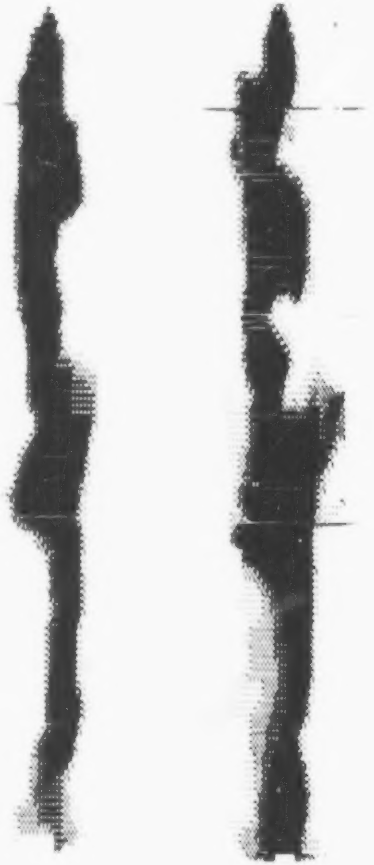

Figure 28. Symbolic plots from two flights August 16, 1968.

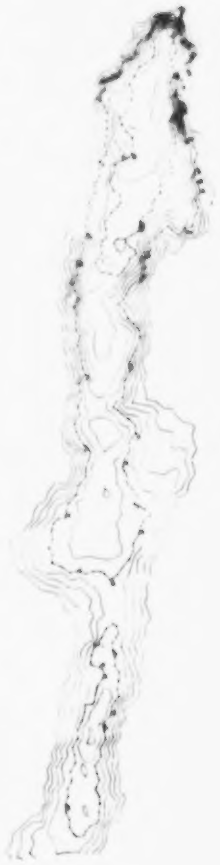

Figure 29. Isoconcentration plot, flight on August 16, 1968.

plot.

The most visually useful form of displaying the photographic waste concentrations is the isoconcentration plot. This plot is similar to a topographic map with the elevation being replaced with the concentration. Figure 29 is a computer printout by this technique of the concentrations shown in the left plot of figure 28. The outfall is located at the top of the plot and the plume extends downward. The plume is 500 to 1000 ft wide and about 7000 ft long.

Steady state diffusion coefficients were determined for a steady state model with unidirectional transport velocity in the X direction. By neglecting the loss to the lower layers and assuming the diffusion in the Y direction was not a function of Y, the basic diffusion equation becomes

$$V_x \frac{\partial W}{\partial X} = D_y \frac{\partial^2 W}{\partial Y^2} \qquad (86)$$

where X is the distance along the centerline of the plume, Y is the distance right or left of the plume center line, $V_x$ is the velocity along the plume center line, W is the waste concentration, and $D_y$ is the diffusion coefficient. A solution to equation is

$$W = \frac{K}{2(\pi D_y t)^{1/2}} \exp\left[-Y^2/rtD_y\right] \qquad (87)$$

For computational purposes this equation can be reduced to

$$W = W_0 \exp\left[-Y^2/2\sigma_y^2\right] \qquad (88)$$

where $W_0$ is the concentration at the center line of the plume and $\sigma^2_y$ is variance of normal curve. The diffusion coefficient is equal to one half the change in variance divided by the time interval or

$$D_y = \frac{1}{2} \frac{\Delta\sigma^2}{\Delta t} \qquad (89)$$

In the computer program, the variance was computed every 300 feet along the center line of the plume. The change in time for this steady state model was equal to the distance between sections in feet divided by the velocity in feet per second. The velocity was determined photogrammetrically from the current floats or dye patches.

The variance ($\sigma^2$) can be estimated for a normal distribution from the sample variance ($S^2_y$). The concentration (W) is equivalent to the frequency of occurrence in the computations. The sample variance is

$$S^2_y = \frac{\Sigma\, W(Y-\bar{Y})^2}{N} \qquad (90)$$

where $\bar{Y}$ is the mean distance from the origin and

$$N = \sum_{i=1}^{n} W_i \qquad (91)$$

In computational form, equation 90 is

$$S_y^2 = \frac{1}{N} \left[ \sum_{i=1}^{n} W_i Y_i^2 - \frac{\left( \sum_{i=1}^{n} W_i Y_i \right)^2}{N} \right] \qquad (92)$$

From equation 92 an estimate of the variance can be made for any section across the plume. Equation 89 was used to determine the diffusion coefficient.

Nonsteady-state diffusion coefficients were determined from two flights over the area using equation 89. In this equation for the non-steady state

$$\Delta\sigma_i^2 = \sigma_{1,i}^2 - \sigma_{2,\ i+c}^2 \qquad (93)$$

where the subscripts 1 and 2 refer to the flight numbers, i refers to the section number across the plume in flight one and i+c is the section number in flight two adjusted for the movement of the waste field between flights. In solving equation 89 for the nonsteady-state case, $\Delta t$ is the time difference between the flights.

The preliminary diffusion coefficients based on the steady state model are shown in table 1. The coefficients are determined from the change in variance along each flight at 300 ft intervals. Assuming a uniform concentration with depth, a vertical thickness of the waste field can be estimated. The columns listed in table 1 are 1) section number where each section represents 60 ft along the axis of the plume, 2) width of the waste field, 3) the estimated average depth of the waste field, 4) the estimate of the standard deviation of Y, 5) the maximum centerline concentration for a normal distribution, 6) and 7) the ground X and Y coordinates of the centerline of the plume, 8) the diffusion coefficient between each fifth section of the plume, and 9) the average diffusion coefficient from the head of the plume. Also shown in the tables are the flow rate, current velocity, sun azimuth from the south, sun altitude, and area within each concentration range.

Nonsteady-state diffusion coefficients are shown in table 2. The coefficients were determined from the change in variance between two photographic flights over the outfall area. Convection of the field was considered in making the comparison.

A detailed description of the computer program used to process the vertical color photography is given in Appendix B.

Table 1. Preliminary diffusion coefficients, flight 1, August 16, 1968.

| Section | Width Ft | Eff. Depth Ft | Sigma Y Ft | Coefficient PPT | State Plane Coordinates X | State Plane Coordinates Y | Diffusion Coefficient $Ft^2/sec$ Fifth Sec. | Diffusion Coefficient $Ft^2/sec$ Average |
|---|---|---|---|---|---|---|---|---|
| 13 | 660 | 3.0 | 1.541E 02 | 3.491E 01 | 1069872 | 376281 | 7.922E 00 | 7.992E 00 |
| 18 | 780 | 2.4 | 1.811E 02 | 3.695E 01 | 1070009 | 376549 | 6.352E 00 | 7.137E 00 |
| 23 | 1020 | 2.1 | 2.156E 02 | 3.515E 01 | 1070033 | 376863 | 9.565E 00 | 7.946E 00 |
| 28 | 1080 | 1.9 | 2.419E 02 | 3.458E 01 | 1070128 | 377148 | 8.441E 00 | 8.070E 00 |
| 33 | 1320 | 2.1 | 2.473E 02 | 3.007E 01 | 1070284 | 377409 | 1.827E 00 | 6.821E 00 |
| 38 | 840 | 2.9 | 1.685E 02 | 3.249E 01 | 1070516 | 377639 | -2.292E 01 | 1.864E 00 |
| 43 | 840 | 3.7 | 1.602E 02 | 2.700E 01 | 1070662 | 377903 | -1.900E 00 | 1.327E 00 |
| 48 | 840 | 3.5 | 1.696E 02 | 2.664E 01 | 1070703 | 378210 | 2.158E 00 | 1.431E 00 |
| 53 | 720 | 4.5 | 1.429E 02 | 2.459E 01 | 1070778 | 378503 | -5.838E 00 | 6.230E-01 |
| 58 | 1200 | 4.0 | 2.338E 02 | 1.718E 01 | 1070783 | 378825 | 2.398E 01 | 2.959E 00 |
| 63 | 1140 | 3.5 | 2.604E 02 | 1.772E 01 | 1070808 | 379138 | 9.181E 00 | 3.524E 00 |
| 68 | 1020 | 3.4 | 2.394E 02 | 1.957E 01 | 1070886 | 379430 | -7.349E 00 | 2.618E 00 |
| 73 | 1200 | 2.8 | 2.645E 02 | 2.142E 01 | 1071094 | 379670 | 8.883E 00 | 3.100E 00 |
| 78 | 1260 | 3.0 | 2.657E 02 | 1.979E 01 | 1071285 | 379916 | 4.818E-01 | 2.910E 00 |
| 83 | 960 | 5.7 | 2.194E 02 | 1.275E 01 | 1071227 | 380263 | -1.573E 01 | 1.667E 00 |
| 88 | 660 | 7.3 | 1.314E 02 | 1.655E 01 | 1071232 | 380584 | -2.159E 01 | 2.134E-01 |
| 93 | 720 | 6.6 | 1.389E 02 | 1.738E 01 | 1071337 | 380865 | 1.410E 00 | 2.838E-01 |
| 98 | 600 | 6.7 | 1.220E 02 | 1.960E 01 | 1071489 | 381127 | -3.086E 00 | 9.654E-02 |
| 103 | 600 | 6.6 | 1.235E 02 | 1.955E 01 | 1071614 | 381400 | 2.587E-01 | 1.051E-01 |
| 108 | 780 | 5.8 | 1.453E 02 | 1.892E 01 | 1071700 | 381689 | 4.105E 00 | 3.051E-01 |
| 113 | 780 | 6.1 | 1.662E 02 | 1.582E 01 | 1071876 | 381942 | 4.554E 00 | 5.074E-01 |

Flow Rate 16.8 CFS
Sun Az. from S. 1.013 Rad.
Current Velocity .42 FPS
Sun Altitude .790 Rad.

Area Within Each Concentration Range

| Range ml/l | Area Sq Ft |
|---|---|
| 0- 2 | 5.580E 05 |
| 2- 4 | 3.924E 04 |
| 4- 6 | 3.672E 05 |
| 6-10 | 9.468E 05 |
| 10-15 | 1.199E 06 |
| 15-20 | 1.188E 06 |
| 20-25 | 5.400E 05 |
| GT25 | 6.948E 05 |

Table 2. Nonsteady-state diffusion coefficients, August 16, 1968.

| Section No. | Width Feet | Diffusion Coefficients $Ft^2/sec$ |
|---|---|---|
| 13 | 660 | 10.1 |
| 18 | 780 | 4.8 |
| 23 | 1020 | 2.5 |
| 28 | 1080 | 1.9 |
| 33 | 1320 | 1.2 |
| 38 | 840 | 13.5 |
| 43 | 840 | 7.5 |
| 48 | 840 | 0.2 |
| 53 | 720 | 13.6 |
| 58 | 1200 | 38.0 |
| 63 | 1140 | 24.9 |
| 68 | 1020 | 12.6 |
| 73 | 1200 | 9.0 |
| 78 | 1260 | 8.9 |
| 83 | 960 | 9.0 |
| 88 | 660 | 10.3 |
| 93 | 720 | 11.6 |
| 98 | 600 | 16.6 |
| 103 | 600 | 13.2 |
| 108 | 780 | 7.6 |

## 1969 Photographic Data

During the 1969 field season, the aerial photography was taken with two 70 mm Hasselblad cameras and a K-17 mapping camera. The large photos from the mapping camera were used for photographic orientation of the smaller cameras. Detailed analysis of the waste field was accomplished from the 70 mm photos.

The aerial film was digitized in the photogrammetry laboratory as shown in figure 30. The densitometer is located on the Kelsh plotter table. The film density is measured as voltage output from the densitometer with a digital voltmeter. The BCD digital voltmeter logic is transmitted through a logic converter to the Autotrol digital recorder. Output from the digitizer is recorded on computer cards by a card punch.

The densitometer and scanning table shown in figure 31 is processing a 70 mm picture. About all that can be seen of the densitometer is the white meter near the center of the figure. The scanning table is designed to handle film up to 9 1/2 inches wide and 250 feet long.

The film is loaded on the reel on the left of the scanning table and the take up reel is on the right. The arm that extends from the meter on the densitometer out over the scanning table contains the filters and the photomultiplier tube. A light source is located below the film. The amount of light that is transmitted through the film is measured by the photomultiplier tube and converted to D. C. voltage.

When digitizing aerial film, the scanning table continuously moves back and forth. The scan limits are marked on the photograph with a black tape or the dark border around the picture. The densitometer senses the end of the scan when its voltage output exceeds 750 volts. At the end of the scan, the scanning table stops and the film is advanced one scan by the take up reel on the table. The direction of the scan is reversed and the scanning table moves in the opposite direction.

The Y axis of the coordinatograph is attached to the scanning table. While scanning, the film density and Y photo coordinates are recorded at a selected interval along the scan. The X coordinate is computed from the scan number.

The operator shown in figure 29 is able to accomplish three processing steps at one time. While the densitometer is digitizing one photo, the operator is usually scanning the line printer listing of a previous photograph searching for illegal characters. At the same time, he can operate the teletype which preliminarily processes the data from another photograph with the computer using program EDIT. This program reduces the voltage output from the densitometer to film densities, rejects extreme values of densities, interpolates photo coordinates and displays the difference in film densities between adjacent bands on the line printer. Output from this program is stored on magnetic tape waiting final processing using program REMOTE. The basic details of this program are essentially the same as those for a single color photograph except that up to ten photographic bands or channels can be processed at one time. Program listings of EDIT and REMOTE are given in Appendix C.

## 1970-71 Photographic Data

Field procedures and processing techniques were revised to include estimating diffusion coefficients from dye patch studies. Field work was conducted during the fall, winter, and spring. Boat sampling was not attempted due to rough sea conditions which generally prevail during this period. More specifically, the aims of this phase of the investigation were to develop a remote sensing tool for the evaluation of waste dispersion from proposed ocean outfalls and to develop a set of characteristic airphoto pattern elements for estimating diffusion coefficients.

Aerial film taken during this period was not digitized with the densitometer but photo coordinates were measured with the x-y coordintograph about both the waste field and dye patch. The area of the waste field

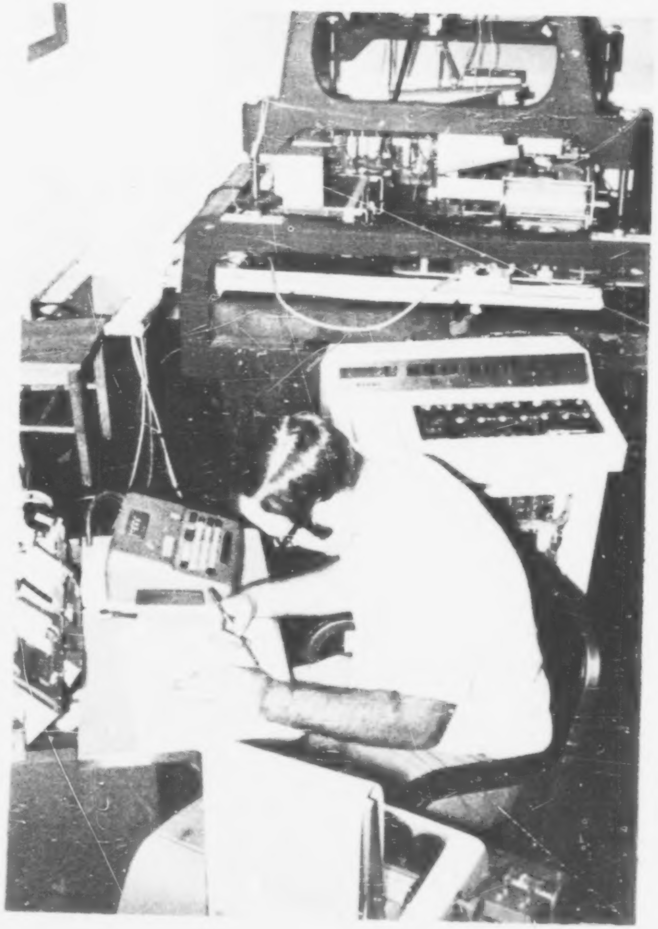

Figure 30. Digitizing aerial film.

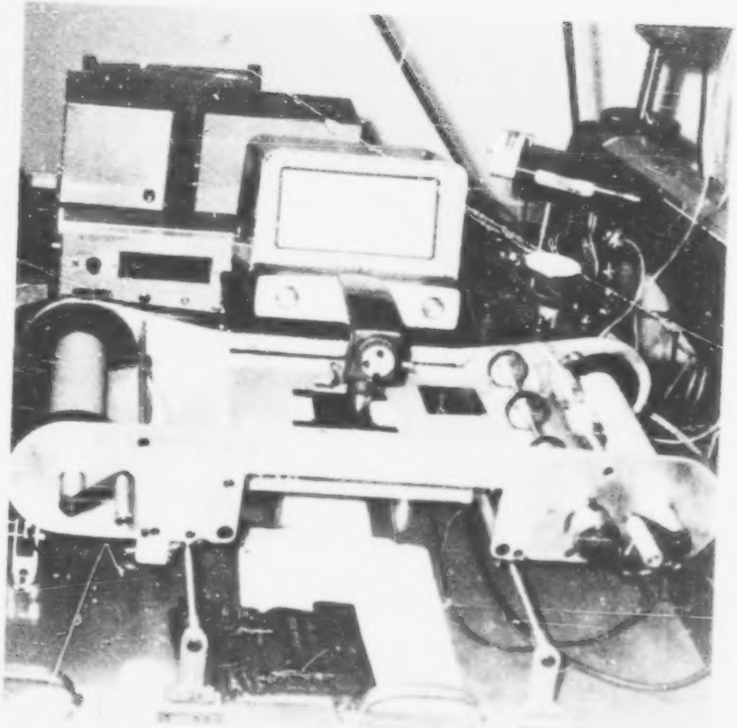

Figure 31. Scanning densitometer.

was computed from the photo coordinates about the plume. In addition, the water current velocity and direction and diffusion coefficients were determined from the dye patch photo coordinates.

The outline of the dye patch was digitized with the x and y coordinatograph along with sufficient ground control for photographic orientation. Photo coordinates about the dye patch were converted to state plane coordinates of the centroid and moments of inertia were computed from the following equations.

$$A = \frac{1}{2} \sum_{i=1}^{n} X_i (Y_{i-1} - Y_{i+1}) \qquad (94)$$

$$\bar{X} = \frac{\sum \bar{X}_i \Delta A_i}{A} \qquad (95)$$

$$\bar{Y} = \frac{\sum \bar{Y}_i \Delta A_i}{A} \qquad (96)$$

$$I_x = \sum X_i^2 \Delta A_i \qquad (97)$$

$$I_y = \sum Y_i^2 \Delta A_i \qquad (98)$$

$$I_{xy} = \sum X_i Y_i \Delta A_i \qquad (99)$$

Care must be taken when programming these equations to avoid roundoff error as state plane coordinates are typically six to seven digit numbers.

The rotation angle ($\alpha$) of the axis to obtain the principal axis is given by

$$\mathrm{Tan}\ (2\alpha) = \frac{2I_{xy}}{I_x - I_y} \qquad (100)$$

The maximum and minimum moments of inertia about the principal axis are computed from

$$I_{max} = \frac{I_x - I_y}{2} + \left[ \left( \frac{I_x - I_y}{2} \right) + I_{xy}^2 \right]^{1/2} \qquad (101)$$

$$I_{min} = \frac{I_x - I_y}{2} - \left[ \left( \frac{I_x - I_y}{2} \right) + I_{xy}^2 \right]^{1/2} \qquad (102)$$

The irregular shaped dye patch is replaced with an ellipse that has the same horizontal area. In addition, the ratio of $I_{max}$ to $I_{min}$ are the same for the ellipse as for the dye patch. The principal moments of inertia for an ellipse are given by

$$I_{max} = \frac{\pi b_e a_e^3}{4} \tag{103}$$

$$I_{min} = \frac{\pi a_e b_e^3}{4} \tag{104}$$

where $a_e$ and $b_e$ are the major and minor semi axes of an equivalent ellipse. If the ratio (IR) of $I_{max}$ to $I_{min}$ remain the same for both the dye patch and the ellipse, the ratio of variances are also the same (equations 74 and 75).

$$IR = \frac{I_{max}}{I_{min}} = \frac{a_e^2}{b_e^2} = \frac{\sigma_x^2}{\sigma_y^2} \tag{105}$$

After computing the area (A) and the ratio of principal moments of inertia (IR) for the dye patch, the semi axes of the equivalent ellipse are determined from

$$a_e^2 = \frac{A}{\pi} (IR)^{-1/2} \tag{106}$$

$$b_e^2 = \frac{A}{\pi} (IR)^{1/2} \tag{107}$$

Equations 74 and 75 are utilized in determining the variances. Diffusion coefficients are determined from the change in variance between two photographic flights as given by equation 69.

Details of the computer program used for this phase of the study are given in Appendix D. In addition to the dye patch analysis, the program prepares the input coordinates for a plotting program. The outline of the waste field, current velocity vector, along with a state plane coordinate grid and displayed on a CRT plotter and a polaroid picture is taken of the face of the tube for a record of the results.

## SECTION X

## SAMPLING RESULTS

### 1968-1969 Data

Detailed descriptions of the 1968-1969 boat sampling and aerial photography acquisition and processing were given by Burgess and James (August 1970). A summary of the results is given in table 3. Field work was conducted in late June, July, August and early September. Fourteen sampling runs were made during this period. For eight of the fourteen sampling runs, the waste field from the ocean outfall was at the sea surface. A submerged plume occurred during the remaining six sampling runs.

When the plume was submerged, both the swell height and the wind velocity were significantly less at a 90 percent confidence level than when the plume formed at the surface. On July 7 and 8, 1969, the sea and weather conditions were very nearly the same, yet on July 7, the plume submerged and on July 8 the plume was at the surface.

On both days the wind was from the north and a foam streak extended southward from the outfall for approximately 1.3 miles. The infrared black and white photo in figure 32 shows the foam streak on July 7, 1969. The photo was taken in a northwest direction with the shore in the foreground and the foam extending southward from the outfall.

The aerial photograph of the plume on July 8, 1969 in figure 33 was taken from 4000 ft with the camera tilted 45 degrees from vertical toward the east. The shore is off the upper edge of the photo and the foam streak extends south from the outfall. The direction from the outfall that the foam travels is not necessarily the same as that of the waste plume and in this case the plume is to the right of the foam.

Temperature profiles taken upstream of the outfall for July 7 and 8 are shown in figure 34. On the first day when the plume was submerged, the temperature profile did not show a definite thermocline but the temperature decreased with depth at a decreasing rate. On the second day a thermocline existed at about four feet below the surface. The wind on the 7th increased from 5 mph at 8:00 to 12 mph at 20:00. On July 8th the wind was stronger and increased from 6 mph at 8:00 to 15 mph at 15:00.

Both steady state and nonsteady state diffusion coefficients were computed when possible for each sampling run. Of the eight days that a surface plume occurred, a one dimensional diffusion model was applicable to the plume pattern on only three days. A two dimensional model was necessary to describe the plume when the current velocity was low. When the velocity was greater than 0.4 ft/sec, a one dimensional diffusion model was adequate.

**Preceding page blank**

Table 3. 1968-1969 sampling summary for Newport.

| Date | Tide[a] | Wave | Wind | | Effluent | PLUME | | | | | Remarks |
|---|---|---|---|---|---|---|---|---|---|---|---|
| | Range Ft. | Height Ft. | Dir. | Velocity mph | Flow Rate gpm | Area[b] Acres | Length Ft. | Max. Concen. ml/L | Current Vel. ft/sec | Dif. Coef. $ft^2/sec$ | |
| 8-8-68 | 10.2 | 4 | NE | 10-20 | 5,550 | 100 | 4600 | 15 | 0.26 | c | |
| 8-10-68 | ------ | ------ | ------ | ------ | ------ | ------ | ------ | ------ | ------ | ------ | Foggy |
| 8-14-68 | 6.0 | 4-6 | SW | 5-10 | 7,600 | ------ | 3400 | 21 | ------ | c | No photography |
| 8-15-68 | ------ | ------ | ------ | ------ | ------ | ------ | ------ | ------ | ------ | ------ | Foggy |
| 8-16-68 | 6.3 | 6-8 | SW | 10-15 | 7,550 | 142 | 7000 | 23 | 0.42 | 11. | |
| 8-21-68 | 8.1 | 8-10 | SW | 0-5 | 7,400 | ------ | 7500 | 20 | ------ | c | |
| 8-22-68 | ------ | ------ | ------ | ------ | ------ | ------ | ------ | ------ | ------ | ------ | Raining |
| 9-10-68 | 6.8 | 1-2 | ------ | 0 | 7,450 | 0 | ------ | ------ | 0.0 | ------ | Plume submerged |
| 9-11-68 | 6.8 | 1-2 | E | 0-5 | 8,950 | 0 | ------ | ------ | ------ | ------ | Plume submerged |
| 9-12-68[e] | 6.5 | 1-2 | E | 0-5 | 6,750 | 0 | ------ | ------ | 0.0 | ------ | Plume submerged |
| 9-12-68[f] | 6.5 | 4-6 | NW | 15-20 | 6,750 | ------ | 3000 | 10 | ------ | ------ | d |
| 6-30-69 | 11.5 | 1-2 | N | 5-10 | 8,100 | 0 | ------ | ------ | ------ | ------ | Plume submerged |
| 7-1-69 | 11.3 | 2-4 | NW | 4-5 | 8,100 | 0 | ------ | ------ | 0.06 | ------ | Plume submerged |
| 7-7-69 | 6.4 | 4-6 | N | 5-12 | 9,000 | 5 | ------ | ------ | 0.4 | ------ | Plume submerged |
| 7-8-69 | 7.7 | 4-6 | N | 6-15 | 9,000 | 93 | 5500 | 10 | 0.5 | 14. | |
| 7-21-69 | ------ | ------ | ------ | ------ | ------ | ------ | ------ | ------ | ------ | ------ | Foggy |
| 7-22-69 | ------ | ------ | ------ | ------ | ------ | ------ | ------ | ------ | ------ | ------ | Foggy |
| 8-12-69 | 8.4 | 2-3 | W | 3-5 | 8,300 | 127 | 4000 | 10 | 0.1 | c | |
| 8-13-69 | ------ | ------ | ------ | ------ | ------ | ------ | ------ | ------ | ------ | ------ | Foggy |
| 9-8-69 | 7.2 | 4 | SW | 5 | 8,400 | 39 | 2000 | 10 | 0.2 | c | |
| 9-9-69 | ------ | ------ | ------ | ------ | ------ | ------ | ------ | ------ | ------ | ------ | Foggy |

[a] Maximum difference between adjacent high and low tides during the day.

[b] Area within the plume with concentrations greater than 2 ml/L.

[c] One dimension model was not applicable.

[d] Vertical photography not processed because of sunlight reflection.

[e] a.m.

[f] p.m.

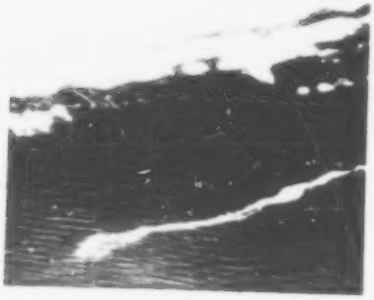

Figure 32. Infrared black and white photo on July 7, 1969.

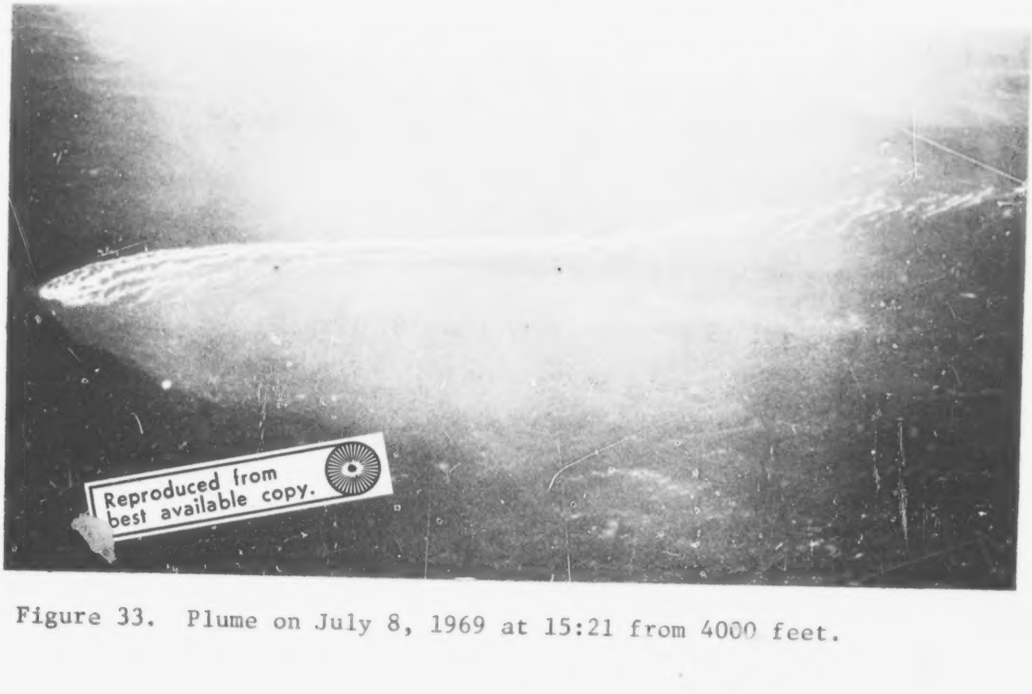

Reproduced from best available copy.

Figure 33. Plume on July 8, 1969 at 15:21 from 4000 feet.

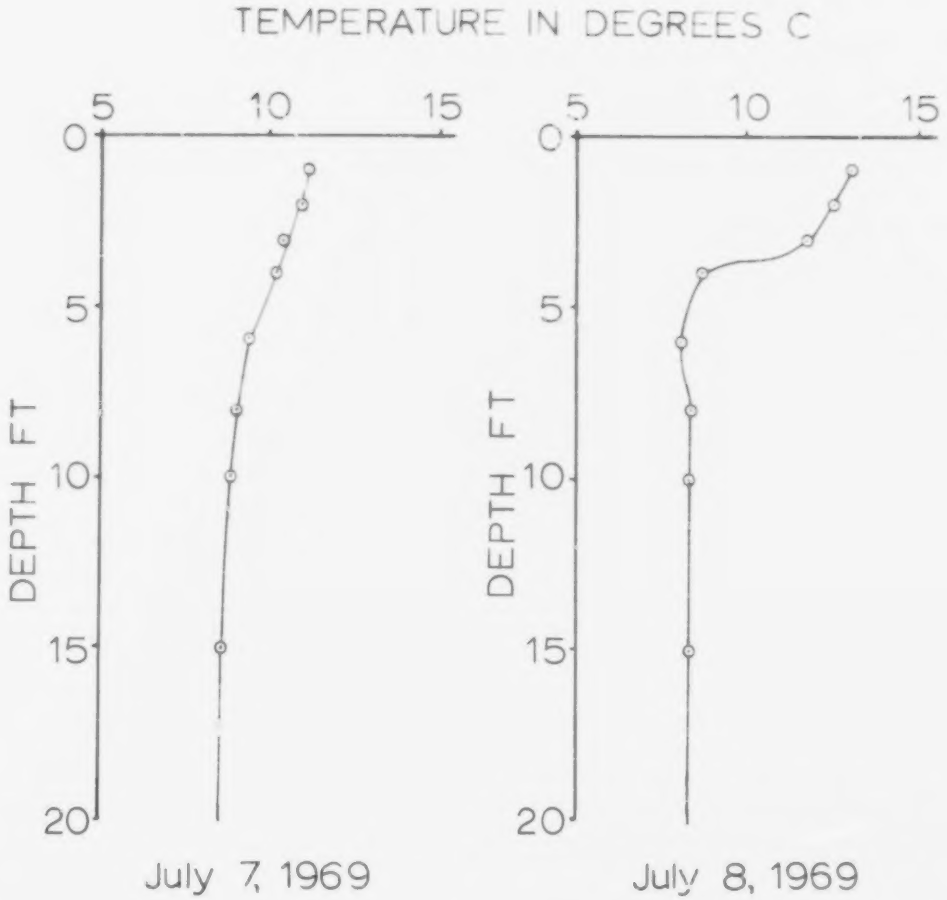

Figure 34. Temperature profiles July 7 and 8, 1969.

On August 16, 1968, the current velocity was 0.42 ft/sec and the waste field was long and narrow as the plume was generally about 600 ft wide; however, there were several locations along the plume that were up to 1200 ft wide. As a result of the nonuniform shape along the axis of the plume, the application of the steady state model to the data resulted in nearly half of the diffusion coefficients being negative. Diffusion coefficients determined from the change in concentrations between flights resulted in all positive values and the average nonsteady diffusion coefficient is listed in table 3 for August 16, 1968.

On July 8, 1969, the current velocity was 0.5 ft/sec and the steady state diffusion coefficient was listed. The nonsteady state model was not applicable. After the first flight, the width of the plume decreased due to horizontal density stratification. In figure 35 dark upwelled water can be seen below the plume. Measurements with the temperature probe indicated that this water was approximately two degrees C warmer than the inshore water. The upwelled water appears to have moved over the plume with limited mixing between masses.

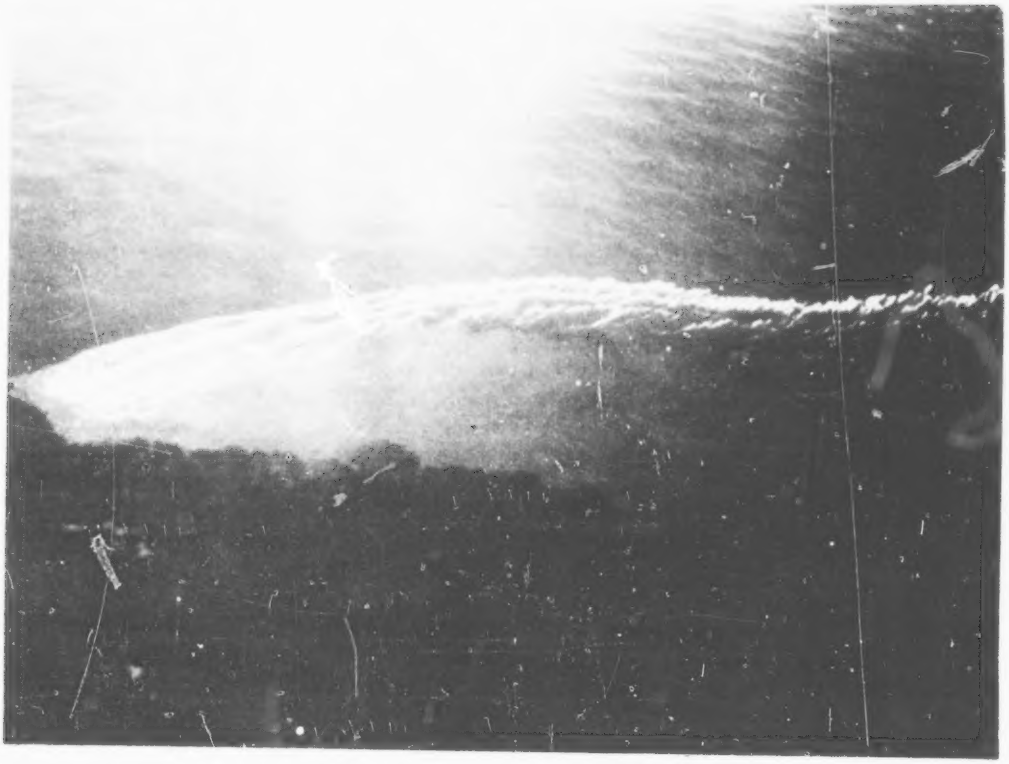

Figure 35. Plume July 8, 1969 at 15:56 from 4000 feet.

The plume was submerged on the morning of September 12, 1968. Weather and sea conditions were calm until 14:00 when a 15-20 mph wind began blowing. The waste field came to the surface and formed a long narrow plume which could have been described with a one dimensional diffusion model. The vertical aerial photography was taken with a six-inch focal length camera at 16:30. Interference caused by sunlight reflection on the choppy water surface made the photography impossible to process.

As listed in the original proposal, the first year of the study was divided into two phases:

1) Photographing the plume and current floats and
2) Photographing dye slugs introduced into the pipeline.

On August 22, 1968, one-gallon dye slugs were injected into the pipeline at 15-minute intervals using compressed air. It was raining on this day and no photography was taken. However, individual dye slugs were not observed from the boat. On September 10, 1968, the time interval was increased to one hour. Because of density stratification, the waste field and dye slugs were submerged. There was no wind on this day and the swell height was one to two ft. The dye slugs and waste field were visible on the aerial photography below the sea surface. The dye slugs did not move away from the outfall in discrete patches as planned, but accumulated about the outfall area. When the dye patches first appeared about the outfall they were doughnut shaped. Two-gallon dye slugs were introduced into the pipeline at one hour intervals on September 11, 1969; however, the aerial photography was cancelled due to cloudy skys. The plume was submerged but the individual boils over the outfall could be seen from the boat. Dye concentrations were detectable visually and with the fluorometers only directly over the outfall.

Had aerial photography been obtained of the dye patches under ideal conditions, it would have been difficult to process. Considering a nonsteady state dye patch within a nearly steady state waste field, the amount of dye, waste and sea water could occur in various combinations which would be impossible to distinguish by measuring the light return with the three broad bands of color photography. At a minimum, four individual narrow pass bands would have been required to obtain meaningful results. This phase of the study was replaced by dye slugs dropped from the airplane away from the waste field.

Summaries of the aerial photography for the 1968 and 1969 field seasons are shown in tables 4 and 5, respectively. The date, flight time, altitude,camera, and type of film are listed in the table.

As listed in the original proposal, water samples were collected during the first year of the study and tested for BOD, COD, PBI, dissolved oxygen and dye tracer concentration. The dissolved oxygen content of

Table 4. Summary of the 1968 vertical aerial photography.

| Date | Photography | | | | Boat-Photo[a] | | F | Boat | | |
|---|---|---|---|---|---|---|---|---|---|---|
| | Time PDT | Altitude (Ft.) | Camera | Film | $MSE_{bp}$ | d.f. | $\frac{MSE_b}{MSE_{bp}}$ | $MSE_b$[b] | d.f. | Sampling PDT |
| 8-8-68 | 17:09 | 8250 | 8-1/4" | Ektachrome | ----- | ----- | ----- | 12. | 3 | 16:06- |
| | 17:20 | 4125 | Zeiss | 8442 | 5.3 | 172 | 2.3 | ----- | ----- | 18:09 |
| | 17:30 | 4125 | RMKA | ----- | 7.3 | 195 | 1.6 | ----- | ----- | |
| | 17:41 | 4125 | ----- | ----- | 7.3 | 142 | 1.6 | ----- | ----- | |
| | 17:50 | 8250 | ----- | ----- | ----- | ----- | ----- | ----- | ----- | |
| 8-16-68 | 15:51 | 8250 | 8-1/4" | Ektachrome | 38. | 178 | 2.4 | 92. | 4 | 14:25- |
| | 16:00 | 4125 | Zeiss | 8442 | 31. | 156 | 3.0 | ----- | ----- | 16:53 |
| | 16:13 | 4125 | RMKA | ----- | 40 | 187 | 2.3 | ----- | ----- | |
| | 16:21 | 8250 | ----- | ----- | ----- | ----- | ----- | ----- | ----- | |
| 8-21-68 | 10:13 | 3500 | 3-1/2" | Ansco | ----- | ----- | ----- | 22. | 5 | 12:10- |
| | 10:21 | 1750 | Wild | D200 | ----- | ----- | ----- | ----- | ----- | 13:41 |
| | 10:36 | 1750 | RC-9 | ----- | ----- | ----- | ----- | ----- | ----- | |
| | 10:44 | 3500 | ----- | ----- | ----- | ----- | ----- | ----- | ----- | |
| 9-10-68 | 10:10 | 5625 | 11-1/4" | Ansco | ----- | ----- | ----- | ----- | ----- | 10:30- |
| | 10:25 | 11250 | K-17 | D200 | ----- | ----- | ----- | ----- | ----- | 12:06 |
| | 10:35 | 5625 | ----- | ----- | ----- | ----- | ----- | ----- | ----- | |
| 9-10-68 | 15:56 | 5625 | 11-1/4" | Ansco | ----- | ----- | ----- | ----- | ----- | 16:15- |
| | 16:11 | 11250 | K-17 | D200 | ----- | ----- | ----- | ----- | ----- | 17:42 |
| | 16:21 | 5625 | ----- | ----- | ----- | ----- | ----- | ----- | ----- | |
| 9-12-68 | 10:12 | 5625 | 11-1/4" | Ansco | ----- | ----- | ----- | ----- | ----- | 9:25- |
| | 10:30 | 11250 | K-17 | D200 | ----- | ----- | ----- | ----- | ----- | 10:49 |
| | 10:43 | 5625 | ----- | ----- | ----- | ----- | ----- | ----- | ----- | |
| 9-12-68 | 16:31 | 3000 | 6" | Ektachrome | ----- | ----- | ----- | 28. | 6 | 15:49- |
| | 16:46 | 6000 | Zeiss | MS | ----- | ----- | ----- | ----- | ----- | 17:11 |
| | 16:54 | 3000 | RMKA | Aerographic | ----- | ----- | ----- | ----- | ----- | |

[a] Statistic from a comparison between boat data and photo results.
[b] Statistic from a comparison within boat data.

Table 5. Summary of the 1969 oblique aerial photography.

| Date | Photography |  |  |  |  | Boat-Photo[c] |  | F | Boat |  |  |
|---|---|---|---|---|---|---|---|---|---|---|---|
|  | Time PDT | Altitude (ft.) | K-17[a] | Film HB-1[b] | HB-2[b] | $MSE_{bp}$ | d.f. | $\frac{MSE_b}{MSE_{bp}}$ | MSE[d] | d.f. | Sampling PDT |
| 7-8-69 | 15:15 | 3000 | 8442 | 8401 | 5424 | 4.0 | 147 | 2.8 | ----- | ----- | 15:10- |
|  | 15:21 | 4000 | 8442 | 8443 | 5424 | 2.9 | 130 | 3.7 | 11.1 | 5 | 16:16 |
|  | 15:56 | 4000 | 8442 | 8443 | 5424 | 2.2 | 148 | 5.0 | ----- | ----- | ----- |
| 8-12-69 | 12:52 | 4000 | 5425 | 5424 | 8442 | 2.8 | 124 | 5.3 | 14.9 | 4 | 12:44- |
|  | 13:01 | 6000 | 5425 | 5424 | 8442 | 3.5 | 193 | 4.3 | ----- | ----- | 13:47 |
| 9-8-69 | 11:21 | 3000 | 2402 | 5424 | 8443 | 7.3 | 110 | ----- | ----- | ----- | 11:19- |
|  | 11:38 | 6000 | 2402 | 5424 | 8443 | 4.8 | 181 | ----- | e | ----- | 12:06 |
|  | 14:44 | 8000 | 2402 | 5424 | 8443 | 4.8 | 70 | ----- | ----- | ----- | ----- |

[a] Mapping camera with 6-inch focal length lens.

[b] 70 mm Hasselblad camera with 150 mm focal length lens.

[c] Statistic from a comparison between boat data and photo results.

[d] Statistic from a comparison within boat data.

[e] No cross lines for the boat sampling.

the water samples were consistently at or near saturation. However, the standard error in conducting the BOD, COD, and PBI tests were about the same magnitude as the test results and the chemical sampling phase of the study was discontinued after the first season.

Originally, nine surface floats with drogues attached at various depths were planned to be set in the receiving water prior to the aerial photography for determining the water currents. Because of the time required to set and retrieve the floats, only three floats were set after the first two sampling runs.

For each day that waste concentrations were computed from both the densitometer measurements taken on the aerial photography and the fluorometer records from the boat sampling, a comparison was made of the concentrations determined by the two methods by matching the ground coordinates. The mean square residuals for this comparison are listed under the column heading of Boat-Photo. Points for the comparison were selected at 60-ft along the boat's track. Only points inside the waste field were used in the comparison. On August 12, 1969, foam from the waste covered the water surface near the outfall and this area was deleted from the comparison.

Plots of the residuals for flight 1 on August 8, 1968, and flight 2 on August 16, 1968, are given in figure 36. In figure 37 are two plots of residuals for the second flights on July 8, 1969, and August 12, 1969. In general, maximum residuals occurred near median concentration values. Plots showing both the concentrations determined from the aerial photography and those measured by boat sampling are given in figures 39 through 41. The X axis of the plot represents distance along the boat's track when inside the waste field. The distance in feet would be equal to the position number times 60. The correlation coefficient between the two methods ranged from 0.85 to 0.95.

Continuous boat sampling of the waste field was conducted while the survey vessel was underway. Where the boat sampling lines crossed, concentrations were measured twice at one point within a relatively short period of time. Continuous boat sampling was generally conducted over a period of about one hour. A measure of the repeatability of the concentrations determined by boat sampling is given by the mean square residual for these observations as listed in tables 4 and 5 under the column heading - $MSE_b$.

The F statistic listed in the tables can be used to test for a significant difference in the residuals computed between the boat and photo data and within the boat data. Using a 95 percent confidence level, the F statistic would have to be greater than 2.5 to indicate that the residual within the boat data is significantly greater than the residual between the boat sampling and the photo values.

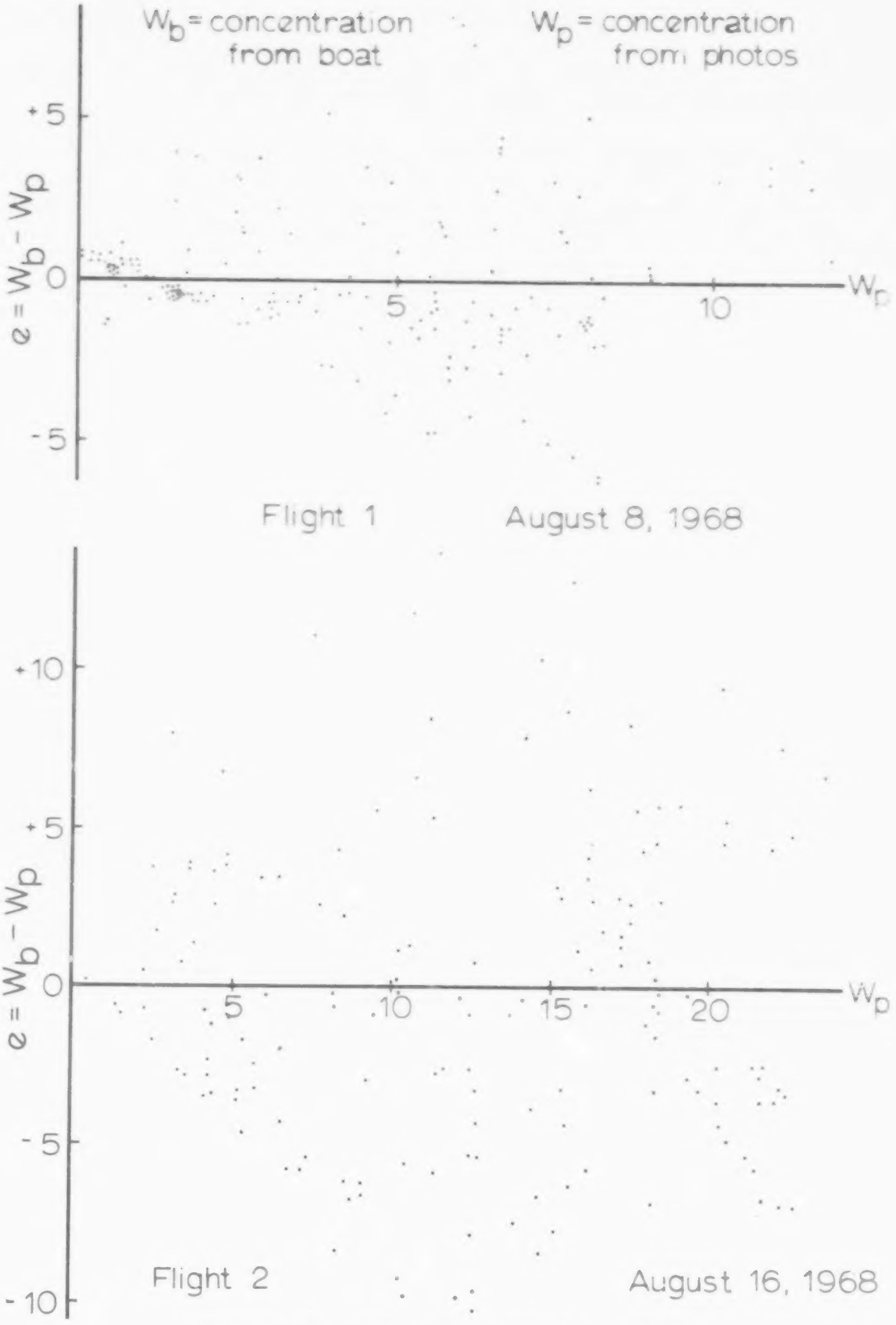

Figure 36. Plot of residuals - 1968

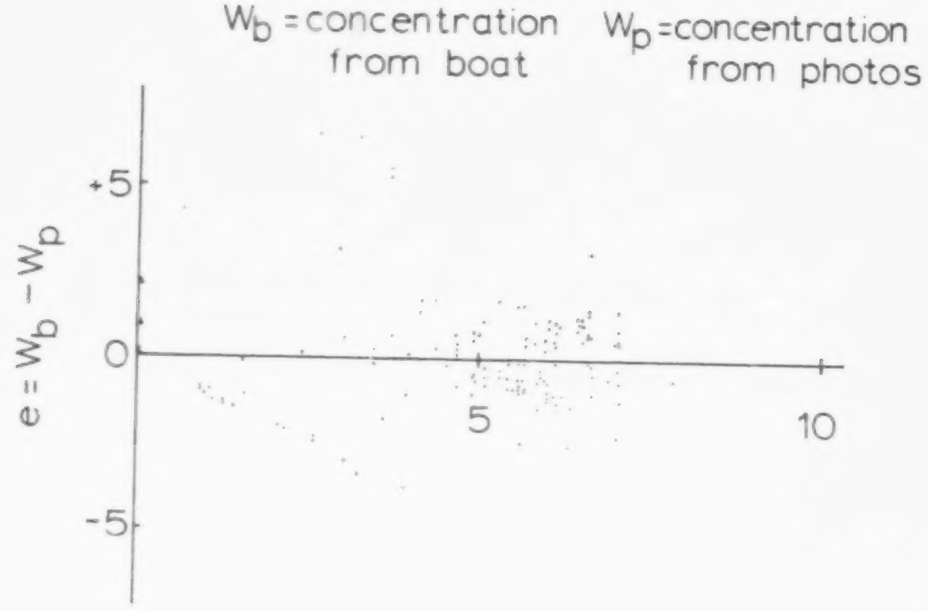

Flight 2 July 8, 1969

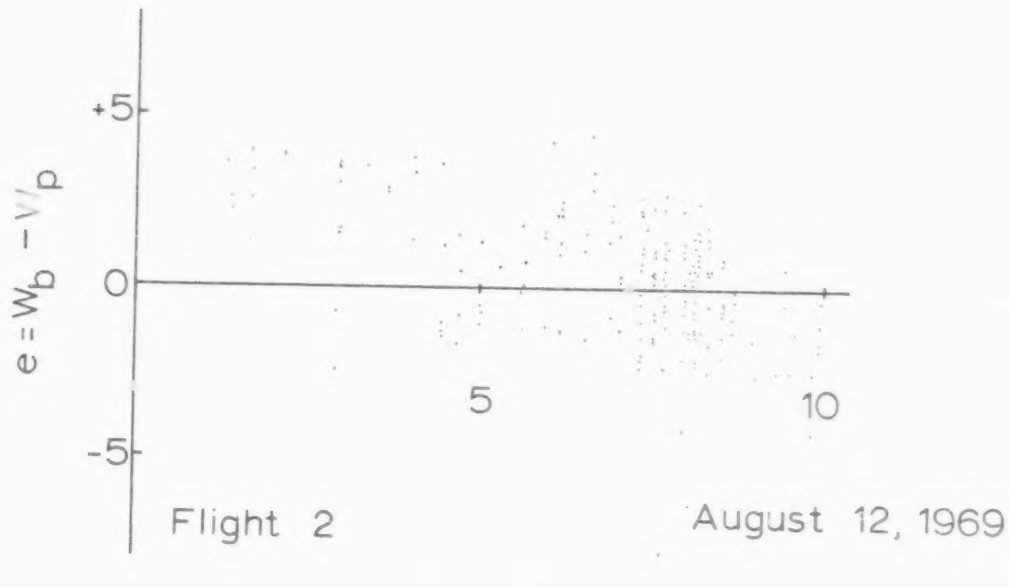

Figure 37. Plot of residuals - 1969

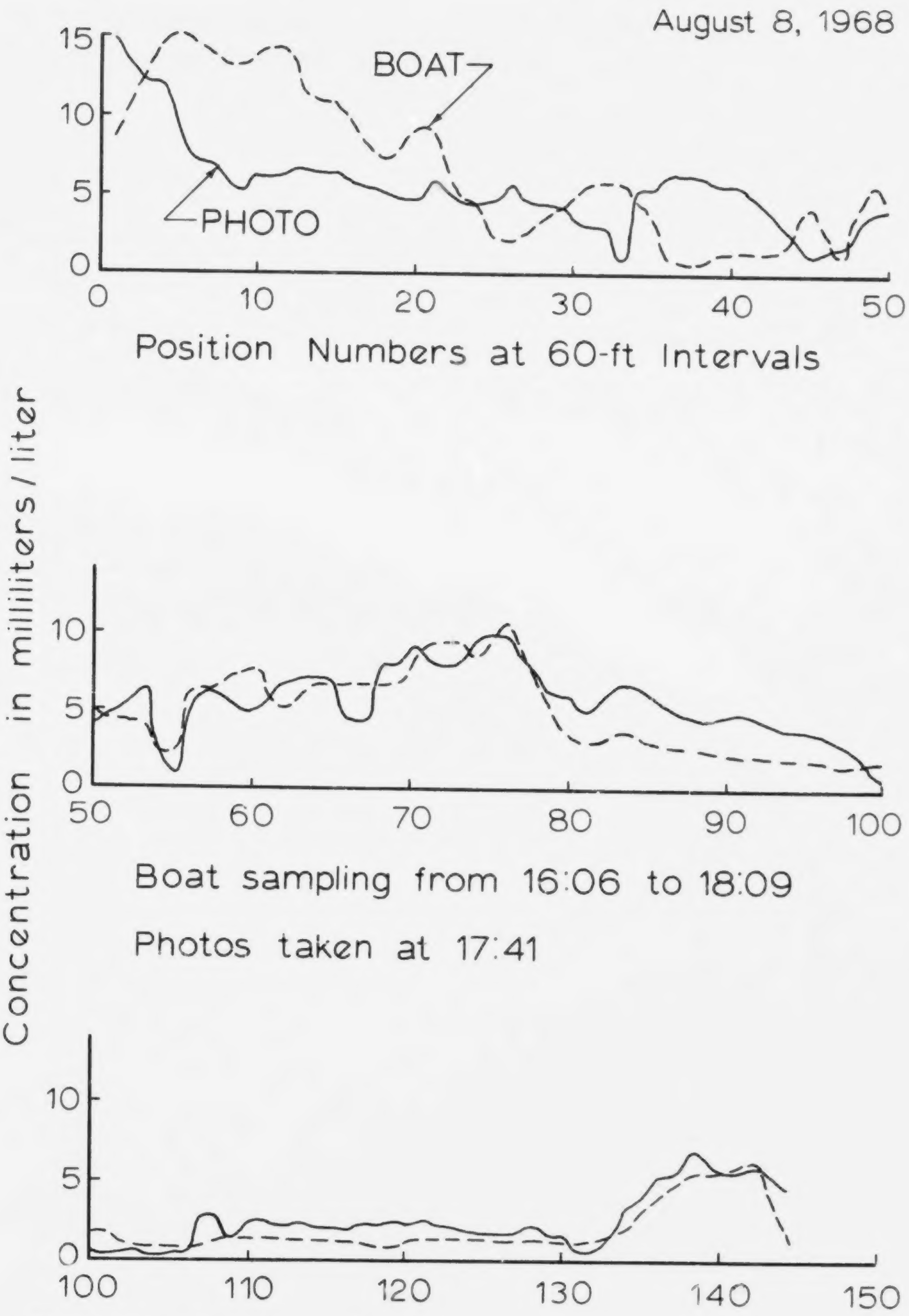

Figure 38. Comparison of boat and photo values on August 8, 1968.

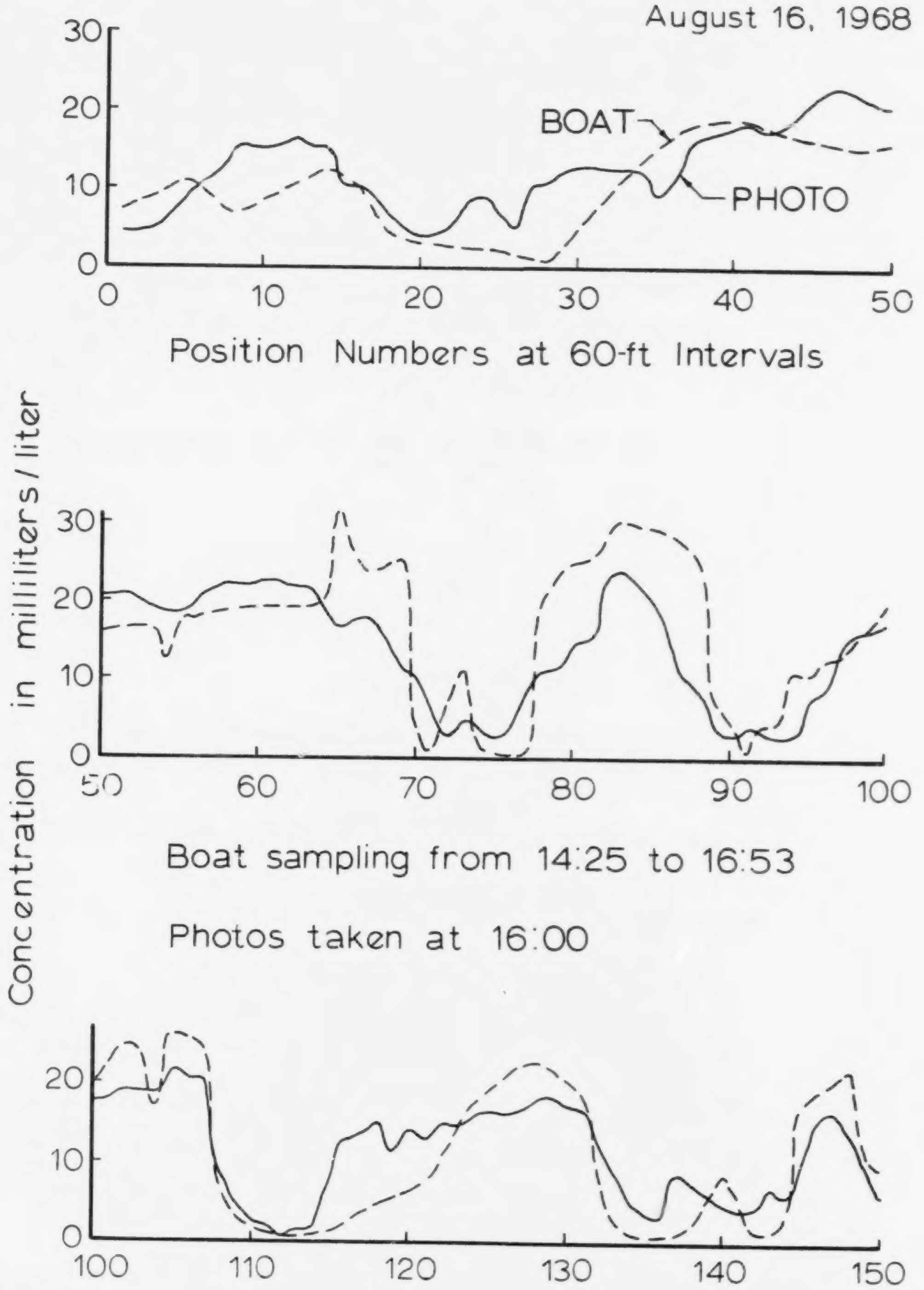

Figure 39. Comparison of boat and photo values on August 16, 1968.

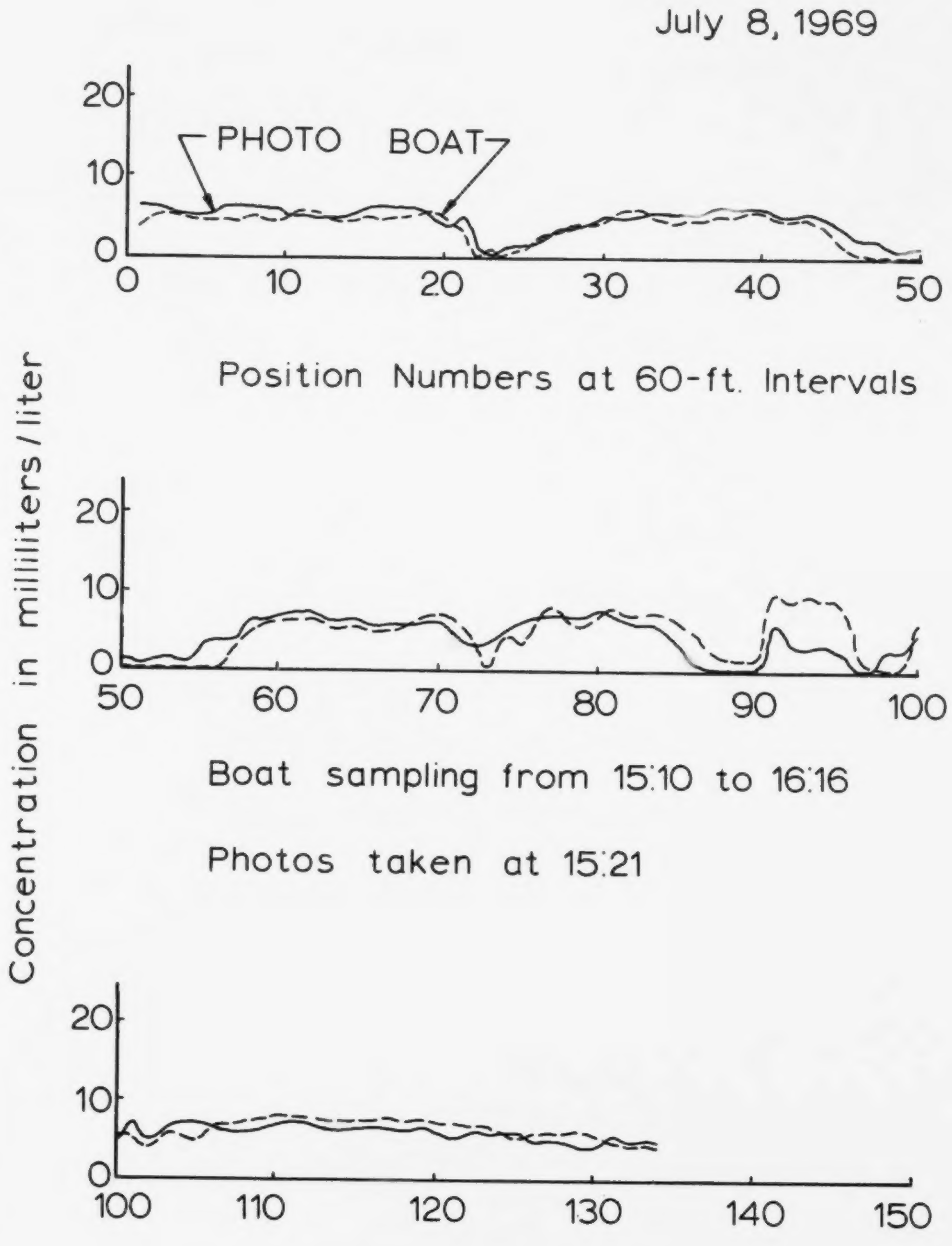

Figure 40. Comparison of boat and photo values July 8, 1969.

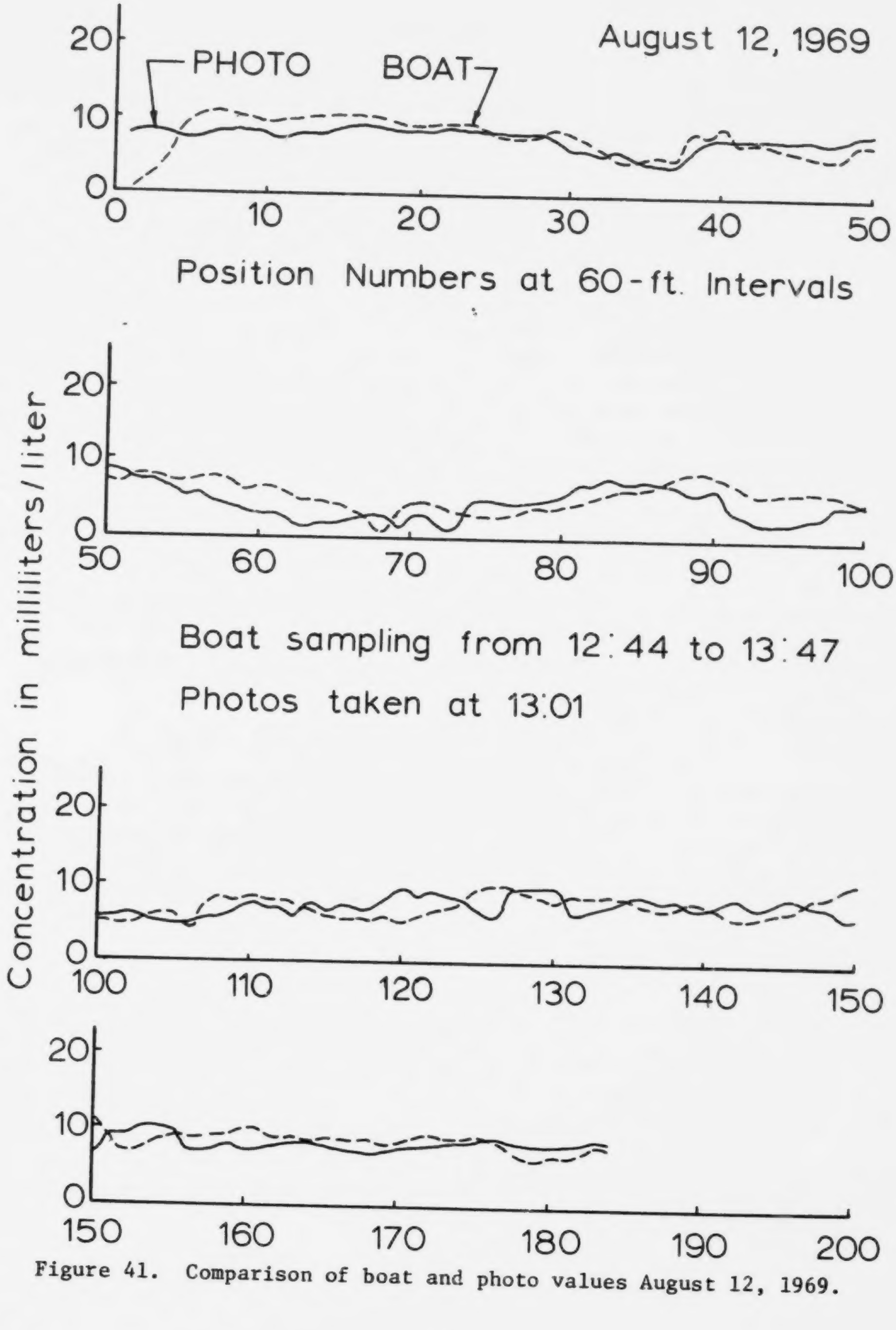

Figure 41. Comparison of boat and photo values August 12, 1969.

## 1970-1971 Data

The data acquired during the 1970-1971 field season are summarized on the following pages. The results of each sampling run are tabulated on two pages. On the left page is a contact print of the outfall area taken with the K-17 mapping camera using panchromatic, type 2402 film with a 25A wratten filter. The oblique photographs were taken with the axis of the camera oriented approximately 50 degrees from the vertical. The general orientation of the photographs can be visualized from the shoreline which extends almost due north and south along this section of the coast. A chart of the outfall area is shown in figure 42.

Depending upon the characteristics of the effluent, the location of the waste field is not always evident in these photographs. If the light scattering of the waste in the red band is high, the plume can be distinguished from the bluish-green background of sea water. However, when the seas are rough suspended sands and silts in the sea water can make the identification of the plume difficult in the red band. When the waste appears black instead of brown, the greatest contrast between the plume and the sea occurs around 500 nm. In this band the light return from the sea water is high while the light scattered in the plume is low.

The plot shown on the right page for a sampling run was made by photographing the CRT of the Tektronix T-4002 graphs display terminal. A state plane coordinate grid is drawn and labeled at 1000-ft intervals. The outline of the waste field is shown on the plot as a solid line. Foam from the effluent is indicated with x's on the plot. The area of the plume is computed in acres and displayed at the top of the plot.

When possible, the water current velocity is computed from the dye patch and the vector drawn on the plot at a scale of 1.0 ft/sec to 1000 ft. The position of the centroid of the dye patch during the first flight over the outfall area is shown on the plot at the tail of the velocity vector. The apparent position of the boil over the outfall is also shown on the plot as a triangle. The position of the outfall as determined from the 1968-1969 data and shown in figure is 1069400E, 375800N.

The wind velocity and direction were listed at the two-hour interval below the tekplot photo for the day of the observation and the previous day. Wind data were obtained from the continuously recording anemometer located on the south jetty. If this station was not in operation or for some other reason the data were not usable, manually recorded weather from the Newport station was plotted at 3 hr intervals. According to the Weather Bureau, the wind velocity at this station is less than that which would be recorded at the south jetty but the wind directions agree closely.

Tidal information is given on the data sheet below the wind vector plot. Pacific Standard Time of day was used for both the wind and tide plots during the period October 25 through April 25. The tidal information was obtained from the Coast and Geodetic Survey tide tables.

Factors which influence the size of wind waves include the wind velocity, wind duration and the fetch. For a given outfall location, the fetch will vary with the direction of the wind. The effect of wind velocity on the condition of the sea is shown in figure 93. The photos show the condition of a developed sea for wind velocities of 15, 20, 25, 30, 40 and 50 kts, respectively. Energy from the wind is transferred to sea as transport velocity energy and turbulent energy. Descriptions of the sea for various wind scales are listed in table 6.

A summary of the 1970-71 data is given in table 7. Effluent discharge rates were not available for December 21 and 23, 1970. During the sampling period the current velocity ranged from 0.1 to 1.4 ft/sec while the area of the waste field ranged from 7 to 464 acres. The diffusion coefficients listed in the table were determined from the dye patch studies. The predicted tide stage at the time of the aerial photography is listed in column eight. In the last column of table 7 is the sea state which was estimated from the aerial photography with the aid of both the descriptions listed in table 6 and the photos of the sea state in figure 93. Detailed descriptions of the observations by dates follows.

The plume on September 9 was one of the largest observed with an area of 275 acres from an effluent discharge rate of 5850 gpm. A current velocity of 0.3 ft/sec was measured near the outfall. The tide was at 4 ft at the time the photo was taken and rising with a maximum of 7.5 ft reached 4 hours later. It can be seen in figure 43 that some foam is visible forming a striated pattern extending southeasterly toward the jetty. The current vector is shown in a southwesterly direction to the north in the afternoon. The waste plume extended northeast from the outfall at the time of the photography. The photo has a mottled tone with scattered whitecaps throughout the area. No definite linear pattern is present due to the wave crests aligned perpendicular to the wind. The diffusion coefficient parallel to the current vector was 12.9 $ft^2$/sec and 0.4 $ft^2$/sec perpendicular to the current.

On September 23, the plume was small with foam streaks originating from the boil over the outfall as shown in figure 45. The foam runs southward due to the prevailing northerly winds while the plume extends northward. The winds on the previous day were 20 kts from the southwest. The area of the waste field was 28 acres and the diffusion coefficients were 3.2 $ft^2$/sec and 0.1 $ft^2$/sec in the x and y directions, respectively. The current velocity was small (0.1 ft/sec), while the tide was 4 ft and rising with a maximum of 6.5 ft 4 hours later. The dye patch can be seen in figure 45 approximately 2000 ft southwest of the outfall. A light haze covers the nearshore area.

A very distinct plume pattern was observed on September 30. The width of the plume increases at a decreasing rate downstream from the outfall. The current velocity was 0.7 ft/sec which is higher than average. The area of the plume was 128 acres with an effluent discharge rate of 6950 gpm. Diffusion coefficients were 7.5 $ft^2$/sec and 0.1 $ft^2$/sec in the x and y directions. Although the wind was approximately 10 kts from the north only a small amount of foam was present. The tide was at 4 ft and decreasing with the minimum being reached 3 hours after the photos were taken. The photo in figure 47 shows the plume as a light area with two thin foam streaks parallel to the shore extending to the right. A few whitecaps can be seen in the photo. The sea has a finely mottled pattern with a definite linear trend normal to the shore due to the wind waves.

On October 7, the plume was one of the smallest observed despite the fact that the effluent flow rate was 7450 gpm. The plume is difficult to see in figure 49 but two small foam streaks can be seen extending southeast from the outfall. The area of the waste field was only 9 acres. At the time of the photo, the stage of the tide was 6.5 ft and rising. The peak was reached about an hour and a half after the flight. The dye patch can be seen in the lower right of figure 49.

A lake-like plume pattern with an area of 89 acres was observed on October 12. The waste discharge rate was 7650 gpm and the sea was choppy. The wind was from the north at 10-15 kts. The current velocity was not measured since only one flight was made over the outfall area. The tide was at 2.5 ft and decreasing, reaching a low of 0.5 ft two hours after the flight. The plume is visible in figure 51 as a lighter patch in the center of the picture just above the dye patch. The swell breaking on the reef can be seen in the lower right of figure 51. The sea has a mottled pattern with a number of whitecaps visible. There is a slight linear trend to the mottled pattern caused by the wind generated waves in the E-W direction.

On December 21, the plume was small and extended offshore from the outfall. Wind from the southwest at 40 kts generated large swell prior to the photography. Breakers can be seen all along the reef in figure 53. The tide stage was at low water. The winds changed and were 10-15 kts from the east for 24 hours before the current velocity was measured at 2.0 ft/sec to the west. The sea has a mottled pattern with a few whitecaps. The swell can be seen peaking throughout the area between the shore and the reef. The Coast Guard recorded a swell of ten ft at the mouth of the Yaquina River. Diffusion coefficients of 7.3 $ft^2$/sec and 1.9 $ft^2$/sec were measured for the x and y directions respectively.

The waste field on December 23 tended to lake about the outfall with an area of 26 acres. A current velocity of 1.1 ft/sec was measured inshore from the outfall. Diffusion coefficients were 5.1 $ft^2$/sec in the x direction and 0.7 $ft^2$/sec in the y direction. The sea was calm with a slight northeasterly breeze. The tide was at 4 ft and falling to one ft 3-1/2 hours later. A long streak of foam extended from the outfall area to the northwest and can be seen in figure 55.

As can be seen in figure 57, the sea was extremely rough on December 31. Although the effluent discharge rate was 8700 gpm, the plume was not visible. While the wind was relatively calm, the swell height was eight feet from the Coast Guard records. The waves were breaking from the outer reef to the beach. A current velocity of 1.4 ft/sec was measured as were diffusion coefficients of 6.9 $ft^2$/sec and 0.6 $ft^2$/sec in the x and y directions. The plot from the Tektronix scope shows only the current vector extending from the position of the dye patch. The tide was at 7.5 ft and reached a maximum of 8 ft about one hour after the flight was taken.

A lake-like waste field was observed on January 2 with an area of 36 acres. The effluent flow rate was 6950 gpm. Diffusion coefficients were 1.7 $ft^2$/sec and 0.5 $ft^2$/sec in the x and y directions. The area near and to the north of the outfall is covered with foam as can be seen in figure 59. The lighter water near shore was caused by the turbulence from the large swell suspending the sand. Wind waves oriented NE-SW can be seen in the upper left. The tide was at 3 ft at the time the photo was taken and reached a peak of 7 ft approximately 3 hours later.

During the morning of the 6th of February, the plume was observed heading toward the north with an area of 193 acres. The current velocity near the outfall was 0.3 ft/sec. The effluent flow rate was 6450 gpm and diffusion coefficients in the area were 3.6 $ft^2$/sec and 0.1 $ft^2$/sec in the x and y directions. The wind had been from the east but was beginning to shift towards the northeast at the time of the photography. The tide stage was 0.5 ft and falling, reaching a minimum of 0.0 ft four hours later. The photo in figure 61 shows foam originating at the boil over the outfall and trailing off toward the northwest. The plume is the lighter area north of the outfall. A few whitecaps are present in the nearshore area but the sea surface when viewed from about 30 degrees from the vertical appears uniform in tone.

In the afternoon of the 6th of February, the plume had shifted approximately 180 degrees from the direction observed in the morning and was headed toward the south. The area of the waste field remained approximately the same as in the morning. The winds had shifted from easterly to northwesterly, and the long foam streak formed a U-shaped pattern, open to the northeast as can be seen in figure 63. The sea was relatively calm, and the tide was at 1.5 ft and nearly reached the minimum of 0.0 ft at 16:00.

The plume on March 16 was small, measuring 22 acres, and extended southward from the outfall. The sea was rough, as the photo in figure 65 shows, and the winds were approximately 20 knots out of the north.

The tide was at a stage of 4 ft and rising to a maximum of 6 ft three hours after the flight. The plume can be seen in figure 65 as the dark area near the lower center of the photo. Extensive whitecaps can be seen everywhere. The photo has a mottled pattern with turbid water near shore and in the shallow area between the outfall and the north jetty. The crests of the wind-generated waves show a linear pattern and the swell can be seen peaking outside the surf zone.

The plume on March 17 tended to lake about the outfall with a leg extending towards the southeast. As can be seen in figure 67, a foam streak extends southward from the outfall, apparently driven by the 15 kt wind from the north. The plume can be seen in figure 67 as the dark area surrounding the boil. Suspended silts and sands in the nearshore area give the water a lighter tone. The sea appears rough with numerous whitecaps in the area. There is a definite linear trend caused by the wind generated waves and the photo has a mottled pattern. A current velocity of 0.3 ft/sec toward the southeast was measured north of the outfall. The tide stage was 5 ft and about 1 hour before high tide.

The area of the plume observed on March 18 was 111 acres with a current velocity of 0.7 ft/sec driving the plume to the south. The effluent flow rate was 5950 gpm and diffusion coefficients of 0.4 $ft^2$/sec in the x and y directions were measured near the plume. The winds were shifting from northeasterly to northwesterly at the time the photo in figure 69 was taken and the tide was at low water. The lighter water near the shore is caused by sand being suspended by the turbulent action of the large waves. This turbulent action continues to suspend material to a depth of 35 ft near the north end of the reef. Waves are breaking on the reef near the outfall.

The lake-like plume in the morning of March 19 measured 73 acres and diffusion coefficients near the plume were determined to be 1.2 $ft^2$/sec in the x direction and 0.4 $ft^2$/sec in the y direction. The current velocity was 0.3 ft/sec in a generally westward direction. The winds were shifting from the northeast to the northwest at the time the observations were made and the tide was at 1 ft. The light water near the shore in figure 71 is caused by sand suspended in the water. The plume extended both onshore and offshore from the outfall. The sea has a mottled pattern with a few whitecaps visible. Waves were breaking on the reef both north and south of the outfall. Swell crests can be seen in the upper left of the photo and near shore. The turbid water along the coast both north and south of Yaquina Head shows a confused circulation pattern.

In the afternoon of March 19, the plume had begun to spread to the south, apparently due to the shifting of the wind from easterly to northerly. The tide had passed the minimum and was at 1 ft and rising. The photo in figure 73 shows the plume as the dark area extending both offshore and onshore. The photo was taken from 6000 ft at 13:50 and, when compared with figure 71, shows the change which occurred. The swell had decreased and the wind had increased from morning and a number of whitecaps can be seen. The refraction wave pattern in the lower right of the photo was caused by a sunken barge on the reef. Photos of the outfall area on both March 18th and 19th showed very turbid water along the coast. Neither the swell height nor wind velocities during these days were particularly large. A heavy rain storm began March 9 and ended March 15. Turbid fresh water runoff from this storm may have caused these conditions in the nearshore coastal waters.

The plume on March 24 was somewhat elongated, extended southwest and covered an area of 58 acres. The current velocity north of the outfall was 0.3 ft/sec and diffusion coefficients were 1.2 $ft^2$/sec in the x direction and 0.0 in the y direction. The wind had been blowing 15-25 kts and generated rough seas as can be seen in figure 75. The waves were breaking on the reef just offshore from the outfall located near the lower center of figure 75. A few whitecaps can be seen near the outfall. The tide was at low water when the photography was taken.

The plume on April 12 was the smallest observed, measuring only 7 acres and extended toward the northwest from the outfall, driven by a current of 0.4 ft/sec. While the wind was 10-15 kts from the east, the sea was calm as the photo in figure 77 shows. The light spot in the center of the photo is the dye patch from which diffusion coefficients of 8.07 $ft^2$/sec and 0.19 $ft^2$/sec were measured. The tide was at 5.5 ft and falling.

The plume on April 15 extended towards the southwest while a foam streak can be seen looping back toward shore in figure 79. The area of the plume was 68 acres with an effluent flow rate of 7700 gpm. The tide is at 4.5 ft and flooding. The wind had been from the east but had changed to the northwest at the time of the observations. The light area in figure 79 extending from shore to the foam streak appears to be a tide rip. Numerous whitecaps are visible and the sea has a mottled tone. A breaker is visible on the reef offshore from the outfall.

The plume on April 21 was long and narrow and extended northward approximately 13,000 ft. The effluent discharge rate was 5850 gpm and the area of the plume was 166 acres. Some foam appears to be generated in the waste by the 10 kt wind with foam streaks extending northeast near the upper left of figure 81. An eddy or a tide rip appears northeast of the outfall and may be the cause of the curved plume pattern. The current velocity was 0.5 ft/sec near the outfall while the x and y diffusion coefficients were only 0.3 and 0.02 $ft^2$/sec, respectively. The observations were made at low tide and the wind was from the southwest.

The largest plume observed during the 1970-71 season was 464 acres on

April 26. The current velocity was 0.3 ft/sec towards the north. The boil over the outfall can be seen near the lower right of figure 83. The plume is the light area extending upwards and to the left from the outfall. The effluent discharge rate was 5800 gpm and diffusion coefficients were 14.0 and 0.2 $ft^2$/sec in the x and y directions, respectively. The elongated dye patch can be seen in the photo just south of the boil. The photo of the sea appears to have a slightly mottled pattern with a few whitecaps present. The wind velocity was only ten knots at the time of the photography. Coast Guard records indicate that the swell was 2-4 ft.

Only one photographic flight was taken over the outfall on May 7 before the area was covered with fog. The fog can be seen on the left in figure 85. The plume was narrow and extended northward from the outfall. A foam streak can be seen along the nearshore edge of the plume. The light spot near the head of the plume is the dye patch. The observation was made during a falling tide when the wind was from the southwest 10-15 kts and the effluent discharge rate was 6350 gpm.

On May 10th, the plume covered an area of 71 acres. The head of the plume formed a sharp point as can be seen near the left of figure 87. The plume extends to the right or south. The current velocity of 0.7 ft/sec was measured near the tail of the plume. Diffusion coefficients from the dye patch in the x and y directions were 2.8 and 0.1 $ft^2$/sec, respectively. A few whitecaps are present near the outfall.

The long plume observed on May 13 extended nearly 9000 ft in a northeasterly direction and covered an area of 197 acres. The flow rate was 6050 gpm on this day. The plume can be seen in figure 89 as a light area with the head of the plume near the right. The photo was taken from 6000 ft at 14:10 and the tide at this time was 4.5 ft and rising toward a peak of 5.5 at 16:00. Numerous whitecaps can be seen in the sea with a finely mottled photo pattern.

The plume on May 14 extended from the outfall toward the west for approximately 2000 ft and then headed southward for a distance of 3500 ft. The area covered by the plume was 112 acres, and the velocity was 0.3 ft/sec in a southwestward direction. The flow rate of the effluent was 5800 gpm and diffusion coefficients were computed to be 2.4 $ft^2$/sec in the x direction and 0.1 $ft^2$/sec in the y direction. The photo in figure 91 was taken from 4000 ft at 14:48 and shows the plume as a large spot with light tone in the darker surrounding water. The tide at this time was at a stage of 5 ft and rising.

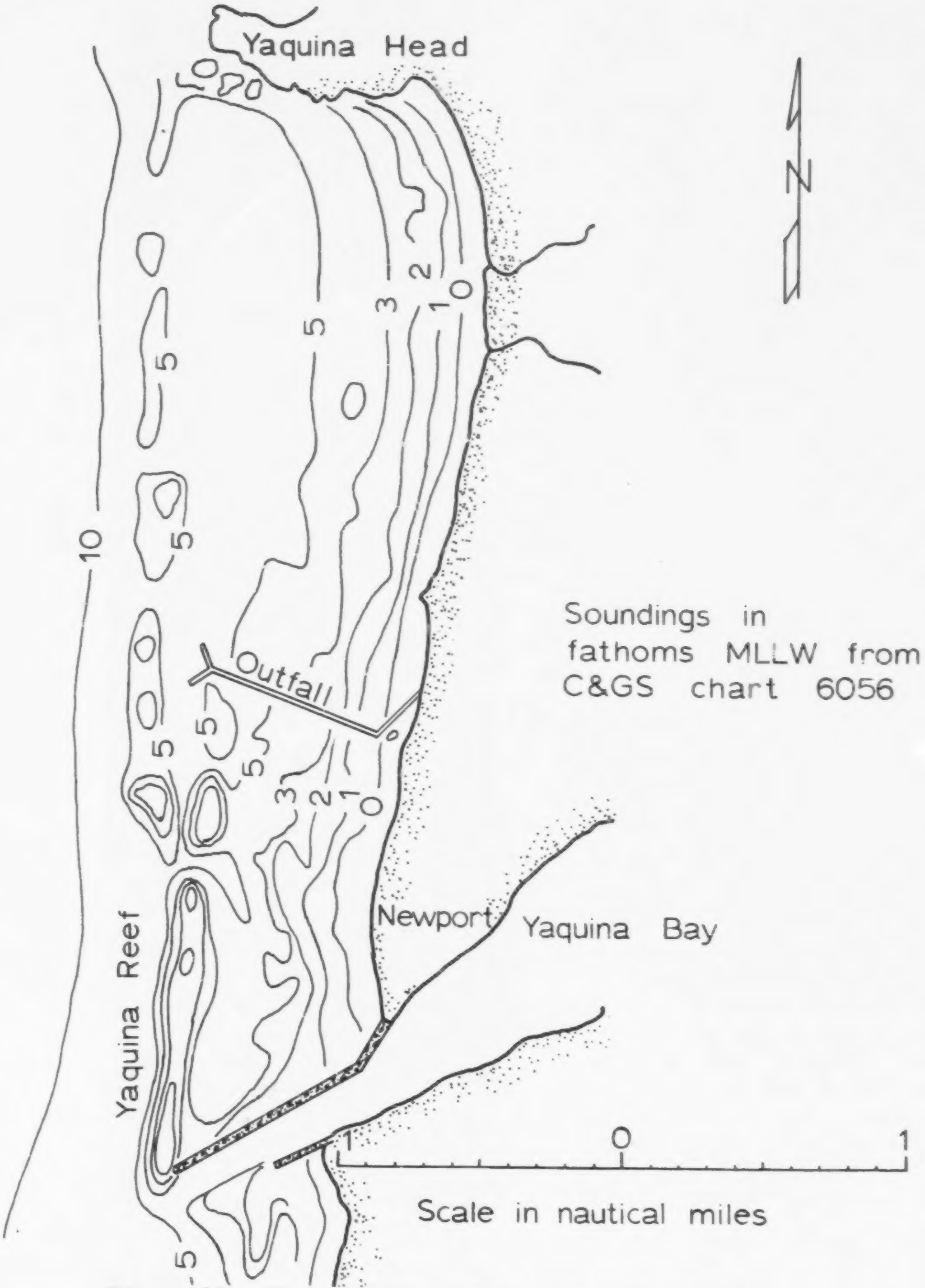

Figure 42. Chart of the outfall area at Newport, Oregon.

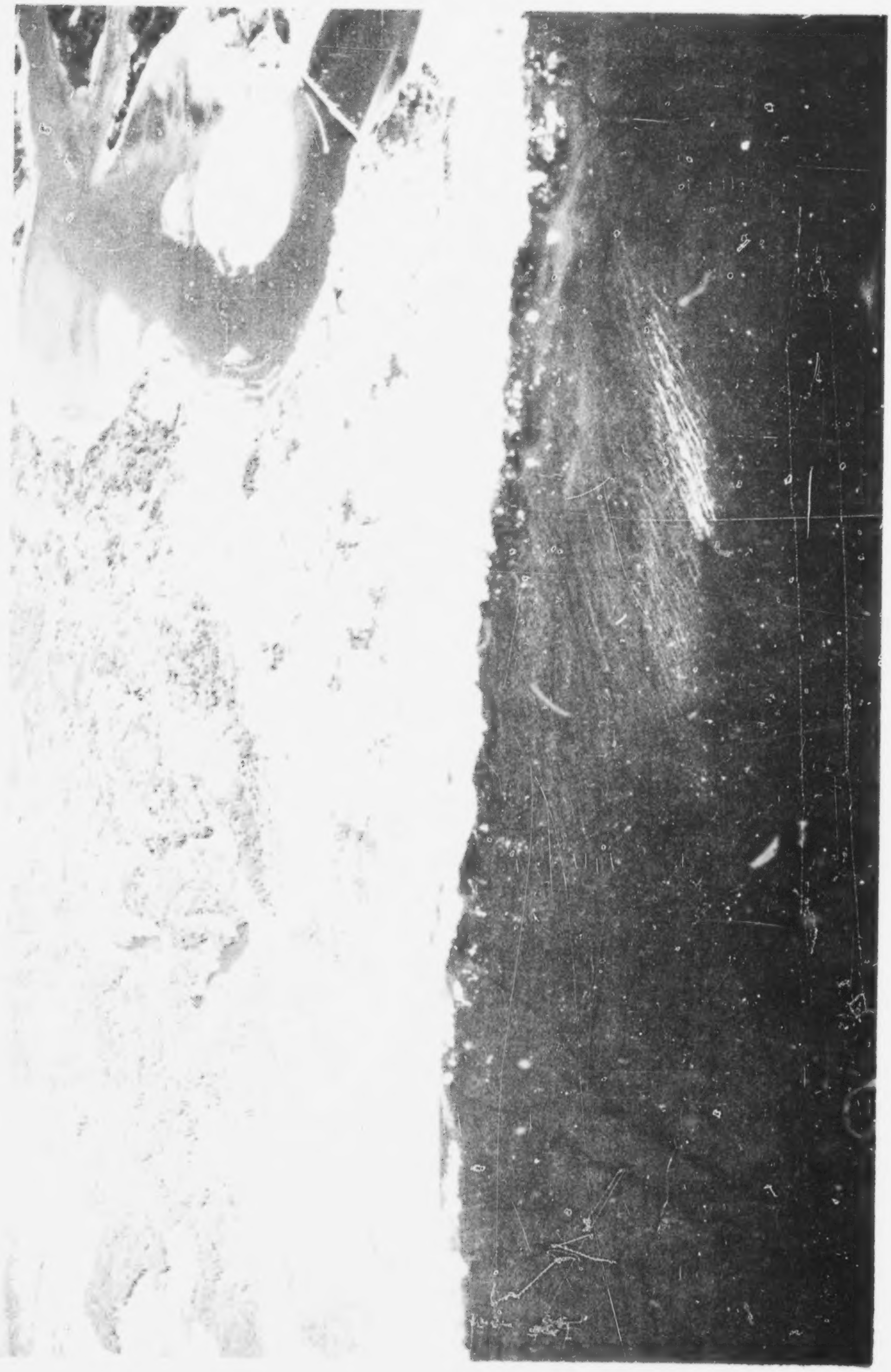

Figure 43. Aerial photo of outfall area on September 9, 1970 from 800 feet at 14:30.

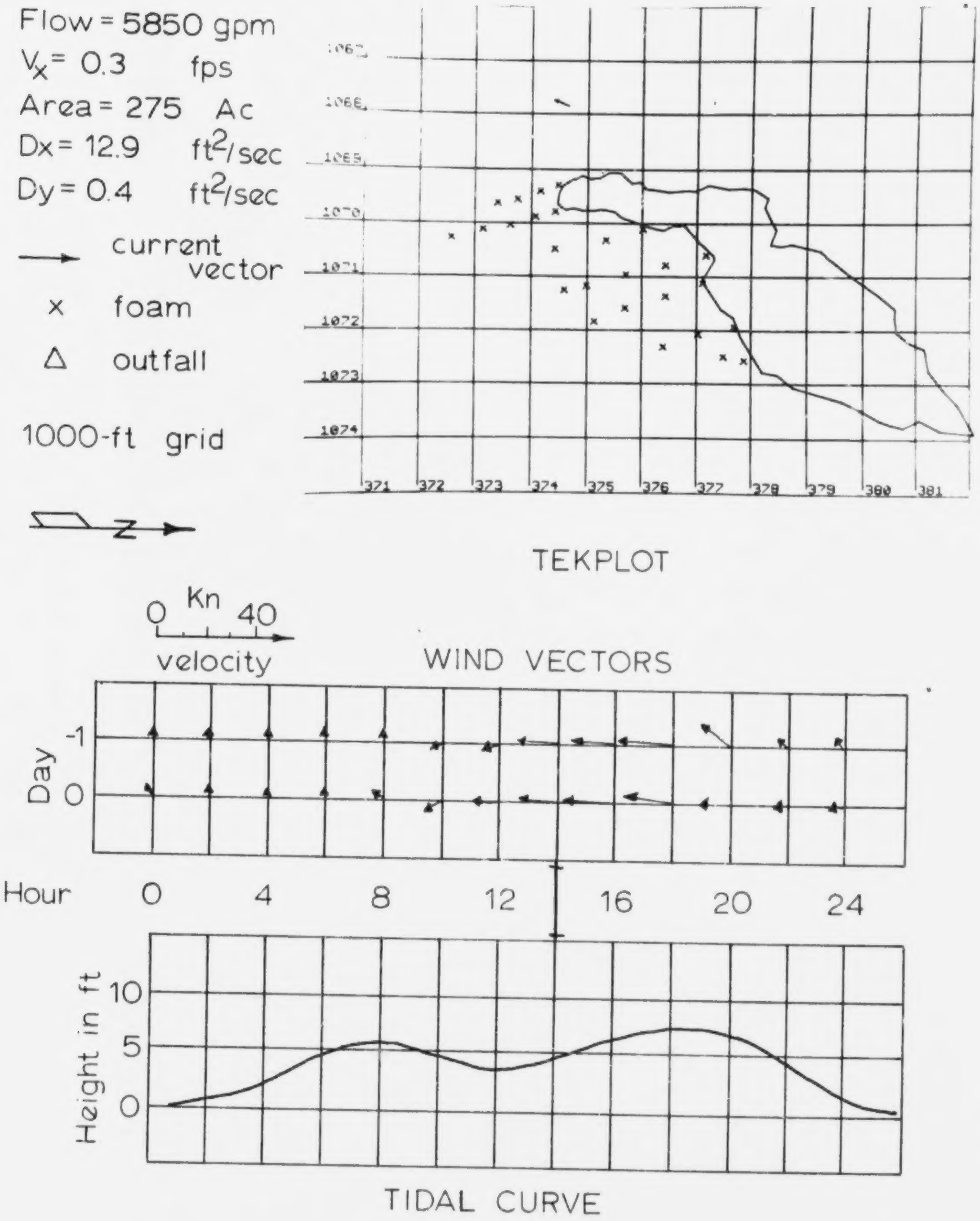

Figure 44. Data for September 9, 1970.

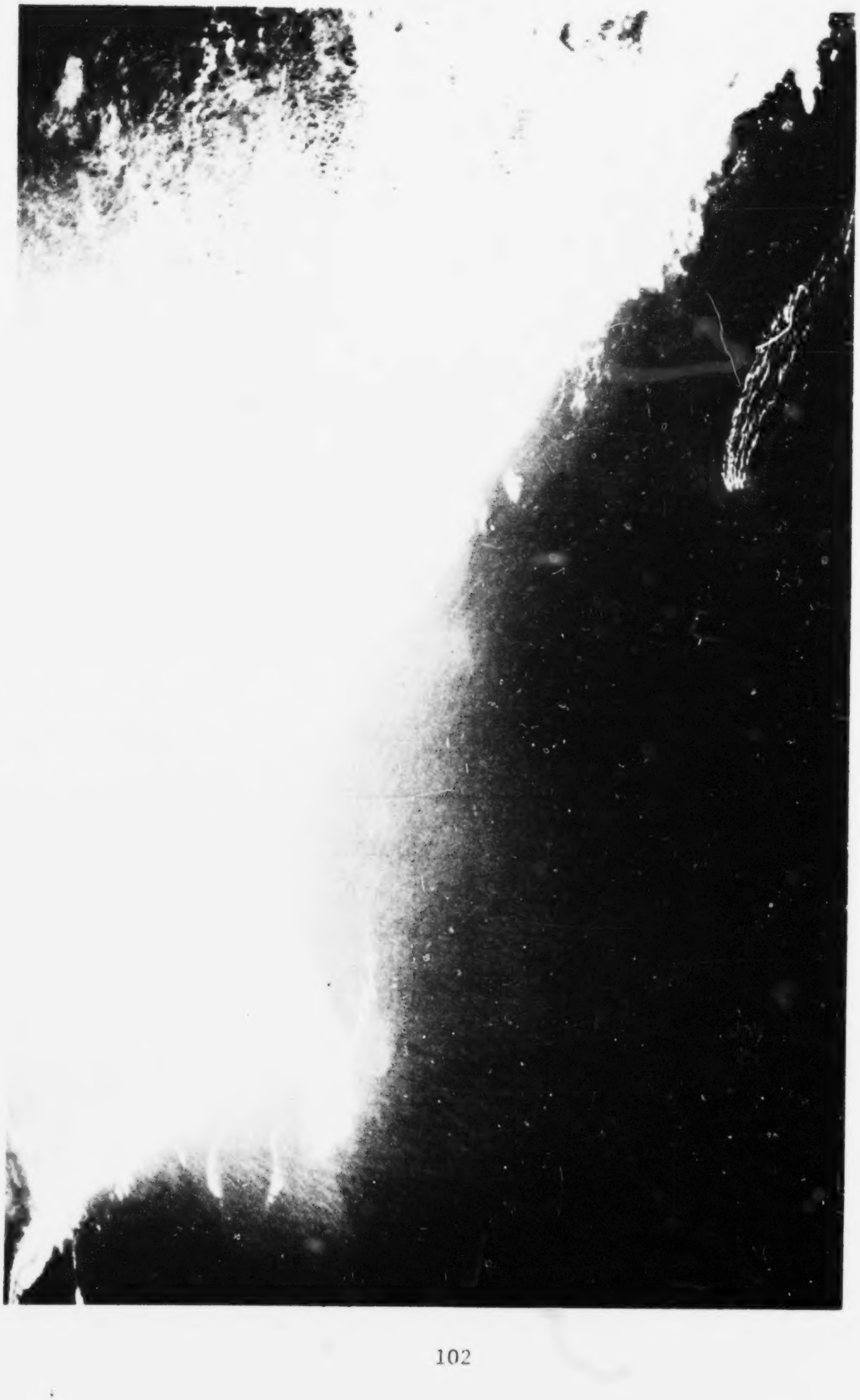

Figure 45. Aerial photo of outfall area on September 23, 1970 from 8000 feet at 15:30.

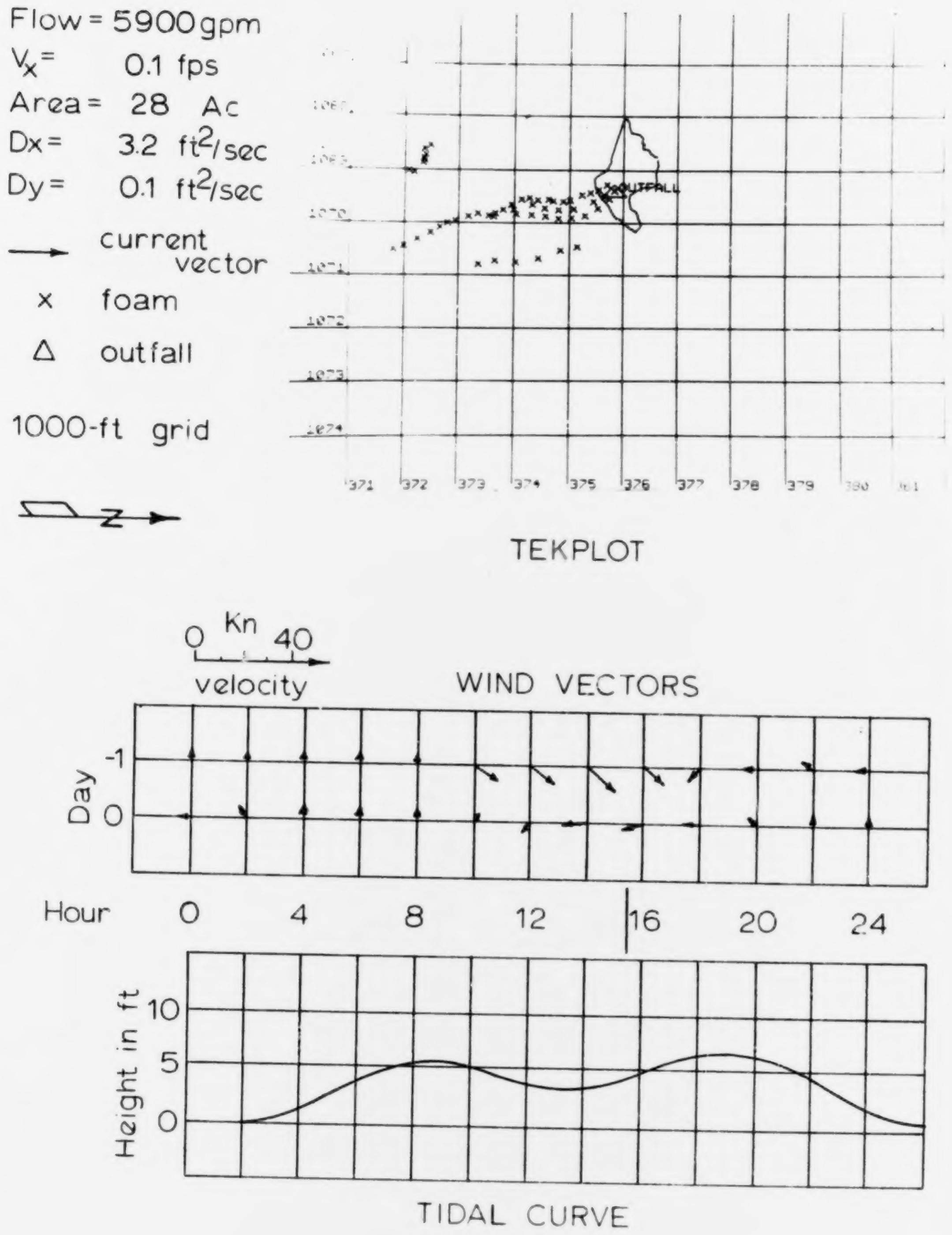

TEKPLOT

WIND VECTORS

TIDAL CURVE

Figure 46. Data for September 23, 1970.

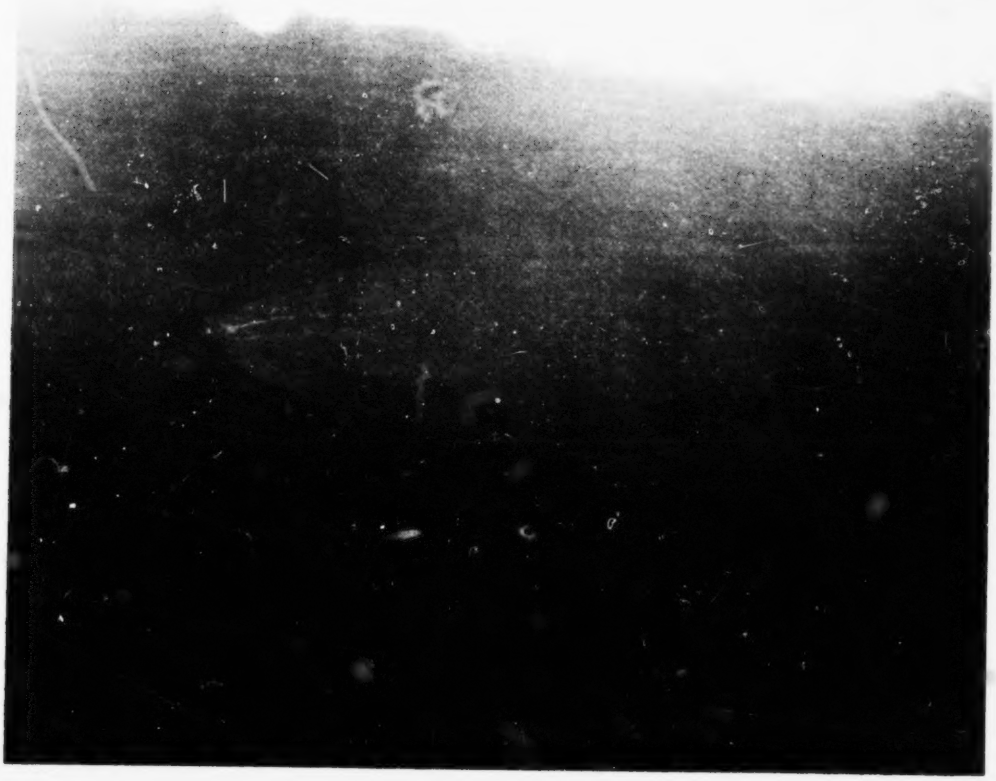

Figure 47. Aerial photo of outfall area on September 30, 1970 from 5000 feet at 14:54.

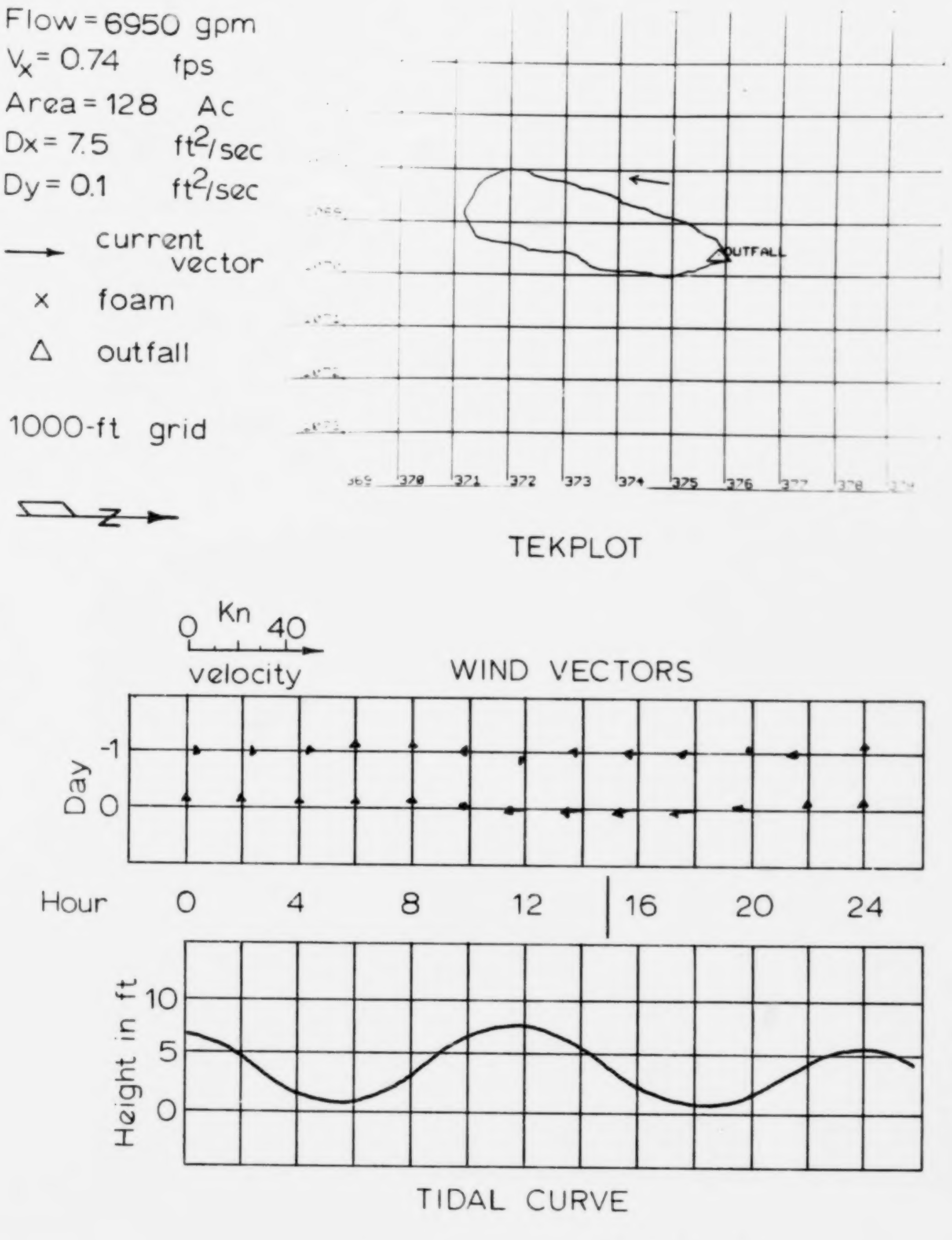

Figure 48. Data for September 30, 1970.

Figure 49. Aerial photo of outfall area on October 7, 1970
from 3000 feet at 14:32.

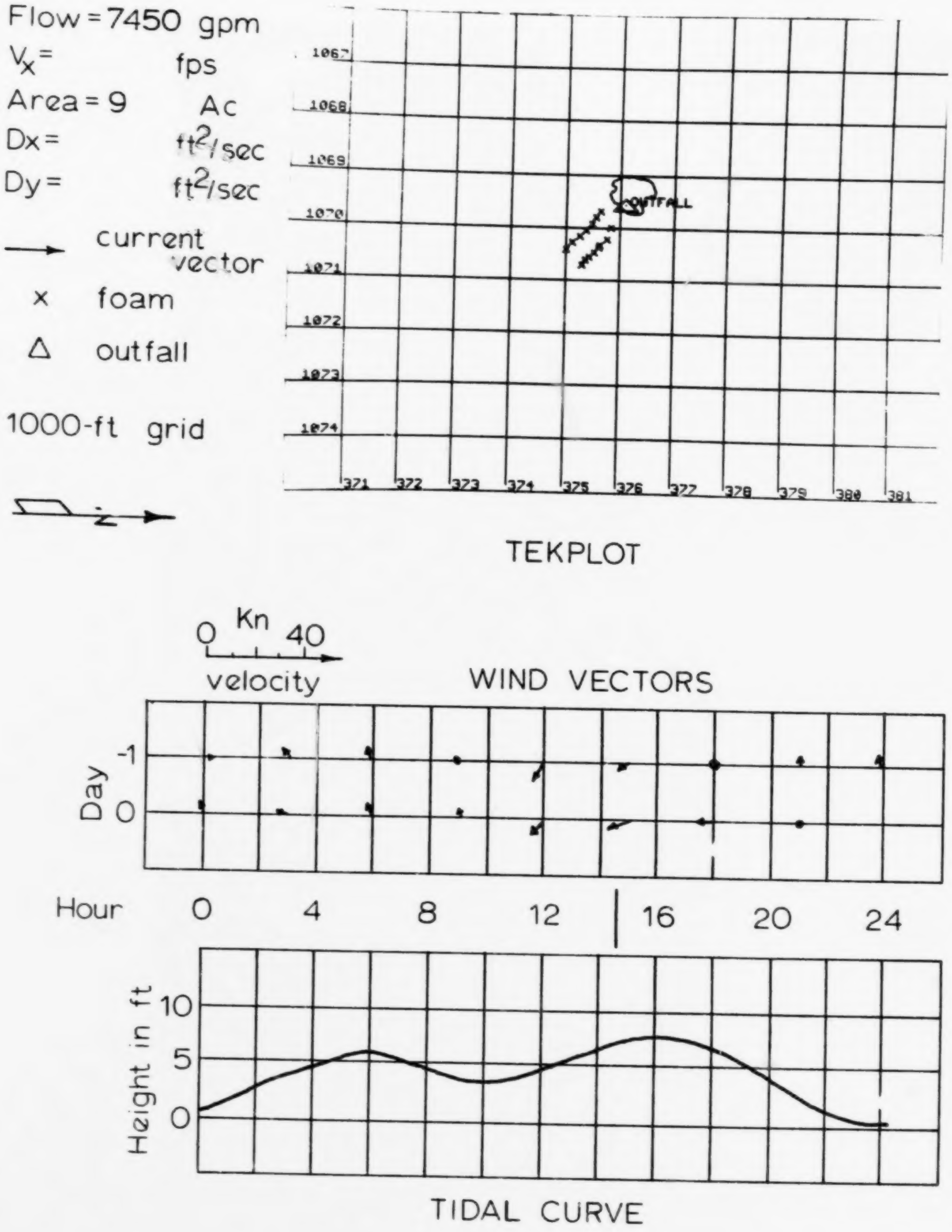

Figure 50. Data for October 7, 1970.

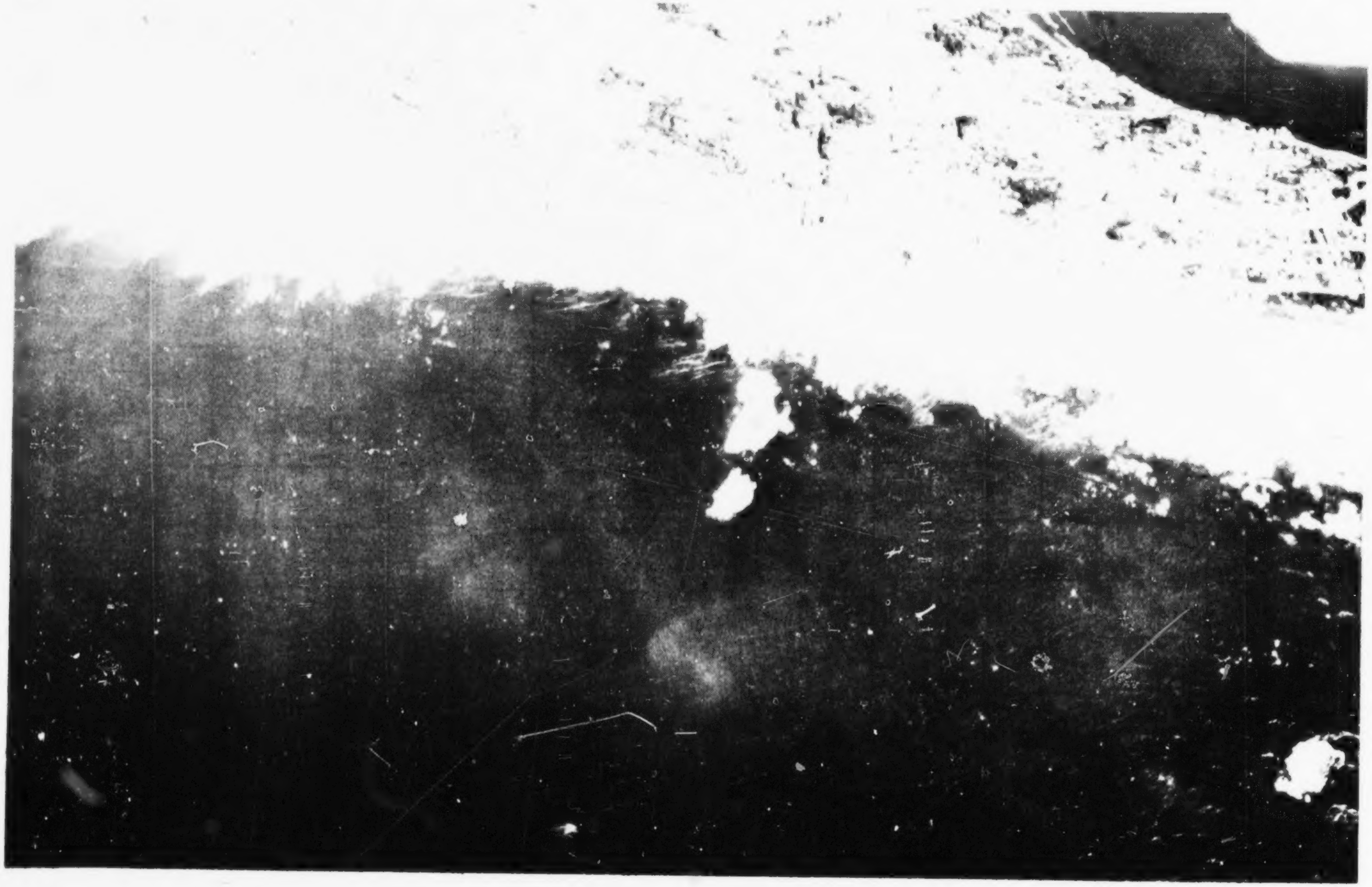

Figure 51.  Aerial photo of outfall area on October 12, 1970 from 4000 feet at 14:10.

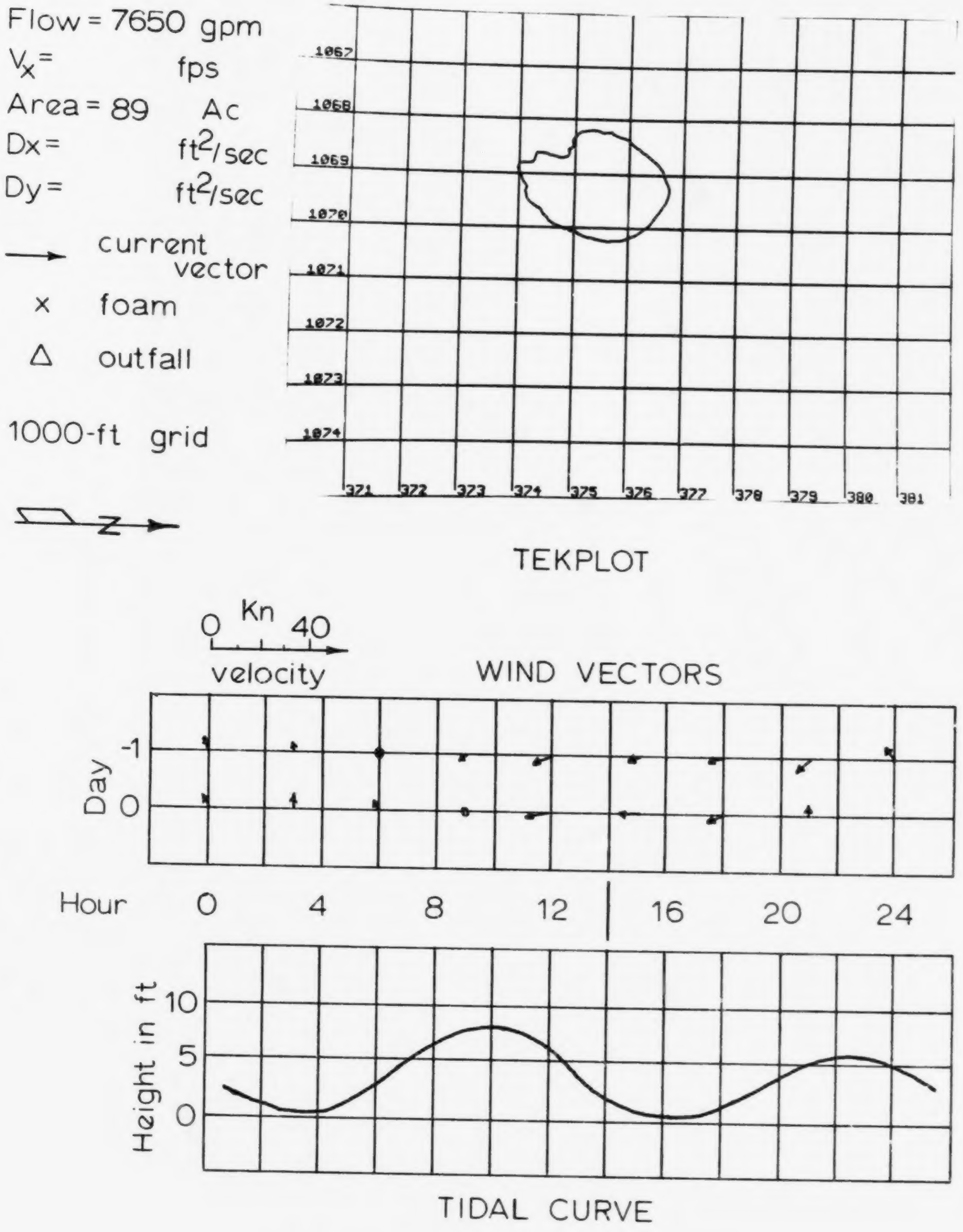

Figure 52. Data for October 12, 1970.

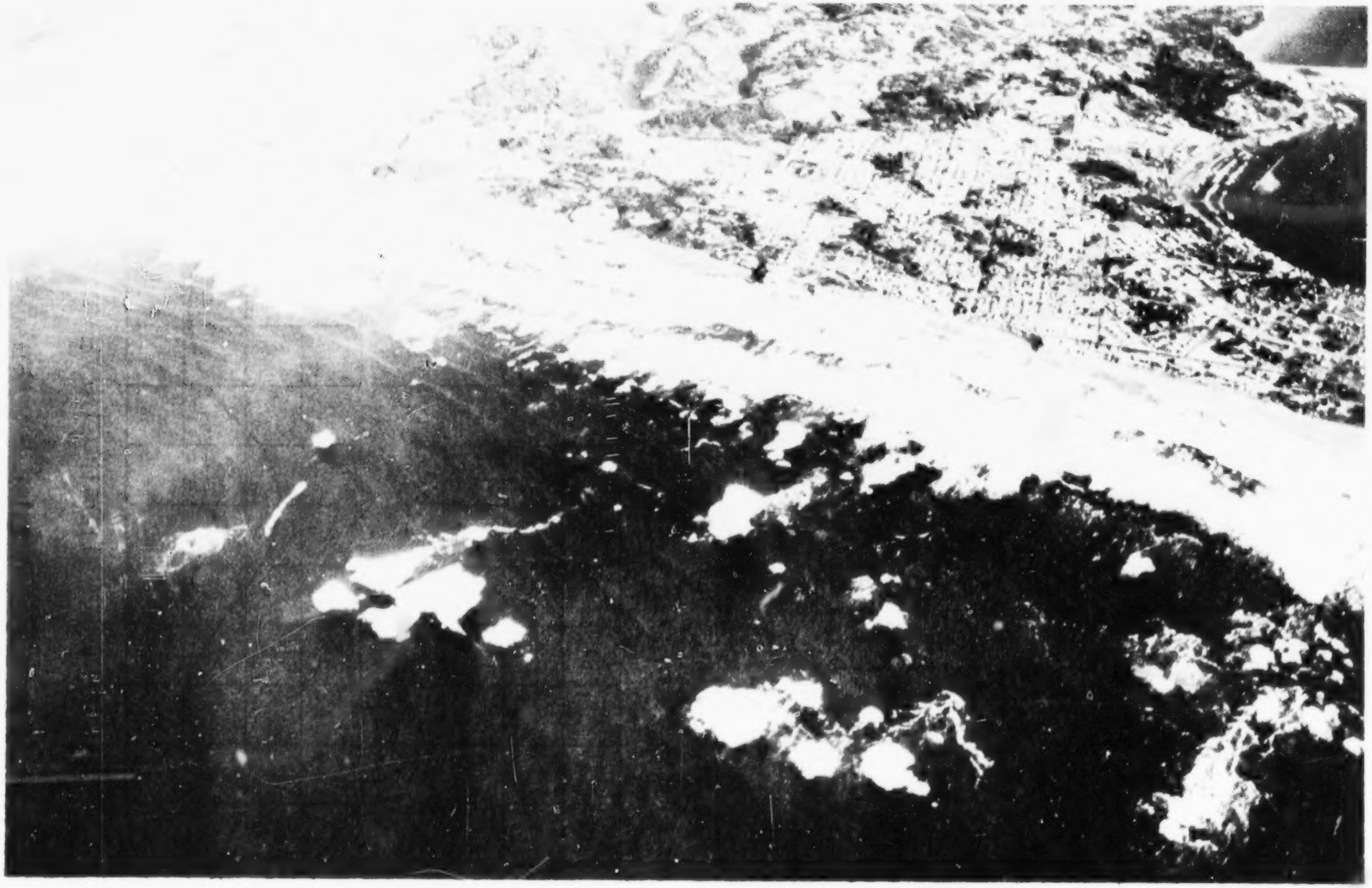

Figure 53. Aerial photo of outfall area December 21, 1970 from 6000 feet at 13:15.

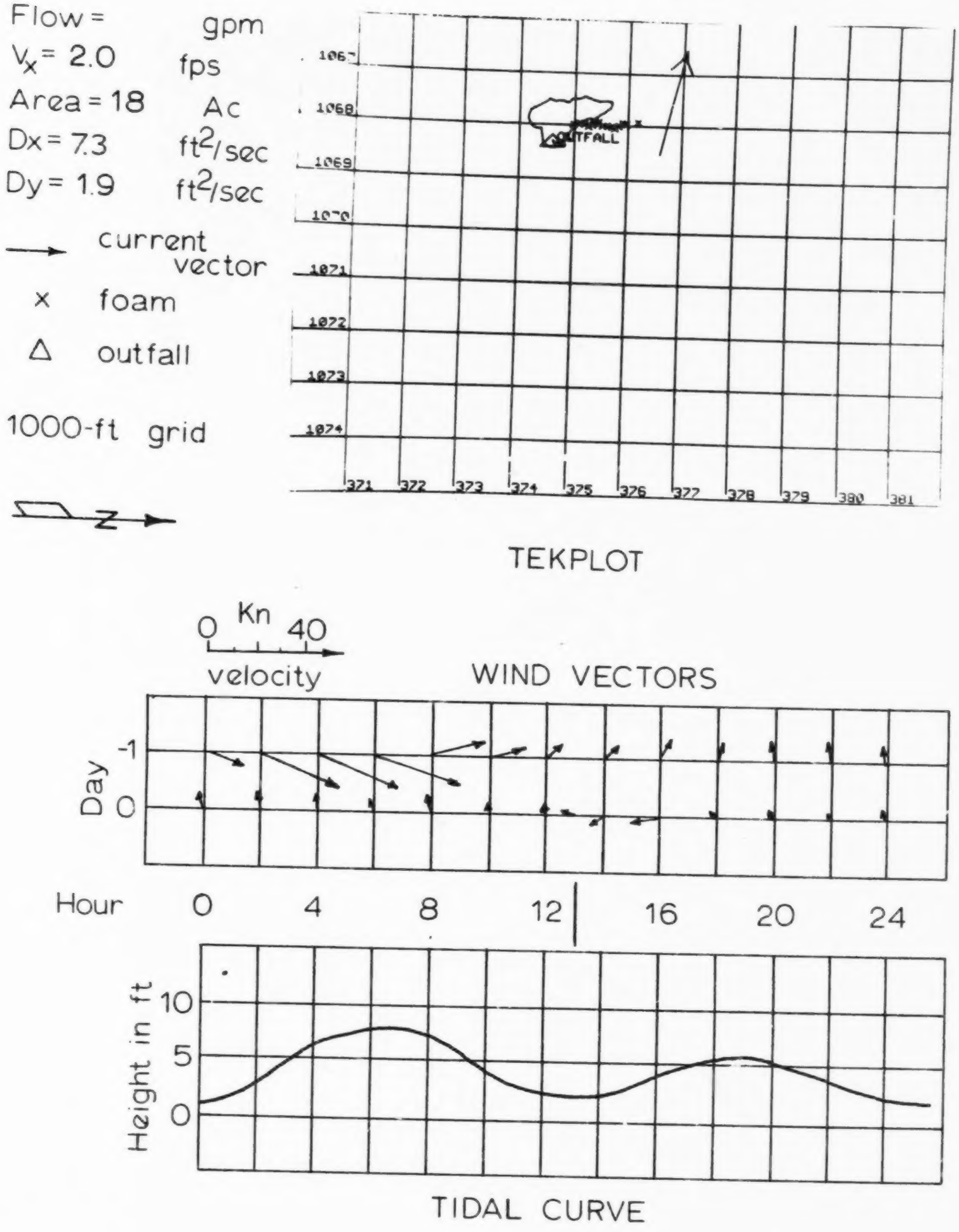

Figure 54. Data for December 21, 1970.

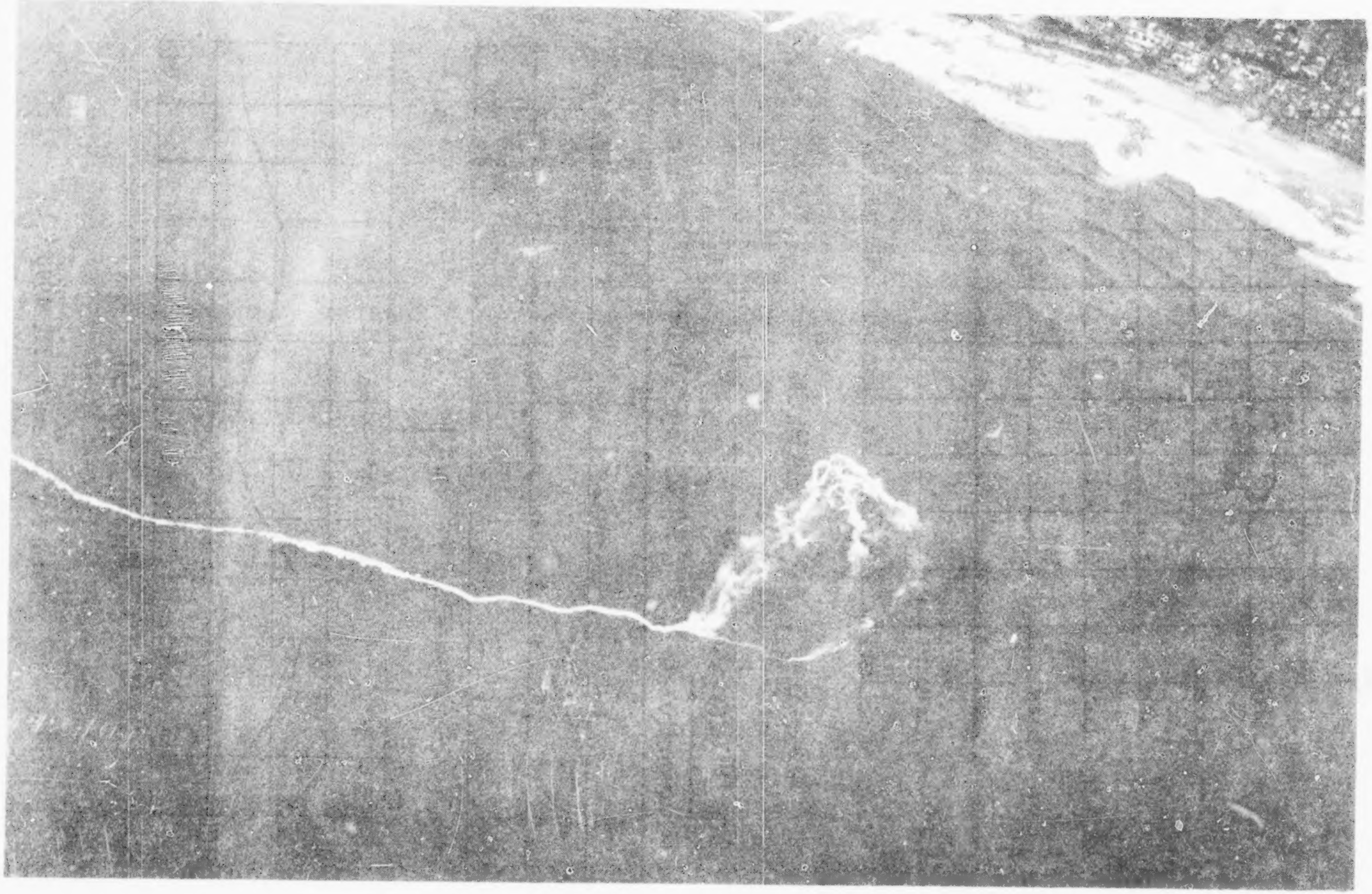

Figure 55. Aerial photo of the outfall area on December 23, 1970 from 3000 feet at 11:25.

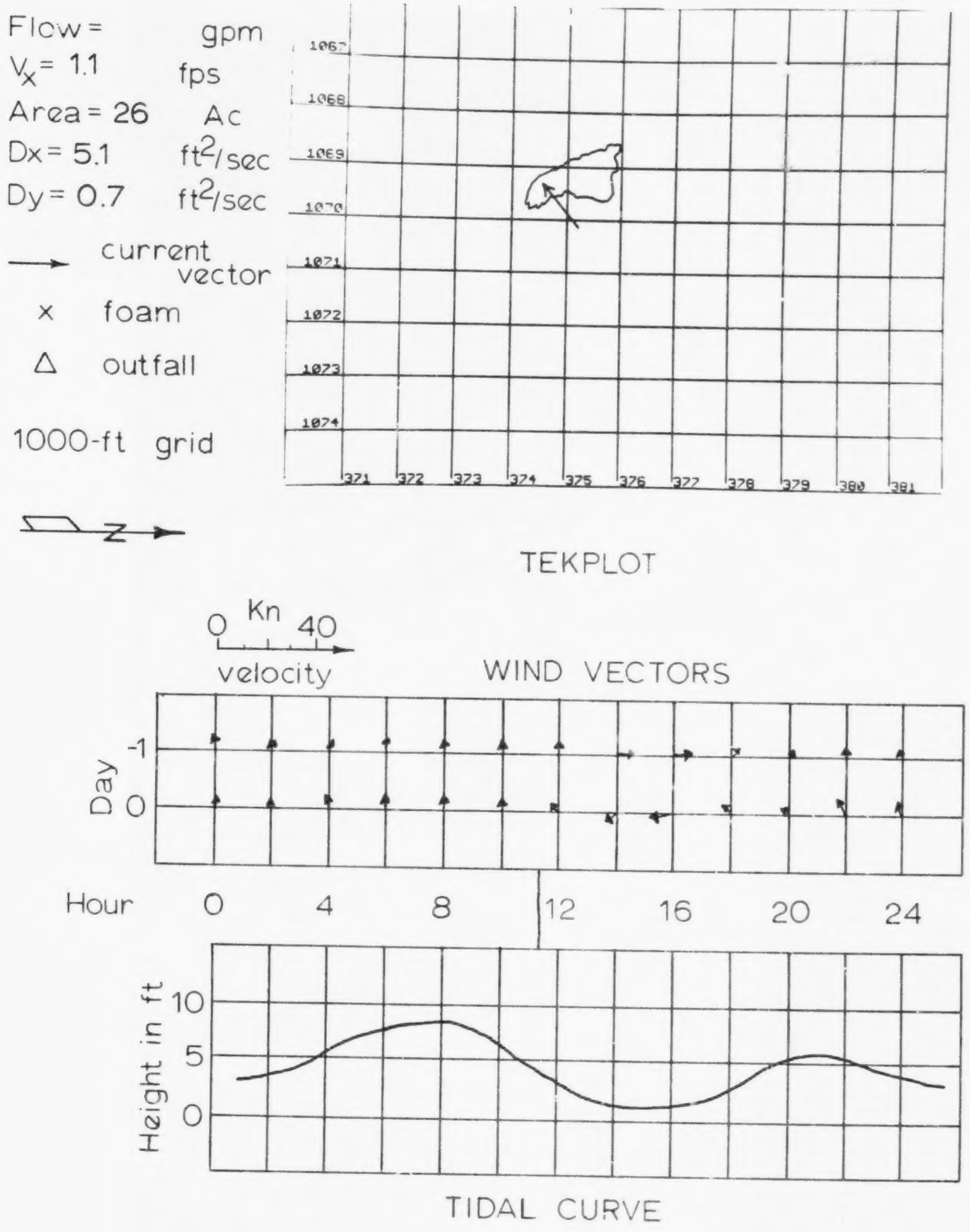

Figure 56. Data for December 23, 1970.

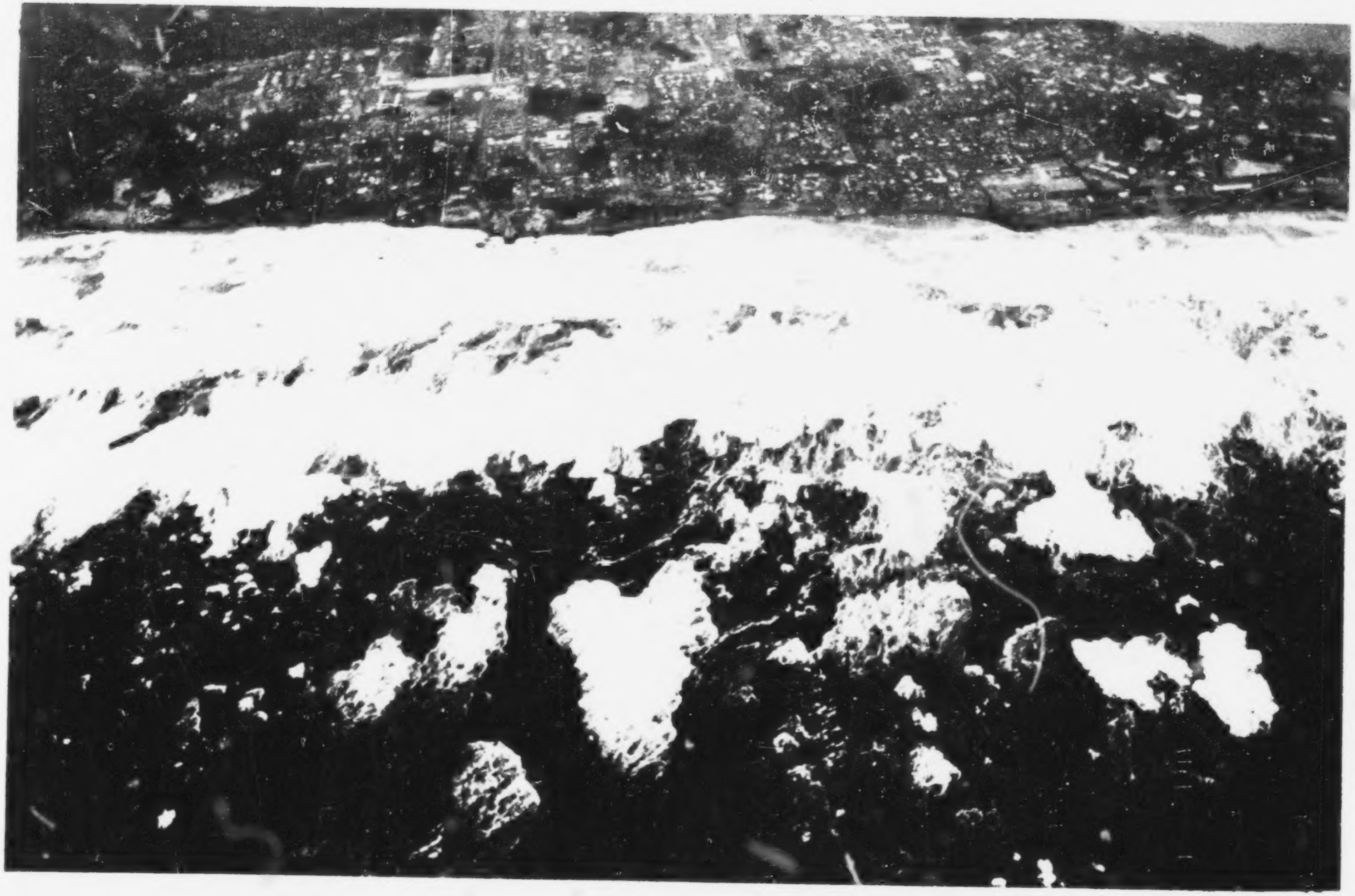

Figure 57. Aerial photo of outfall area on December 31, 1970 from 3000 feet at 12:10.

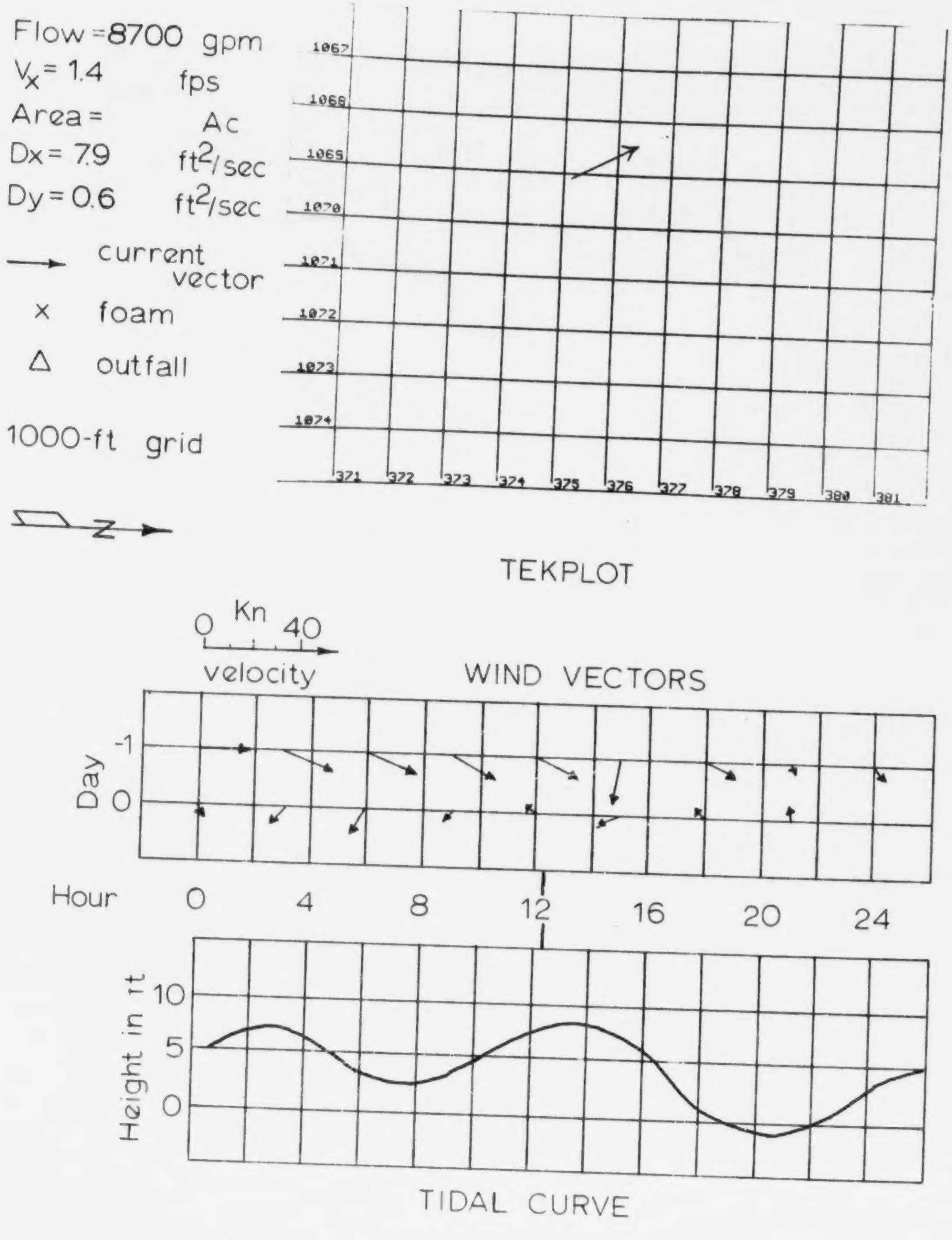

Figure 58. Data for December 31, 1970.

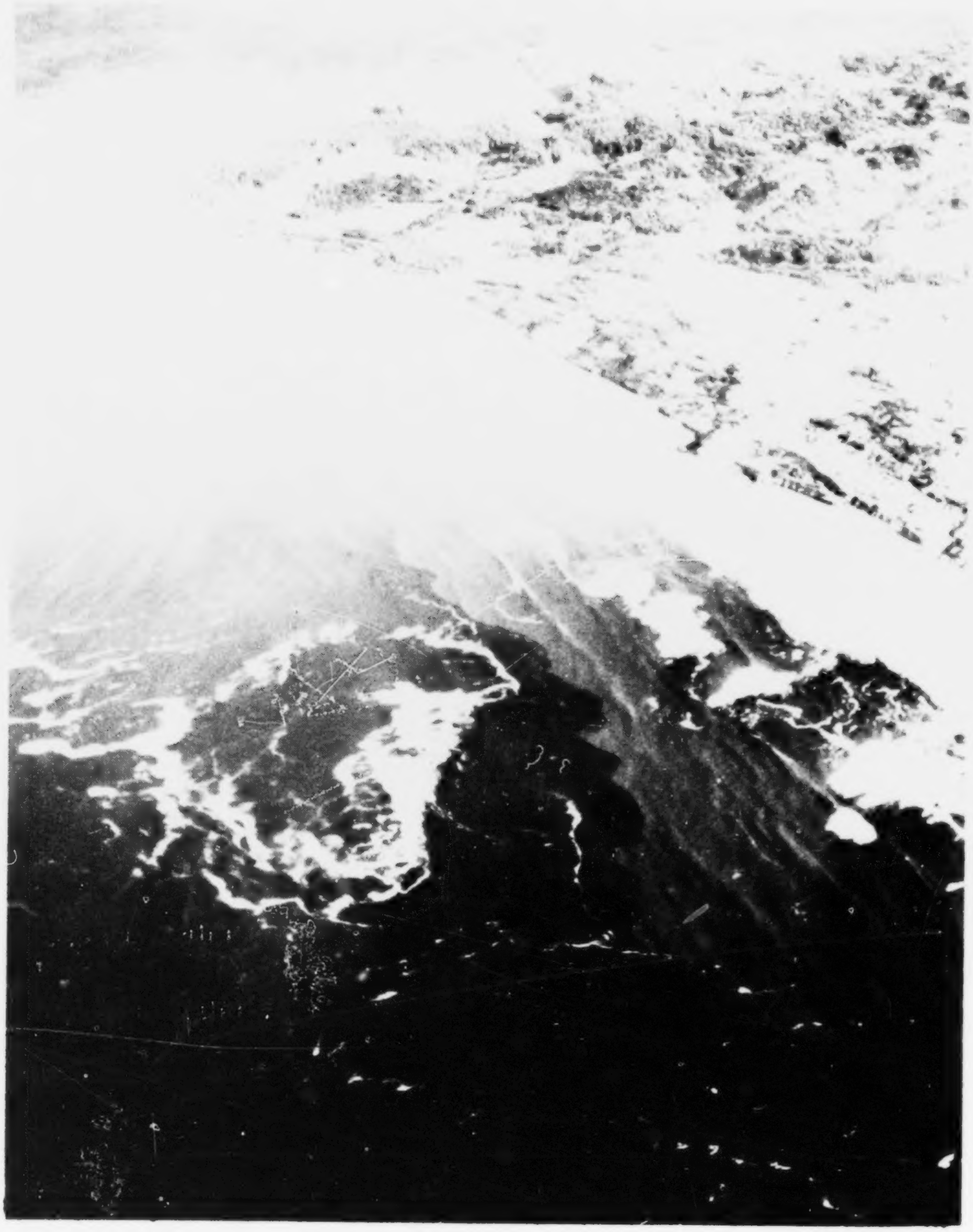

Figure 59. Aerial photo of outfall area on January 2, 1971 from 4000 feet at 11:40.

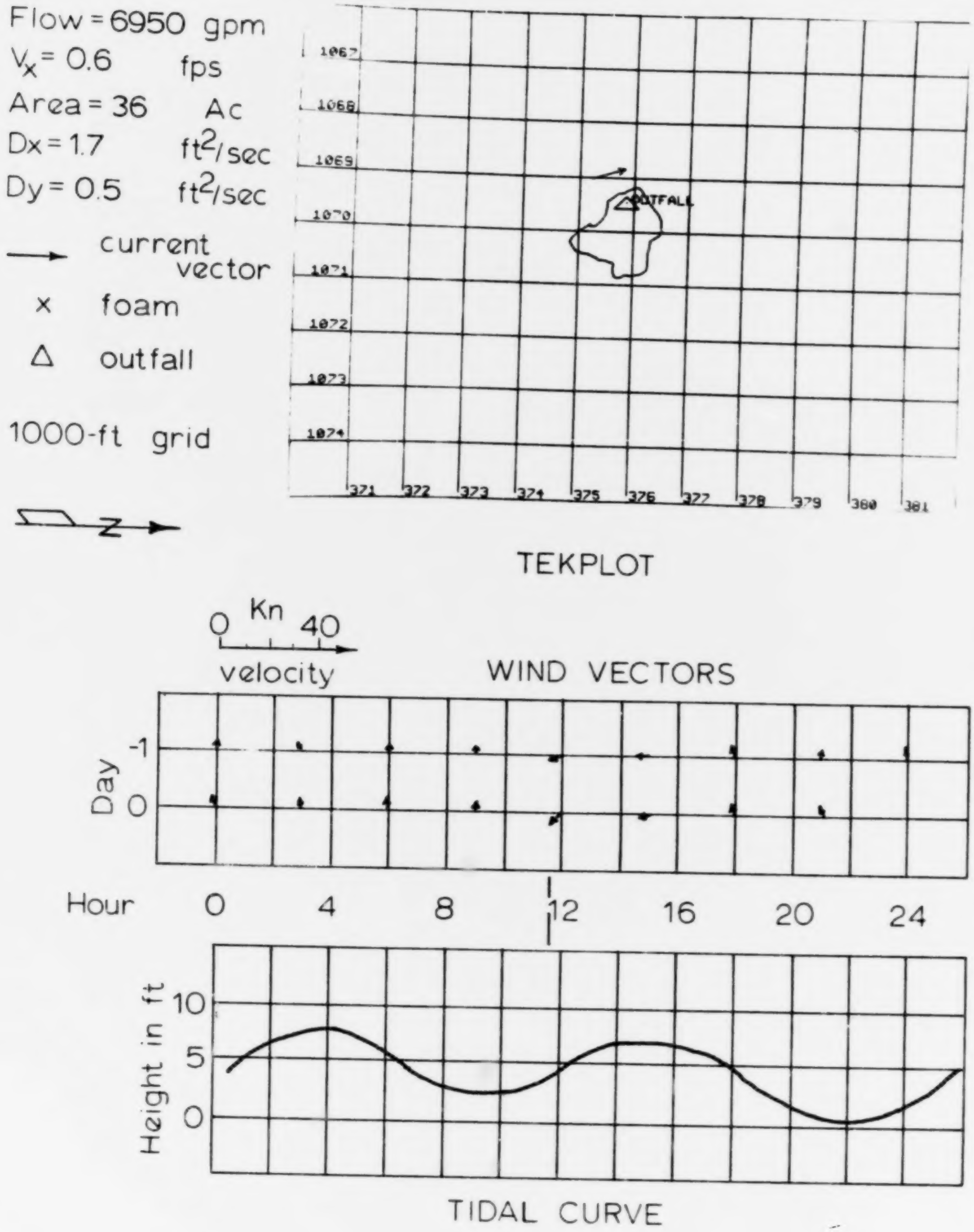

Figure 60. Data for January 2, 1971.

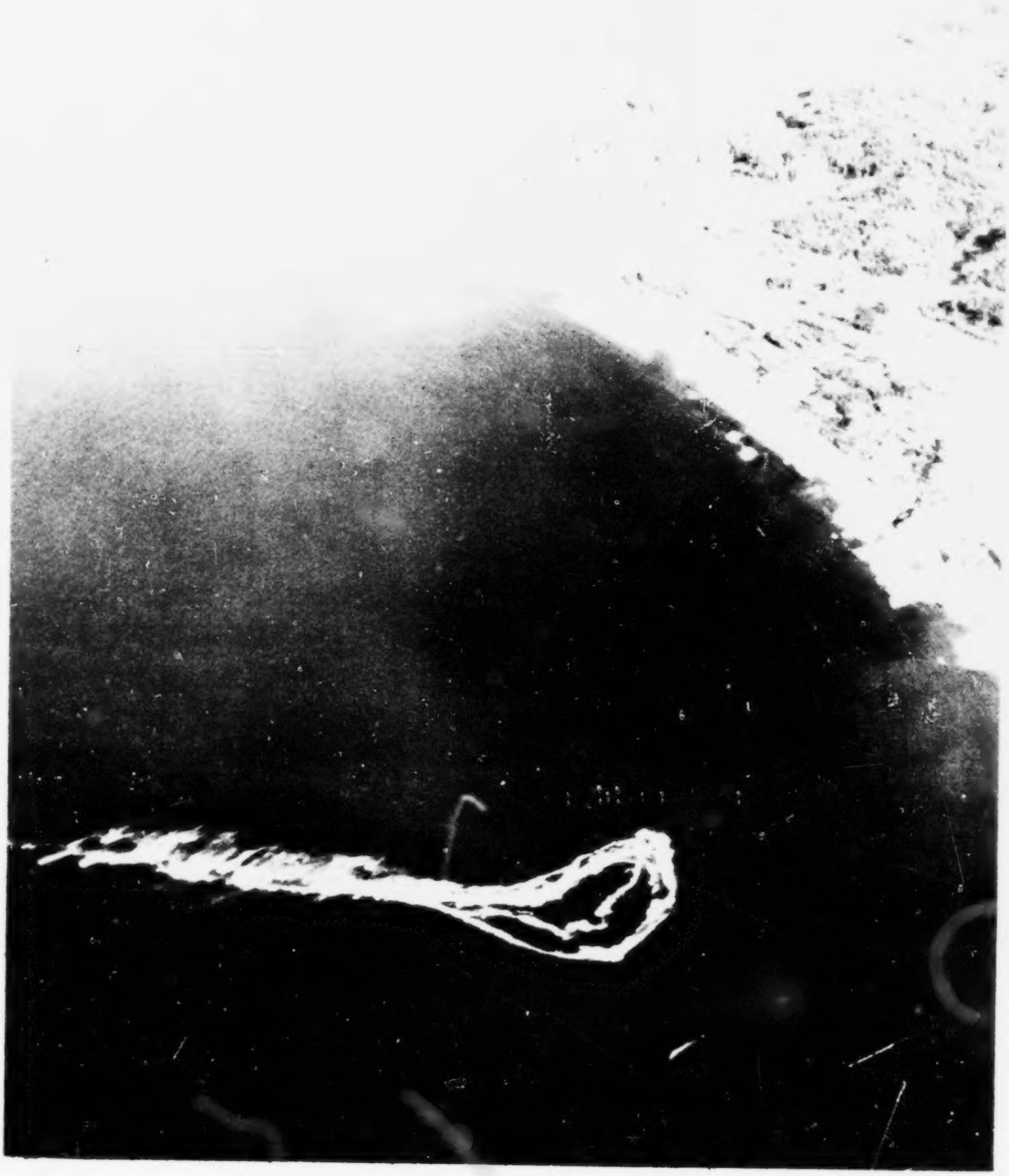

Figure 61. Aerial photo of outfall area on February 6, 1971 from 6000 feet at 11:55.

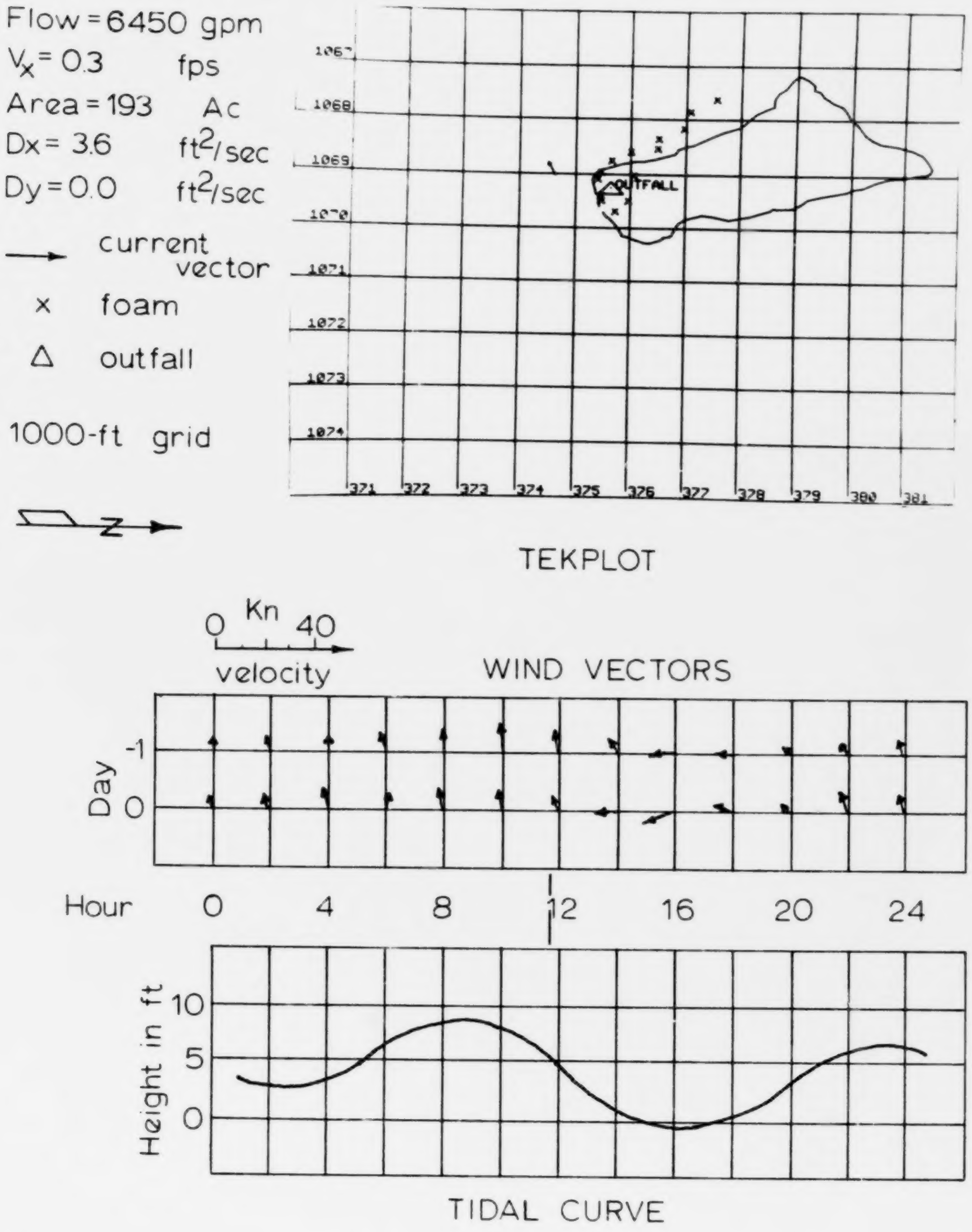

Figure 62. Data for February 6, 1971 AM.

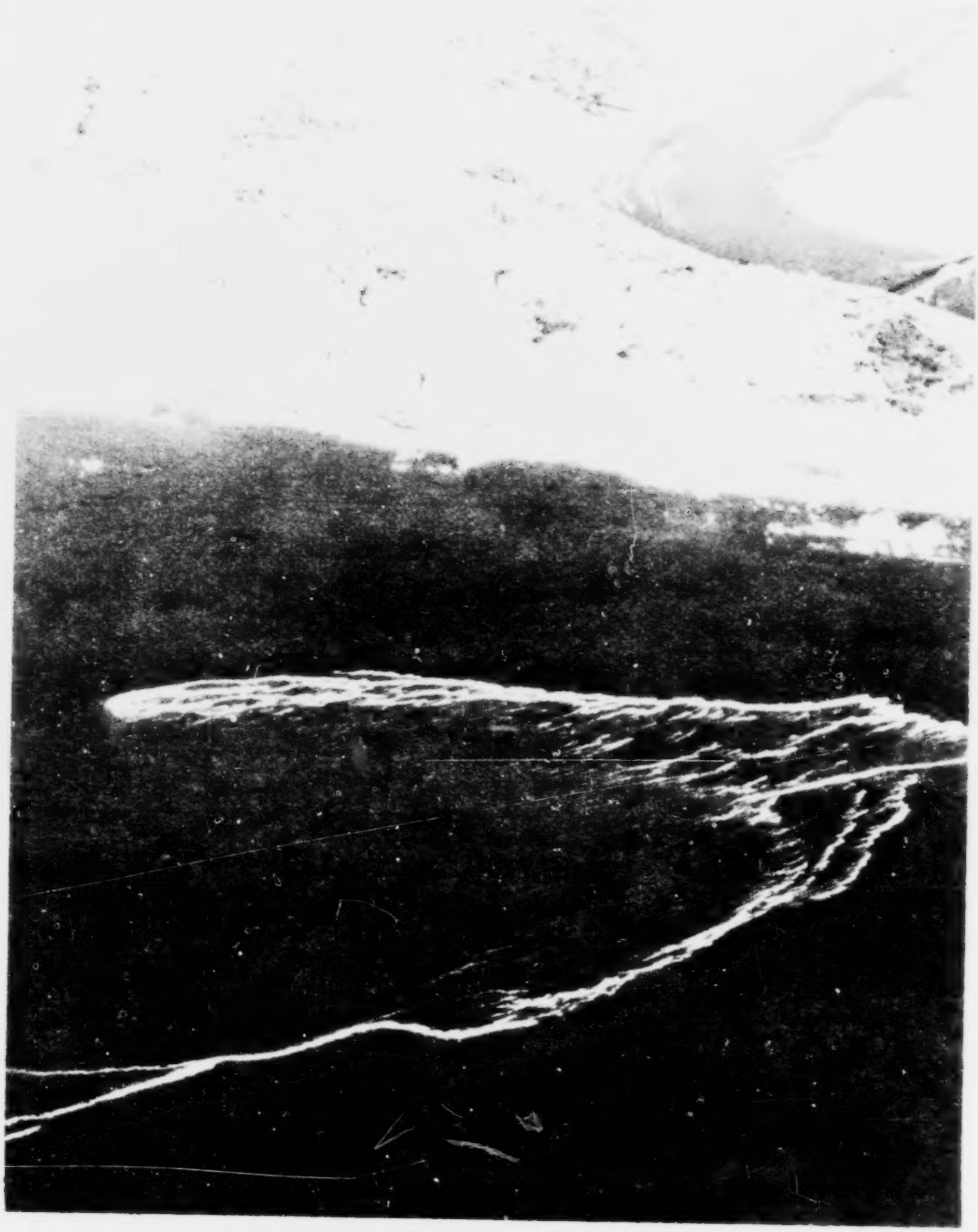

Figure 63. Aerial photo of outfall area on February 6, 1971 from 4000 feet at 14:18.

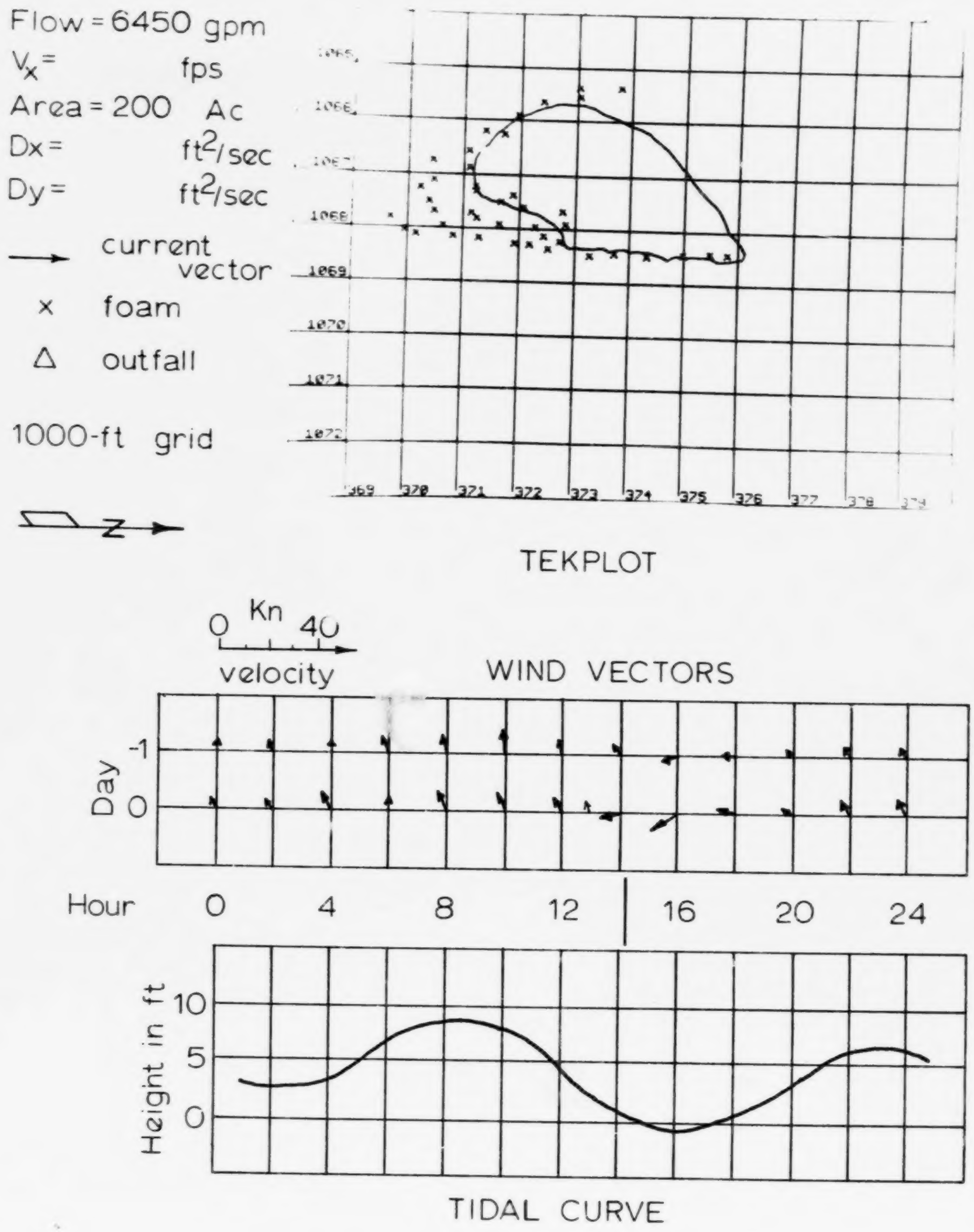

Figure 64. Data for February 6, 1971 PM.

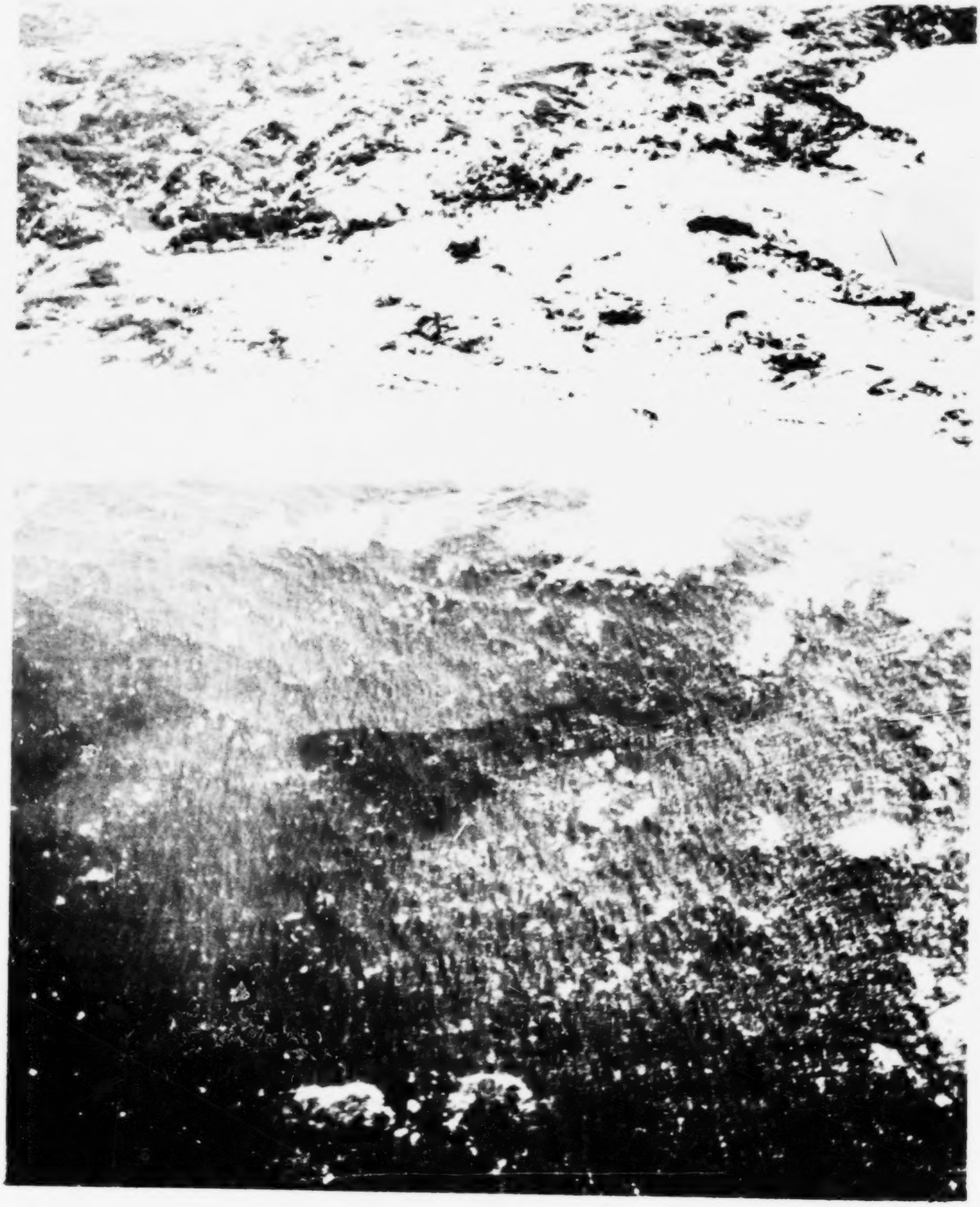

Figure 65. Aerial photo of outfall area on March 16, 1971 from 4250 feet at 12:20.

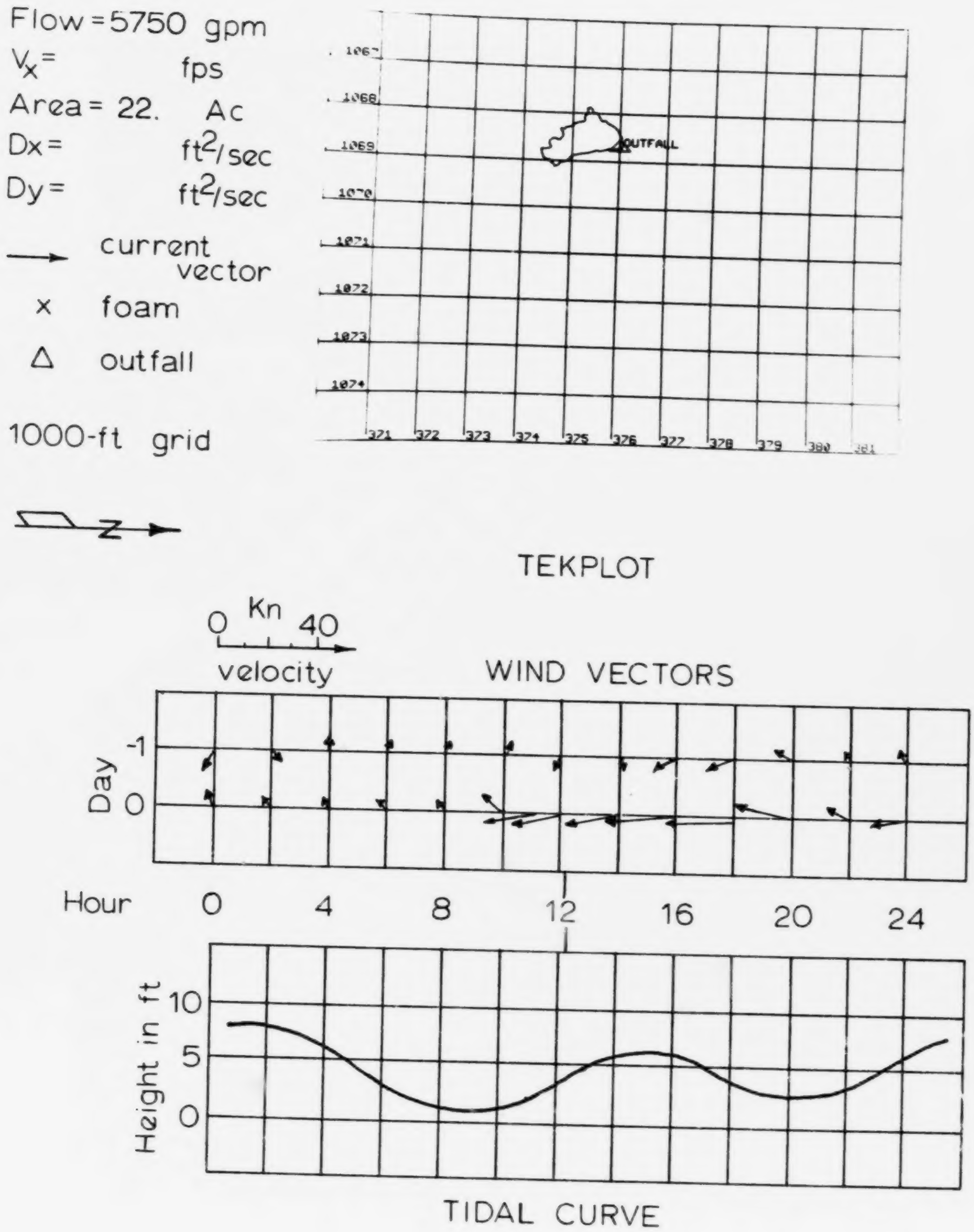

Figure 66. Data for March 16, 1971.

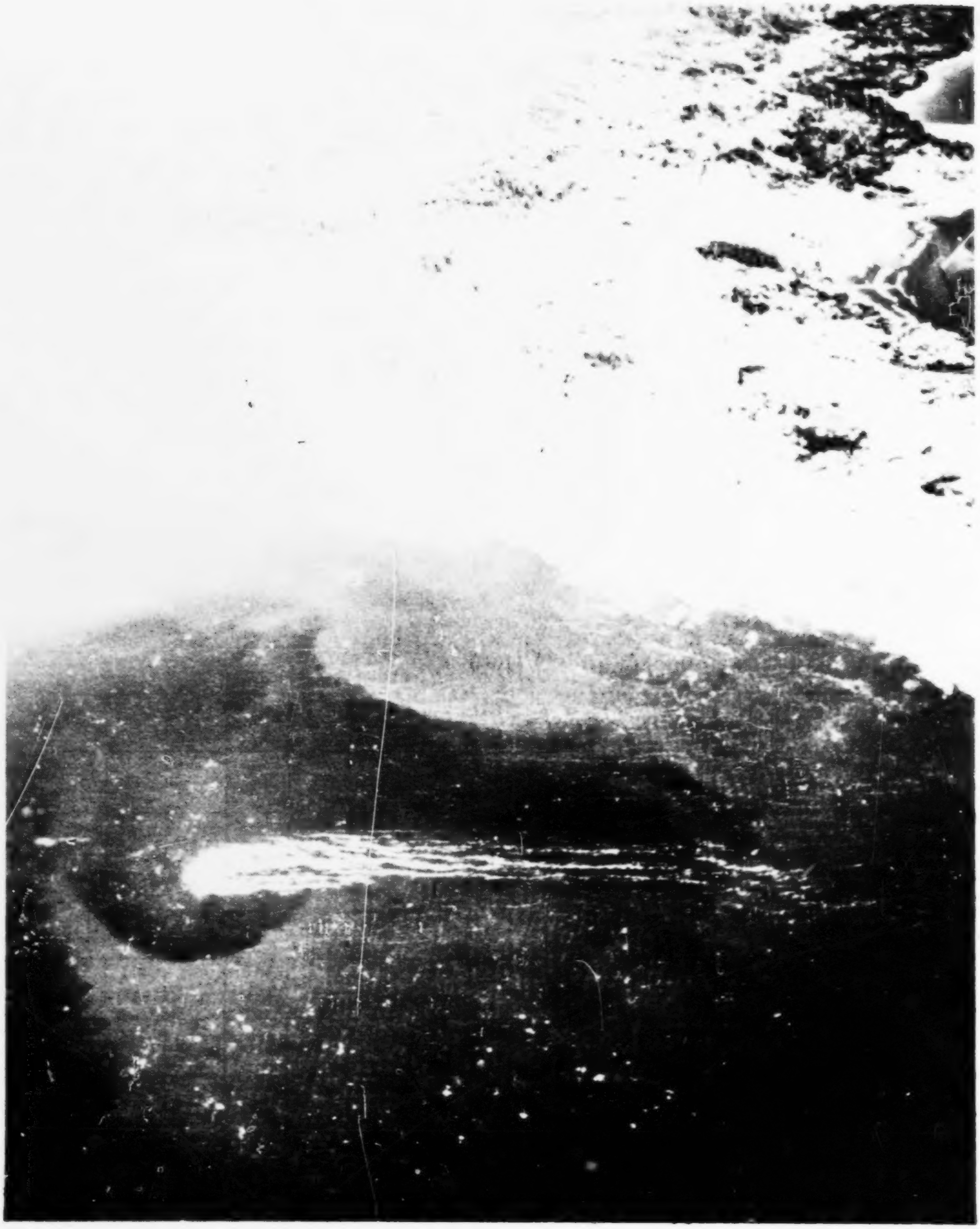

Figure 67. Aerial photo of outfall area on March 17, 1971 from 4000 feet at 14:25.

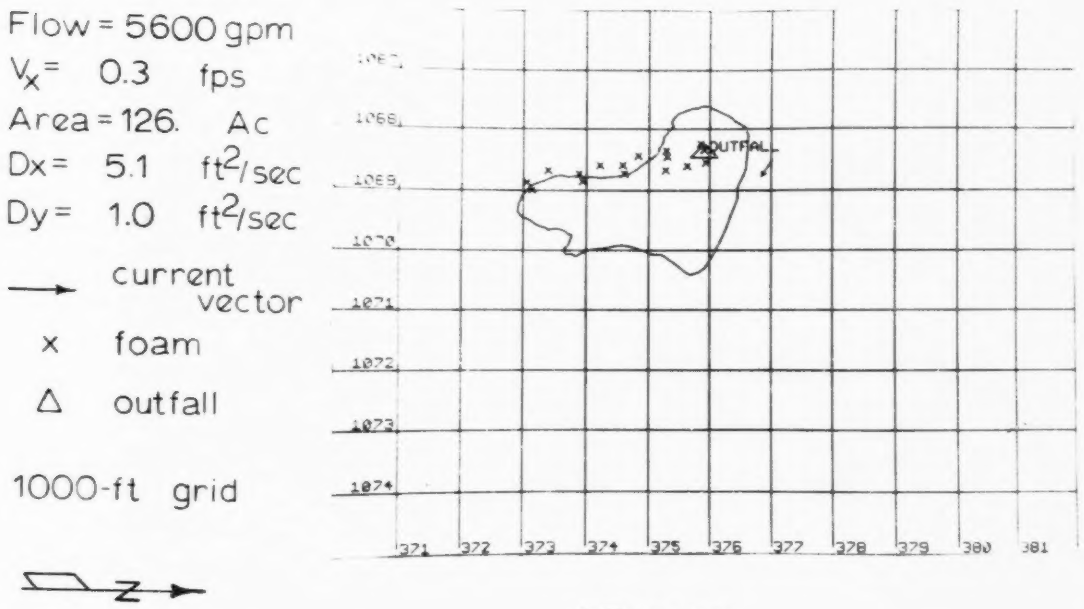

TEKPLOT

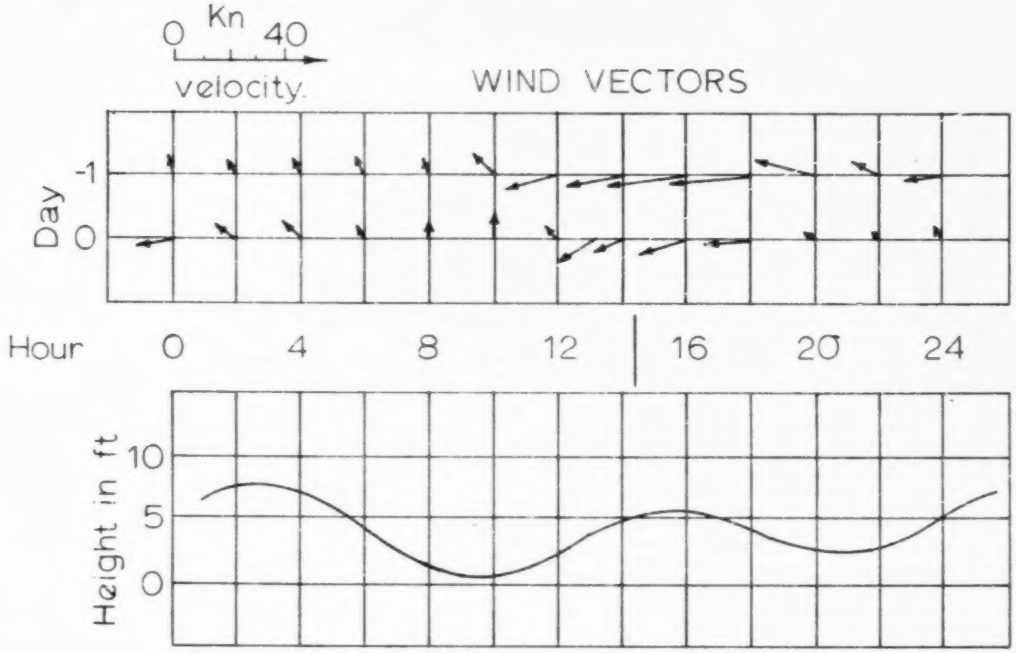

TIDAL CURVE

Figure 68. Data for March 17, 1971.

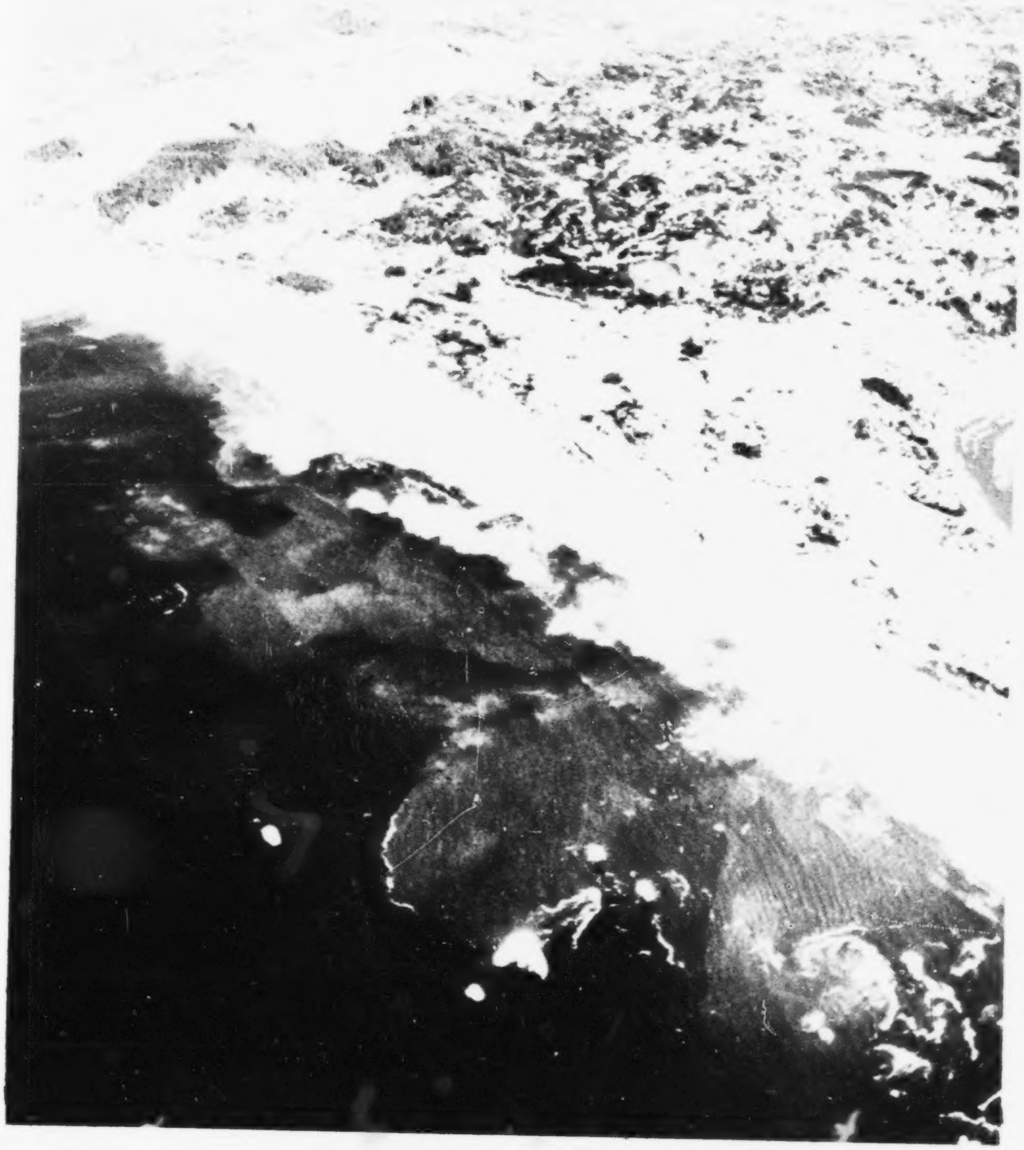

Figure 69. Aerial photo of outfall area on March 18, 1971 from 8000 feet at 11:42.

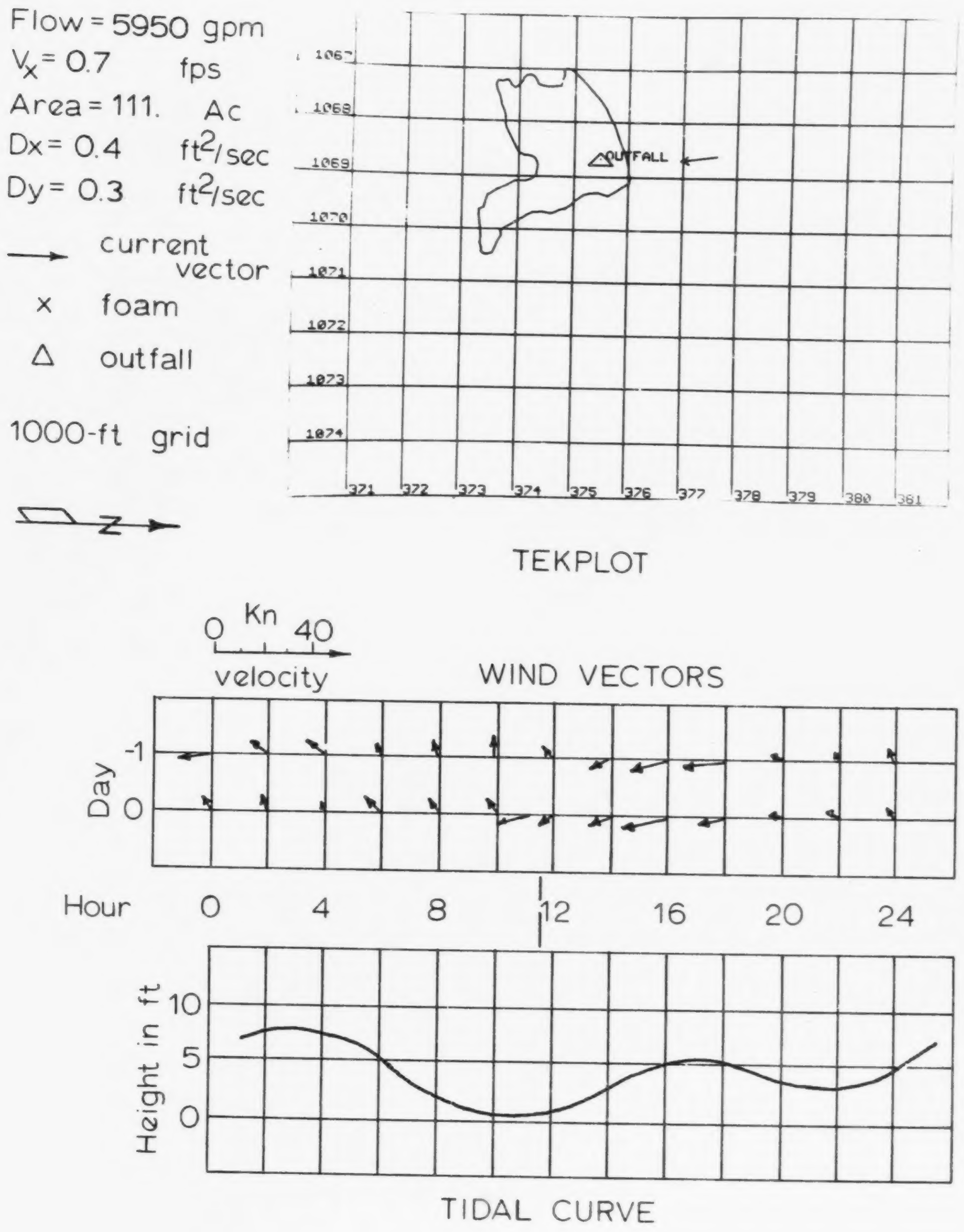

Figure 70. Data for March 18, 1971.

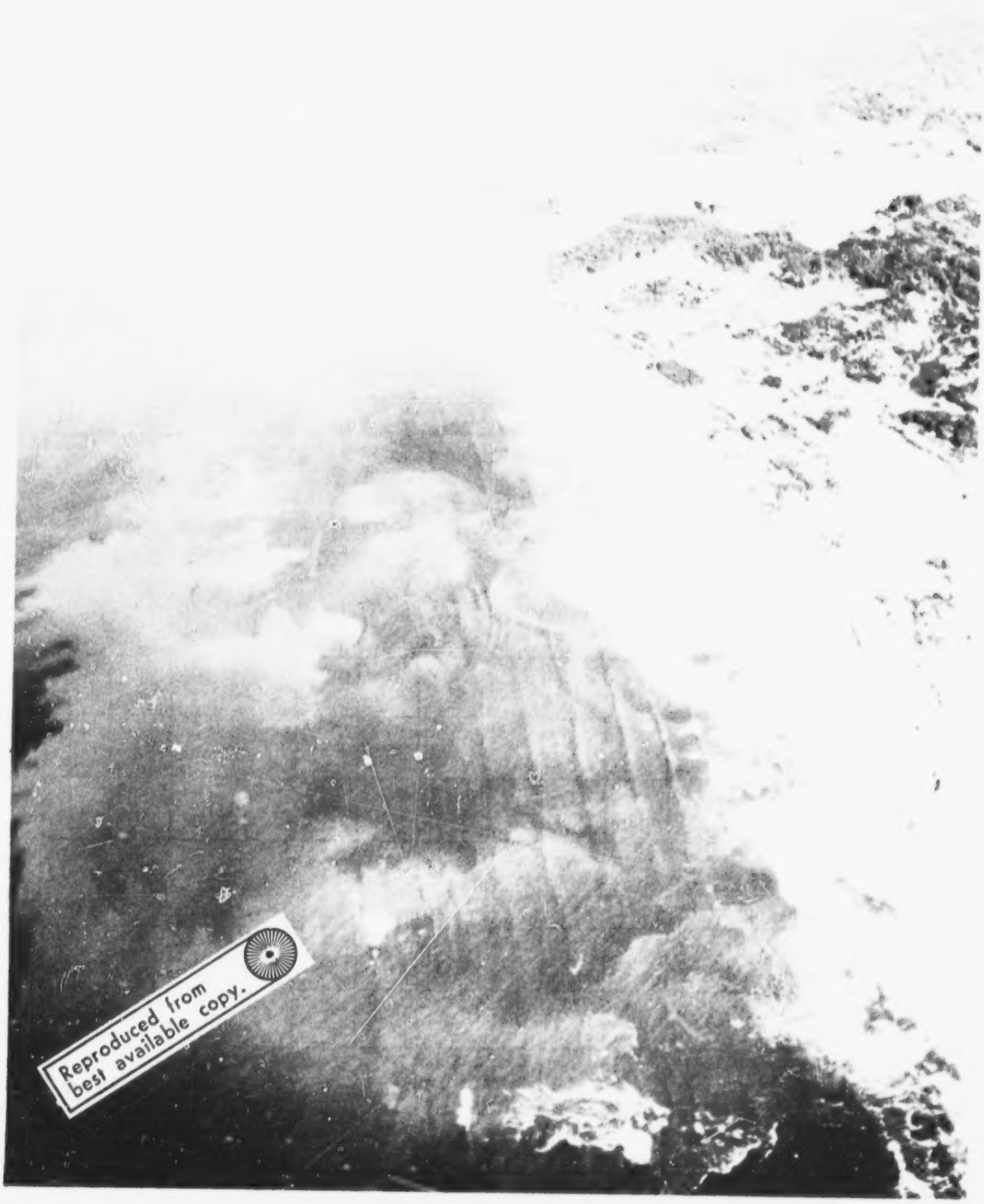

Reproduced from
best available copy.

Figure 71. Aerial photo of outfall area on March 19, 1971
from 8000 feet at 11:27.

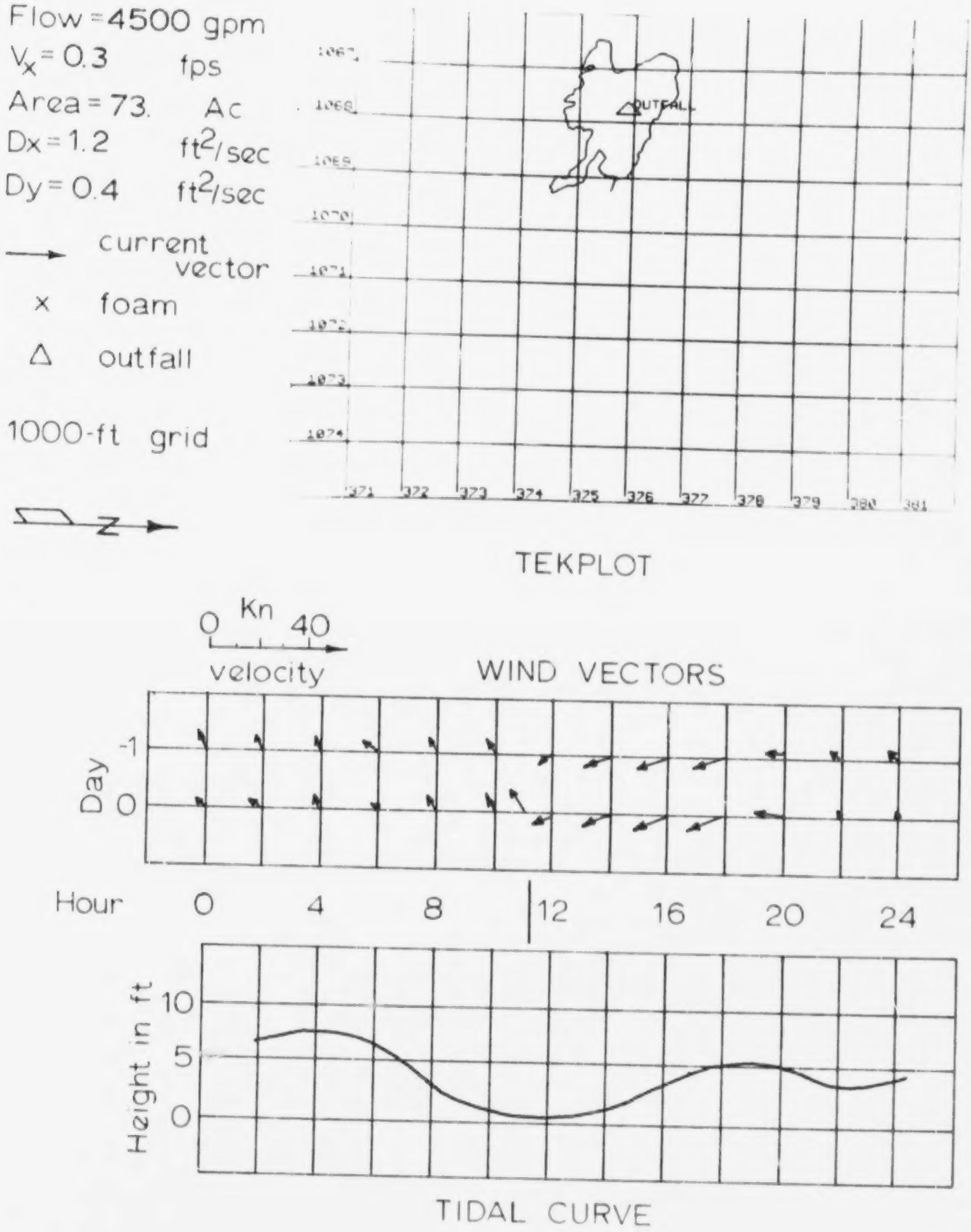

Figure 72. Data for March 19, 1971 AM.

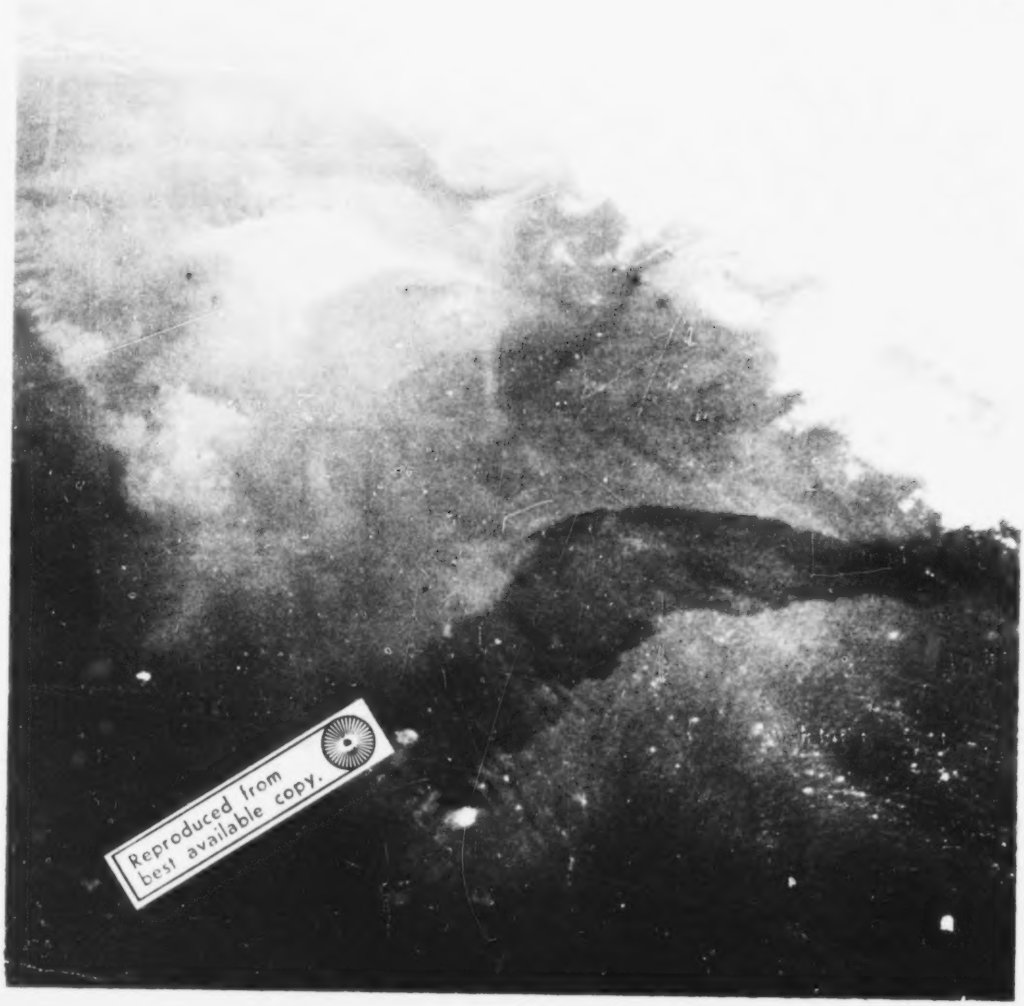

Reproduced from best available copy.

Figure 73. Aerial photo of outfall area on March 19, 1973 from 6000 feet at 13:50.

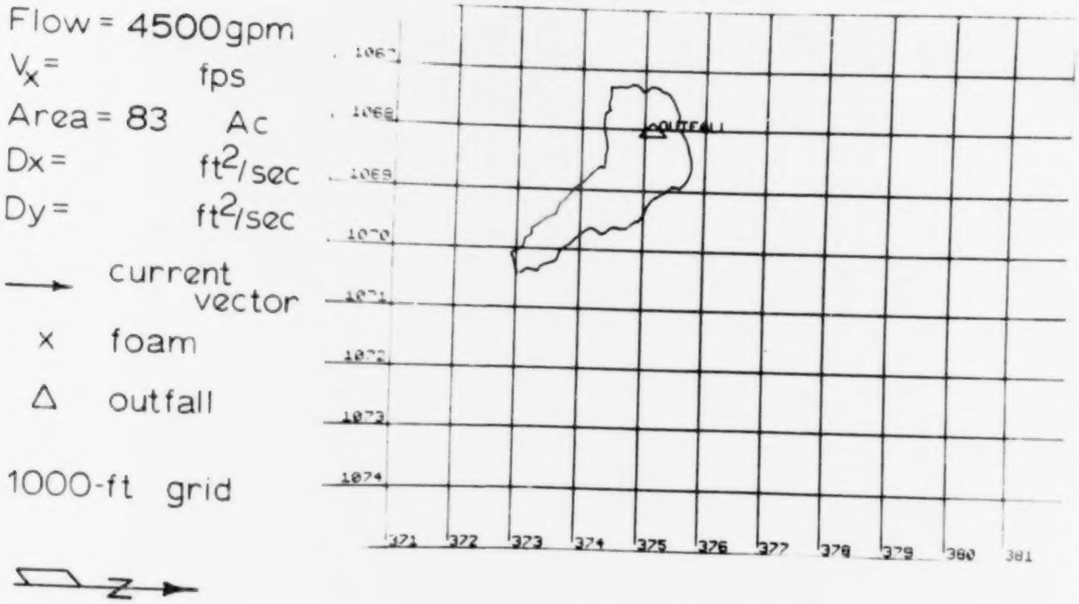

TEKPLOT

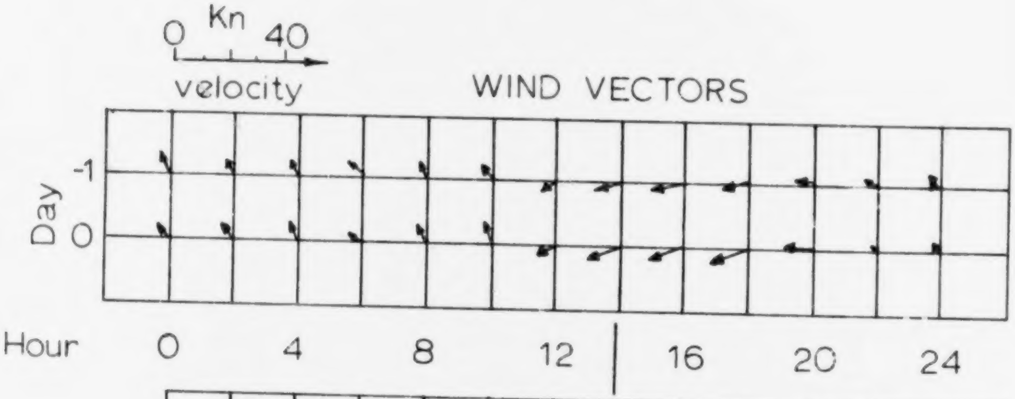

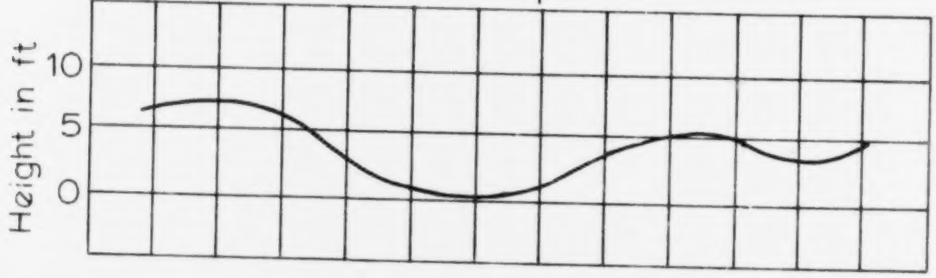

TIDAL CURVE

Figure 74. Data for March 19, 1971 PM.

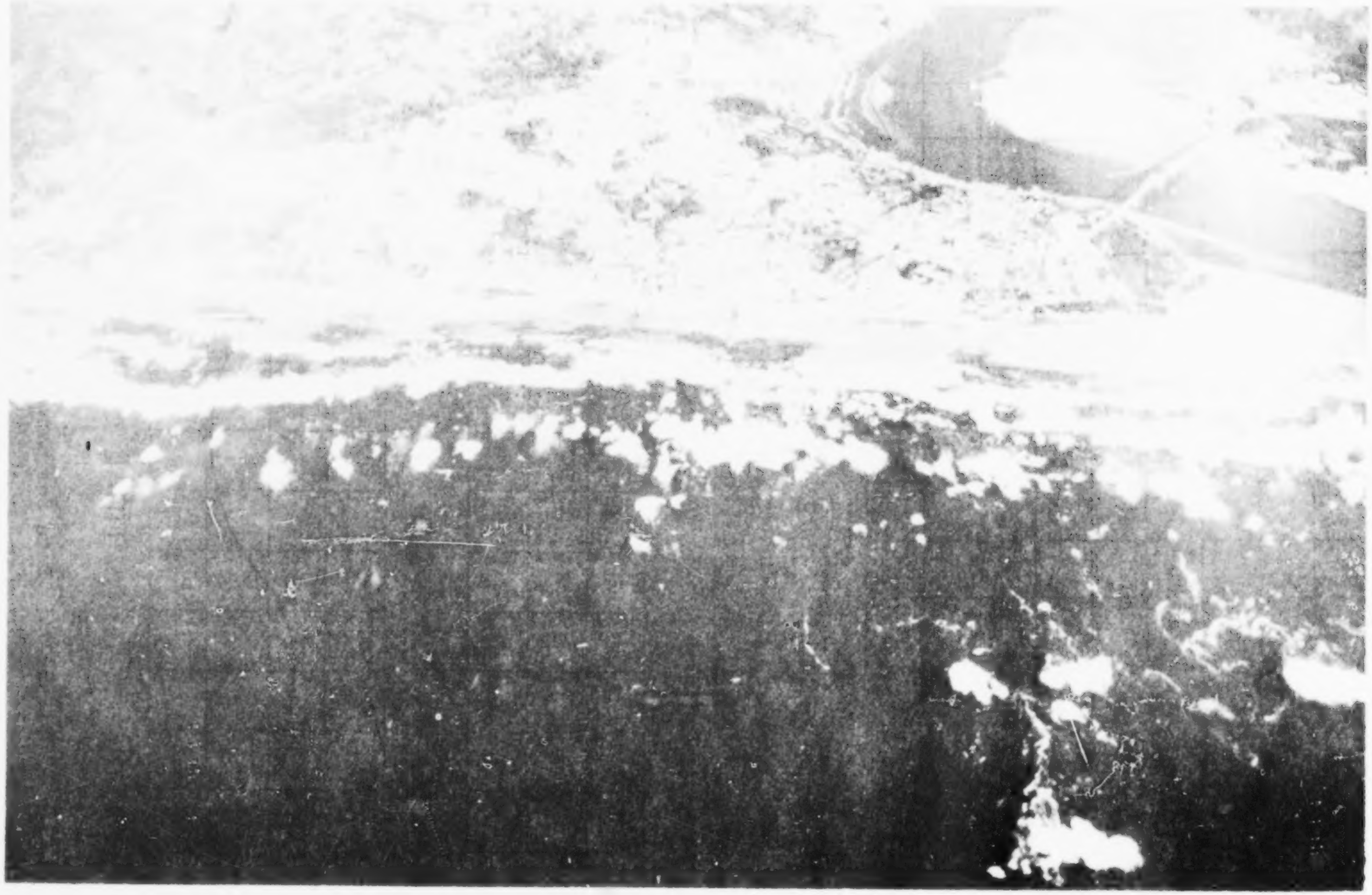

Figure 75. Aerial photo of outfall area on March 24, 1971 from 6000 feet at 16:00.

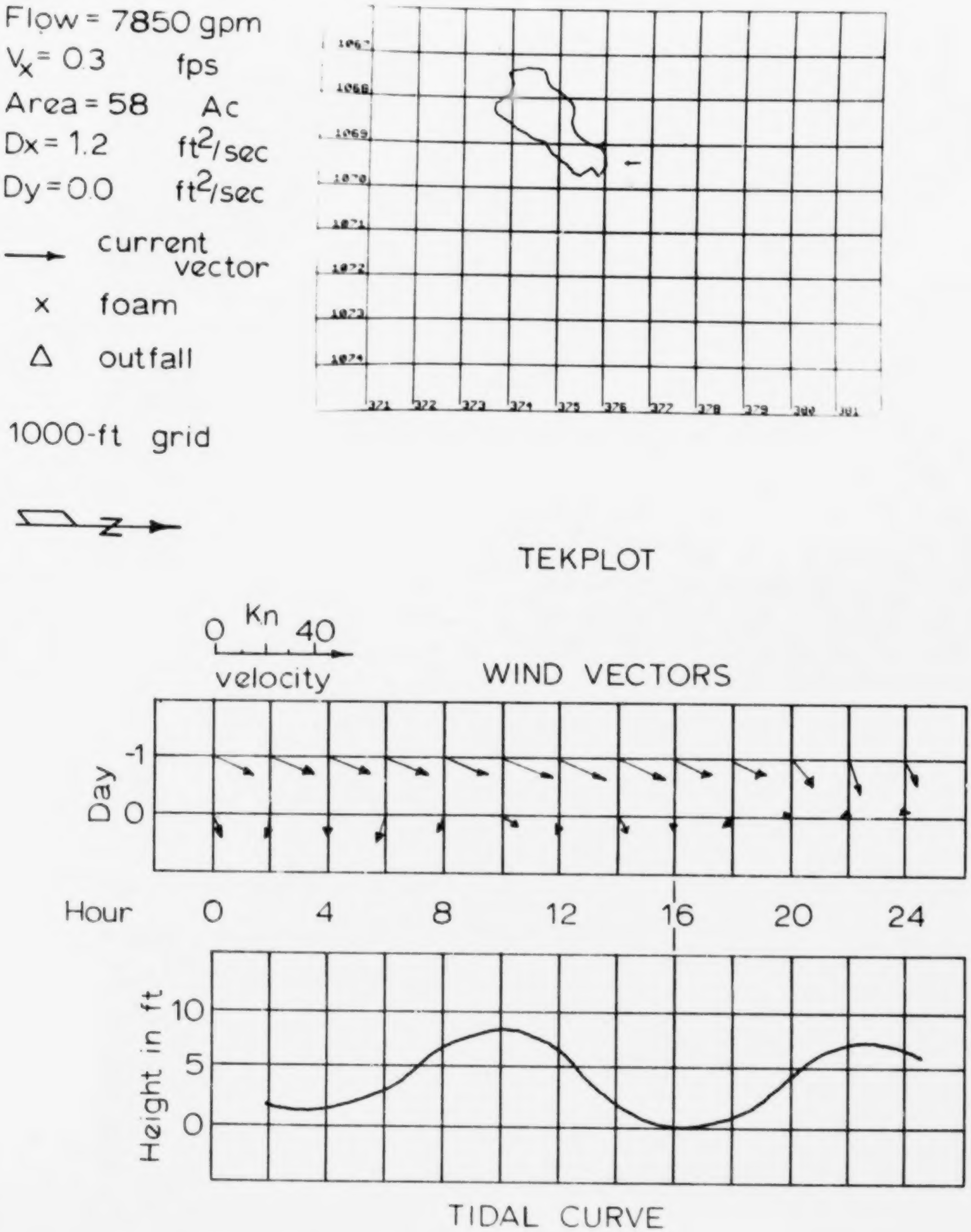

TEKPLOT

WIND VECTORS

TIDAL CURVE

Figure 76. Data for March 24, 1971.

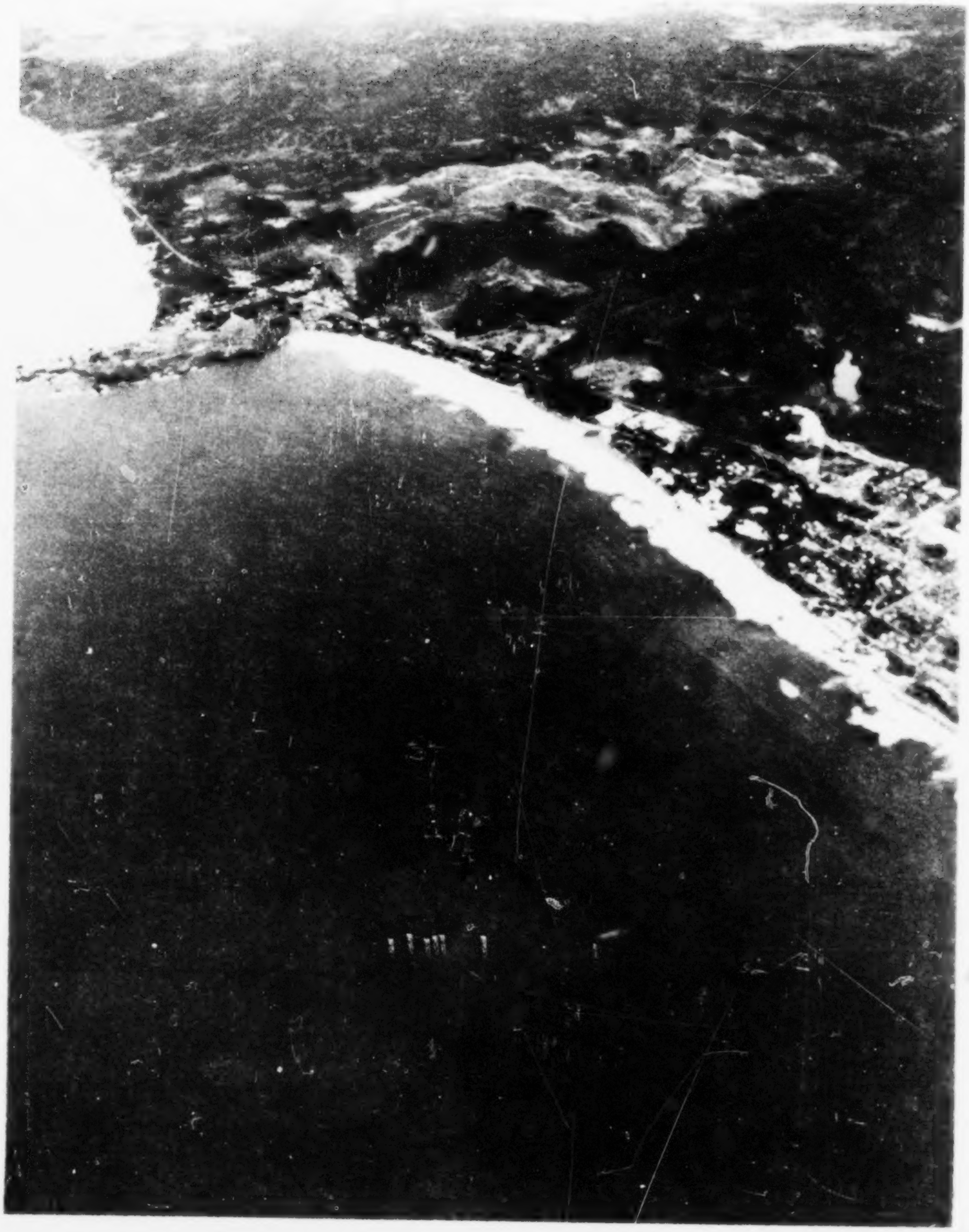

Figure 77. Aerial photo of outfall area on April 12, 1971 from 6000 feet at 14:45.

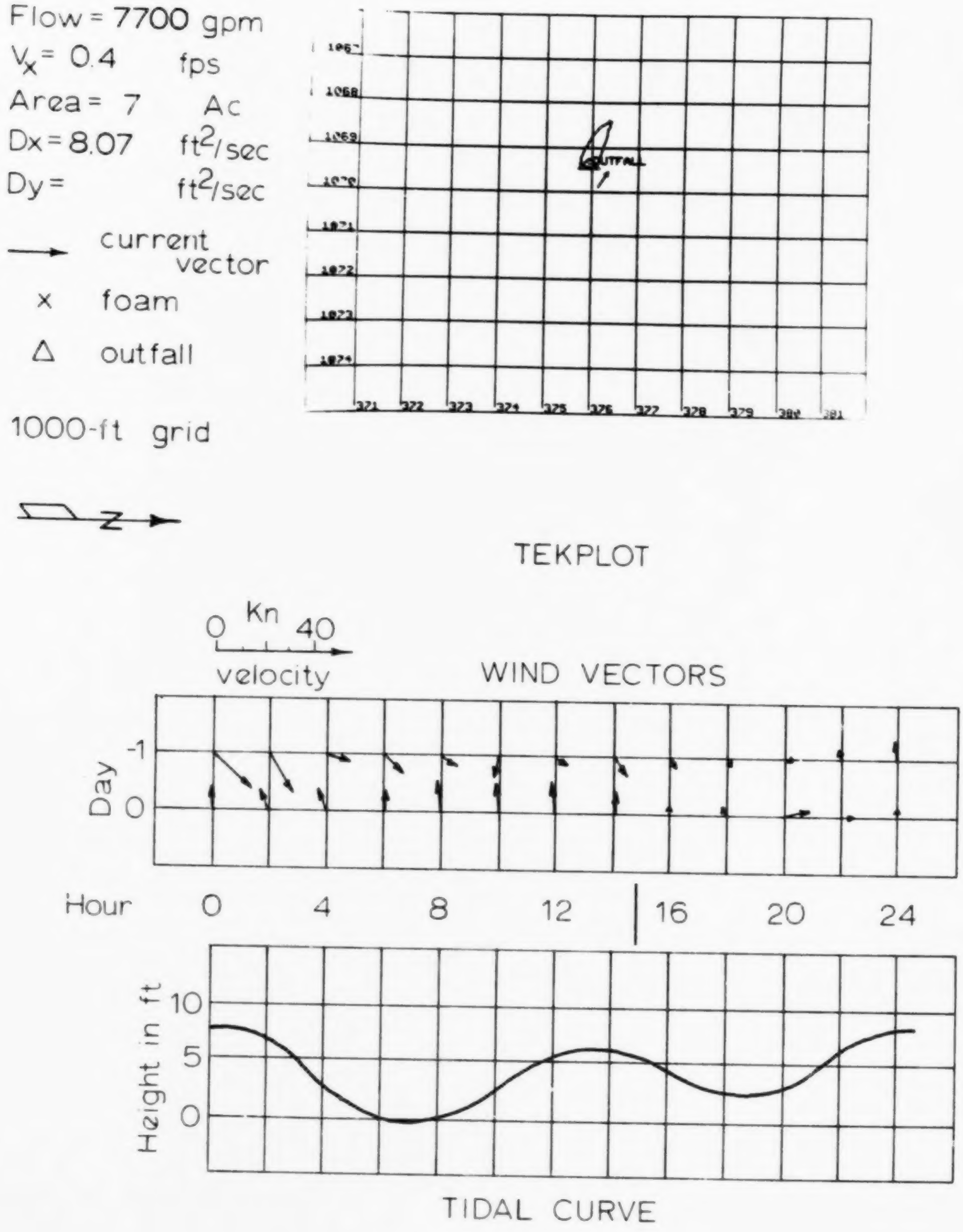

Figure 78. Data for April 12, 1971.

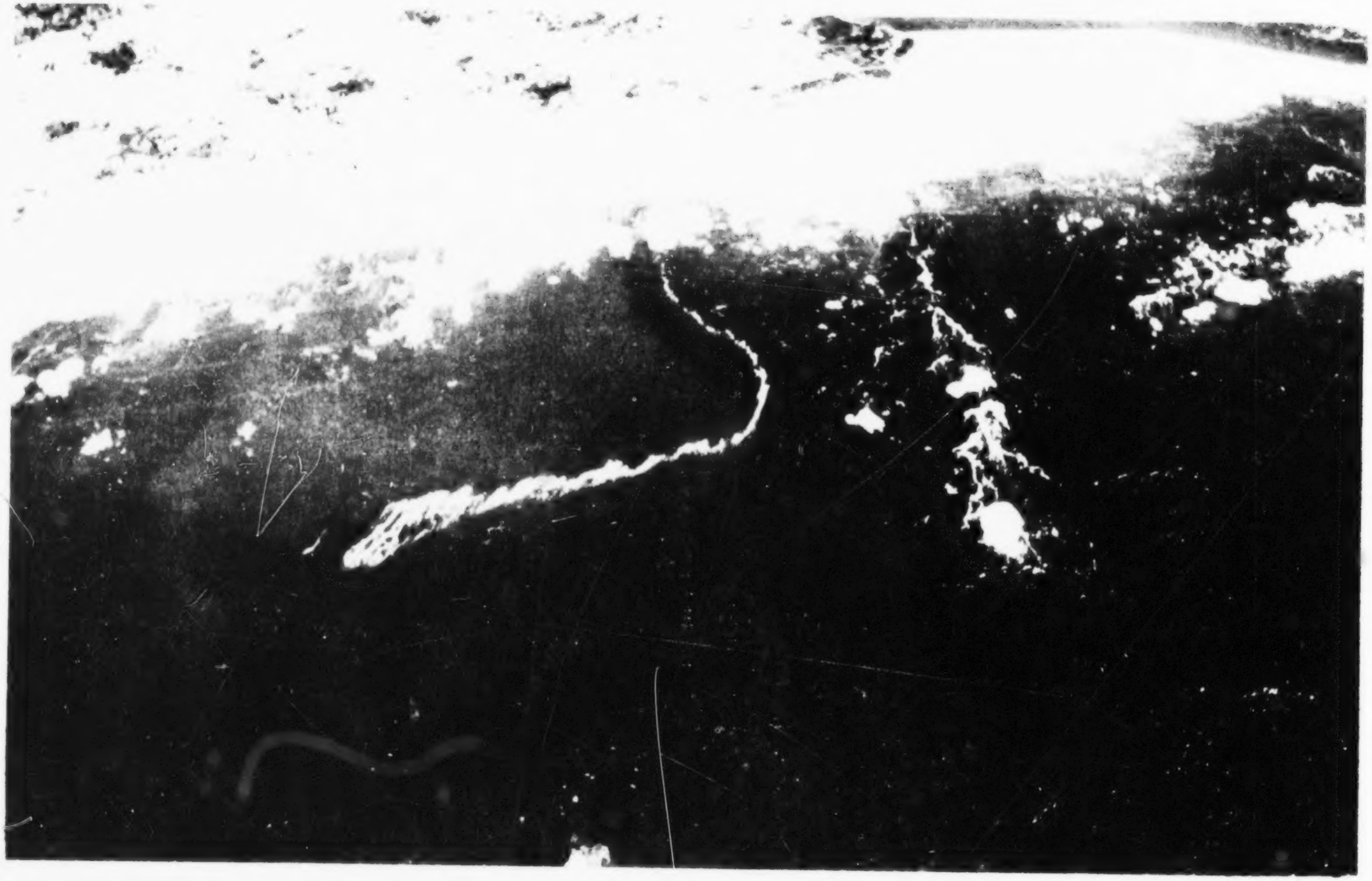

Figure 79. Aerial photo of outfall area on April 15, 1971 from 4000 feet at 14:07.

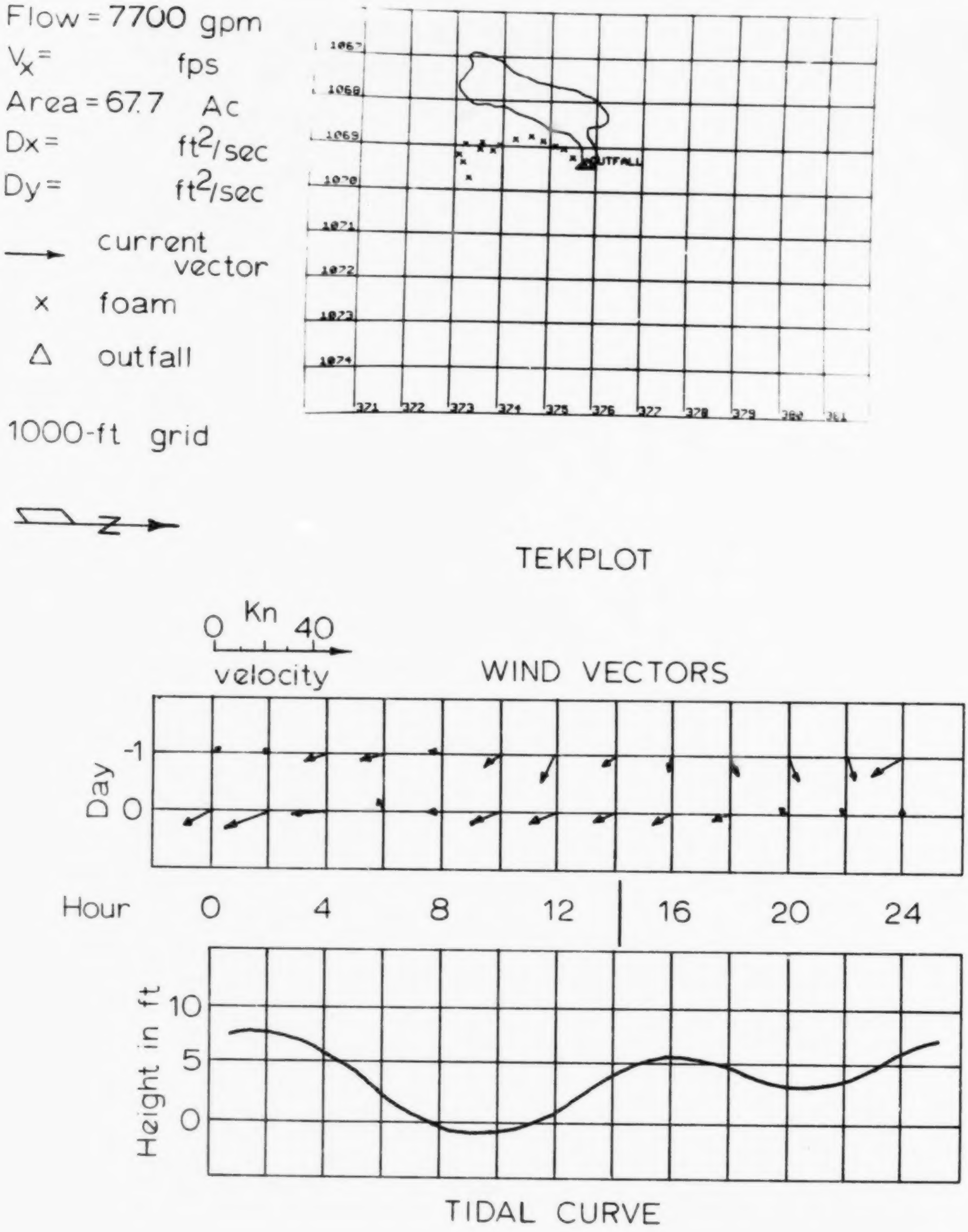

Figure 80. Data for April 15, 1971.

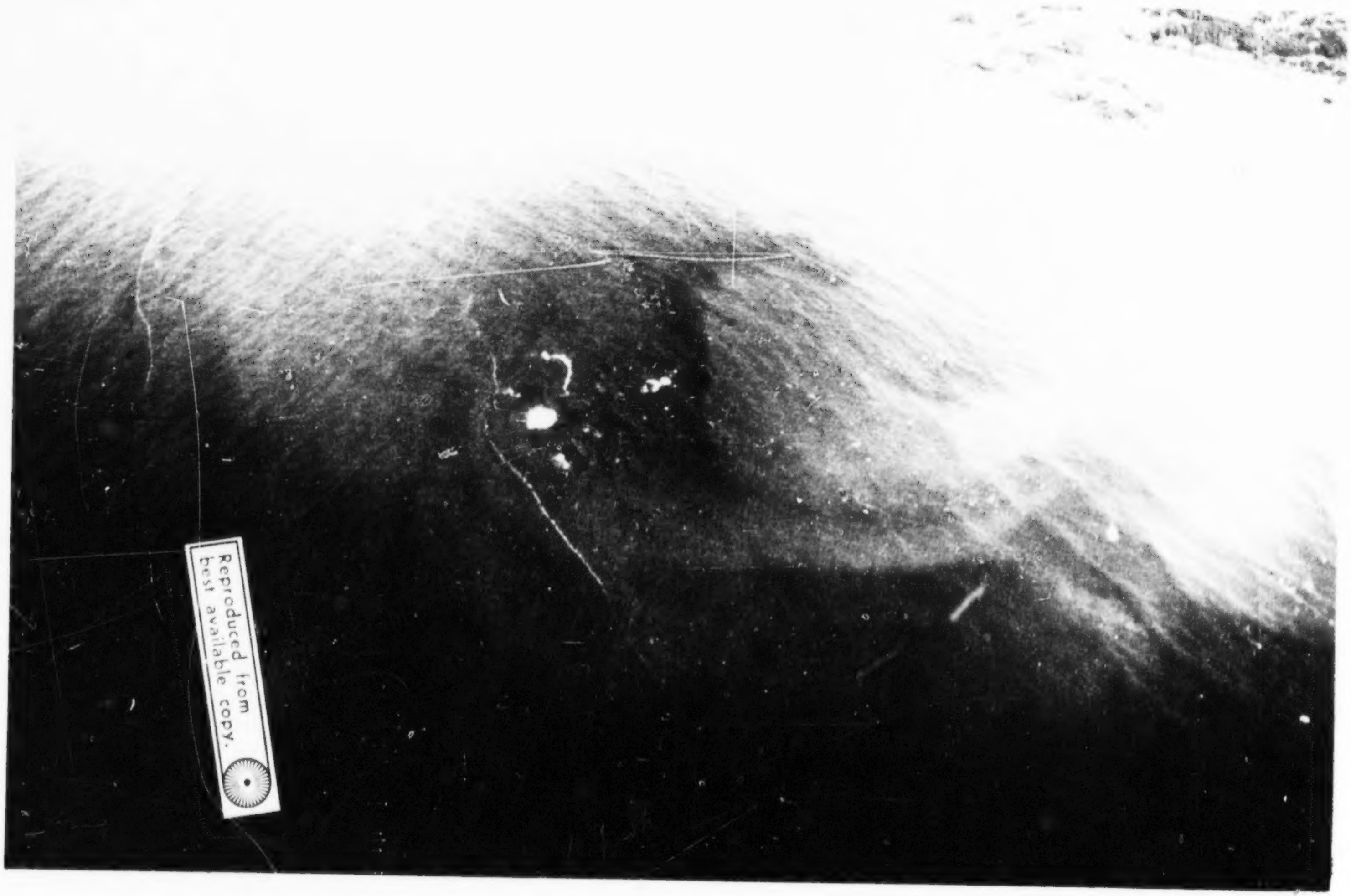

Reproduced from
best available copy.

Figure 81. Aerial photo of outfall area on April 21, 1971 from 4000 feet at 13:46.

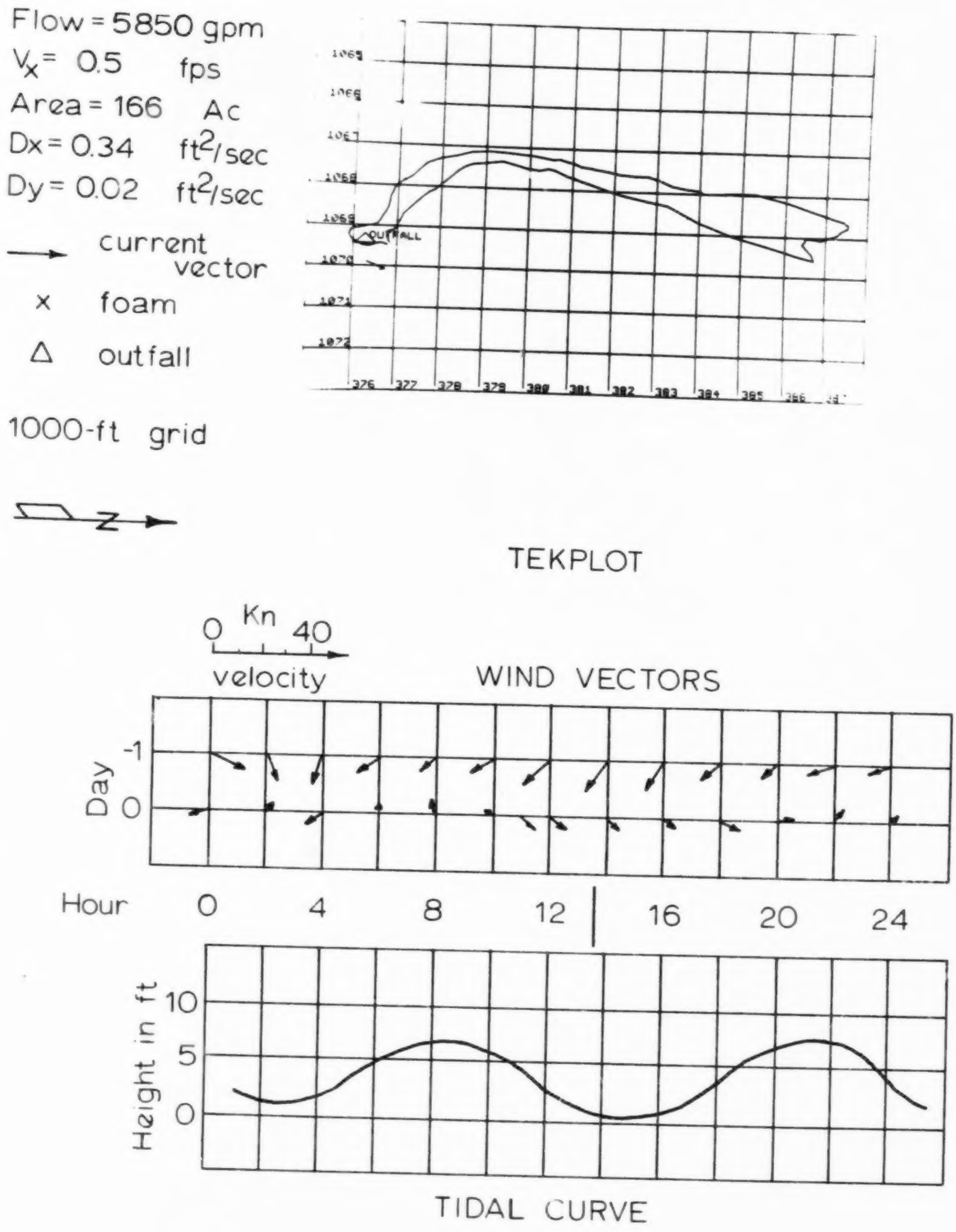

Figure 82. Data for April 21, 1971.

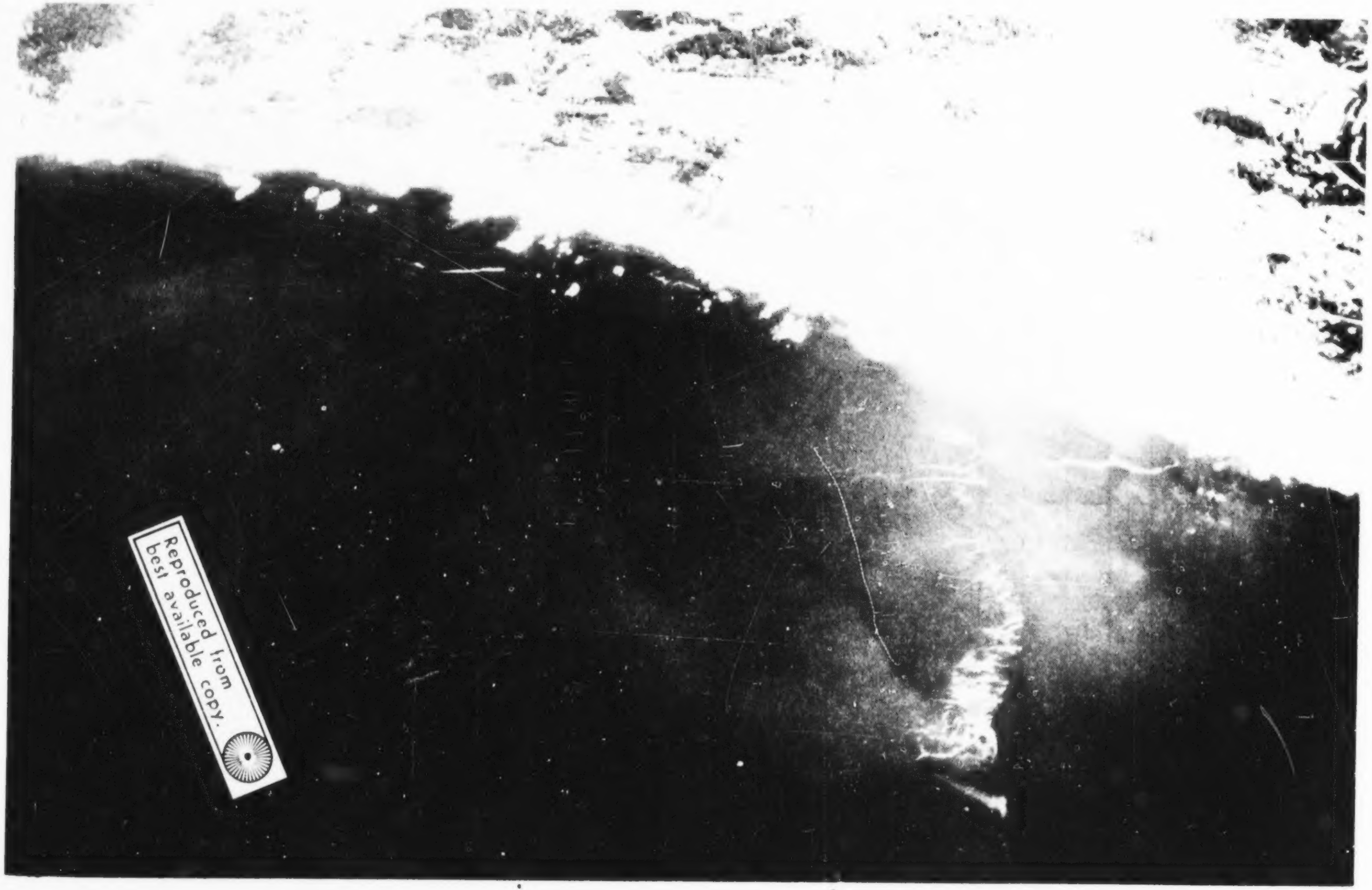

Reproduced from
best available copy.

Figure 83. Aerial photo of outfall area on April 26, 1971 from 6000 feet at 14:20.

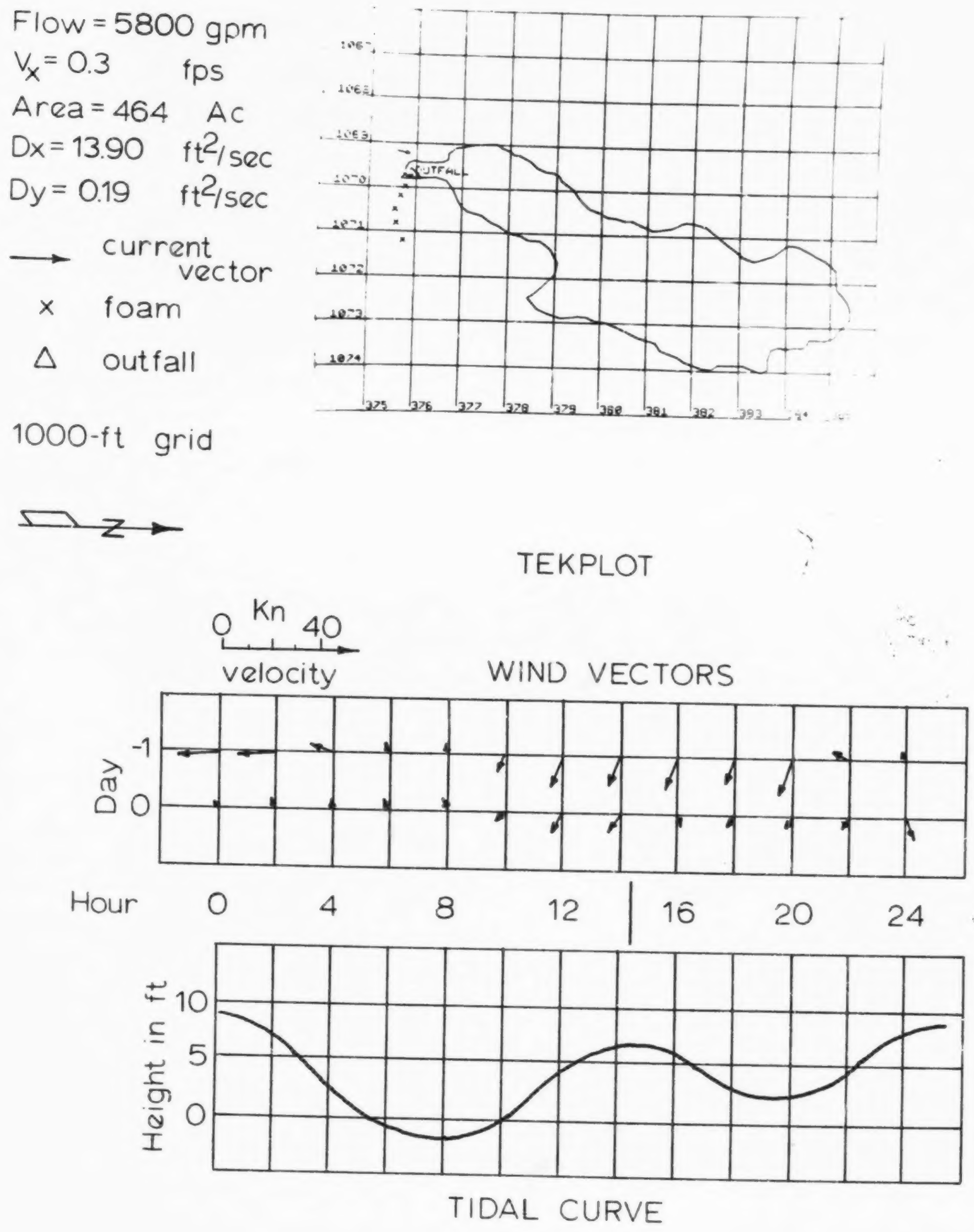

Figure 84. Data for April 26, 1971.

Reproduced from best available copy.

Figure 85. Aerial photo of outfall area on May 7, 1971 from 4000 feet at 15:13.

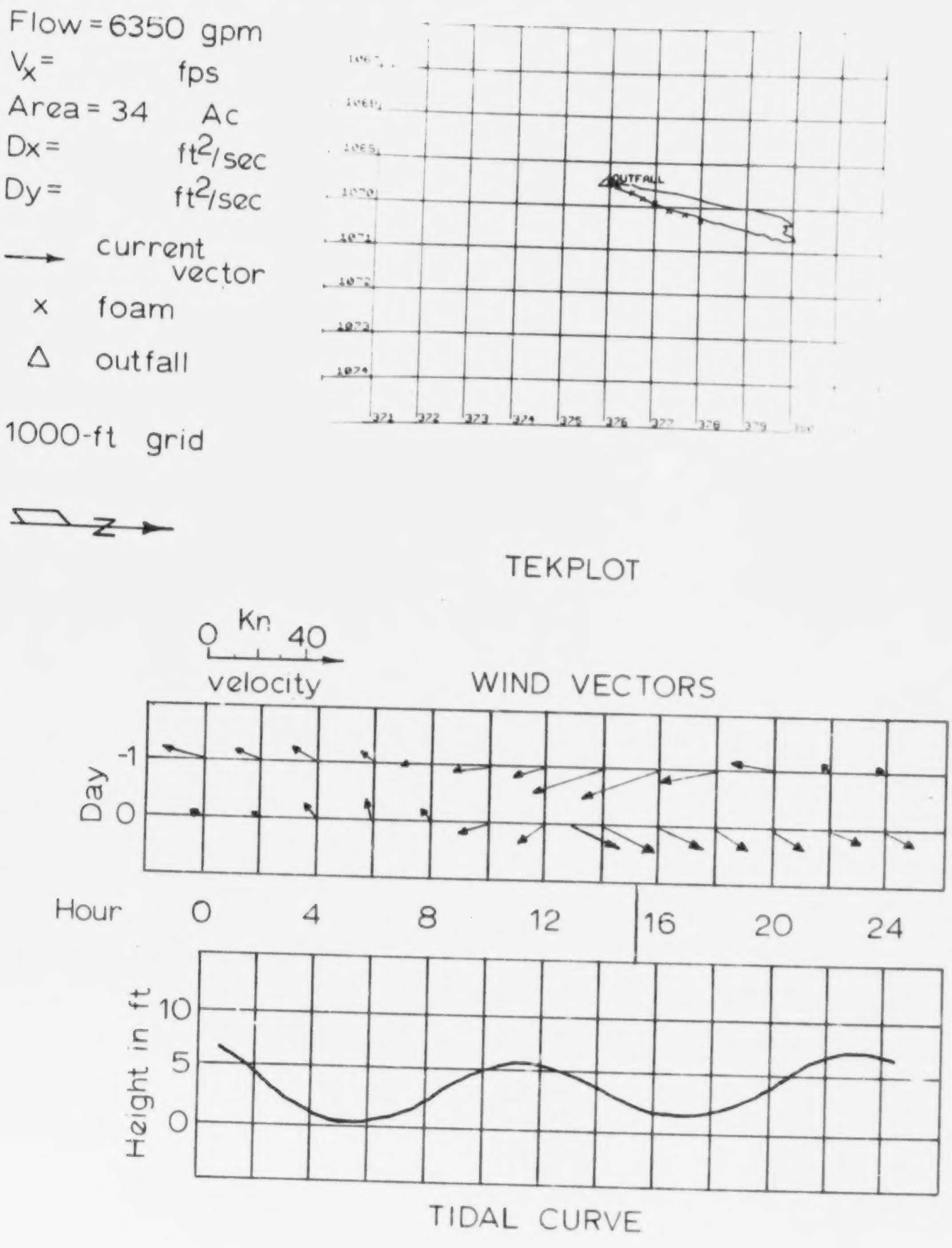

Figure 86. Data for May 7, 1971.

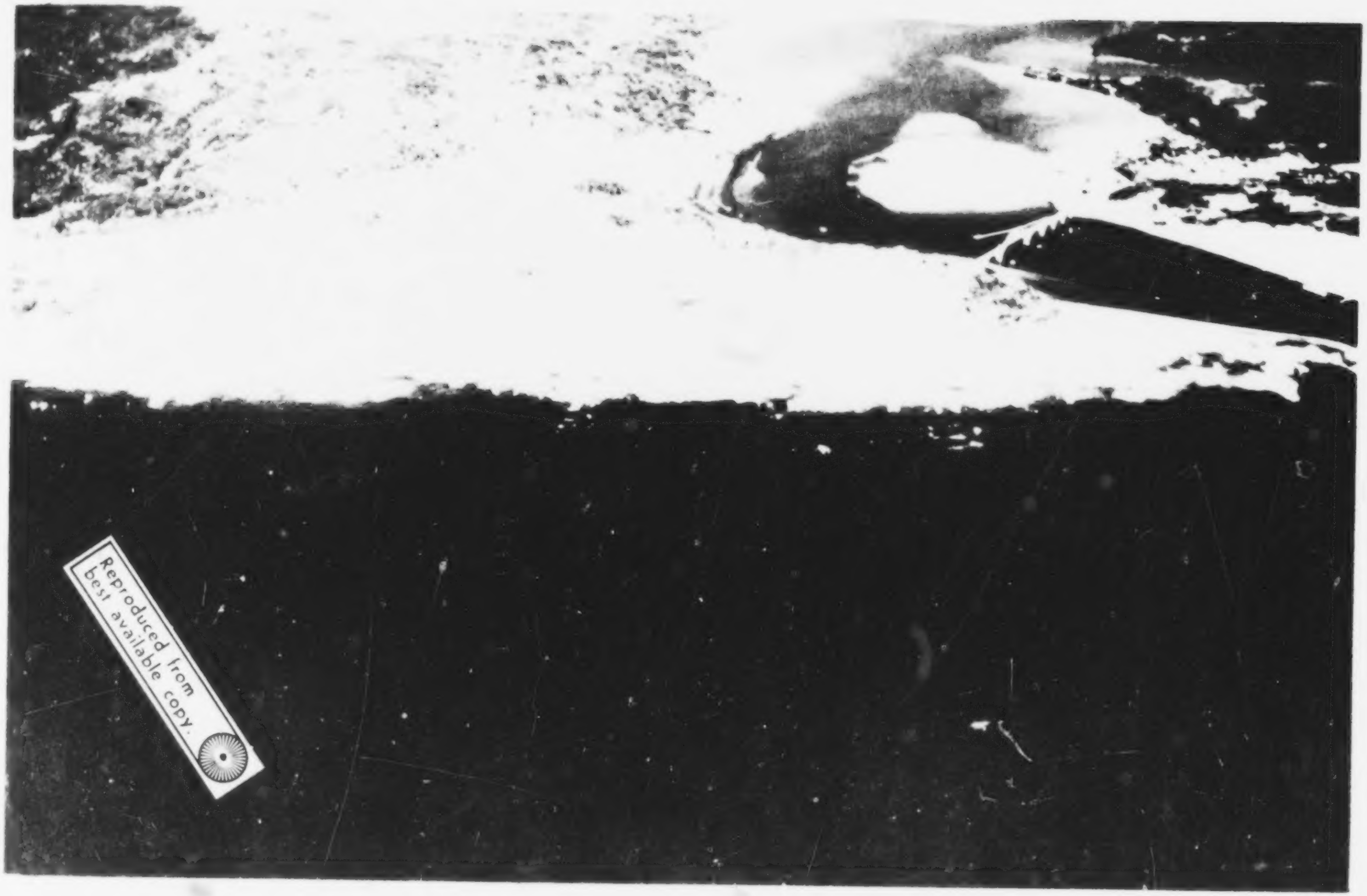

Reproduced from best available copy.

Figure 87. Aerial photo of outfall area on May 10, 1971 from 4000 feet at 16:10.

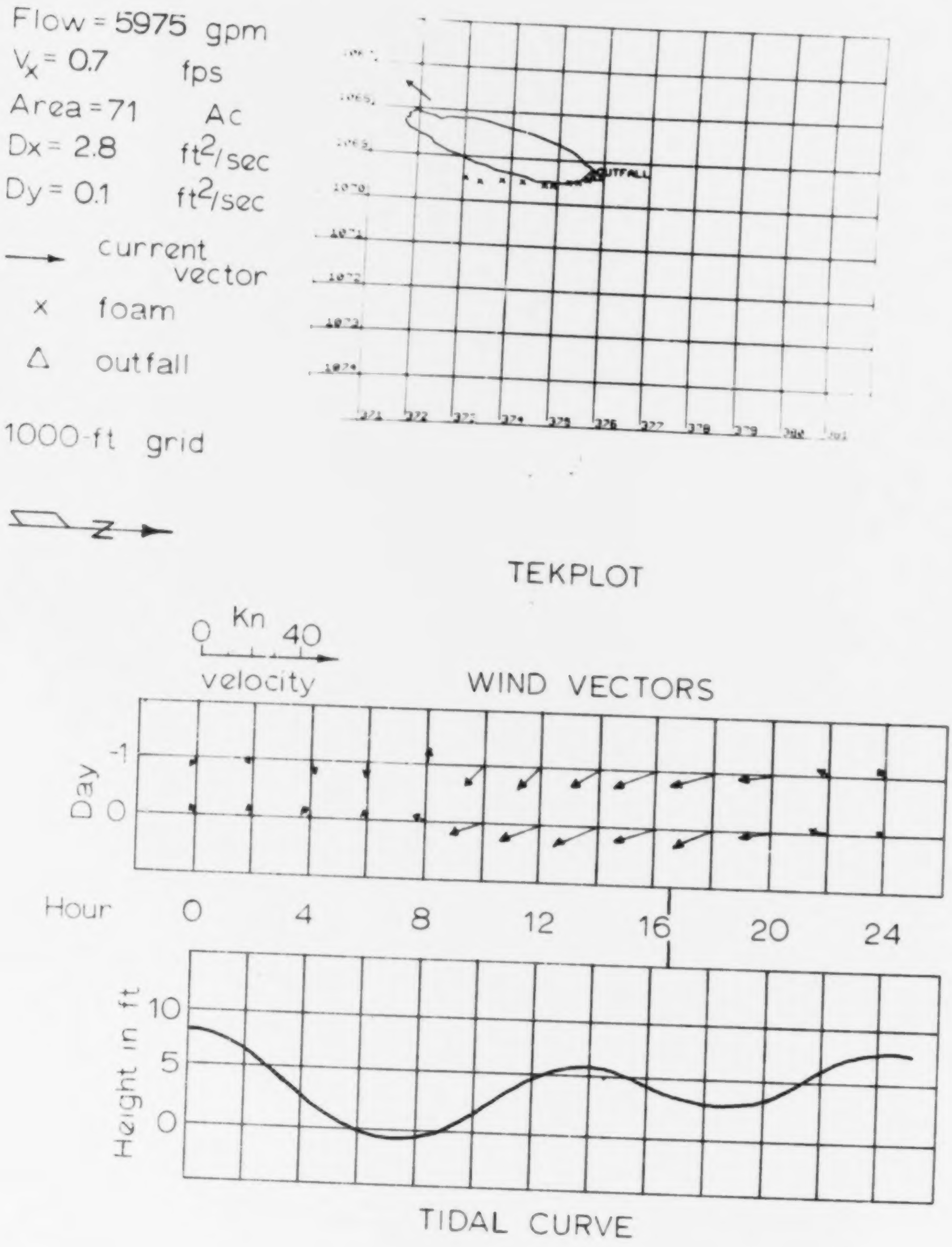

Figure 88. Data for May 10, 1971.

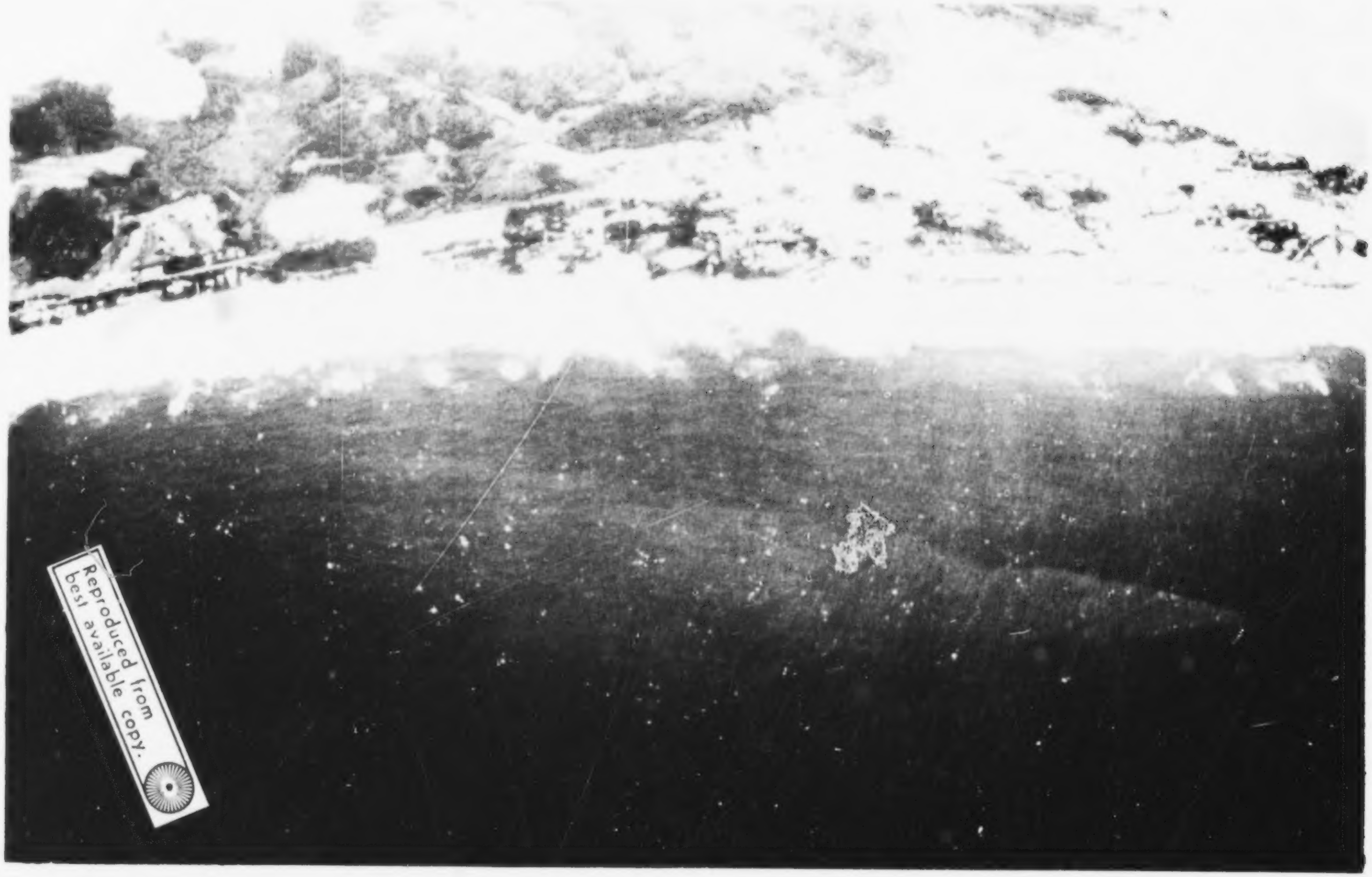

Reproduced from
best available copy.

Figure 89. Aerial photo of outfall area on May 13, 1971 from 6000 feet at 14:10.

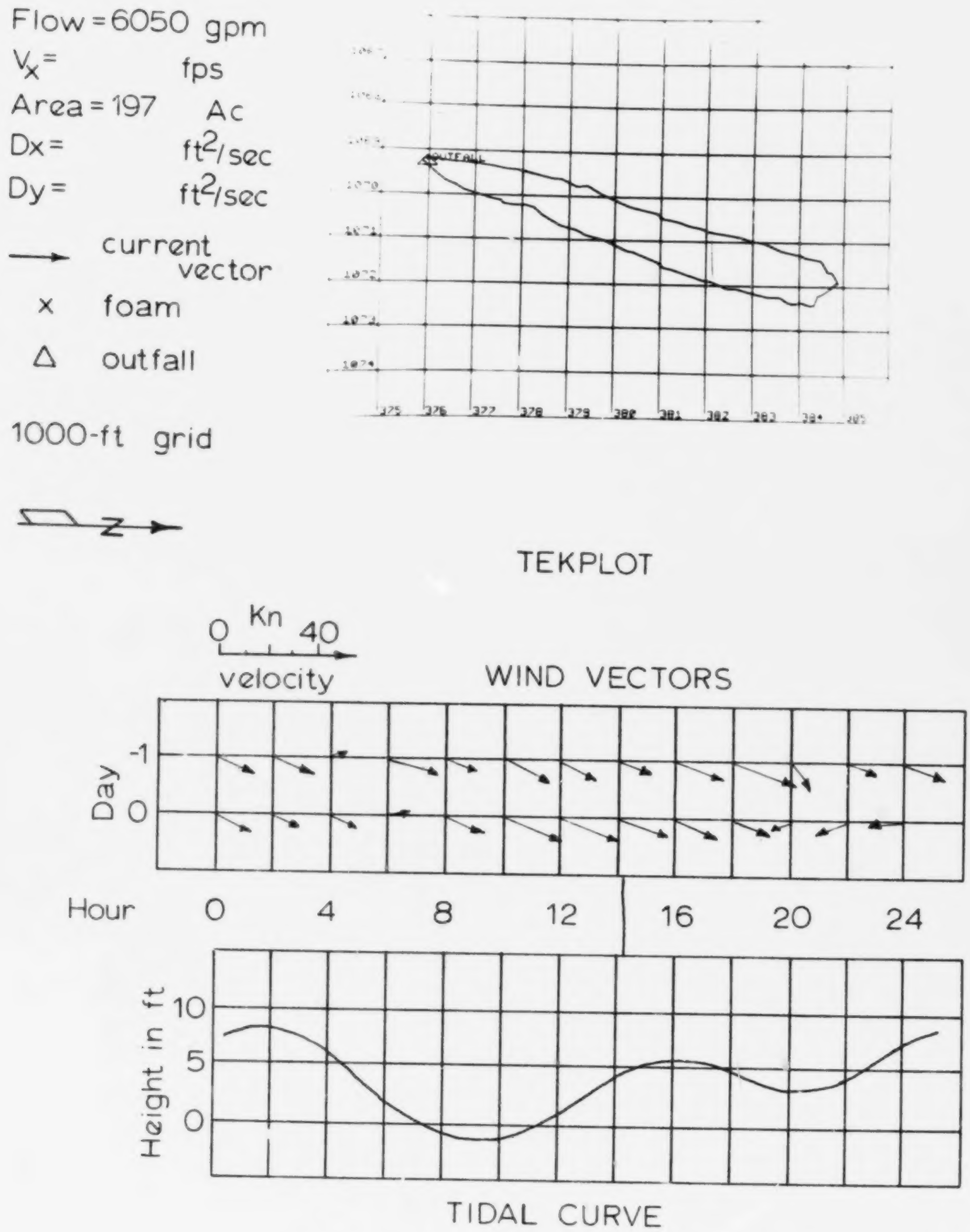

Figure 90. Data for May 13, 1971.

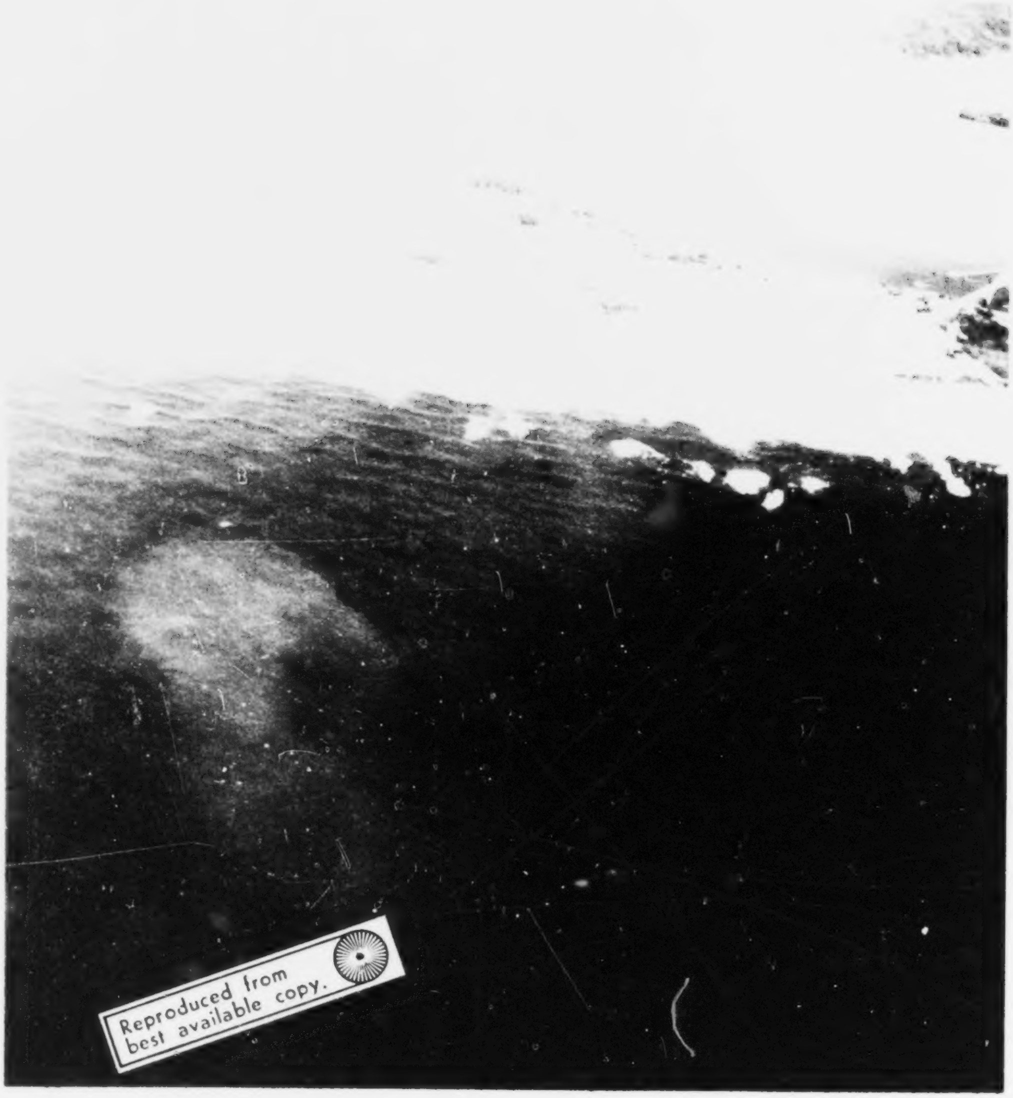

Reproduced from best available copy.

Figure 91. Aerial photo of outfall area on May 14, 1971 from 4000 feet at 14:48.

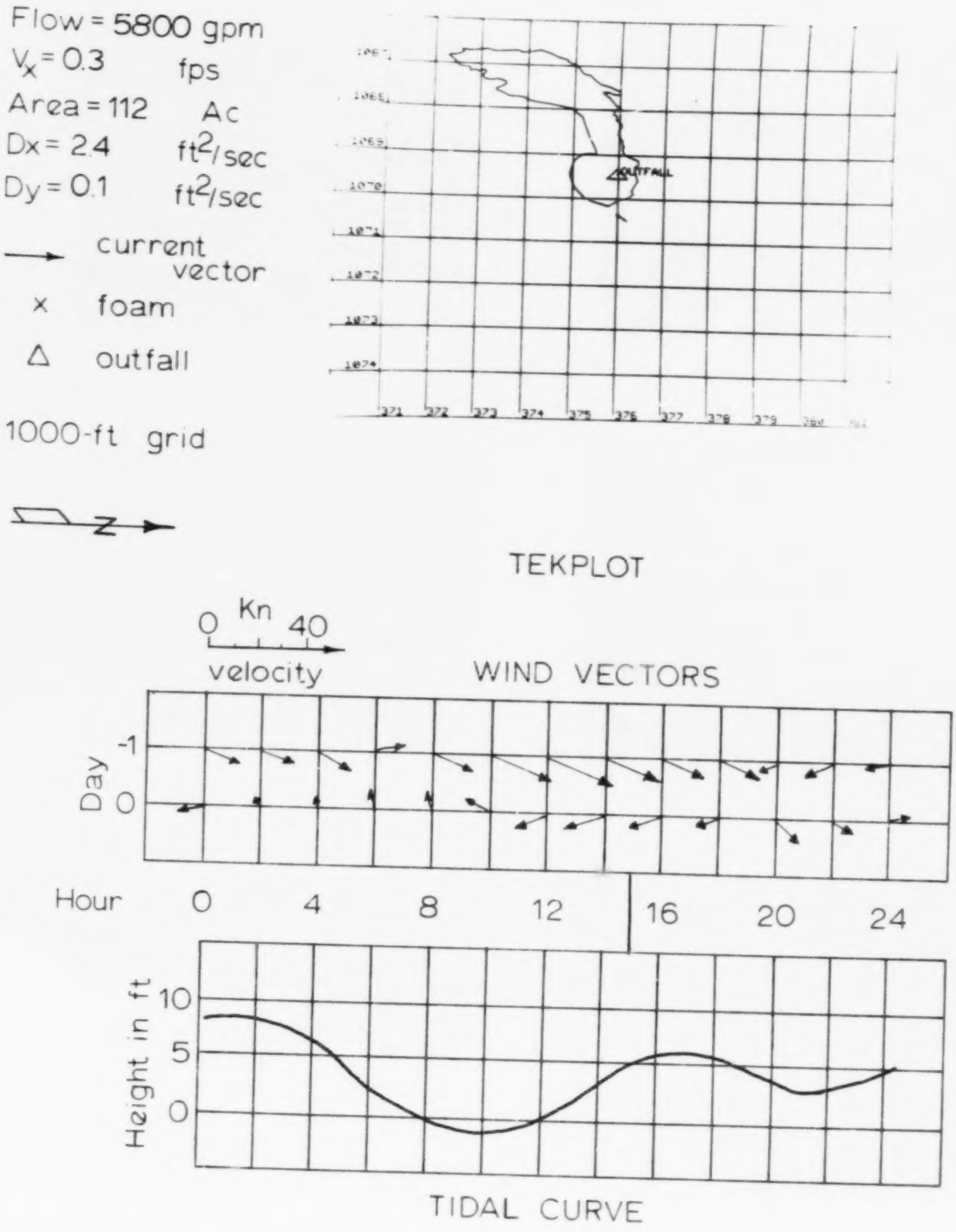

Figure 92. Data for May 14, 1971.

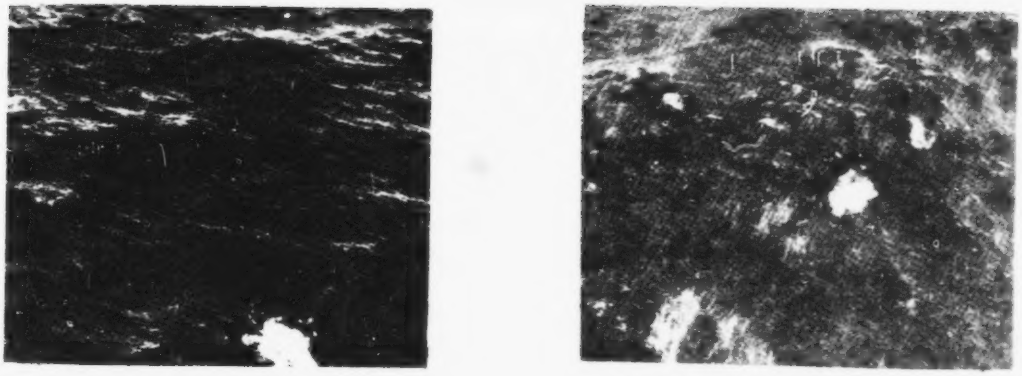

Wind 15 kts

Wind 20 kts

Reproduced from best available copy.

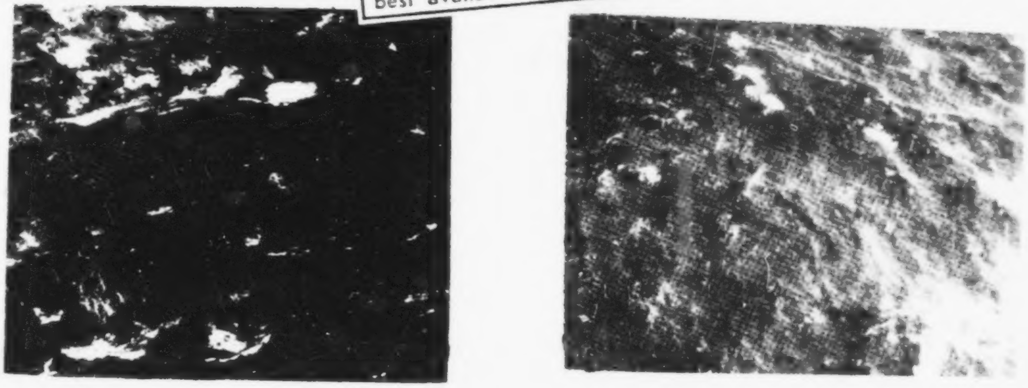

Wind 25 kts

Wind 30 kts

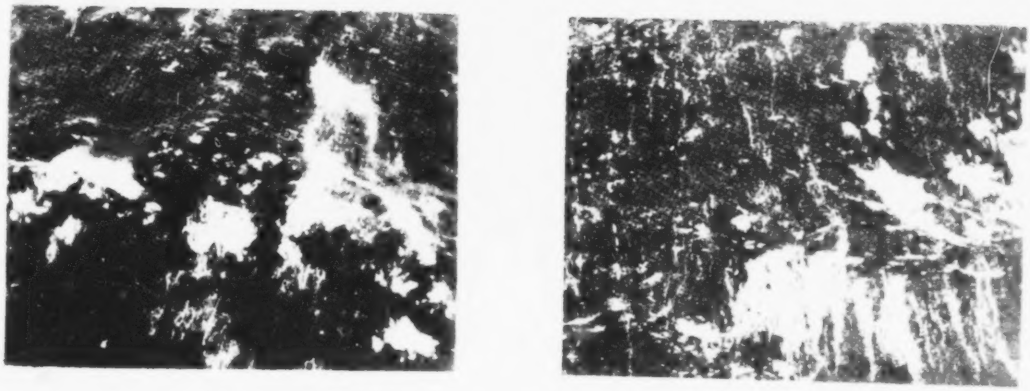

Wind 40 kts

Wind 50 kts

Figure 93. Photos of sea conditions (from Neumann & Pierson, Jr., 1966).

Table 6. Wind scales and sea descriptions (after Bascom 1964).

| Beaufort Scales | Wind Velocity Knots | Description | Wave Heights feet | State of Sea Code |
|---|---|---|---|---|
| 1 | 1-3 | Light air; ripples-no foam crests. | 0 | 0 |
| 2 | 5 | Light breeze; small wavelets, crests have glassy appearance and do not break. | 0-1 | 1 |
| 3 | 10 | Gentle breeze; large wavelets, crests begin to break. Scattered whitecaps. | 1-2 | 2 |
| 4 | 15 | Moderate breeze; small waves becoming longer. Frequent whitecaps. | 2-4 | 3 |
| 5 | 20 | Fresh breeze; moderate waves taking a more pronounced long form; mainly whitecaps, some spray. | 4-8 | 4 |
| 6 | 25 | Strong breeze; large waves begin to form extensive whitecaps everywhere, some spray. | 8-13 | 5 |
| 7 | 30 | Moderate gale; sea heaps up and white foam from breaking waves begins to be blown in streaks along the direction of the wind. | 13-16 | 5-1/2 |
| 8 | 40 | Fresh gale; edges of crests break into spindrift. The foam is blown in well-marked streaks along the direction of the wind. | 16-20 | 6 |
| 10 | 50 | Whole gale. The surface of the sea takes on a white appearance. The rolling of the sea becomes heavy. | 20-30 | 7 |

Table 7. Summary of the 1970-71 data.

| Date | Effluent Flow, gpm | Time Between Flights Seconds | Current Velocity, ft/sec | Plume Area, Acres | Diffusion | Coefficients | Tide ht - ft + flood - ebb | State of Sea Code |
|---|---|---|---|---|---|---|---|---|
| | | | | | $D_x$ $ft^2/sec$ | $D_y$ $ft^2/sec$ | | |
| 9-9-70 | 5850 | 1920 | 0.3 | 275 | 12.9 | 0.4 | 4 + | 4 |
| 9-23-70 | 5900 | 1500 | 0.1 | 28 | 3.2 | 0.1 | 4 + | 2 |
| 9-30-70 | 6950 | 780 | 0.74 | 128 | 7.5 | 0.1 | 4 - | 3 |
| 10-7-70 | 7450 | ------ | ------ | 9 | ------ | ------ | 6.5+ | 2 |
| 10-12-70 | 7650 | ------ | ------ | 89 | ------ | ------ | 2.5- | 3 |
| 12-21-70 | ------ | 1200 | 2.0 | 18 | 7.3 | 1.9 | 2.5- | 3 |
| 12-23-70 | ------ | 540 | 1.1 | 26 | 5.1 | 0.7 | 4 - | 2 |
| 12-31-70 | 8700 | 360 | 1.4 | ------ | 7.9 | 0.6 | 7.5+ | 5 |
| 1-2-71 | 6950 | 600 | 0.6 | 36 | 1.7 | 0.5 | 3 + | 2 |
| 2-6-71 am | 6450 | 720 | 0.3 | 193 | 3.6 | 0.0 | 5 - | 2 |
| 2-6-71 pm | 6450 | ------ | ------ | 200 | ------ | ------ | 1.5- | 2 |
| 3-16-71 | 5750 | ------ | ------ | 22 | ------ | ------ | 4 + | 5 |
| 3-17-71 | 5600 | 2100 | 0.3 | 126 | 5.1 | 1.0 | 5 + | 4 |
| 3-18-71 | 5950 | 1920 | 0.7 | 111 | 0.4 | 0.3 | 0.5+ | 2 |
| 3-19-71 am | 4500 | 900 | 0.3 | 73 | 1.2 | 0.4 | 1 - | 2 |
| 3-19-71 pm | 4500 | ------ | ------ | 83 | ------ | ------ | 1 + | 2 |
| 3-24-71 | 7850 | 1500 | 0.3 | 58 | 1.2 | 0.0 | 0 + | 3 |
| 4-12-71 | 7700 | 2040 | 0.4 | 7 | 8.1 | 0.2 | 5.5- | 2 |
| 4-15-71 | 7700 | ------ | ------ | 68 | ------ | ------ | 4.5+ | 3 |
| 4-21-71 | 5850 | 1020 | 0.5 | 166 | 0.3 | 0.0 | 0.5- | 2 |
| 4-26-71 | 5800 | 1980 | 0.3 | 464 | 13.9 | 0.2 | 6.5- | 3 |
| 5-7-71 | 6350 | ------ | ------ | 34 | ------ | -- -- | 2.5- | 3 |
| 5-10-71 | 5975 | 1680 | 0.7 | 71 | 2.8 | 0.1 | 4 - | 3 |
| 5-13-71 | 6050 | ------ | ------ | 197 | ------ | ------ | 4.5+ | 4 |
| 5-14-71 | 5800 | 1980 | 0.3 | 112 | 2.4 | 0.1 | 5 + | 3 |

# SECTION XI

## DISCUSSION OF RESULTS

During the 1968 and 1969 field seasons, field work was conducted during the summer. Since boat work was required in the nearshore area, data acquisition was limited to periods of relatively calm seas when the swell seldom exceeded five ft and the current velocity was generally less than 0.5 ft/sec. Boat work was discontinued during the 1970-1971 season and field work was conducted during the fall, winter and spring when rough sea conditions prevailed and current velocities greater than 0.5 ft/sec were common.

### One Dimensional Diffusion Model

As a result of the various plume patterns observed over the period of the project, the Fickian diffusion model with a unidirectional transport velocity appears to provide a reasonably accurate description of the surface transport and dilution process when the current velocity in the receiving water is high. A sketch showing the steady state plume patterns expected from a line source with a unidirectional velocity is given in figure 94. If the diffusion coefficient ($D_y$) is constant, the widths of the plume should increase with the distance downstream from the outfall at a decreasing rate or the sides of the plume should be concaved inward. The center sketch in figure 94 shows the plume shape for a diffusion coefficient that increases linearly with the scale. For this model the sides of the plume are straight. If, however, the diffusion coefficient varies to a larger power of the scale such as the 4/3 power, the plume width should increase at an increasing rate or the sides of the plume should be concaved outward.

Sinusoidal oscillations along the length of the plume will cause the width to increase faster than normal. From the dye patch studies, the diffusion coefficient in the x-direction was generally several times greater than that in the y-direction or normal to the flow. In a steady state plume, the longitudinal diffusion coefficient is not effective in reducing the waste concentration because of the small change in concentration gradients in the x-direction. Oscillations along the length of the plume will cause the width of the plume to increase at a faster rate than would normally be expected from the magnitude of the lateral diffusion coefficient. A curved plume pattern will create large changes in the concentration gradient in the x-direction and the longitudinal diffusion coefficient will become effective in reducing the waste concentration.

A diffusion model with a unidirectional transport velocity is not applicable to the plume pattern when the current velocity in the receiving water is low. Figure 95 is an isoconcentration plot of the waste field on August 8, 1968. The outfall is located near the upper

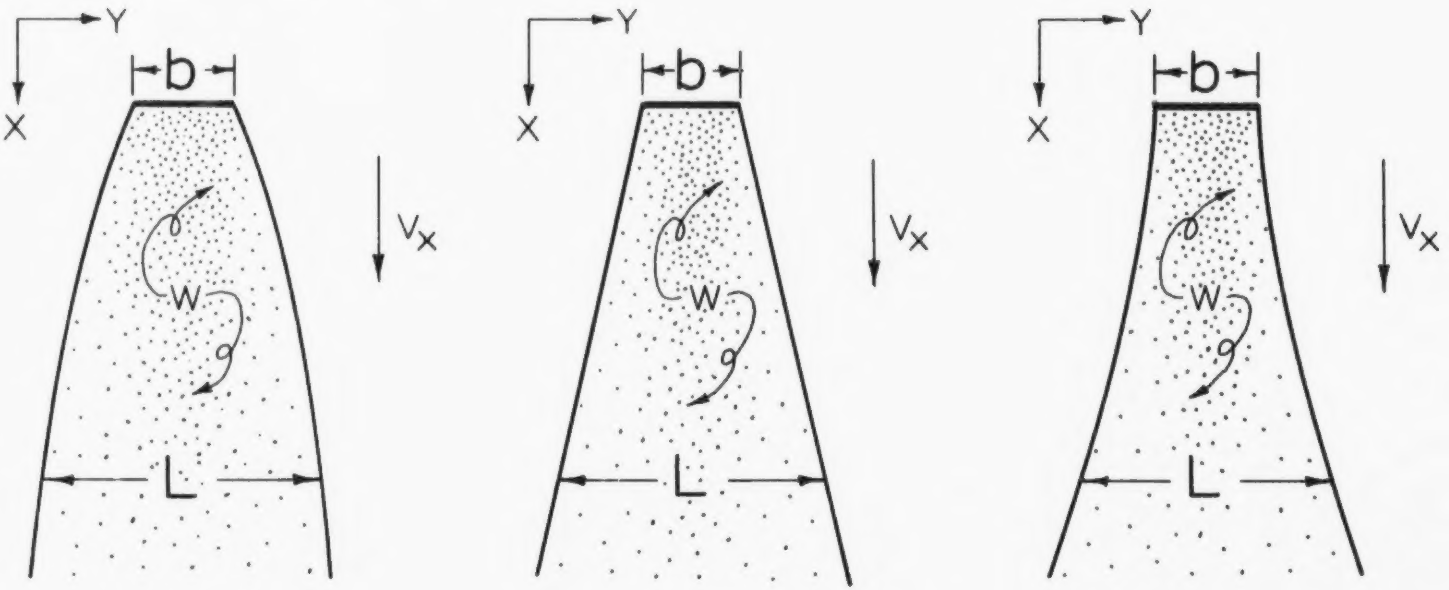

$D_y = \text{Constant}$ $\qquad$ $D_y = K\left(\frac{L}{b}\right)$ $\qquad$ $D_y = K\left(\frac{L}{b}\right)^{4/3}$

$$D_y \frac{\partial^2 W}{\partial Y^2} - V_x \frac{\partial W}{\partial X} + aW = 0$$

Figure 94. Plume patterns for a unidirectional transport velocity.

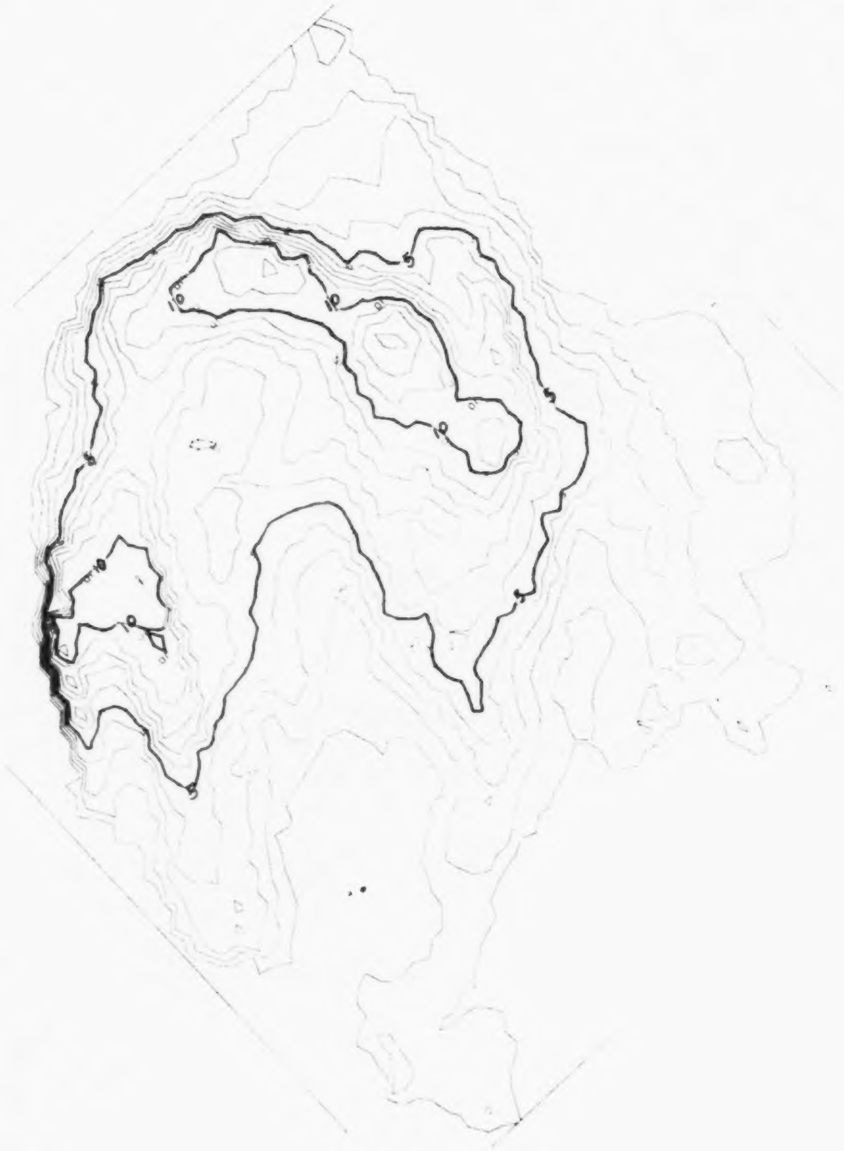

Figure 95. Isoconcentration plot, August 8, 1968.

center of the plot and the plume extends downward. The plume is 2400 ft wide and 3000 ft long. Concentrations shown on the plot are in ml/L. The diffusion coefficients computed from the one dimensional model are listed in table 8 for August 8, 1968. It can be seen that the diffusion coefficients computed from the change in variance between each fifth section along the axis of the plume are extremely high at the head of the plume with a few negative values toward the tail of the plume. While the sea was choppy, the initial spreading of the waste field was not due to diffusion but rather to the surface spreading of a source in a uniform stream. The average initial dilution over the outfall was about 1:100. The sea water, when combined with an effluent discharge rate of 12.4 cfs, would create a source with a strength of 1240 cfs over the outfall near the surface and a sink of nearly equal strength below the surface. The subsurface sink in general draws water upstream from the outfall similar to the draw down on a well in an aquifier, while the surface source discharges its water downstream. The vertical jet from the diffuser section of the outfall provides the connection for the transfer between the sink and source and supplies the energy necessary to lift the dense subsurface water from the bottom to the sea surface.

## Potential Flow

Figure 96 shows a line source of strength $\alpha$ in a uniform flowing stream. The velocity of the uniform flow is U and

$$\alpha = \frac{Q\ (DIL)}{b\ (DEP)\ 2\pi} \qquad (108)$$

Where Q is the effluent discharge rate in cfs, DIL is the dilution over the outfall, b is the length of the diffuser section and DEP is the average depth of the waste field. The potential flow is given by

$$\begin{aligned} \Omega &= \phi + i\,\psi \\ &= -UZ + \int_{-b/2}^{b/2} \ln\,(iZ-y')\,dy' \end{aligned} \qquad (109)$$

Where $\phi$ is the potential function, $\psi$ is the stream function and

$$Z = x + iy \qquad (110)$$

Equation 109 can be reduced to

$$\begin{aligned} \psi &= -UZ \\ &\quad + \alpha(iZ + b/2\ \ln\,(iZ + b/2) \\ &\quad - \alpha(iZ-b/2)\ \ln\,(iZ-b/2) \end{aligned} \qquad (111)$$

Table 8. Preliminary diffusion coefficients, flight 2, August 8, 1968.

| Section | Width Ft | Eff. Depth Ft | Sigma Y Ft | Coefficient PPT | State Plane Coordinates X | State Plane Coordinates Y | Diffusion Coefficient Ft$^2$/sec Fifth Sec | Diffusion Coefficient Ft$^2$/sec Average |
|---|---|---|---|---|---|---|---|---|
| 11 | 1007 | 9.6 | 3.160E 02 | 6.221E 00 | 1069767 | 375748 | 4.145E 01 | 4.145E 01 |
| 16 | 1429 | 3.5 | 4.215E 02 | 1.273E 01 | 1069428 | 375611 | 3.372E 01 | 3.758E 01 |
| 21 | 2059 | 3.3 | 5.252E 02 | 1.090E 01 | 1069277 | 375351 | 4.250E 01 | 3.922E 01 |
| 26 | 2475 | 3.3 | 6.169E 02 | 9.309E 00 | 1069136 | 375084 | 4.539E 01 | 4.076E 01 |
| 31 | 2613 | 3.5 | 7.055E 02 | 7.634E 00 | 1069031 | 374795 | 5.078E 01 | 4.277E 01 |
| 36 | 2784 | 4.4 | 7.147E 02 | 6.028E 00 | 1068938 | 374497 | 5.677E 00 | 3.659E 01 |
| 41 | 3091 | 6.5 | 6.748E 02 | 4.315E 00 | 1068904 | 374162 | -2.406E 01 | 2.792E 01 |
| 46 | 3080 | 9.4 | 6.461E 02 | 3.104E 00 | 1068785 | 373881 | -1.638E 01 | 2.238E 01 |
| 51 | 2207 | 14.2 | 6.958E 02 | 1.915E | 1068407 | 373769 | 2.886E 01 | 2.310E 01 |

Flow Rate 12.4 CFS
Sun Az. from S. 1.398 Rad.
Current Velocity .26 FPS
Sun Altitude .567 Rad.

Area Within Each Concentration Range

| Range ml/l | Area Sq Ft |
|---|---|
| 0- 2 | 2.477E 06 |
| 2- 4 | 1.616E 06 |
| 4- 6 | 9.036E 05 |
| 6-10 | 1.613E 06 |
| 10-15 | 2.376E 05 |

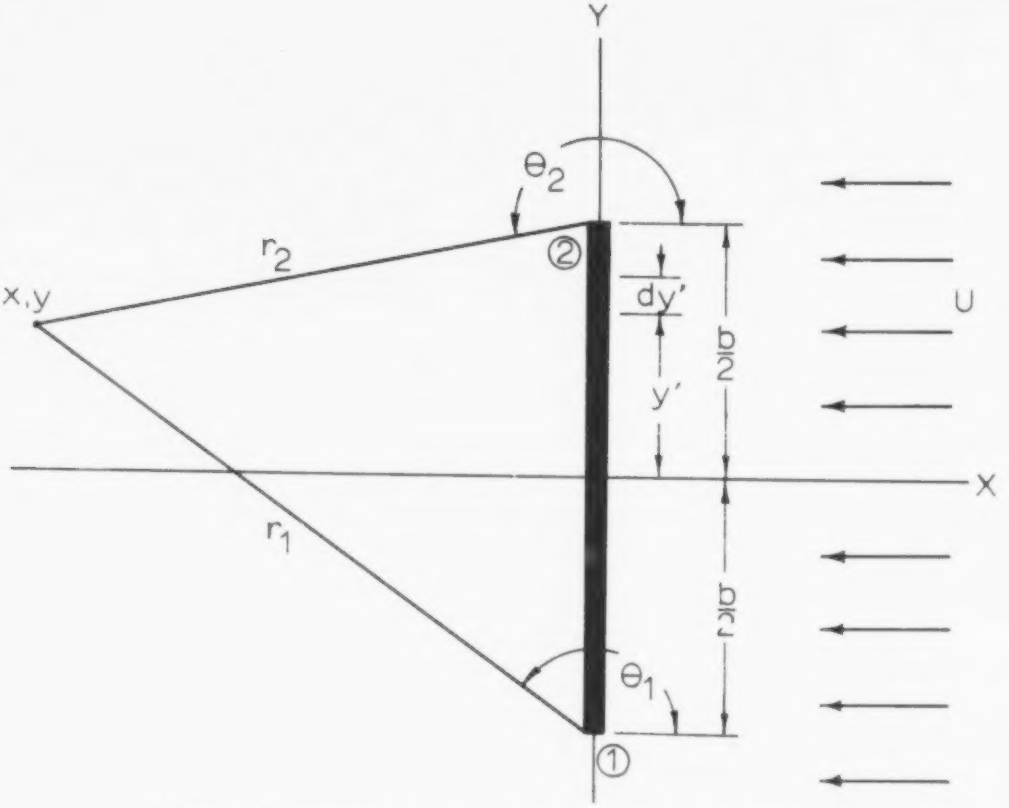

Line Source in a Uniform Stream

Figure 96. Geometry for a line source in a uniform stream.

from which the stream function is

$$\psi = -UY + \alpha[(Y + \frac{b}{2})\ \theta_1 - (Y - \frac{b}{2})\ \theta_2 - X \ln \frac{r_1}{r_2})] \tag{112}$$

where

$$\tan \theta_1 = \frac{(Y + \frac{b}{2})}{X} \tag{113}$$

$$\tan \theta_2 = \frac{Y - \frac{b}{2}}{X} \tag{114}$$

The value of the stream function along the axis of the plume (y = 0) is

$$\psi = \alpha\ b\ \pi \qquad (115)$$

While the value of y when $\psi = 0$ and x approaches $\infty$ is

$$y = \frac{\alpha\ b\ \pi}{U} \qquad (116)$$

The values of the x and y velocity components are given by

$$V_x = \frac{\partial\psi}{\partial y} = -U + \alpha(\theta_1 - \theta_2) \qquad (117)$$

$$V_y = \frac{-\partial\psi}{\partial x} = \alpha\ \ln\ (\frac{r_1}{r_2}) \qquad (118)$$

Equation 112 was programmed to solve for the x and y coordinates of the streamlines. Two plots from the Tektronix plotter are shown in figure 97. The source strength for each plot is 300 cfs per ft of depth. A state plane coordinate grid is drawn and labeled at 1000-ft intervals. The outer streamline defines the plume boundary if the diffusion effluents were equal to zero. This plume can also be reproduced from the following modification of the diffusion model (equation 56).

$$\frac{\partial W}{\partial t} = -\ [\frac{\partial}{\partial Y}\ (V_y W) + \frac{\partial}{\partial X}\ (V_x W)] \qquad (119)$$

where the x and y components of the velocity are determined from equations 117 and 118. The model given by equation 119 would be applicable when the sea is calm and the diffusion coefficients low.

On each plot in figure 97 the outer streamline has a value of zero while the centerline has a value of 150 as given by equation 115. The two plots are for line sources oriented perpendicular to a uniform stream of 0.1 and 0.5 ft/sec, respectively.

The four streamline sketches in figure 98 are for a line source of strength 300 cfs per ft of depth in a uniform stream of 0.0, 0.1, 0.3 and 0.5 ft/sec, respectively. The streamlines were traced from Tektronix plots such as those shown in figure 97. At zero current velocity, the waste field lakes or ponds about the outfall area. As shown in figure 98, the potential flow solution would give a downstream plume width of 3000 ft in a uniform stream of 0.1 ft/sec. As the current velocity increases, the plume width decreases to 1000 ft at 0.3 ft/sec and 600 ft at 0.5 ft/sec. The minimum width of the plume would be the length of the diffuser section.

When a waste water stream discharged from a submerged outfall spreads at the surface, the resulting drift flow plume pattern is influenced

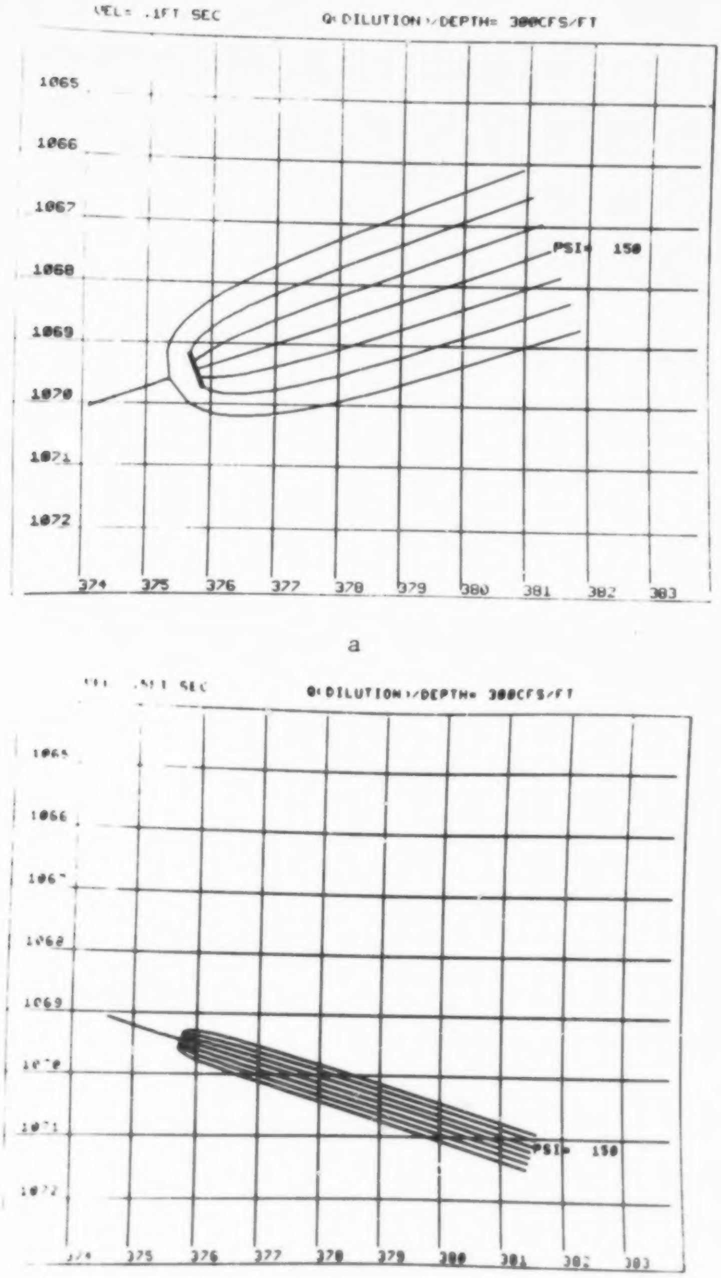

a

b

Figure 97. Plots of a source in a uniform stream.

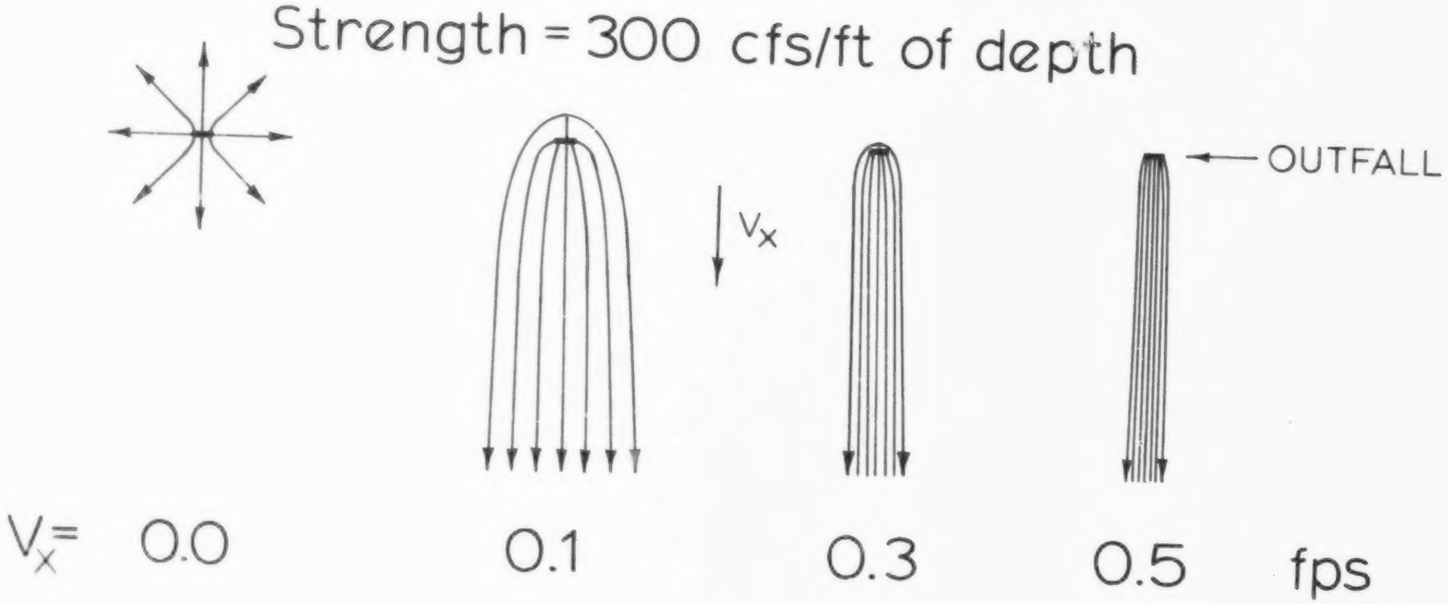

Figure 98. Potential flow solutions for a line source.

by the ambient current velocity and the amount of residual buoyancy and momentum (if any) in the waste stream (Baumgartner and Trent, 1970). Rather accurate methods are available to calculate dilutions in the buoyant jet, neglecting the influence of ambient currents in this region. When density stratification occurs in the region surrounding the outfall, a plume can form without residual buoyancy and these dilution models can be used to determine the depth at which the lens first forms, whether or not portions of the plume rise to the surface (Baumgartner, Trent and Byram). This model offers a means for estimating the initial concentration and depth of the drift flow plume. The initial width and curvature of the surface plume can be estimated using a potential flow solution for a source in a uniform stream. For a single outfall port a point source would be used and for a multiport diffuser, a line source over the diffuser length can be used. In this way the relative influence of the ambient current, diffuser length and orientation can be evaluated.

## Diffusion Model

In order to gain insight into the Fickian diffusion model and to determine the relative importance of the terms in the equation on the plume shape, a modified form of equation 56 was programmed so that the waste field could be simulated on the computer. For the computer model, the vertical diffusion coefficient ($D_z$) and the velocity in the vertical direction ($V_z$) in equation 56 were set equal to zero. In the resulting two-dimensional model the loss of waste to the lower layers due to vertical mixing was considered by substituting a decay term (-kW) for the sink term in equation 56. The resulting two-dimensional diffusion equation is:

$$\frac{\partial W}{\partial T} = \frac{\partial}{\partial Y} (D_y \frac{\partial W}{\partial Y}) + \frac{\partial}{\partial X} (D_x \frac{\partial W}{\partial X})$$

$$- [\frac{\partial}{\partial Y} (V_y W) + \frac{\partial}{\partial X} (V_x W)] - kW \qquad (120)$$

The initial condition for the model was that the concentrations throughout the waste field were zero. At the start of each incremental time period, the waste concentration for the elements in the array at the outfall were set equal to the concentration that resulted from the initial jet dilution. During each incremental time period the waste field is moved or convected in the array, diffused and decayed according to the model.

Two isoconcentration plots from this model are shown in figure 99. The outfall is located at the top of each plot and the plume extends downward. Current velocities for the two plots were 0.1 ft/sec and 0.5 ft/sec, respectively, while the diffusion coefficients were $D_y = D_x = 2$ ft$^2$/sec. A source strength of 300 cfs/ft of depth was used to determine the current velocity components. The print out time was 90 minutes from the start of the effluent discharge, and the decay

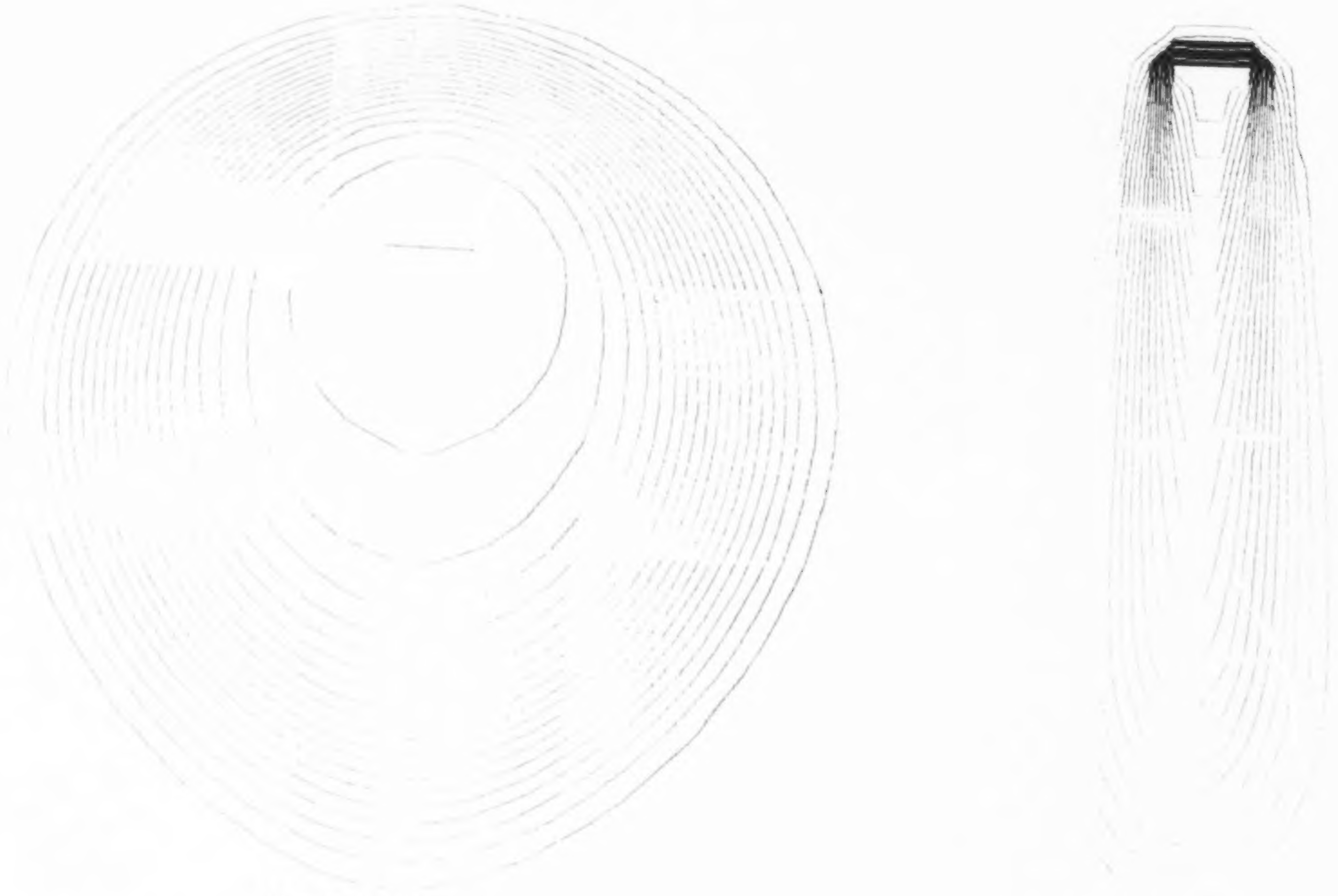

U = 0.1 ft/sec

U = 0.5 ft/sec

Figure 99. Isoconcentration plots from diffusion model.

coefficient was 0.1 per hour.

## Temperature

Vertical density stratification can cause the waste field to be formed below the sea surface. Of the 21 sampling runs conducted during the summers of 1968 and 1969, a surface plume was observed on eight days, the plume was submerged on six days and the waste field was not observed on seven days due to fog or rain. During these two summers a surface plume occurred for only 60% of the observations. Generally, the plume was not visible when the sea was calm. However, of the 25 observations conducted in the fall of 1970 and the winter and spring of 1971, the plume was not visible on only one day which was when the sea was extremely rough.

Changes in density can be caused by a variation in temperature and or salinity. Fresh water runoff from the coastal streams is at a minimum during the summer months and variations in temperature are generally the major cause of vertical density stratification in the nearshore area during the summer. Upwelling, which occurs during the summer, brings to the surface the more dense subsurface water rich in nutrients. Upon reaching the surface, plankton begin growing. This suspended material reduces the transparency of the water and increases the sunlight absorption coefficient. Under relatively calm sea conditions, a thin surface layer of dark green water warms rapidly and can become lighter than the less saline subsurface water. During periods of upwelling, there is generally a narrow band of clear water between the land and the dark green offshore water. In addition to the seasonal variation in temperature there is also a diurnal variation. The diurnal thermocline is especially prominent during calm summer days. The sketch in figure 100 shows the progressive variation in vertical temperature structure for various times of the day.

The absorption of solar radiation by the upper layers is readily apparent as the surface temperature increases to a late afternoon maximum and then decreases as the sun sets. Typical diurnal thermoclines may be as much as 30 feet deep and perhaps as much as 1° or 2° C in magnitude, though usually they are somewhat less. If a good breeze is blowing, the upper layers will become mixed, carrying the warm water to greater depths, having the effect of increasing the depth of the diurnal thermocline, but decreasing its magnitude, as the absorbed heat is spread out over a large volume of seawater.

## Wind

Water currents in the nearshore area can be caused by a combination of factors including wind, tide, waves, and the general ocean circulation patterns. The importance of each of the several factors vary with both time and location. The topographic configuration of the shore, bathymetry of the area, pressure gradients and Coriolis forces will tend to

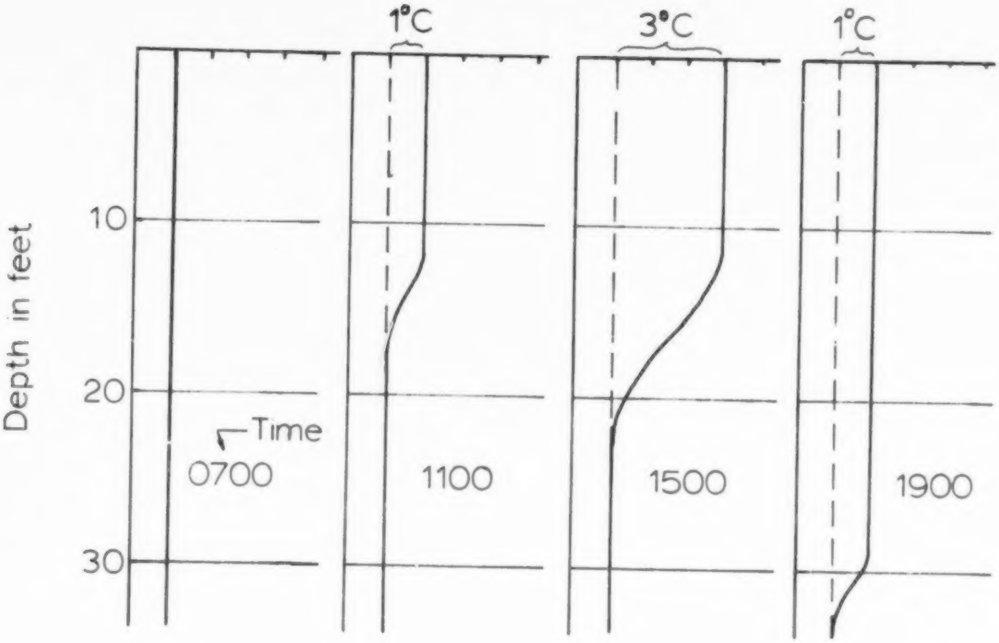

Figure 100. Typical diurnal thermoclines.
(After Williams, Higginson & Rohrbough, 1968).

modify the flow pattern. Near the entrance to Yaquina Bay, there are large tidal currents while along the surf zone the wave height, beach slope and the angle the wave crests make with the beach are important considerations in estimating the longshore current. In the nearshore area of the outfall, wind appears to be the dominant factor in estimating water currents (Burgess and James, 1970 and Keene, 1971). The wind not only supplies energy for water transport but also energy in the form of turbulence.

The relationship between the wind and the water current velocity depends on the fetch, duration and magnitude of the wind as modified by the topography near the boundary of the sea. Diurnal variations in the coastal winds are common. An example of the effect of a shifting wind on the current velocity profile is given in figure 101. As the wind begins blowing, only the surface is affected. As the duration increases, the sea becomes turbulent and the energy is transferred deeper into the water. If the wind continues long enough in the same direction, the effect of the bottom drag may influence the velocity profile in the shallow areas. A reversal of the wind will affect the surface water first and will cause a change in the surface velocity vector. The surface waters can move in a direction opposite that of the subsurface water.

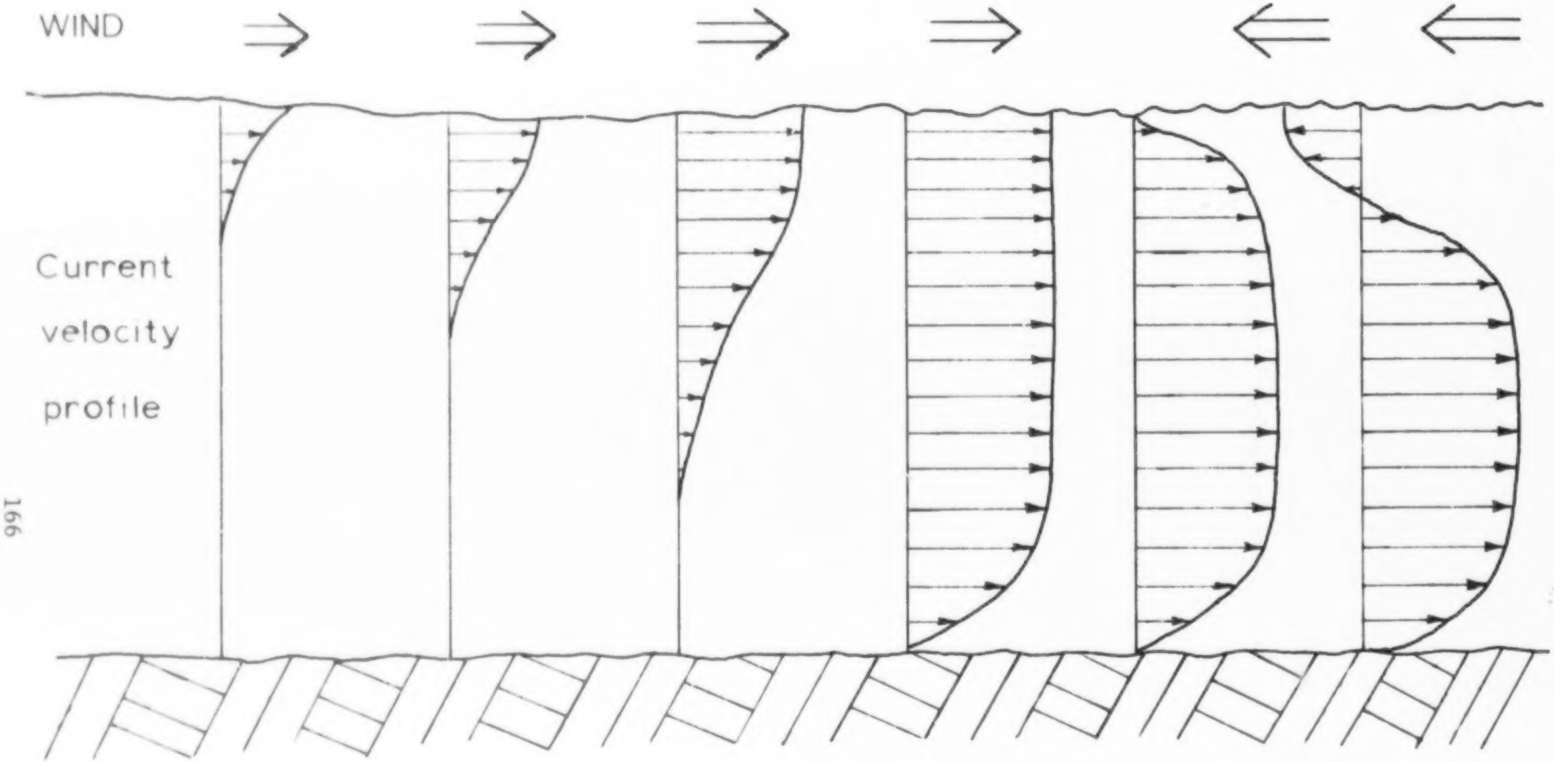

Figure 101. Development of current velocity profile.

## Sea State

Wind provides turbulent energy for mixing of wastes discharged into the ocean. When the horizontal velocity changes with depth, vertical turbulence will transfer mass between layers and will cause a slug discharge of waste to spread faster along the direction of motion than normal to the current direction. From the dye patch studies, large longitudinal diffusion coefficients can be expected when the wind first starts blowing or it changes direction.

The observations of the waste field during the 1970-71 field season were divided into three categories depending on the apparent dominant form of turbulent energy. These classes were: 1) sea surface roughness caused primarily by the wind, 2) sea roughness due to heavy swell, and 3) the sea state influenced by both the wind and breakers in the area.

Table 9 lists the observations for which wind was the main cause of the sea state. These dates are listed in order of increasing sea turbulence as determined by a visual interpretation of the photos. For all except two observations, the dye patch was elongated parallel to the wind. On April 26 the dye patch was oriented parallel to the water current while on September 9 the dye patch was v-shaped with one leg oriented parallel to the water current and the other leg oriented parallel to the wind.

Diffusion coefficients ranged from 3.0 to 14 $ft^2$/sec in the longitudinal direction and 0.0 to 1.0 in the transverse direction. The diffusion coefficient determined for a one dimensional model from the 1968-1969 data were 11 $ft^2$/sec and 14 $ft^2$/sec on August 16, 1968, and July 8, 1969, respectively. The state of the sea code for both of these days was 3. The wind was 10-15 kts on August 16 with 6-ft swell and 15-kt wind on July 8 with a choppy sea.

Table 10 shows the sea state when the turbulence is due mainly to heavy swell. The diffusion coefficients ranged from 1.2 to 8 $ft^2$/sec in the longitudinal direction and 0.0 to 1.9 in the transverse directions for a sea state code ranging from 3 to 5.

Table 11 lists the sea state for turbulence due to both wind and swell. Diffusion coefficients were not determined for rough sea condition but only for a sea state of 2. The values of the longitudinal and transverse diffusion coefficients were more nearly equal to each other for this condition than for either of the conditions represented in tables 9 or 10.

The waves normally observed at sea are composed of two types. The swell is a long and relatively symmetrical wave form having a period greater than 10 seconds, generated by winds at some distance from the area, and in the nearshore area is oriented nearly parallel to the

Table 9. Sea state due primarily to wind.

| Date | Figure no. | Diffusion coef ft$^2$/sec | | State(1 of sea | Remarks |
|---|---|---|---|---|---|
| | | Dx | Dy | | |
| April 12 | 77 | 8.1 | 0.2 | 2 | Strong east wind in opposite direction to swell. |
| Oct. 7 | 49 | - | - | 2 | Very lightly mottled photo pattern. |
| Dec. 23 | 55 | 5.1 | 0.7 | 2 | A curved dye patch. Wind changed from E to NE. |
| Feb. 6 am | 61 | 3.6 | 0.0 | 2 | Lightly mottled photo tone. A few scattered whitecaps. |
| Feb. 6 pm | 63 | - | - | 2 | Lightly mottled photo tone with a few scattered whitecaps. |
| Sept. 23 | 45 | 3.2 | 0.1 | 2 | Finely mottled photo tone with scattered whitecaps. |
| May 10 | 87 | 2.8 | 0.1 | 3 | Wind from the northwest at 15 kts for six hours. Scattered whitecaps with a mottled photo tone. |
| May 7 | 85 | - | - | 3 | Wind changed from NW to SW at 25 kts. Finely mottled photo tone with scattered whitecaps. |
| May 14 | 91 | 2.4 | 0.1 | 3 | Finely mottled photo pattern with scattered whitecaps. |
| April 26 | 84 | 13.9 | 0.2 | 3 | Finely mottled photo pattern with scattered whitecaps. Excessive longitudinal dispersion of dye patch ahead of main slug. |
| Sept. 30 | 47 | 7.5 | 0.1 | 3 | Wind parallel to the x component for 4 hours. A mottled photo pattern with a linear trend normal to the wind direction and frequent whitecaps. |

Table 9. Continued

| Date | Figure no. | Diffusion coef ft$^2$/sec | | State(1 of Sea | Remarks |
|---|---|---|---|---|---|
| | | Dx | Dy | | |
| May 13 | 89 | - | - | 4 | Wind 30 kts from the SW for 6 hours. Coarsely mottled pattern with same linear trend parallel to the wind. |
| Sept. 9 | 43 | 12.9 | 0.4 | 4 | Mottled photo tone with numerous whitecaps. Dye patch is v-shaped. |
| Mar. 17 | 67 | 5.1 | 1.0 | 4 | High turbidity near shore. Wind changed direction 2 hours before. Strong linear trend due to wind waves. Numerous whitecaps. Wind from the NW 15 kts. |

(1 see table 6.

Table 10. Sea state due primarily to swell.

| Date | Figure no. | Diffusion coef ft$^2$/sec | | State(1 of Sea | Remarks |
|---|---|---|---|---|---|
| | | Dx | Dy | | |
| March 21 | 75 | 1.2 | 0.0 | 3 | Waves breaking on reef S of outfall. Lightly mottled photo pattern with scattered whitecaps. |
| Dec. 21 | 53 | 7.3 | 1.9 | 3 | Waves breaking along reef. Mottled photo pattern with a few scattered whitecaps. |
| Dec. 31 | 57 | 7.9 | 0.6 | 5 | Waves breaking everywhere. |

(1 see table 6.

Table 11. Sea state due to wind and swell.

| Date | Figure no. | Diffusion coef $ft^2/sec$ |  | State of Sea[1] | Remarks |
|---|---|---|---|---|---|
|  |  | Dx | Dy |  |  |
| Mar. 18 | 69 | 0.4 | 0.3 | 2 | Turbid nearshore water. Finely mottled photo tone a few whitecaps. |
| Mar. 19 am | 71 | 1.2 | 0.4 | 2 | Turbid nearshore water mottled photo tone. |
| Mar. 19 pm | 73 | - | - | 2 | Wind 15 kts from NW. Mottled photo tone with scattered whitecaps. |
| Jan. 2 | 59 | 1.7 | 0.5 | 2 | Low wind velocity. Dye patch oriented normal to wind and parallel to direction of swell. |
| April 21 | 81 | 0.3 | 0.0 | 2 | Wind 10 kts from the SW. Wind wave from both the NW and SW. |
| April 15 | 79 | - | - | 3 | Frequent whitecaps. Finely mottled photo pattern. Wind 15 kts from NW. |
| Oct. 12 | 51 | - | - | 3 | Finely mottled photo pattern with frequent whitecaps. Wind 15 kts from NW. |
| Mar. 16 | 65 | - | - | 5 | Wind 20 kts NW for two hours. Linear trend normal to wind. Coarsely mottled photo tone with whitecaps everywhere. |

(1 see table 6.

coast. The second wave type is the sea which is generated by the local winds, has a short wave period and a steep, unsymmetrical wave form.

As the wind begins flowing over the water surface, the sea changes from a mirror lake surface to a surface that includes a number of wave trains superimposed on each other. The length of each crest is short and both the wave length and height are irregular. If fetch is large enough and the wind continues long enough as listed in table 12, the significant wave height and peak energy period would be as listed in this table.

The wave forms appear on the aerial photography as a mottled pattern. The curved surfaces of the wave tend to concentrate the sunlight under the wave crest as shown in figure 102. The wave crests appear light while the trough appears dark on the photo, since the wind generated waves are unsymmetrical, the sea in general will appear rougher when viewed looking into the wind than when viewed down wind. This is also true of the oblique aerial photography.

As the wind velocity increases, the average wave length also becomes larger. On the aerial photos the photo pattern changes from a finely mottled tone to a coarse pattern. For a steady wind the mottling will generally show a linear trend normal to the wind direction. When the wind is blowing at 10 kts a few scattered whitecaps will begin appearing; as the wind increases to 15 kts there are frequent whitecaps and at 25 kts whitecaps are everywhere. When the wind exceeds about 25 kts, streaks parallel to the wind direction begin appearing.

## Photographic Limitations

The photographic method of studying waste dispersion is subjected to interferences from several sources. Clear sky with the sun altitude above 25 degrees has given the best results. Clouds in the sky increase the water surface brightness and reduce the subsurface contrast. With the oblique camera mounting, the photography is taken to avoid the direct sunlight reflection. Polarizing filters reduce but do not eliminate the skylight reflection. Shadows from scattered clouds cause uneven lighting and will interfere with the quantitative data processing.

Kraft pulp mill effluent under certain conditions will foam when discharged into the sea. The white foam can cover areas of the plume and, where present, will prevent any photographic measurement of the waste concentration. Whitecaps and spray generated when wind velocities exceed about 15 kts can also interfere with the photographic techniques.

The natural color of the sea varies, with color gradients generally greatest perpendicular to the beach. Near the shore, turbulence in the surf zone entrains and suspends sand and silt particles. The width of this discoloration zone depends on the sea roughness and may extend

Table 12. Conditions in fully developed seas (from Bascom, 1964).

| Wind velocity (kts) | Fetch (miles) | Duration (hours) | Wave height (ft) (1 | Wave period (sec) (2 |
|---|---|---|---|---|
| 10 | 10 | 2.4 | 1.4 | 4 |
| 15 | 34 | 6.0 | 3.5 | 6 |
| 20 | 75 | 10.0 | 8.0 | 8 |
| 25 | 160 | 16.0 | 14.0 | 10 |
| 30 | 280 | 23.0 | 22.0 | 12 |
| 40 | 710 | 42.0 | 44.0 | 16 |
| 50 | 1420 | 69.0 | 78.0 | 20 |

(1 Average of highest 1/3

(2 Period where most of the energy is concentrated.

several thousand feet offshore. During the summer months, dark green upwelled water may appear offshore. If the plume is completely surrounded by the green water, the upwelling does not interfere with the processing; however, often due to horizontal density stratification, the dark upwelled water will form the offshore boundary of the effluent plume. Computer processing of the photographic film requires that film densities be measured throughout the photographs. This processing step can either be done automatically or semi-automatically. When the photograph is digitized automatically, film densities and photo coordinates are measured on a selected grid pattern and a large volume of data is generated. The effect of the interferences listed above can be reduced but not eliminated by computer programming techniques. In the semi-automatic digitizing procedure, the location of points for digitizing is selected manually. This method results in fewer but better data points as areas on the photograph with interferences can be avoided in this step.

## Aerial Photography

Aerial photography provides a comprehensive method of analyzing the dispersion of wastes from existing or proposed outfall sites and is not restricted to periods of calm seas. Field data for measuring concen-

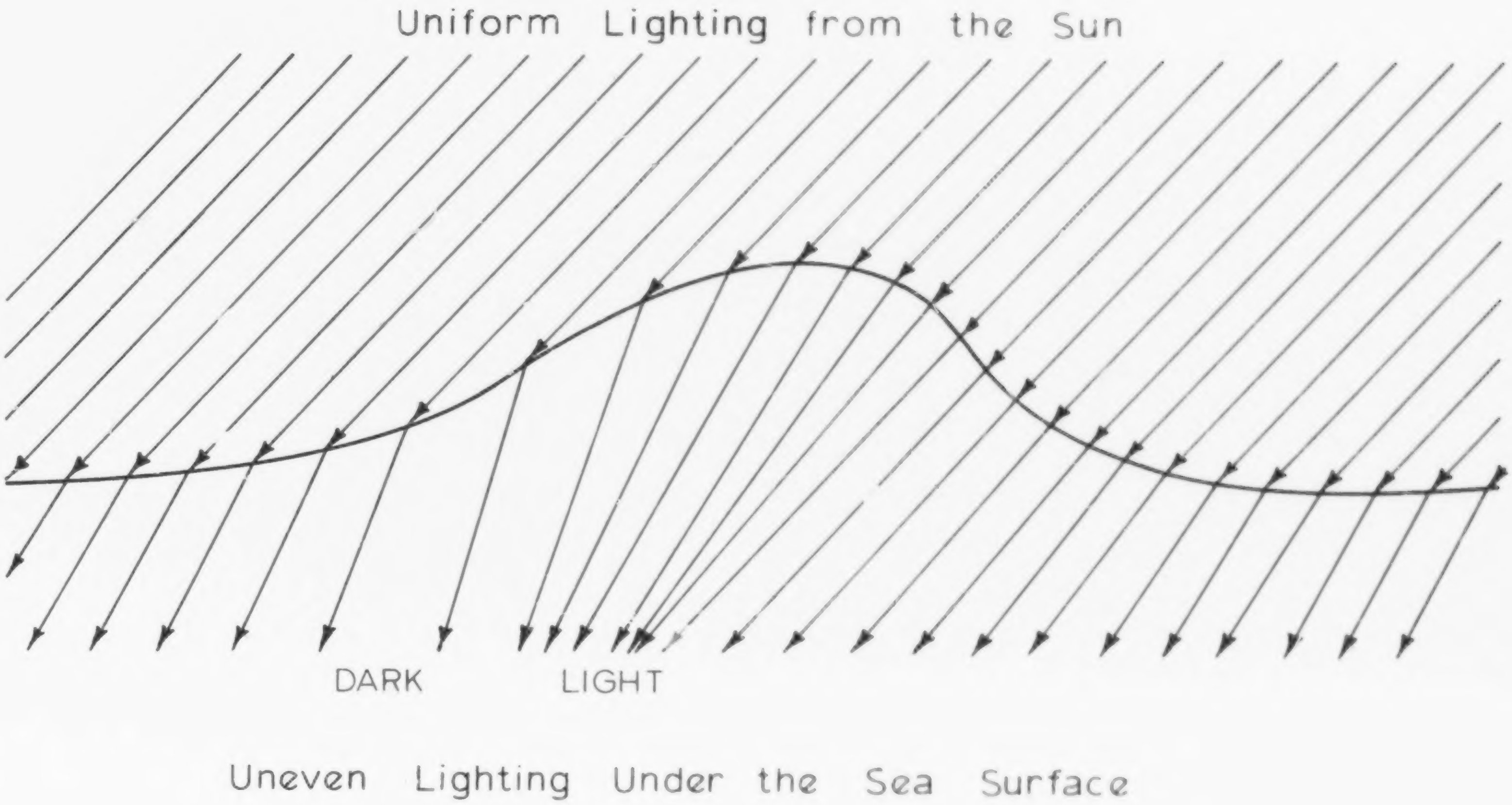
Uniform Lighting from the Sun
DARK
LIGHT
Uneven Lighting Under the Sea Surface

Figure 102. Mottled photo pattern from surface waves.

trations throughout the waste disposal area can be collected in a fraction of a second.

While the time required for gathering concentration data photogrammetrically is short, the computation of current velocities and diffusion coefficients require a minimum of two flights over the area. Generally photographic flights were made at 15-minute intervals. The time between flights need not be lost if several neighboring locations can be studied at the same time.

Boat sampling is hazardous in the nearshore area and is impossible during heavy seas. In order to adequately define a waste ordye field, a boat survey is conducted over an extended period of time. Since the tide, wind and currents are continuously changing, the survey does not represent a pattern at any one instant but is a composite pattern during the sampling period.

During the summer of 1969, aerial photographic surveys and conventional boat sampling surveys were conducted at the same time. The conventional survey was conducted over an eight to twelve hour period including travel time from the dock and required in addition to the boat operator, three people on the vessel to run equipment and two people on shore to locate the boat. The aerial survey team consisted of a pilot and photographer. Two 2-hour photographic flights were made, one in the morning and the second in the afternoon.

The cost of the aerial survey was essentially the same as the conventional survey. The fluorometer aboard the survey vessel cost the same as the three cameras aboard the airplane. The oblique camera mounting eliminated the need for establishing horizontal control markers in the water. A seaworthy boat and experienced operator cost about $200 per day while an airplane and pilot cost about $120 for four hours. The cost of the film and photographic processing range from $30 to $100 per day depending on the type of film.

Computerized techniques were developed for data processing of both the boat records and the aerial photography. Strip chart records from the boat instruments were digitized with the same equipment that was used to measure photographic coordinates. A densitometer would not be required for processing aerial photos from a dye patch study conducted for the purpose of acquiring design information at proposed outfall sites. The computer time for data processing would be nearly the same for the two survey methods.

The aerial survey is not limited by sea conditions, provides comprehensive information on the diffusion process and can be conducted fast with a minimum of personnel. It is a technically and economically feasible method for acquiring ocean outfall design data.

# SECTION XII

## SUMMARY

The objective of this research was to develop a remote sensing tool for the evaluation of dispersion of wastes from existing or proposed ocean outfalls. Photogrammetric and photo interpretation methods are used to determine dispersion patterns, diffusion coefficients, waste concentrations and nearshore currents. This study is unique in that the aerial photography is not only used to determine the position of points and the size of objects as in normal photogrammetry, but the photograph is also used as an energy sensor. The amount of light reflected from an object is recorded by the photograph as the film density of the image. The light scattered from within the sea is measured from the film with a photo densitometer and can be related to certain water quality parameters.

Ocean outfall sewers for the disposal of waste along the Pacific Northwest coastline are, in general, located on the relatively shallow coastal shelf which is subjected to heavy seas. Sampling from a boat in these areas is dangerous at all times and impossible much of the time due to rough water. The use of aerial photography and photogrammetric methods presents a possible method for overcoming this difficulty. From two to eight hours of continuous sampling from a boat is required to adequately define the waste field in the vicinity of an ocean outfall. The waste field is usually shifting thus making a comprehensive study nearly impossible by conventional methods. The aerial photographic technique presents a method where concentrations throughout the waste field can be measured in one instant. Consideration of these factors suggest that photogrammetry can be a most useful tool for water quality investigations. Prior to this time the use of aerial photography for water quality studies has been limited to identifying pollution sources but has not been used for making quantitative measurements from the photographs.

In order to obtain design information at proposed outfall locations, aerial photography is taken of dye patches. The dye markers are dropped from the aircraft at selected locations in the waste disposal area. Current velocities and diffusion coefficients are determined from the change in position and size of the dye patches between two photographic flights over the proposed site.

The field work was conducted at the Georgia-Pacific Kraft pulp mill outfall at Newport because of its convenient location. This site provided an additional advantage since the natural color of the waste effluent was visible on aerial photography. However, the results of this study are not limited to Kraft pulp mill outfalls. If the effluent from an outfall has the same light scattering and light absorption properties as the receiving water, dye can be added to the effluent to distinguish the waste field from the receiving body of water. The natural color characteristics of the Kraft pulp waste will vary with time while the addition of dye to a colorless waste will give greater control over the test.

Three different field procedures were used on the project. During the 1968 and 1969 field seasons, work was carried out by conducting simultaneous studies of the waste plumes by aerial photographic methods and by conventional boat sampling. Concentrations in the plume were determined by metering rhodamine WT tracer into the pipeline and measuring the tracer concentration in the waste field with a fluorometer aboard the survey boat.

During the first field season, two fluorometers were used to sample from one foot and five feet below the water surface. Since there was no significant difference in the concentration at these two depths, only one fluorometer was used during the following field season. A ten-foot sampling probe for the fluorometer intake was constructed for the 1969 field season. Boat sampling was discontinued during the 1970-71 field season and field work continued throughout the fall, winter, and spring when boat operations were impossible due to rough sea conditions most of the time.

Vertical color aerial photography was taken with a single camera by a commercial aerial photography firm during the 1968 field season. As the firm was located approximately 100 miles from the study area, scheduling of the photography was difficult. Photography was taken at scales of 1:6,000 and 1:12,000 using precise mapping cameras. The small scale photography was intended to be used for buoy location by analytical strip bridging. However, it was found more convenient to triangulate the position of the buoys from the shore stations.

As listed in the original proposal, the first year of the study was divided into two phases: 1) Photographing the plume and current floats and 2) Photographing dye slugs introduced into the pipeline. Aerial photography of the dye slugs was difficult to process. Considering a nonsteady state dye patch within a nearly steady state waste field, the amount of dye, waste and sea water could occur in various combinations which would be impossible to distinguish by measuring the light return with the three broad bands of color photography. At a minimum, four individual narrow pass bands would have been required to obtain meaningful results. This phase of the study was later replaced by dye slugs dropped from the airplane away from the waste field.

One of the primary problems encountered in processing the 1968 vertical photography was the direct sunlight reflection from the water surface. Photography after 1968 was taken with an oblique camera mounting to avoid the sun spot. Three cameras were purchased and mounted in the baggage compartment of a small high wing aircraft. The oblique camera mounting reduced the requirement for horizontal control in the water. The large camera photographs included the horizon and two horizontal control points could be identified on shore. The mapping camera, because of its large angular coverage, permitted photographic orientation of the two smaller cameras. Films from the two 70 mm cameras were used for detailed analyses and measurements of the waste field. Polarizing filters on the 70 mm cameras reduced the skylight reflection from the water surface.

During the 1968-1969 field seasons, work was conducted in late June, July, August and early September. Fourteen sampling runs were made during this period. For eight of the fourteen sampling runs, the waste field from the ocean outfall was at the sea surface. A submerged plume occurred during the remaining six sampling runs. When the plume was submerged both the swell height and the wind velocity were significantly less at a 90 percent confidence level than when the plume formed at the surface. Both steady state and nonsteady state diffusion coefficients were computed when possible for each sampling run. Of the eight days that a surface plume occurred, a one dimensional diffusion model was applicable to the plume pattern on only three days. A two dimensional model was necessary to describe the plume when the current velocity was low. When the velocity was greater than 0.4 ft/sec, a one dimensional diffusion model was adequate.

For each day that waste concentrations were computed from both the densitometer measurements taken on the aerial photography and the fluorometer records from the boat sampling, a comparison was made of the concentrations determined by the two methods by matching the ground coordinates. The correlation coefficients for these comparisons ranged from 0.85 to 0.95. When the boat sampling was conducted, there were several locations where the sampling lines crossed and the concentrations were measured twice at one point. The mean square residual determined at these points was significantly greater than the mean square residual between the concentrations determined by boat sampling and aerial photography (generally at a 95% confidence level).

During the final year of the project, 25 field observations were conducted starting in September of 1970 and ending in May of 1971. Diffusion coefficients and water current velocities were computed from the transport and spread of a dye slug dropped from the airplane. Continuous wind records were available from anemometers located on the south jetty. Longitudinal diffusion coefficients determined from the dye patch study ranged from 0.3 to 13.9 while the transverse diffusion coefficients range from 0.0 to 1.9 ft$^2$/sec. The dye patch was nearly always oriented parallel to the wind. When the wind velocity was low, the major axis of the elliptical dye patch would usually be oriented perpendicular to the swell crest.

Of the 25 observations conducted during the fall, winter and spring, the plume was not visible on only one day, covered less than 30 acres on seven days and less than 100 acres on 15 days. The size of the plume was not directly related to the state of the sea code, diffusion coefficients nor related to the effluent discharge rate within the range covered by the study.

The water current velocities ranged from 0.1 to 2.0 ft/sec. The surface water current was found to be the dominant factor in the resulting plume pattern. By a visual comparison, the general direction of the current could be explained by the wind record for 12 of the 17 days that the current velocity was measured.

The Fickian diffusion equation with a unidirectional transport velocity was not applicable to the majority of the observations. A two dimensional model with losses of waste to the lower layers considered by using a decay coefficient was able to better explain the observed plume patterns. The x and y velocity components for this model were determined from the equation as for a line source in a uniform stream.

The characteristic airphoto pattern elements can be used to estimate state of the sea, wind velocity and diffusion coefficients. As the sea becomes rough, the finely mottled tone changes to a coarsely mottled pattern. The density of whitecaps increases with the wind speed and when the wind velocity exceeds 25 kts, streaks parallel to the direction of the wind begin appearing. Within the generating area of the wind curves, the waves are irregular and confused, they appear to have no particular period or common wave height, giving rise to a randomly mottled photo tone. As a dominant wave train develops, the photo pattern has a linear trend normal to the wave movement. With the wave length measured from the photos, the wave period and speed can be estimated using wave formulas.

# SECTION XIII

## ACKNOWLEDGMENTS

The writers wish to express their gratitude to the following: Messrs. T. Fenwick and P. O'Hara of the Georgia Pacific Corporation at Toledo, Oregon.

To members of the Pacific Northwest Water Laboratory, especially Messrs. D. Baumgartner, L. Bentsen, R. Callaway, W. Clotheir, W. DeBen, G. Dittsworth, R. Scott, and D. Trent for their guidance and assistance in collection of the data;

Captain R. Redmond and Messrs. D. McKeel, B. Danby and R. Ervin of Marine Science Center at Newport, Oregon, for their help with the boat operations;

Professors R. Schultz, M. Northcraft, D. Phillips and D. Bella of Oregon State University for their advice and assistance on the project;

Students J. Graham, L. Doester, B. Valentine, R. Spaw, D. Monroe, R. Scholl, W. Hart, T. Basgen, Ching-Lin Chang, M. Soderquist, R. Collier, R. Mann, P. Klampe, B. Barnes, G. Carman, J. Plasker, W. Halverson, A. Langdon, K. Cerotsky and W. Gilbert for their assistance in collection of data, construction of equipment and processing data; and

the Federal Water Quality Office for financial support of the project.

# SECTION XIV

## REFERENCES

Allen Hancock Foundation. 1964. An investigation on the fate of organic and inorganic wastes discharged into the marine environment and their effects on biological productivity. Los Angeles, University of Southern California. 118 p. (California State Water Quality Control Board Publication 29).

American Society of Photogrammetry. 1968. Manual of color aerial photography. Menasha, George Banta Company. 550 p.

American Society of Photogrammetry. 1960. Manual of photographic interpretation. Menasha, George Banta Company. 868 p.

Bascom, Willard. 1964. Waves and beaches. Garden City, Doubleday & Co. 267 p.

Baumgartner, D. J., W. P. James and G. L. O'Neal. 1969. A study of two ocean outfalls. National Council for Air and Stream Improvement Technical Bulletin No. 231. p 27-53.

Baumgartner, D. J. and D. S. Trent. 1970. Ocean outfall design, part I, literature review and theoretical development. USDI, FWQA, Pacific Northwest Water Laboratory, Corvallis, Oregon. April. 129 p.

Baumgartner, D. J., D. S. Trent and K. V. Byram. 1971. User's guide and documentation for outfall plume model. EPA, WQO, Pacific Northwest Water Laboratory, Corvallis, Oregon. Working Paper No. 80, May.

Brooks, Norman H. 1960. Diffusion of sewage effluent in an ocean current. Proceedings of the First International Conference on Waste Disposal in Marine Environment, London, Pergamon Press. p. 246-267.

Burgess, F. J. and W. P. James. 1970. An aerial photographic tracing of pulp mill effluent in marine waters. Federal Water Quality Office, EPA, Water Pollution Control Research Series 12040EBY, Grant WP-00524. 152 p.

Burt, Wayne V. 1953. A note on the reflection of diffusion radiation by the sea surface. Transactions, American Geophysical Union 34(2): 199-200.

Cox, C. and W. Munk. 1954. Measurement of the roughness of the sea surface from photographs of the sun's glitter. Journal of the Optical Society of America 44:838-850.

Cox, Charles and Walter Munk. 1955. Some problems in optical oceanography. Journal of Marine Research 14(1):63-78.

**Preceding page blank**

Elterman, Louis and Robert B. Toolin. 1965. Atmospheric optics. In: Handbook of Geophysics and Space Environment, ed. by Shea L. Valley, Cambridge, Air Force Cambridge Research Laboratories. p 7.1-7.36.

Faas, V. A. 1960. The procurement of aerial photography of underwater objects. In: Manual of photographic Interpretation, American Society of Photogrammetry, Menasha, George Banta Company. p. 96.

Fisher, Davis, and Sousa. 1966. Fresh-water springs of Hawaii from infrared images. U.S. Geological Survey Hydrologic Investigations Atlas HA-218. Washington, D. C.

Fritz, N. L. 1967. Optimum methods for using infrared-sensitive color films. Photogrammetric Engineering 33:1128-1138.

Holter, Marvin R. 1967. Infrared and multispectral sensing. BioScience June. p. 376-383.

Hutchinson, G. E. 1957. A treatise on limnology. Vol. 1. New York, John Wiley and Sons, Inc. 1015 p.

Ichiye, T. and N. B. Plutchak. 1966. Photodensitometric measurements of dye concentration in the ocean. Limnology and Oceanography 2:364-370.

Jensen, Niels. 1968. Optical and photographic reconnaissance systems. New York, John Wiley and Sons, Inc., 211 p.

Jerlov, N. G. 1964. Optical classification of ocean water. In: Symposium on Physical Aspects of Light in the Sea, ed. J. E. Typer, Honolula, University of Hawaii Press. p. 45-49.

Jerlov, N. G. 1968. Optical oceanography. Amsterdam, Elseview Publishing Company. 194 p.

Jones, L. A. and H. R. Condit. 1948. Sunlight and skylight as determinants of photographic exposure. Optical Society of America 38:123-178.

Keller, Morton. 1963. Tidal current surveys by photogrammetric methods. U.S. Coast and Geodetic Survey, Technical Bulletin 22. 20 p.

Keller, M. and G. C. Tewinkel. 1966. Space resection in photogrammetry. U.S. Coast and Geodetic Survey Technical Bulletin 32. 10 p.

Keene, D. F. 1971. A physical oceanographic study of the nearshore zone at Newport, Oregon. M.S. thesis. Corvallis, Oregon State University.

Masch, F. D. 1961. Mixing and dispersive action of wind waves. Berkeley, University of California, IER Technical Report 138-6.

Molineux, C. E. 1965. Multiband spectral system for reconnaisance. Photogrammetric Engineering 31:131-143.

Neumann, G. and W. J. Pierson, Jr. 1966. Principles of physical oceanography. Prentice-Hall, Englewood Cliffs, N. J. 545 p.

Neumaier, G., F. Silvestro, H. Thung, and R. Frank. 1967. Project aqua-map development of aerial photography as an aid to water quality management. Buffalo, Cornell Aeronautical Laboratory, Inc. (Contract No. HC-9768 of the State of New York Conservation Department).

Ory, T. R. 1965. Line scanning reconnaissance systems in land utilization and terrain studies. In: Third symposium on remote sensing of environment. Ann Arbor, University of Michigan. p. 393-398.

Pearson, E. A. 1955. An investigation of the efficacy of submarine outfall disposal of sewage and sludge. California Waste Pollution Control Board Publication 14. 154 p.

Pearson, E. A., P. N. Storrs and R. E. Selleck. 1967. Some physical parameters and their significance in marine waste disposal. In: Pollution and Marine Ecology, ed. by F. J. Burgess and T. A. Olson, New York, Interscience. p. 297-315.

Romanovsky, V. 1966. Coastal currents. In: Proceedings of the Third International Conference on Advances in Water Pollution Research, Munich. Baltimore, Port City Press, Inc. Vol. 3, p. 290-292.

Scherz, James P. 1967. Aerial photographic techniques in pollution detection. Doctoral dissertation. Madison, University of Wisconsin. 82 numb. leaves. (Microfilm)

Strandberg, C. H. 1966. Water quality analysis. Photogrammetric Engineering 32 (2):234-248.

Strandberg, C. H. 1967. Aerial discovery manual. New York, John Wiley and Sons. 249 p.

Sverdrup, H. V., M. W. Johnson and R. H. Fleming. 1942. The oceans. New York, Prentice-Hall. 1087 p.

Swanson, L. W. 1964. Aerial photography and photogrammetry in the Coast and Geodetic Survey. Photogrammetric Engineering, 30(5):699-726.

Tarkington, Raife G. 1966. The photographic process. In: Manual of photogrammetry, 3d ed., Menasha, George Banta Company. p. 243-293.

Tyler, J. E. and W. H. Richardson. 1958. Nephelometer for volume scattering function in situ. Journal of the Optical Society of America 48(5):354-357.

Waldichuk, Michael. 1966. Currents from aerial photography in coastal pollution studies. Proceedings of the Third International Conference on Advances in Water Pollution Research, Munich. Baltimore, Port City Press, Inc. Vol. 3, p. 263-284.

Water Pollution Research Board. 1964. Coastal pollution. Report of the Director, Department of Scientific and Industrial Research, London. p. 136-142.

Wiegel, R. L. 1964. Oceanographical engineering. London, Prentice Hall International. 532 p.

Williams, J.,J. J. Higginson and J. D. Rohdbough. 1968. Air and sea-the naval environment. Menasha, George Banta Company. 338 p.

Wilson, James F., Jr. 1968. Fluorometric procedures for dye tracing. U.S. Geological Survey, Chapter A12 of Book 3 (Applications of Hydraulics). 31 p.

Yost, E. F. and S. Wenderoth. 1967. Multispectral color aerial photography. Photogrammetric Engineering 33:1020-1033.

# SECTION XV

## PUBLICATIONS

1. Burgess, F. J. and W. P. James. 1970. Pulp mills take to the air to monitor ocean outfalls. *Pulp and Paper*, September.

2. James, W. P. and F. J. Burgess. 1969. The use of photogrammetry in predicting outfall diffusion. *National Council for Air and Stream Improvement Technical Bulletin No. 231*. p. 2-26.

3. James, W. P. and F. J. Burgess. 1970. Ocean outfall dispersion. *Photogrammetric Engineering Journal* 36(12):1241-1250.

4. James, W. P. and F. J. Burgess. 1971. Pulp mill outfall analysis by remote sensing techniques. *Journal of the Technical Association of the Pulp and Paper Industry*. 54(3):414-418.

5. James, W. P., F. J. Burgess and D. Baumgartner. 1971. An aerial photographic study of waste fields from three ocean outfalls. *Offshore Technology Conference Proceedings*, Houston, Texas; April 19-21. OTC paper 1374, PPI 483-I498.

## SECTION XVI

## APPENDICES

Page

A. Definition of Terms. . . . . . . . . . . . . . . . . . . . . . 189

B. Computer Program for Processing Vertical Photography . . . . 193

Figure
B-1 Flow diagram for computer program DIFFUSION . . . . 200
B-2 Listing of program. . . . . . . . . . . . . . . . . . 204
B-3 Listing of subroutines. . . . . . . . . . . . . . . . 216
B-4 Sample input, LUN 1 . . . . . . . . . . . . . . . . 222
B-5 Sample input LUNS 3 and 19. . . . . . . . . . . . . 223

C. Processing 1969 Photographic Data. . . . . . . . . . . . . . 224

Figure
C-1 Flow diagram for computer program EDIT. . . . . . . 231
C-2 Listing of program EDIT . . . . . . . . . . . . . . 233
C-3 Sample input for program EDIT . . . . . . . . . . . 241
C-4 Sample output from program EDIT . . . . . . . . . . 242
C-5 Flow diagram of program REMOTE. . . . . . . . . . . 243
C-6 Flow diagram of subroutine PROCESS. . . . . . . . . 245
C-7 Program listing for REMOTE. . . . . . . . . . . . . 247
C-8 Subroutines used with program REMOTE. . . . . . . . 260
C-9 Sample input data for REMOTE. . . . . . . . . . . . 271

D. Processing of 1970-71 Photographic Data. . . . . . . . . . . 272

Figure
D-1 Flow diagram for computer program INSHORE . . . . . 275
D-2 Listing of program INSHORE. . . . . . . . . . . . . 277

E. Streamlines for a Source in a Uniform Flow . . . . . . . . . 284

Figure
E-1 Flow diagram of program FLOWNET . . . . . . . . . . 285
E-2 Listing of program FLOWNET. . . . . . . . . . . . . 286

**Preceding page blank**

# APPENDIX A

## DEFINITION OF TERMS

The following terms that were used in The Rationale are defined as follows:

| | |
|---|---|
| A | is the extinction optical thickness for a standard atmosphere. When subscripted the subscripts b, g and r refer to the blue, green and red bands of the color photograph, respectively. |
| a | is the sea water attenuation coefficient per meter. |
| Az | is the azimuth of the sun from true north. |
| AZ | is the azimuth of the sun from grid north. |
| $\alpha$ | is the angle at the incremental scattering volume between incident and scattered beams. |
| b | is the waste absorption coefficient in (Meter-ml/liter)$^{-1}$. |
| $\beta(\alpha)$ | is the volume scattering function per meter. |
| C | is the attenuation coefficient for the sea water and waste per meter. |
| c | is the angle between the ray to the camera and the camera axis. |
| $D_b(x,y)$, $D_g(x,y)$ | and $D_r(x,y)$ are the film densities measured at photo coordinates x and y for the blue, green and red bands, respectively. |
| dJ | is the scattered light intensity from the incremental scattering volume. |
| $d\Omega$ | is the solid angle in steradians. |
| dV | is the incremental scattering volume. |
| E | is the extinction optical thickness for the atmosphere from the sea surface to the camera. When subscripted the subscripts b, g and r refer to the blue, green and red bands of color photograph, respectively. |
| EX | is the photographic exposure. |

| | |
|---|---|
| $f$ | is the cameras focal length. |
| FNO | is the relative aperture of the lens. |
| $G$ | is a constant representing film contrast. |
| $H$ | is the irradiance in watts per square centimeter. |
| $H_o$ | is the irradiance from the sun at the outer atmosphere normal to the ray. |
| $H_s$ | is the irradiance on a horizontal plane from the sun at the sea surface. |
| $H_{sky}$ | is the irradiance from skylight at the sea surface. |
| $H_a$ | is the irradiance at the sea surface from the scattering volume. |
| $H_w$ | is the irradiance from the sun on a plane normal to the ray below the water surface. |
| $H_z$ | is the irradiance from the sun at a depth z below the water surface. |
| $H'$ | is the irradiance of the film image. |
| $i$ | is the angle of incidence of the direct sunlight at the water surface. |
| $i_2$ | is the angle of incidence of the scattered light at the water surface. |
| $j$ | is the angle of refraction of the direct sunlight at the water surface. |
| $j_2$ | is the angle between the vertical and the object ray. |
| $K$ | is a constant. |
| Ka | is the rotation angle about the Z camera axis. |
| $M$ | is a constant representing film speed. |
| $n$ | is the refractive index of water. |
| $N$ | is the total radiance from the sea in watts per square centimeter-steradian. |
| $N_a$ | is the radiance from the scattering volume above the |

| | |
|---|---|
| | sea surface. |
| $N_b$, $N_g$ and $N_r$ | are the total radiance at the sea surface including reflected skylight, reflected direct sunlight and scattered light from within the sea for the blue, green and red bands of the photograph, respectively. |
| $N_c$ | is radiance from the sea measured at the camera station. |
| $N_d$ | is the radiance of direct sunlight reflection from the water surface. |
| $N_{sky}$ | is the skylight radiance reflected from the water surface. |
| $N_w$ | is the radiance from the scattering volume under the sea surface. |
| $P_a$ | is the reflectivity of direct sunlight from the sea surface. |
| $P_s$ | is the reflectivity of skylight from the water surface. |
| $P_w$ | is the reflectivity of uplighting from the sea at the surface. |
| RA | is the variation in the ratio of red to green light returned from within the sea due to the waste. |
| RM | is photographic orientation matrix. |
| $R_p$ | is the ratio of red to green radiance at the camera station. |
| $R_{ph}$ | is the ratio of red to green radiance at the sea surface. |
| $R_{pho}$ | is the estimated ratio of red to green radiance at the sea surface if there was no waste present. |
| SUNR | is the angle between the object ray and the direct sunlight reflection from a horizontal plane. |
| TIM | is the photographic exposure time in seconds. |
| TR | is the lens transmittance. When it is subscripted the subscripts b, g and r refer to the blue, green and red bands, respectively. |

| | |
|---|---|
| $W$ | is the waste concentration in milliliters per liter. |
| $W_o$ | is the rotation angle about the X axis of the camera. |
| $Z$ | is the flying height in feet. |
| $z$ | is the distance in meters below the water surface. |
| $\phi$ | is the rotation angle about the Y axis of the camera. |

# APPENDIX B

## COMPUTER PROGRAM
## FOR
## PROCESSING VERTICAL PHOTOGRAPHY

### Introduction

Included in this appendix are the program and subprogram listings and sample input data for processing of vertical photography. The program determines diffusion coefficients from two flights of aerial color photographs and was written for the CDC 3300 system in Fortran IV computer language. The unique feature of this system is the remote access to the computer by teletypes on a time sharing basis.

Input data for the program is either from a logical unit number (LUN) or from the teletype keyboard. The input statements include the standard READ statement, FFIN (1), or TTYIN(4H X = ). The free form input (FFIN) will accept data in any format in columns 1 to 72 as long as the words are separated by at least one space. The number in parentheses with the call command is the input LUN. The teletype free form input command (TTYIN) allows the user to enter data from the teletype. The parameter in the TTYIN function must be a hollerith constant containing four characters. When the fortran statement is executed, the hollerith message is printed on the user's teletype. Only a single variable can be entered each time the function is executed.

### Program Listing

Flow diagram for the program used to process the 1968 photographic data is shown in figure B-1. The numbers in parentheses on the diagram refer to the line numbers on the program listing shown in figure B-2. The main array was declared an integer to save storage space and is dimensioned 2, 120, 60. If the size of this array is changed, only lines 3, 30, 31, 539 and 540 in the main program will require modification.

All except two of the subroutines called in the main program are listed in figure B-3. These subroutines, date and time, return the time and date of computer processing. If they are not available, lines 26 through 29 of the main program should be erased. The following subroutines are included in the listing:

| | |
|---|---|
| Rotate | - Converts state plane coordinates to coordinates based on system oriented about waste field. |
| Sunlite | - Determines sun altitude and azimuth. |
| Resect | - Determines the orientation of near vertical photographs and was modified from USC & GS |

program resection. Each time the subroutine is called, the camera station coordinates and orientation matrix are printed on LUN 2.

Leastfit - Determines the least squares solution of the regression coefficients for a linear model to data with one independent and up to nine dependent variables. Each time the subroutine is executed, values of the regression coefficients, standard deviation, variance-covariance matrix, and $Y$, $\hat{Y}$, and e for each observation are written on LUN 2.

Matinv - Determines the inverse of a square matrix.

Trncoord - Converts the photographic vector to a unit vector oriented with the state plane coordinate system.

Grdcoord - Determines the ground coordinates of the unit vector.

Angles - Determines the angles between the object ray and the vertical in air and under the water. Determines the angles between the sun ray and the object ray above and below the water surface.

## Input Data

Input data for the program are from five sources. These are the teletype, photo coordinates and film densities from LUN 1, ground control coordinates from LUN 3, general information from LUN 5 and waste concentration as measured by fluorometers with ground coordinates from LUN 19.

### Teletype

The following information is to be typed on the teletype after the hollerith constant is printed during program execution.

| No. | Hollerith Constant | Remarks |
|---|---|---|
| 1. | IGO | Type in 1 if the photo values in the array are to be averaged and the maximum value printed on the teletype for each section across the waste field or 2 if this is not required. |
| 2. | B1= | Coefficient for the linear term relating the photo value to waste concentration. |
| 3. | B2= | Coefficient for the squared term relating the photo value to waste concentration. |

| No. | Hollerith Constant | Remarks |
|---|---|---|
| 4. | VEL= | Estimated velocity if there were no current floats. |
| 5. | | Repeat above items 1-3 for second flight. |

LUN 1

Sample input from LUN 1 is shown in figure B-4. As the input on this LUN is mostly from the digitizer the Z value (densitometer voltage) is always recorded but is not always used in the computations. In the sample input there were two photos in the first flight (lines 1 through 359) and three in the second flight (lines 360 through 1336). In figure B-4, lines 1 through 33 and lines 360 through 398 are read with free form input while the other lines are read on a fixed format.

Description of the input data one LUN 1 follows

| Item | Line No. | Remarks |
|---|---|---|
| 1. | 1 | Camera focal length in mm for photo 1 of flight 1. |
| 2. | 2 | Photo number in flight (00001), number of photo control points on the photograph (0006) and the X, Y, Z photo coordinates of the principal point. |
| 3. | 3-4 | Point identification number and the X, Y, Z values of control points. This series is repeated six times to input photo coordinates. |
| 4. | 5 | 0.0 to indicate end of current float coordinates (none in this example). |
| 5. | 6 | Identification number and the X, Y, Z photo coordinates at the head of the plume and at a point along the plume. These points are used to orient the array about the plume. |
| 6. | 8-9 | Eighteen film densities on the standard grey scale. |
| 7. | 10-15 | Identification number and the X, Y, Z values |

| Item | Line No. | Remarks |
|---|---|---|
| | | measured on the grey scale with the red filter in the densitometer. Only the voltage in the Z coordinate is used in computations. |
| 8. | 16-21 | Same as lines 10-15 except readings are with the green filter. |
| 9. | 22-27 | Same as lines 10-15 except readings are with the blue filter. |
| 10. | 28 | Focal length in mm for photo number two of the first flight. |
| 11. | 29 | Photo number, number of control points and X, Y, Z photo coordinates. |
| 12. | 30-31 | Same as lines 2-4. |
| 13. | 33 | 0.0 to indicate end of current float coordinates (none in this case). |
| 14. | 34-70 | Film densities for points outside the plume with one line being required for each point. The first number on each line is the photo number followed by the point number which is less than 200. The point number with the X, Y, Z values are repeated three times to input the red, green and blue film density voltages. The green film density voltage is the Z value of the center group while the blue or red can be in either the first or third group. The red film density voltage is always larger than the blue value. |
| 15. | 71-358 | Same as lines 34-70 except the points are in the waste field and are numbered between 300 and 399. |
| 16. | 359 | Blank card to indicate end of flight 1. |
| 17. | 360 | Same as item 1 except for photo 1 of flight 2. |
| 18. | 361 | Same as item 2. |
| 19. | 362-363 | Same as item 3. |

| Item | Line No. | Remarks |
|---|---|---|
| 20. | 364 | Same as item 4. |
| 21. | 366-367 | Same as item 7. |
| 22. | 368-385 | Same as items 8, 9 and 10. |
| 23. | 386 | Same as item 1 except for photo 2 of flight 2. |
| 24. | 387 | Same as item 2. |
| 25. | 388 | Same as item 3. |
| 26. | 389-390 | Point identification number (900 or greater) and X, Y, Z photo coordinates of current floats. |
| 27. | 392 | Same as item 4. |
| 28. | 393 | Same as item 1 except for photo 3 of flight 2. |
| 29. | 394 | Same as item 2. |
| 30. | 395-396 | Same as item 3. |
| 31. | 398 | Same as item 4. |
| 32. | 399-458 | Same as item 15. |
| 33. | 459-1335 | Same as item 16. |
| 34. | 1336 | Blank card to indicate end of input data. |

LUN 3

Sample input from LUN 3 is shown in figure B-5. This LUN contains the ground coordinates of the photo control stations and some initial orientation parameters for the five photographs. On the lines containing four numbers, the numbers are the point identification number, and the X, Y, Z state plane coordinates for the photo control. The control data must be listed in the same sequence as the photo coordinates were listed on LUN 1. Lines in figure B-5 containing three numbers list the initial approximation of the camera station coordinates (X, Y, Z). The lines containing 0.0 and 1.0 list the sine and cosine values of the initial approximation of the photo azimuth.

### LUN 5

LUN 5 contains the general information required for the program. The information is read with free form input and is described as follows:

| No. | Description |
|---|---|
| 1. | Number of flights to be processed. |
| 2. | Time difference between flights in seconds. |
| 3. | Effluent flow rate in gpm. |
| 4. | Number of photos in flight 1. |
| 5. | Time of day of first flight in hours. |
| 6. | Time of day - minutes past even hour. |
| 7. | Declination in degrees at 0 hr GCT. |
| 8. | Declination - minutes over even degree. |
| 9. | Change in declination in minutes per hour. |
| 10. | Equation of time in minutes. |
| 11. | Equation of time - seconds over even minute. |
| 12. | Change in equation of time in seconds per hour. |
| 13. | Longitude of exposure station in degrees. |
| 14. | Latitude of exposure station in degrees. |
| 15. | Reciprocal of exposure time. |
| 16. | F - number of lens setting. |
| 17. | Film gamma to base 10. |
| 18. | Photo identification for symbolic plot. |
| 19. | Day for heading on symbolic plot. |
| 20. | Month for heading of symbolic plot. |

If two flights are being processed, the following information is required:

| No. | Description |
|---|---|
| 21. | Number of photos in second flight. |
| 22. | F - number of lens setting. |
| 23. | Film gamma to base 10. |
| 24. | Photo identification for symbolic plot. |
| 25. | Day for heading on symbolic plot. |
| 26. | Month for heading on symbolic plot. |

### LUN 19

A partial listing of data on LUN 19 is also shown in figure B-5. Each line contains the position number, X, Y state plane coordinates of the boat, waste concentration in milliliters per liter and the sampling depth. A blank line is inserted after the data to indicate end of data.

## Output from Program

Output from program DIFFUSION is on LUNS 2, 4 and 20. The output on LUN 2 includes the photo orientation matrix, current float coordinates, statistical information from subroutine LEASTFIT, symbolic plots, a plot of difference in concentration between flights and diffusion coefficients. The output on LUN 4 is used for more detailed statistical analyses of photo values ($R_{ph} - R_{pho}$) and boat concentrations and ground coordinates are read out on LUN 20.

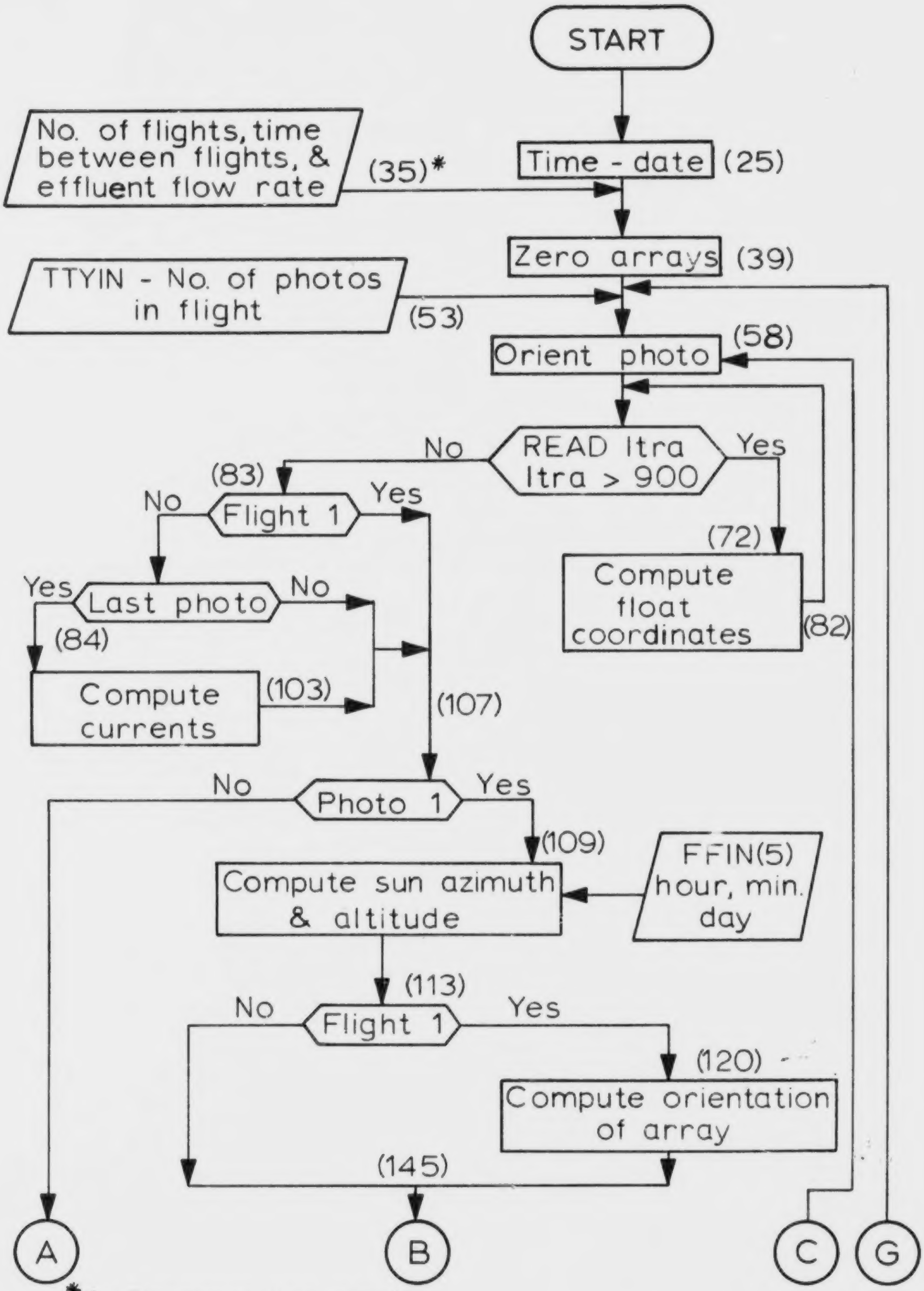

*( ) Program line number

Figure B-1. Flow diagram for computer program DIFFUSION.

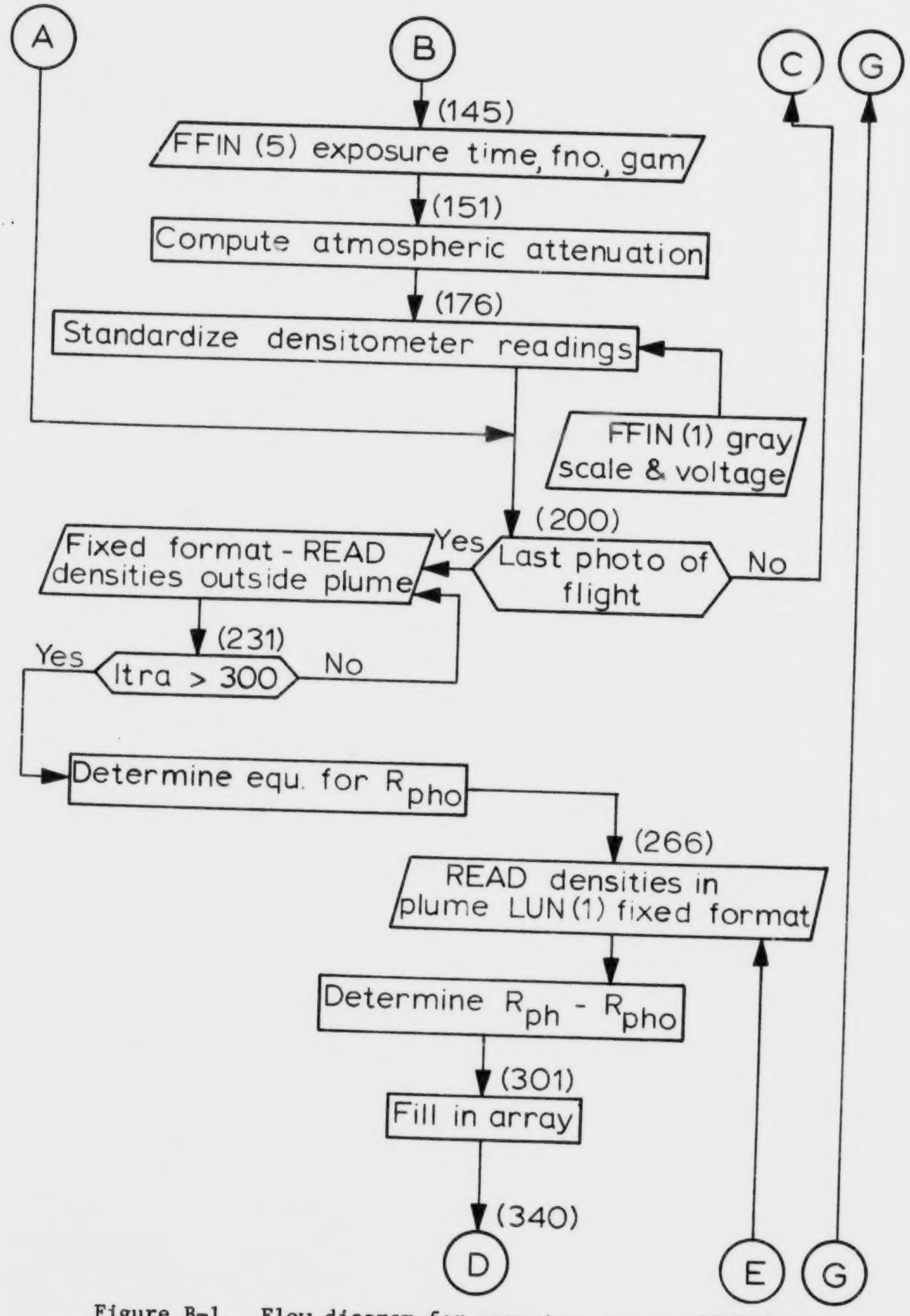
A
B
C
G
(145)
FFIN (5) exposure time, fno., gam
(151)
Compute atmospheric attenuation
(176)
Standardize densitometer readings
FFIN (1) gray scale & voltage
(200)
Yes
Last photo of flight
No
Fixed format - READ densities outside plume
(231)
Yes
Itra > 300
No
Determine equ. for R pho
(266)
READ densities in plume LUN (1) fixed format
Determine R ph - R pho
(301)
Fill in array
(340)
D
E
G

Figure B-1. Flow diagram for computer program DIFFUSION.

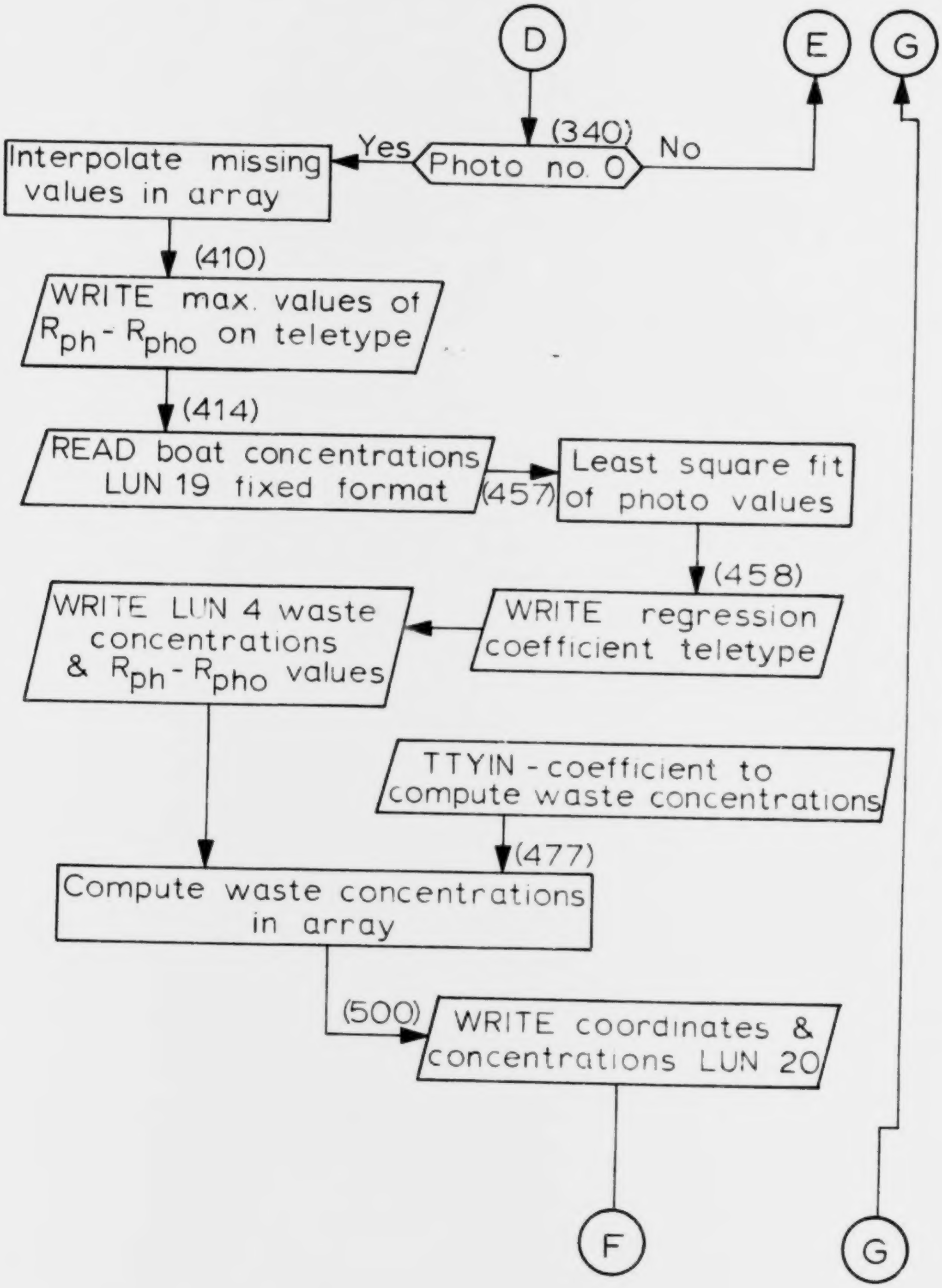
D
E
G
(340)
Yes
Photo no. 0
No
Interpolate missing values in array
(410)
WRITE max. values of $R_{ph} - R_{pho}$ on teletype
(414)
READ boat concentrations LUN 19 fixed format
(457)
Least square fit of photo values
(458)
WRITE LUN 4 waste concentrations & $R_{ph} - R_{pho}$ values
WRITE regression coefficient teletype
TTYIN - coefficient to compute waste concentrations
(477)
Compute waste concentrations in array
(500)
WRITE coordinates & concentrations LUN 20
F
G

Figure B-1. Flow diagram for computer program DIFFUSION.

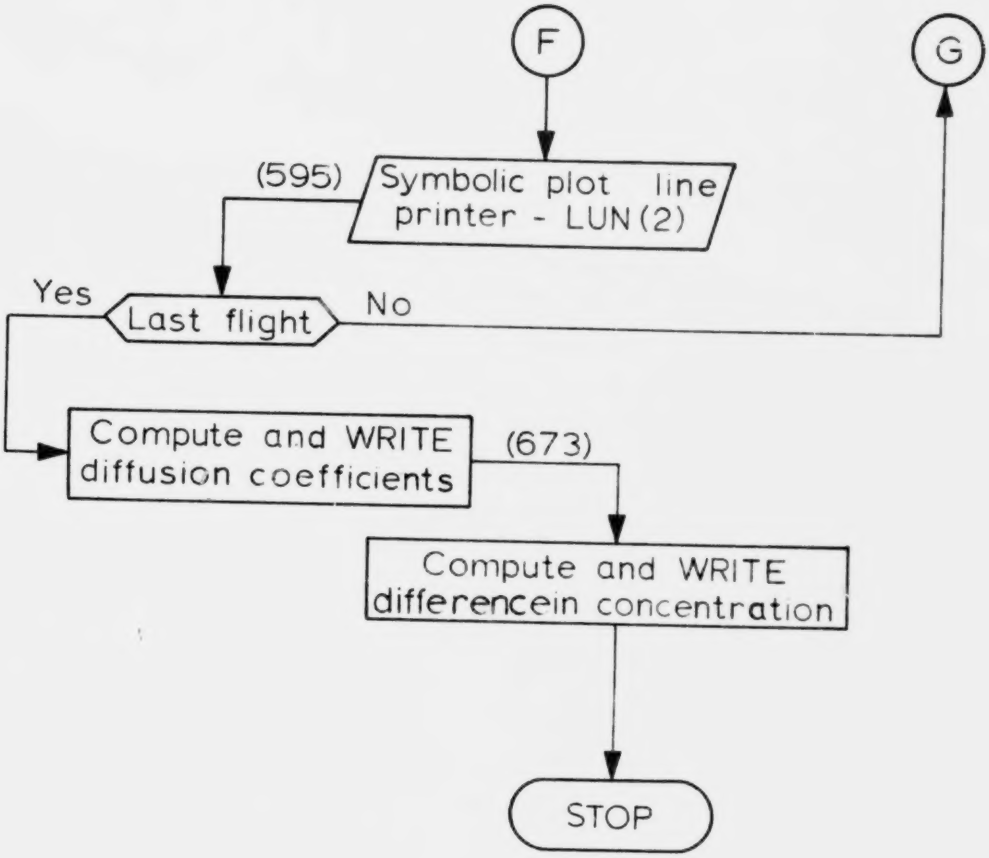
F
G
(595)
Symbolic plot line printer - LUN(2)
Yes
Last flight
No
Compute and WRITE diffusion coefficients
(673)
Compute and WRITE differencein concentration
STOP

Figure B-1. Flow diagram for computer program DIFFUSION.

```
      PROGRAM DIFFUSION
      DIMENSION C(20,3),XFTS(2,10,2),XT(3),XS(9),DEN(3),THI(3),B(9),
     1 RATIO(2,120,60),XPG(2),CAMO(3,5,3),RAD(3),XAR(2,8),
     2 DB(4,3)
      COMMON X(10,200)
      INTEGER RATIO,HARDWARE
      IF (HARDWARE(2) .EQ. 1) GO TO 62
      CALL EQUIP(2,5HFILE )
      GO TO 63
   62 REWIND 2
   63 IF (HARDWARE(4) .EQ. 1) GO TO 64
      CALL EQUIP(4,5HFILE )
      GO TO 65
   64 REWIND 4
   65 IF (HARDWARE(20) .EQ. 1) GO TO 66
      CALL FQUIP(20,5HFILE )
      GO TO 67
   66 REWIND 20
   67 IF (HARDWARE(19) .EQ. 1) 68,1000
   68 IF (HARDWARE(3) .EQ. 1) 69,1000
   69 REWIND 3
      IF (HARDWARE(1) .EQ. 1) 70,1000
   70 REWIND 1
      IF (HARDWARE(5) .EQ. 1) 71,1000
   71 REWIND 5
      CALL TIME(ETIME)
      CALL DATE(EDATE)
      WRITE(02,56) EDATE,ETIME
   56 FORMAT(//////10X,A8,30X,A8//////)
      NNXS=120
      NNYS=60
      YMIDY=30*NNYS
C     NO. OF FLIGHTS OVER AREA, TIME DIFFERENCE BETWEEN
C     FLIGHTS IN SECONDS, AND FLOW RATE OF EFFLUENT IN GPM
      IRUNM=FFIN(5)
      DTIM=FFIN(5)
      RATE=FFIN(5)
      RATE=RATE/(7.48*60.)
C     ZERO ARRAY
      DO 50 LX=1,NNXS
      DO 50 LY=1,NNYS
      DO 50 K=1,2
      RATIO(K,LX,LY)=0
   50 CONTINUE
      DO 55 I=1,2
      DO 55 J=1,10
      DO 55 K=1,2
      XFTS(I,J,K)=0.
   55 CONTINUE
      IRUN=1
   54 REWIND 19
C     NO OF PHOTOS IN THIS FLIGHT
      IPMX=FFIN(5)
      IPHOT=1
      WRITE (02,31)
      KFTS=1
C     ORIENT PHOTO
  100 CALL RESECT (FL,XP,YP,C)
      CAMO(IPHOT,5,1)=XP/1000.
      CAMO(IPHOT,5,2)=YP/1000.
      DO 105 J=1,3
      CAMO(IPHOT,I,J)=C(I,J)
  105 CONTINUE
```

Figure B-2. Listing of program.

```
      DO 106 J=2,4
      K=J+2
      DO 106 I=1,3
      CAMO(IPHOT,J,I)=C(K,I)
  106 CONTINUE
      J=1
  104 ITRA=FFIN(1)
      IF (ITRA-900) 108,107,107
  107 X(2,J)=(FFIN(1)-XP)/1000.
      X(1,J)=(FFIN(1)-YP)/1000.
      BB=FFIN(1)
      CALL TRNCOORD (CAMO,XT,J,FL,IPHOT)
      CALL GRDCOORD(CAMO,XT,XPG,J,IPHOT)
      WRITE (02,34) ITRA,XPG(1),XPG(2)
   34 FORMAT (' FLOAT  ',I5,2F10.0)
      XFTS(IRUN,KFTS,1)=XPG(1)
      XFTS(IRUN,KFTS,2)=XPG(2)
      KFTS=KFTS+1
      GO TO 104
  108 GO TO (109,130),IRUN
  130 IF(IPMX-IPHOT) 131,131,109
  131 J=0
      DO 135 K=1,10
      DX=XFTS(1,K,1)-XFTS(2,K,1)
      DY=XFTS(1,K,2)-XFTS(2,K,2)
      DX=SQRT(DX*DX+DY*DY)
      IF (DX .LE. 100. .OR. DX .GT. 3000.) 135,133
  133 J=J+1
      X(1,J)=DX/DTIM
      WRITE (02,16) J,X(1,J)
   16 FORMAT(' VELOCITY   ',I5,10X,F10.2,'   FT PER SEC')
  135 CONTINUE
      K=J+1
      VEL=0.0
      GO TO (111,132),K
  132 DX=J
      DO 140 K=1,J
      VEL=VEL+X(1,K)
  140 CONTINUE
      VEL=VEL/DX
  111 IF (VEL-0.001) 142,142,143
  142 VEL=TTYIN(4HVEL=)
  143 LDFX=VEL*DTIM/60.+0.5
  109 GO TO (110,219),IPHOT
C     COMPUTE ALTITUDE AND AZIMUTH OF THE SUN
  110 CALL SUNLITE (H,AZ,IRUN,DTIM)
      SAZ=AZ+3.14159
      IF (SAZ-6.28318) 114,114,112
  112 SAZ=SAZ-6.28318
  114 GO TO(115,116),IRUN
  116 ROT=-ROT
      XLOW=XORG
      YMID=YORG
      GO TO 211
C READ IN THE DIRECTION OF THE  PLUME AND ORIENT RATIO ARRAY
C FIRST POINT DEFINES ZERO O.  GRID FOR PLUME
  115 DO 200 J=1,2
      ITRA=FFIN(1)
      X(2,J)=(FFIN(1)-XP)/1000.
      X(1,J)=(FFIN(1)-YP)/1000.
      BB=FFIN(1)
      CALL TRNCOORD(CAMO,XT,J,FL,IPHOT)
      CALL GRDCOORD(CAMO,XT,XPG,J,IPHOT)
```

**Figure B-2.  Listing of program (continued).**

```
      IF (J-1) 196,196,198
  196 XLOW=XPG(1)
      YMID=XPG(2)
  198 X(3,J)=XT(1)
      X(4,J)=XT(2)
  200 CONTINUE
      BOT=X(3,2)-X(3,1)
      TOP=X(4,2)-X(4,1)
      DIV=BOT/TOP
      ROT=ATANF(DIV)
      IF (TOP) 206,211,211
  206 ROT=ROT+3.14159
  211 SROT=SINF(ROT)
      CROT=COSF(ROT)
      WRITE(02,2) ROT,XLOW,YMID
    2 FORMAT(' ROT ANGLE = ' ,F10.5,5X,'XLOW',F10.0,5X,'YMID',F10.0)
      SXF=-SINF(AZ)
      SYF=-COSF(AZ)
C     EXPOSURE TIME ,F/D, AND FILM GAMMA TO BASE 10
      ETIME=FFIN(5)
      FNUM=FFIN(5)
      GAM=FFIN(5)/2.30
      CEXP=ETIME*FNUM**2
C      OPTICAL THICKNESS 3000 TO 10,000 FT
      THI(1)=0.108+0.069*LOGF(C(1,3)/3280.)
      THI(2)=THI(1)*1.15
      THI(3)=THI(1)*1.4
      RAD(1)=EXPF(-0.252/SINF(H))
      RAD(2)=EXPF(-0.331/SINF(H))
      DTHI=-0.024*LOGF(C(1,3)/3280.+1)
      TENR=RAD(1)/RAD(2)
      RAD(3)=EXPF(-0.45/SINF(H))
      HI=3.14159/2.-H
      SINH=0.75*SINF(HI)
      COSH=SQRT(1.0-SINH**2)
      TANH=SINH/COSH
C      ANGLE BETWEEN SUN RAY AND VERTICAL UNDER WATER
      HW=ATANF(TANH)
      WRITE (02,3) HW
    3 FORMAT(' UNDERWATER SUN ANGLE = ' ,F10.5)
      XS(1)=SINF(HW)*(-SXF)
      XS(2)=SINF(HW)*(-SYF)
      XS(3)=-COSF(HW)
      XS(4)=COSF(H)*(-SXF)
      XS(5)=COSF(H)*(-SYF)
      XS(6)=-SINF(H)
      XS(7)=-COSF(H)
      XS(8)=SINF(SAZ)
      XS(9)=COSF(SAZ)
C     READ IN FILM DENSITIES  FROM GREY SCALE
      DO 215 J=1,18
      X(5,J)=FFIN(1)
      X(1,J)=1.0
  215 CONTINUE
C     READ IN  VOLTAGES RED GREEN AND BLUE
      DO 217 I=1,3
      DO 216 J=1,18
      ITRA=FFIN(1)
      ITRA=FFIN(1)
      ITRA=FFIN(1)
      X(2,J)=FFIN(1)/10.
      X(3,J)=X(2,J)*X(2,J)
      X(4,J)=X(3,J)*X(2,J)
```

Figure B-2. Listing of program (continued).

```
  216 CONTINUE
      N=5
      NO=18
      CALL LEASTFIT(N,NO,B)
      DB(1,I)=B(1)
      DB(2,I)=B(2)
      DB(3,I)=B(3)
      DB(4,I)=B(4)
  217 CONTINUE
  219 IPHOT=IPHOT+1
      IF (IPHOT-IPMX) 100,100,218
  218 J=1
  220 READ(01,35) IPHOT,ITRA,X(2,J),X(1,J),DEN1,DEN(2),DEN3
      IF (DEN1-DEN3) 222,222,224
  222 DEN(3)=DEN1
      DEN(1)=DEN3
      GO TO 225
  224 DEN(1)=DEN1
      DEN(3)=DEN3
  225 DO 227 I=1,3
      DEN(I)=DB(1,I)+DB(2,I)*DEN(I)+DB(3,I)*DEN(I)*DEN(I)
     1 +DB(4,I)*DEN(I)**3
  227 CONTINUE
      IF (DEN(1) .LE. 0.9 .OR. DEN(1) .GT. 3.25) 220,228
  228 IF (DEN(2) .LE. 0.7 .OR. DEN(2) .GT. 3.25) 220,229
  229 IF (DEN(3) .LE. 0.4 .OR. DEN(3) .GT. 3.25) 220,231
   35 FORMAT (I5,I4,2F6.3,F5.1,17X,F5.1,17X,F5.1)
  231 X(1,J)=X(1,J)-CAMO(IPHOT,5,2)
      X(2,J)=X(2,J)-CAMO(IPHOT,5,1)
C      ANGLE BETWEEN CAMERA AXIS AND RAY
      R=SQRT(X(1,J)**2+X(2,J)**2)
      CAM=ATANF(R/FL)
      CALL TRNCOORD(CAMO,XT,J,FL,IPHOT)
      CALL ANGLES(XT,XS,FL,J,CAN,CCA,TAB,SUNR)
      X(10,J)=SUNR
      X(5,J)=COSF(CAN)
      X(6,J)=DEN(1)-DEN(2)
      X(6,J)=EXPF(X(6,J)/GAM+(DTHI)/X(5,J))/TENR
      X(7,J)=EXPF(DEN(3)/GAM)*CEXP/COSF(CAM)**4
      X(8,J)=CAN
      J=J+1
      IF (ITRA-300) 220,230,220
  230 INO=J-2
      K=1
      DO 238 J=1,INO
      X(1,K)=1.0
      X(2,K)=X(8,J)
      X(3,K)=X(2,K)*X(2,K)
      X(4,K)=1.0/X(7,J)
      WRITE (02,44) X(1,K),X(2,K),X(3,K),X(4,K)
   44 FORMAT (4E11.3)
      K=K+1
  238 CONTINUE
      NO=K-1
      N=4
      CALL LEASTFIT(N,NO,B)
      A1=B(1)
      A2=B(2)
      A3=B(3)
      DO 243 J=1,INO
      TRB=A1+A2*X(8,J)+A3*X(8,J)*X(8,J)
      X(1,J)=1.
      X(2,J)=X(10,J)
```

Figure B-2. Listing of program (continued).

```
      X(3,J)=X(7,J)*TRE
      X(4,J)=X(6,J)
      WRITE (02,43) X(1,J),X(2,J),X(3,J),X(4,J)
   43 FORMAT (4E11.3)
  243 CONTINUE
      N=4
      NO=INO
      CALL LEASTFIT (N,NO,B)
      B1=B(1)
      B2=B(2)
      B3=B(3)
      XLAST=0.0
      J=1
  245 READ (01,35) IPHOT,ITRA, X(2,J),X(1,J),DEN1,DEN(2),DEN3
      IF (IPHOT) 260,260,244
  244 IF (DEN1-DEN3) 322,322,324
  322 DEN(1)=DEN3
      DEN(3)=DEN1
      GO TO 325
  324 DEN(1)=DEN1
      DEN(3)=DEN3
  325 DO 327 I=1,3
      DEN(I)=DB(1,I)+DB(2,I)*DEN(I)+DB(3,I)*DEN(I)*DEN(I)
     1 +DB(4,I)*DEN(I)**3
  327 CONTINUE
      IF (DEN(1) .LE. 0.9 .OR. DEN(1) .GT. 3.25) 245,328
  328 IF (DEN(2) .LE. 0.7 .OR. DEN(2) .GT.  3.25) 245,329
  329 IF (DEN(3) .LE. 0.4 .OR. DEN(3) .GT. 3.25) 245,246
  246 IF(X(1,J)-XLAST) 260,260,247
  247 XLAST=X(1,J)
      X(1,J)=X(1,J)-CAMO(IPHOT,5,2)
      X(2,J)=X(2,J)-CAMO(IPHOT,5,1)
      R=SQRT(X(1,J)**2+X(2,J)**2)
      CAM=ATANF(R/FL)
      CALL TRNCOORD(CAMO,XT,J,FL,IPHOT)
      CALL GRDCOORD(CAMO,XT,XPG,J,IPHOT)
      CALL ANGLES(XT,XS,FL,J,CAN,CCA,TAB,SUNR)
      CALL ROTATE(XPG,XLON,YMID,CROT,SROT,J)
      COSC=COSF(CAN)
      YRRA=CEXP/COSF(CAM)**4
      DEN(1)=EXPF((DEN(1)-DEN(2))/GAM+DTHI/COSC)
     1 /TENR
      DEN(3)=EXPF(DEN(3)/GAM)*YRRA
      TRB=A1+A2*CAN+A3*CAN*CAN
      BLUE=DEN(3)*TRB
      X(10,J)=DEN(1)-B1-B2*SUNR-B3*BLUE
      J=J+1
      IF (J-200) 245,245,260
C  FILL IN ARRAY WITH PHOTO VALUES
C X AXIS ALONG THE CENTER LINE OF PLUME
  260 KK=J-1
      DO 285 J=1,KK
      LX=X(1,J)/60.+0.5
      IF (LX .LE. 0 .OR. LX .GT. NNXS) 285,262
  262 LY=(X(2,J)+YMIDY)/60.+0.5
      IF (LY .LE. 0 .OR. LY .GT. NNYS) 285,264
  264 RATIO(IRUN,LX,LY)=X(10,J)*1000.
      IF (J-1) 280,280,267
  267 DDEN=X(10,J)-X(10,J-1)
      DKX=LX-LLX
      DKY=LY-LLY
      XKX=ABSF(DKX)
      YKY=ABSF(DKY)
```

Figure B-2. Listing of program (continued).

```
      IF (XKX-YKY) 268,269,269
  268 KY=YKY-1.
      DIV=YKY
      GO TO 270
  269 KY=XKX-1.
      DIV=XKX
  270 IF (DIV-6.)272,272,280
  272 DO 275 K=1,KY
      YYK=K
      DE=X(10,J-1)+DDEN*YYK/DIV
      KKX=LLX+YYK*DKX/DIV+0.5
      KKY=LLY+YYK*DKY/DIV+0.5
      RATIO(IRUN,KKX,KKY)=DE*1000.
  275 CONTINUE
  280 LLX=LX
      LLY=LY
  285 CONTINUE
      J=1
      KK=KK+1
      IF (KK-200) 284,283,283
  283 XLAST=0.0
      IF (IPHOT) 300,300,245
  284 X(1,J)=X(1,KK)
      X(2,J)=X(2,KK)
      IF (IPHOT) 300,300,247
C     INTERPOLATE MISSING VALUES IN ARRAY
  300 KND=7
      KDN=5
  301 NXS=NNXS-2
      NYS=NNYS-2
      DO 340 I=1,NNYS
      DO 340 J=1,NXS
      IF (RATIO(IRUN,J,I)) 330,340,330
  330 IF (RATIO(IRUN,J+1,I)) 340,332,340
  332 DO 334 K=2,KND
      KJ=J+K
      IF (KJ-NNXS) 333,333,340
  333 IF (RATIO(IRUN,KJ,I)) 336,334,336
  334 CONTINUE
      GO TO 340
  336 LJ=KJ-J-1
      DJ=KJ-J
      DIF=RATIO(IRUN,J,I)-RATIO(IRUN,KJ,I)
      DO 338 K=1,LJ
      AJ=K
      LLJ=J+K
      RATIO(IRUN,LLJ,I)=RATIO(IRUN,J,I)-DIF*AJ/DJ
  338 CONTINUE
  340 CONTINUE
      DO 320 I=1,NNXS
      DO 320 J=1,NYS
      IF (RATIO(IRUN,I,J)) 310,320,310
  310 IF (RATIO(IRUN,I,J+1)) 320,312,320
  312 DO 314 K=2,KDN
      KJ=J+K
      IF (KJ-NNYS) 313,313,320
  313 IF (RATIO(IRUN,I,KJ)) 316,314,316
  314 CONTINUE
      GO TO 320
  316 LJ=KJ-J-1
      DJ=KJ-J
      DIF=RATIO(IRUN,I,J)-RATIO(IRUN,I,KJ)
      DO 318 K=1,LJ
```

Figure B-2. Listing of program (continued).

```
      AJ=K
      LLJ=J+K
      RATIO(IRUN,I,LLJ)=RATIO(IRUN,I,J)-DIF*AJ/DJ
  318 CONTINUE
  320 CONTINUE
      IF (KND-6) 302,302,303
  302 KND=10
      KDN=6
      GO TO 301
C  AVERAGE VALUES IN ARRAY
  303 WRITE(61,1)
    1 FORMAT ( ' TYPE IN 1 TO AVERAGE VALUES OR 2 IF NOT')
      IGO=TTYIN(4HIGO=)
      GO TO (304,380) IGO
  304 ITEST=1
      DO 370 I=1,NXS
      DO 360 J=2,NYS
      GO TO (362,364),ITEST
  362 X(1,J)=(RATIO(IRUN,I,J)+RATIO(IRUN,I,J-1)+RATIO(IRUN,I,J+1)+
     1 RATIO(IRUN,I+1,J))/4
  364 X(2,J)=(RATIO(IRUN,I,J)+RATIO(IRUN,I+1,J)+RATIO(IRUN,I+2,J)+
     1 RATIO(IRUN,I+1,J+1)+RATIO(IRUN,I+1,J-1))/5
  360 CONTINUE
      ITEST=2
      XMAX=0.0
      DO 365 J=2,NYS
      RATIO(IRUN,I,J)=X(1,J)
      IF (XMAX-X(1,J)) 361,363,363
  361 XMAX=X(1,J)
  363 X(1,J)=X(2,J)
  365 CONTINUE
      WRITE (61,39) XMAX
   39 FORMAT (E11.3)
  370 CONTINUE
  380 J=1
      RFAD (19,12) FIX,XL,YL,CONL
  500 READ (19,12) FIX,XF,YF,CONF
      IF (FIX) 520,520,505
  505 DDEN=CONF-CONL
      DKX=(XF-XL)
      DKY=(YF-YL)
      XKX=ABSF(DKX)/50.
      YKY=ABSF(DKY)/50.
      IF (XKX-YKY) 450,460,460
  450 KY=YKY
      DIV=YKY
      GO TO 470
  460 KY=XKX
      DIV=XKX
  470 IF (DIV-8.) 472,472,490
  472 DO 485 K=1,KY
      YYK=K
      CONC=CONL+DDEN*YYK/DIV
      IF (CONC-0.5) 490,490,475
  475 XPG(1)=XL+DKX*YYK/DIV
      XPG(2)=YL+DKY*YYK/DIV
   12 FORMAT (F7.1,2F14.0,F10.1)
      CALL ROTATE(XPG,XLOW,YMID,CROT,SROT,J)
      LX=X(1,J)/60.+0.5
      IF (LX .LE. 0 .OR. LX .GT. NNXS) 490,512
  512 LY=(X(2,J)+YMIDY)/60.+0.5
      IF (LY .LE. 0 .OR. LY .GT. NNYS) 490,514
  514 IF (RATIO(IRUN,LX,LY)) 516,490,516
```

Figure B-2. Listing of program (continued).

```
516 CONTINUE
    X(1,J)=RATIO(IRUN,LX,LY)
    X(2,J)=X(1,J)*X(1,J)
    X(3,J)=CONC
    WRITE (04,13) (X(I,J),I=1,3)
 13 FORMAT (7E11.3)
    J=J+1
    IF (J-200) 485,485,520
485 CONTINUE
490 XL=XF
    YL=YF
    CONL=CONF
    GO TO 500
520 NO=J-1
    N=3
    CALL LEASTFIT(N,NO,B)
    WRITE (61,37) B(1),B(2)
 37 FORMAT ( ' B1',E11.3,'B2',E11.3)
    WRITE (02,42) XLOW,YMID,ROT
 42 FORMAT(1H1,'XORG=',F8.0,'  YORG=',F7.0,'  ROTATION ANGLE=',F5.3)
    DO 540 I=1,NNXS,20
    WRITE (02,31)
 31 FORMAT (1H1)
    DO 540 J=1,NNYS
    KK=I+19
    WRITE (02,30) (RATIO(IRUN,K,J),K=I,KK)
 30 FORMAT (20I5)
540 CONTINUE
    ROT=-ROT
    SROT=-SINF(ROT)
    CROT=-COSF(ROT)
    XORG=XLOW
    YORG=YMID
    XLOW=0.0
    YMID=YMIDY
    CB=TTYIN(4HB1= )
    CA=TTYIN(4HB2= )
    XSUM=0.
    DO 522 J=1,NO
    XSUM=XSUM+(CB*X(1,J)+CA*X(2,J)-X(3,J))**2
522 CONTINUE
    XNO=NO
    XSUM=XSUM/XNO
    WRITE (61,38) XSUM,NO
 38 FORMAT(' MEAN SQUARE ',E11.3,'  DF',I5)
    DO 530 I=1,NNXS
    DO 530 J=1,NNYS
    IF (RATIO(IRUN,I,J)) 524,530,524
524 AJ=J
    AI=I
    XPG(1)=AI*60.
    XPG(2)=AJ*60.
    CALL ROTATE(XPG,XLOW,YMID,CROT,SROT,J)
    XPG(1)=X(1,J)+XORG
    XPG(2)=X(2,J)+YORG
    AXZ=RATIO(IRUN,I,J)
    AXZ=CB*AXZ+CA*AXZ*AXZ
    IF (AXZ-0.6) 530,537,537
537 WRITE(20,10) I,XPG(1),XPG(2),AXZ
 10 FORMAT(I3,3F15.2)
    RATIO(IRUN,I,J)=AXZ*10.
530 CONTINUE
    J=1
```

Figure B-2. Listing of program (continued).

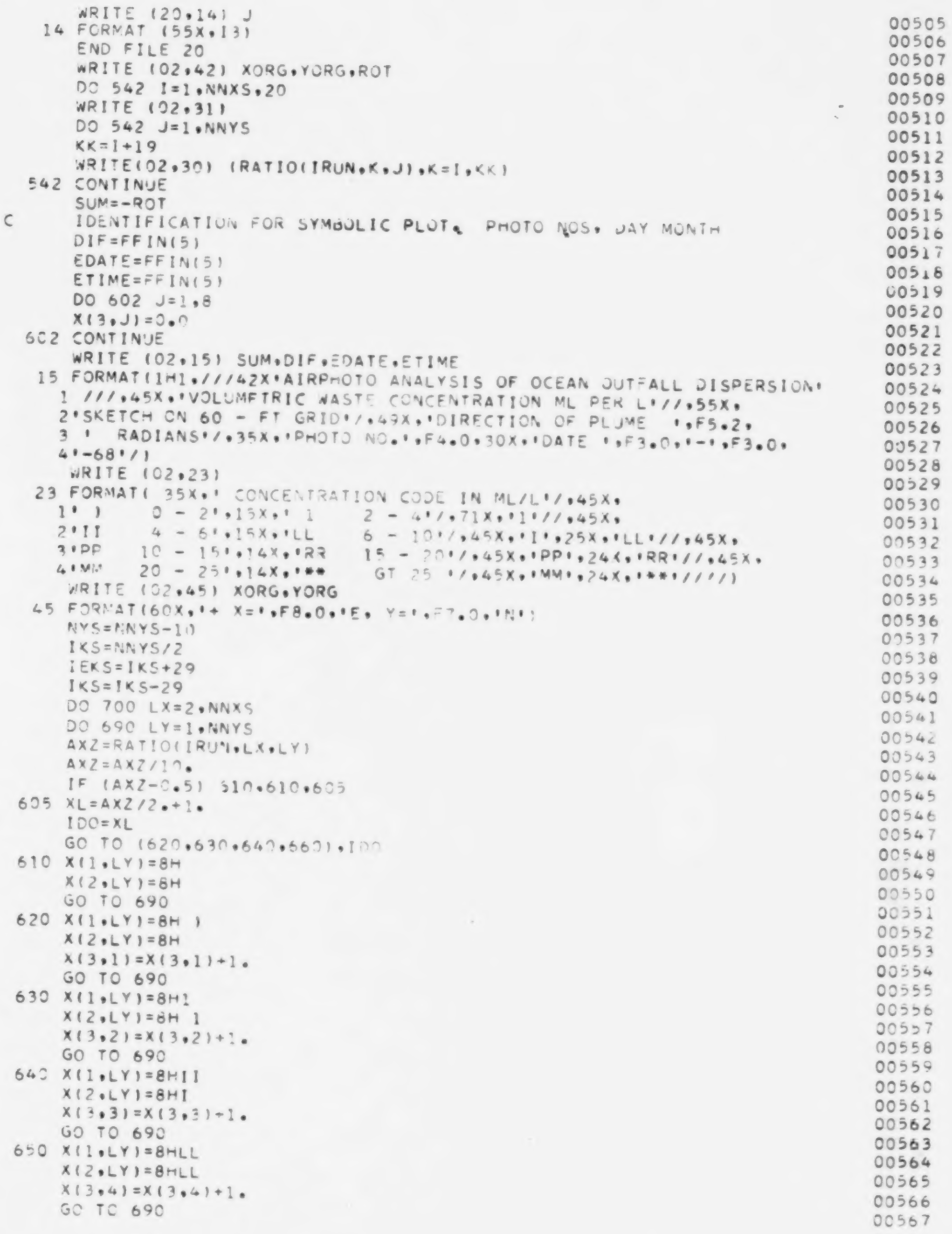

```
      WRITE (20,14) J
   14 FORMAT (55X,I3)
      END FILE 20
      WRITE (02,42) XORG,YORG,ROT
      DO 542 I=1,NNXS,20
      WRITE (02,31)
      DO 542 J=1,NNYS
      KK=I+19
      WRITE(02,30) (RATIO(IRUN,K,J),K=I,KK)
  542 CONTINUE
      SUM=-ROT
C     IDENTIFICATION FOR SYMBOLIC PLOT,  PHOTO NOS, DAY MONTH
      DIF=FFIN(5)
      EDATE=FFIN(5)
      ETIME=FFIN(5)
      DO 602 J=1,8
      X(3,J)=0.0
  602 CONTINUE
      WRITE (02,15) SUM,DIF,EDATE,ETIME
   15 FORMAT(1H1,///42X'AIRPHOTO ANALYSIS OF OCEAN OUTFALL DISPERSION'
     1 ///,45X,'VOLUMETRIC WASTE CONCENTRATION ML PER L'//,55X,
     2'SKETCH ON 60 - FT GRID'/,49X,'DIRECTION OF PLUME  ',F5.2,
     3 '  RADIANS'/,35X,'PHOTO NO.',F4.0,30X,'DATE ',F3.0,'-',F3.0,
     4'-68'/)
      WRITE (02,23)
   23 FORMAT( 35X,' CONCENTRATION CODE IN ML/L'/,45X,
     1' )     0 - 2',15X,' 1     2 - 4'/,71X,'1'//,45X,
     2'II     4 - 6',15X,'LL     6 - 10'/,45X,'I',25X,'LL'//,45X,
     3'PP    10 - 15',14X,'RR    15 - 20'/,45X,'PP',24X,'RR'//,45X,
     4'MM    20 - 25',14X,'**     GT 25 '/,45X,'MM',24X,'**'////)
      WRITE (02,45) XORG,YORG
   45 FORMAT(60X,'+ X=',F8.0,'E, Y=',F7.0,'N')
      NYS=NNYS-10
      IKS=NNYS/2
      IEKS=IKS+29
      IKS=IKS-29
      DO 700 LX=2,NNXS
      DO 690 LY=1,NNYS
      AXZ=RATIO(IRUN,LX,LY)
      AXZ=AXZ/10.
      IF (AXZ-0.5) 610,610,605
  605 XL=AXZ/2.+1.
      IDO=XL
      GO TO (620,630,640,660),IDO
  610 X(1,LY)=8H
      X(2,LY)=8H
      GO TO 690
  620 X(1,LY)=8H )
      X(2,LY)=8H
      X(3,1)=X(3,1)+1.
      GO TO 690
  630 X(1,LY)=8H1
      X(2,LY)=8H 1
      X(3,2)=X(3,2)+1.
      GO TO 690
  640 X(1,LY)=8HII
      X(2,LY)=8HI
      X(3,3)=X(3,3)+1.
      GO TO 690
  650 X(1,LY)=8HLL
      X(2,LY)=8HLL
      X(3,4)=X(3,4)+1.
      GO TO 690
```

Figure B-2. Listing of program (continued).

```
660 IF (AXZ-10.) 650,650,670
670 XL=AXZ/5.-1.
    IDO=XL
    GO TO (675,680,685,688),IDO
675 X(1,LY)=8HPP
    X(2,LY)=8HPP
    X(3,5)=X(3,5)+1.
    GO TO 690
680 X(1,LY)=8HRR
    X(2,LY)=8HRR
    X(3,6)=X(3,6)+1.
    GO TO 690
685 X(1,LY)=8HMM
    X(2,LY)=8HMM
    X(3,7)=X(3,7)+1.
    GO TO 690
688 X(1,LY)=8H**
    X(2,LY)=8H**
    X(3,8)=X(3,8)+1.
690 CONTINUE
    WRITE (02,24) (X(1,J),J=IKS,IEKS)
    WRITE (02,24) (X(2,J),J=IKS,IEKS)
 24 FORMAT (70A2)
700 CONTINUE
    DO 603 J=1,8
    XAR(IRUN,J)=X(3,J)*3600.
603 CONTINUE
    IRUN=IRUN+1
    IF(IRUN-IRUNM) 54,54,593
593 AMASS=RATE*60./ABSF(VEL)
    DO 594 IRUN=1,IRUNM
    WRITE(02,18) IRUN
 18 FORMAT(1H1,47X,'PRELIMINARY  DIFFUSION  COMPUTATIONS'//,
   1 58X,'FLIGHT NO.',I3,//19X,
   2' SECTION WIDTH  EFF DEPTH         SIGMA  Y'
   3 '  COEFFICIENT    GROUND X    GROUND Y     DIFFUSION COEF'/
   4 ,29X,'FT',7X,'FT',14X,'FT',9X,'PPT',7X,'STATE PLANE '
   5 ,' COORDINATES',3X,'FT SQ PER SEC'//)
    L=1
    GO TO (550,552),IRUN
550 LDF=9
    LDD=7
    LDST=3
    GO TO 554
552 LDF=10
    LDD=8
    LDST=LDFX+3
554 NXS=NNXS-2
    DO 600 I=LDST,NXS,5
    DO 560 J=1,NNYS
    IF (RATIO(IRUN,I,J)) 560,560,570
560 CONTINUE
    GO TO 600
570 JST=J
    LNY=0
    DIV=0.0
    SUM=0.0
    DIF=0.0
    DO 580 J=1,NNYS
    AJ=J*60
    ACD=(RATIO(IRUN,I,J)+RATIO(IRUN,I-1,J)+RATIO(IRUN,I+1,J)+
   1 RATIO(IRUN,I-2,J)+RATIO(IRUN,I+2,J))/50
    SUM=SUM+ACD*AJ
```

Figure B-2. Listing of program (continued).

```
      DIF=DIF+ACD
      DIV=DIV+ACD*AJ*AJ
      IF (RATIO(IRUN,I,J)) 580,580,575
  575 LNY=LNY+1
  580 CONTINUE
      XMEAN=SUM/DIF
      X(10,L)=DIV/DIF-XMEAN*XMEAN
      X(4,L)=LNY*60
      X(5,L)=AMASS/(DIF*3.6)
      X(6,L)=SQRT(X(10,L))
      X(7,L)=DIF*60./(2.51*X(6,L))
      XPG(1)=I*60
      XPG(2)=XMEAN
      J=1
      CALL ROTATE(XPG,XLOW,YMID,CROT,SROT,J)
      X(8,L)=X(1,J)+XORG
      X(9,L)=X(2,J)+YORG
      IF (L-1) 585,585,590
  585 DJ=0.
      GO TO 595
  590 DJ=ABSF(VEL)*(X(10,L)-X(10,L-1))/600.
  595 LL=L+150
      X(LDF,LL)=X(10,L)
      X(LDD,LL)=X(4,L)
      WRITE(02,17) I, X(4,L),X(5,L),X(6,L),X(7,L),X(8,L),X(9,L),DJ
   17 FORMAT(19X,I6,F9.0,F9.1,8X,2E11.3,2F13.0,E14.3)
      L=L+1
  600 CONTINUE
      WRITE(02,26) RATE,VEL
   26 FORMAT(///55X,' FLOW RATE',F5.1,'  CFS',17X,
     1'CURRENT VELOCITY',F4.2,'  FPS'//)
      WRITE(02,27) AZ,H
   27 FORMAT(35X,' SUN AZ FM S.',F6.3,'  RAD'
     1,17X,'SUN ALTITUDE',F6.3,'  RAD')
      WRITE (02,40)
   40 FORMAT(47X,'AREA  WITHIN  EACH  CONCENTRATION  RANGE'/,
     1 55X,'RANGE',13X,'AREA'/,55X,'ML/L',13X,'SQ FT')
      WRITE (02,41) (XAR(IRUN,J),J=1,8)
   41 FORMAT(55X,'0 - 2',8X,E11.3/,55X,'2 - 4',8X,E11.3/,
     1 55X,'4 - 6',8X,E11.3/,55X,'6 -10',8X,E11.3/,
     2 55X,'10-15',8X,E11.3/,55X,'15-20',8X,E11.3/,
     3 55X,'20-25',8X,E11.3/,55X,'GT 25',8X,E11.3)
  594 CONTINUE
      AJ=0.0
      DIV=0.0
      SUM=0.0
      AXZ=0.0
      WRITE (02,31)
      NXS=NNXS-1
      DO 728 I=1,NXS
      DO 725 J=1,NNYS
      DKX=RATIO(2,I,J)-RATIO(1,I,J)
      IF (DKX) 722,724,722
  722 DKX=DKX/10.
      AJ=AJ+1.
      DIV=DIV+DKX
      SUM=SUM+DKX*DKX
      AXZ=AXZ+ABSF(DKX)
  724 RATIO(2,NNXS,J)=DKX
  725 CONTINUE
      WRITE (02,49) (RATIO(2,NNXS,J),J=1,NNYS)
   49 FORMAT(5X,60I2/)
  728 CONTINUE
```

Figure B-2. Listing of program (continued).

```
      DKX=DIV/AJ
      DKY=SUM-DIV*DIV/AJ
      DKY=SQRT(DKY/(AJ-1.))
      AXZ=AXZ/AJ
      AJ=AJ-1.0
      WRITE (02,48) DKX,AXZ,DKY,AJ
   48 FORMAT(1H1,////' MEAN DIFFERENCE IN CONCENTRATION',F6.2,
     1/' ABSOLUTE MEAN DIFFERENCE ',F6.2,/
     2' STANDARD DEVIATION OF THE MEAN',F6.2,/' DEGREES OF '
     3'FREEDOM',F6.0)
      L=3
      WRITE (02,53)
   53 FORMAT (1H1,///20X,'N O N S T E A D Y   S T A T E'
     1'   D I F F U S I O N   C O E F F I C I E N T S'//
     2 ,23X,'SECTION',12X,'WIDTH 1',12X,'WIDTH 2',8X,
     3 'COEFFICIENTS'/)
      DIV=0.
      SUM=0.
      DTIM=DTIM*2.
      LXF=150
      LXL=150
  730 DJ=(X(10,LXF)-X(9,LXL))/DTIM
      WRITE (02,52) L,X(7,LXL),X(8,LXF),DJ
   52 FORMAT (23X,I5,14X,F6.0,12X,F6.0,10X,F8.2)
      L=L+5
      SUM=SUM+DJ
      DIV=DIV+1.
      LXF=LXF+1
      LXL=LXL+1
      IF(LXF-LL) 730,730,740
  740 DIV=SUM/DIV
      WRITE (02,60) DIV
   60 FORMAT(23X,' MEAN DIFFUSION COEFFICIENT',F10.2)
      STOP
      END
..
..
```

Figure B-2. Listing of program (continued).

```
      SUBROUTINE ROTATE(XPG,XLOW,YMID,CROT,SROT,J)
      DIMENSION XPG(2)
      COMMON X(10,200)
      RGX=XPG(1)-XLOW
      RGY=XPG(2)-YMID
      X(1,J)=RGX*SROT+RGY*CRUT
      X(2,J)=-RGX*CROT+RGY*SROT
      RETURN
      END
      SUBROUTINE SUNLITE (H,AZ,IRUN,DTIM)
C      COMPUTE THE ALTITUDE AND AZIMUTH OF THE SUN
C      TIME IS PACIFIC DAYLIGHT TIME
      GO TO (10,20),IRUN
C     READ IN TIME OF DAY IN HRS AND MIN FOR FIRST FLIGHT
   10 DPT=FFIN(5)
      DP=FFIN(5)
      DPT=DPT+DP/60.
C     READ IN DECLINATION OF SUN IN DEGREES (AA),AND MIN (B)
C     AND CHANGE IN MIN PER HOUR (CC). EQUATION OF TIME
C     IN MINUTES (DD), SECONDS (E), AND CHANGE PER HOUR (F)
C     LONGITUDE (WLON) AND LATITUDE (ALAT).
      AA=FFIN(5)
      B=FFIN(5)
      CC=FFIN(5)
      DD=FFIN(5)
      E=FFIN(5)
      F=FFIN(5)
      WLON=FFIN(5)
      ALAT=FFIN(5)
      GO TO 30
   20 DPT=DPT+DTIM/3600.
   30 GCT=DPT+7.
      DEC=(AA+(B+CC*GCT)/60.)*3.14159/180.
      EQT=(DD+(E+F*GCT)/60.)/60.
      GHA=(GCT+EQT)*15.0-180.
      TT=GHA-WLON
      TT=TT*3.14159/180.
      T=ABS(TT)
      ALAT=ALAT*3.14159/180.
      Z=SINF(T)/(COSF(ALAT)*TANF(DEC)-SINF(ALAT)*COSF(T))
      AZ=ATANF(Z)
      IF (TT) 120,120,123
  120 IF (AZ) 121,121,122
  121 AZ=2.*3.14159+AZ
      GO TO 126
  122 AZ=3.1359+AZ
      GO TO 126
  123 IF (AZ) 124,124,125
  124 AZ=-AZ
      GO TO 126
  125 AZ=3.14159-AZ
  126 CONTINUE
      SINH=SINF(ALAT)*SINF(DEC)+COSF(ALAT)*COSF(DEC)*COSF(T)
      COSH=SINF(T)*COSF(DEC)/SINF(AZ)
      ALT=ABS(SINH/COSH)
      HH=ATANF(ALT)
      REF=((1.+25./60.)/60.)*3.14159/180.
      H=HH+REF
      WRITE (02,1) H,REF,AZ
    1 FORMAT(11H SUN'S ALT. ,F10.6,12H REFRACTION ,F10.6,
     1/16H AZIMUTH OF SUN ,F10.6)
      RETURN
      END
```

Figure B-3. Listing of subroutines.

```
      SUBROUTINE RESECT (FL,XP,YP,C)
      DIMENSION B(15,6),C(20,3),P(2,8),D(6,7)
C     PHOTO RESECTION PHASE
C     READ IN  REFINED PLATE AND GROUND COORDS OF RESECTION POINTS
      IGO=1
      FL=FFIN(1)/25.4
C      FL IS FOCAL LENGTH
      IPLATE=FFIN(1)
      IMAGE=FFIN(1)
      XP=FFIN(1)
      YP=FFIN(1)
      BB=FFIN(1)
      DO 10 I=1,IMAGE
      B(I,1)=FFIN(1)
      B(I,3)=(FFIN(1)-XP)/1000.
      B(I,2)=(FFIN(1)-YP)/1000.
      BB=FFIN(1)
   10 CONTINUE
      DO 15 I=1,IMAGE
      BB=FFIN(3)
      B(I,4)=FFIN(3)
      B(I,5)=FFIN(3)
      B(I,6)=FFIN(3)
   15 CONTINUE
C     INITIAL APPROXIMATION OF CAMERA PARAMETERS
      C(1,1)=FFIN(3)
      C(1,2)=FFIN(3)
      C(1,3)=FFIN(3)
      C(2,1)=FFIN(3)/57.2928
      C(3,1)=COSF(C(2,1))
      C(2,1)=SINF(C(2,1))
      C(2,2)=FFIN(3)/57.2928
      C(3,2)=COSF(C(2,2))
      C(2,2)=SINF(C(2,2))
      C(2,3)=FFIN(3)/57.2928
      C(3,3)=COSF(C(2,3))
      C(2,3)=SINF(C(2,3))
C     ORIENTATION FACTORS IN C ARRAY
  610 C(4,1)=C(3,2)*C(3,3)
      C(5,1)=-C(3,2)*C(2,3)
      C(6,1)=C(2,2)
      C(10,1)=-C(2,2)*C(3,3)
      C(11,1)=C(2,2)*C(2,3)
      C(12,1)=C(3,2)
      C(10,2)=C(4,1)*C(2,1)
      C(11,2)=C(5,1)*C(2,1)
      C(12,2)=C(2,1)*C(2,2)
      C(10,3)=-C(4,1)*C(3,1)
      C(11,3)=-C(5,1)*C(3,1)
      C(12,3)=-C(3,1)*C(2,2)
      C(4,2)=C(3,1)*C(2,3)+C(12,2)*C(3,3)
      C(5,2)=C(3,1)*C(3,3)-C(12,2)*C(2,3)
      C(6,2)=-C(2,1)*C(3,2)
      C(4,3)=C(2,1)*C(2,3)+C(10,1)*C(3,1)
      C(5,3)=C(2,1)*C(3,3)+C(11,1)*C(3,1)
      C(6,3)=C(3,1)*C(3,2)
      DO 612 I=7,9
      C(I,1)=0.
      C(I,2)=-C(I-3,3)
      C(I,3)=C(I-3,2)
      C(13,I-6)=C(5,I-6)
      C(14,I-6)=-C(4,I-6)
  612 C(15,I-6)=0.
```

Figure B-3. Listing of subroutines (continued).

```
      GO TO (613,763),IGO
C     CLEAR NORMAL EQUATION D ARRAY TO ZERO
  613 DO 614 I=1,6
      DO 614 J=I,7
  614 D(I,J)=0.
C     COMPUTE P TERMS FOR RESECTION PASS POINTS
      DO 618 NU=1,IMAGE
      DO 619 K=1,3
  619 C(16,K)=B(NU,K+3)-C(1,K)
      K=4
      DO 620 L=17,20
      DO 620 I=1,3
      C(L,I)=C(K,1)*C(16,1)+C(K,2)*C(16,2)+C(K,3)*C(16,3)
  620 K=K+1
      DO 621 I=1,2
      DO 622 L=1,4
  622 P(I,L)=(B(NU,I+1)*C(L+16,3)-(-FL)*C(L+16,I))/C(17,3)
      DO 623 L=5,7
  623 P(I,L)=(-B(NU,I+1)*C(6,L-4)+(-FL)*C(I+3,L-4))*C(1,3)/C(17,3)
  621 P(I,8)=-P(I,1)
C     CONTRIBUTION TO NORMAL EQUATIONS
      DO 618 I=1,6
      DO 618 J=I,7
      DO 618 K=1,2
  618 D(I,J)=D(I,J)+P(K,I+1)*P(K,J+1)
C     FOREWARD SOLUTION
      DO 699 I=1,6
      SQR=SQRT(D(I,I))
      DO 698 J=I,7
  698 D(I,J)=D(I,J)/SQR
      IF (I-6)697,696,696
  697 IP1=I+1
      DO 699 L=IP1,6
      DO 699 J=L,7
  699 D(L,J)=D(L,J)-D(I,L)*D(I,J)
C     BACK SOLUTION
  696 D(6,7)=D(6,7)/D(6,6)
      DO 691 I=1,5
      NMI=6-I
      NMIP1=NMI+1
      DO 690 J=NMIP1,6
  690 D(NMI,7)=D(NMI,7)-D(J,7)*D(NMI,J)
  691 D(NMI,7)=D(NMI,7)/D(NMI,NMI)
      DO 625 I=4,6
  625 D(I,7)=D(I,7)*C(1,3)
C     ADD LEAST SQUARES RESULTS TO CAMERA PARAMETERS IN C ARRAY
      DO 626 J=1,3
      C(1,J)=C(1,J)+D(J+3,7)
      C(4,J)=D(J,7)
      C(5,J)=SQRT(1.-C(4,J)*C(4,J))
      C(6,J)=C(2,J)*C(5,J)+C(3,J)*C(4,J)
      C(7,J)=C(3,J)*C(5,J)-C(2,J)*C(4,J)
      C(2,J)=C(6,J)
  626 C(3,J)=C(7,J)
C     TEST MAGNITUDE OF CORRECTIONS FOR ORIENTATION PARAMTERES
      DO 628 I=1,3
      IF (ABS(D(I,7))-.00001)628,628,610
  628 CONTINUE
      IGO=2
      GO TO 610
C     CAMERA PARAMETERS OUTPUT
  763 WRITE(02,532)
      WRITE(02,527)
```

Figure B-3. Listing of subroutines (continued).

```
      WRITE (02,528) IPLATE,(C(1,J),J=1,3)
      WRITE (02,529)
      WRITE (02,528) IPLATE,(C(2,J),J=1,3)
      WRITE (02,528) IPLATE,(C(3,J),J=1,3)
      WRITE (02,530) IPLATE
      WRITE (02,533) ((C(I,J),J=1,3),I=4,6)
  527 FORMAT(/49H PLATE                XO               YO               ZO)
  528 FORMAT(I7,3(2X,E14.7))
  529 FORMAT(/50H PLATE             OMEGA            PHI              KAPPA)
  530 FORMAT(/30H ORIENTATION MATRIX FOR PLATE ,I7)
  532 FORMAT(/50H ORIENTATION PARAMETER CORRECTION LIMIT IS 0.00001)
  533 FORMAT (1X,3(2X,E14.7))
      RETURN
      END
      SUBROUTINE LEASTFIT (N,NO,B)
      DIMENSION XX(10,10),XY(10),B(9),ZITX(10,1)
      COMMON X(10,200)
C     N=NO OF VARIABLES,NO=NO. OF DATA,B=COFF
      KK=N-1
      DO 15 J=1,KK
      XY(J)=0.
      DO 10 I=1,NO,1
      XY(J)=XY(J)+X(J,I)*X(N,I)
   10 CONTINUE
   15 CONTINUE
      DO 20 K=1,KK
      DO 20 J=1,KK
      XX(J,K)=0.
      DO 20 I=1,NO
      XX(J,K)=XX(J,K)+X(J,I)*X(K,I)
   20 CONTINUE
      CALL MATINV (XX,KK,ZITX,0,DETERM)
      DO 30 J=1,KK
      B(J)=0.
      DO 30 I=1,KK
      B(J)=B(J)+XX(J,I)*XY(I)
   30 CONTINUE
      WRITE (02,1)
      WRITE (02,5) (B(J),J=1,KK)
      YY=0.
      DO 40 J=1,NO
      YY=YY+X(N,J)*X(N,J)
   40 CONTINUE
      BXX=0.
      DO 50 J=1,KK
      BXX=BXX+B(J)*XY(J)
   50 CONTINUE
      IDF=NO-KK
      RES=(YY-BXX)/IDF
      WRITE (02,3) RES,IDF
    1 FORMAT (32H LEAST SQ ESTIMATE OF PARAMETERS )
    3 FORMAT (23H MEAN SQ OF RESIDUALS= ,E16.7,5X,4HDF= ,I3)
    4 FORMAT (28H VARIANCE-COVARIANCE MATRIX )
    5 FORMAT (/4E15.5)
      WRITE (02,4)
      WRITE (02,5) ((XX(I,J),I=1,KK),J=1,KK)
      WRITE (02,7)
    7 FORMAT ('          Y                    EST OF Y              Y-EST Y')
      DO 70 J=1,NO
      ESTY=0.0
      DO 60 K=1,KK
      ESTY=ESTY+B(K)*X(K,J)
   60 CONTINUE
```

Figure B-3. Listing of subroutines (continued).

```
      DIF=X(N,J)-ESTY
      WRITE (02,6) X(N,J),ESTY,DIF
    6 FORMAT(3F15.7)
   70 CONTINUE
      RETURN
      END
      SUBROUTINE MATINV(A,N,B,M,DETERM)
C     MATRIX INVERSION WITH ACCOMPANYING SOLUTION OF LINEAR EQUATIONS
      DIMENSION IPIVOT(10), A(10,10), B(10,1), INDEX(10,2), PIVOT(10)
      DETERM=1.0
      DO 20 J=1,N
   20 IPIVOT(J)=0
      DO 550 I=1,N
C     SEARCH FOR PIVOT ELEMENT
      AMAX=0.0
      DO 105 J=1,N
      IF (IPIVOT(J)-1) 60, 105, 60
   60 DO 100 K=1,N
      IF (IPIVOT(K)-1) 80, 100, 740
   80 IF (ABSF(AMAX)-ABSF(A(J,K))) 85, 100, 100
   85 IROW=J
      ICOLUM=K
      AMAX=A(J,K)
  100 CONTINUE
  105 CONTINUE
      IPIVOT(ICOLUM)=IPIVOT(ICOLUM)+1
C     INTERCHANGE ROWS TO PUT PIVOT ELEMENT ON DIAGONAL
      IF (IROW-ICOLUM) 140, 260, 140
  140 DETERM=-DETERM
      DO 200 L=1,N
      SWAP=A(IROW,L)
      A(IROW,L)=A(ICOLUM,L)
  200 A(ICOLUM,L)=SWAP
      IF(M) 260, 260, 210
  210 DO 250 L=1, M
      SWAP=B(IROW,L)
      B(IROW,L)=B(ICOLUM,L)
  250 B(ICOLUM,L)=SWAP
  260 INDEX(I,1)=IROW
      INDEX(I,2)=ICOLUM
      PIVOT(I)=A(ICOLUM,ICOLUM)
      DETERM=DETERM*PIVOT(I)
C     DIVIDE PIVOT ROW BY PIVOT ELEMENT
      A(ICOLUM,ICOLUM)=1.0
      DO 350 L=1,N
  350 A(ICOLUM,L)=A(ICOLUM,L)/PIVOT(I)
      IF(M) 380, 380, 360
  360 DO 370 L=1,M
  370 B(ICOLUM,L)=B(ICOLUM,L)/PIVOT(I)
C     REDUCE NON-PIVOT ROWS
  380 DO 550 L1=1,N
      IF(L1-ICOLUM) 400, 550, 400
  400 T=A(L1,ICOLUM)
      A(L1,ICOLUM)=0.0
      DO 450 L=1,N
  450 A(L1,L)=A(L1,L)-A(ICOLUM,L)*T
      IF(M) 550, 550, 460
  460 DO 500 L=1,M
  500 B(L1,L)=B(L1,L)-B(ICOLUM,L)*T
  550 CONTINUE
C     INTERCHANGE COLUMNS
      DO 710 I=1,N
      L=N+1-I
```

Figure B-3. Listing of subroutines (continued).

```
      IF (INDEX(L,1)-INDEX(L,2)) 630, 710, 630
  630 JROW=INDEX(L,1)
      JCOLUM=INDEX(L,2)
      DO 705 K=1,N
      SWAP=A(K,JROW)
      A(K,JROW)=A(K,JCOLUM)
      A(K,JCOLUM)=SWAP
  705 CONTINUE
  710 CONTINUE
  740 RETURN
      END
      FUNCTION REFLECT (AI,AR)
      A=AI-AR
      B=AI+AR
      C=SINF(A)**2
      D=SINF(B)**2
      E=TANF(A)**2
      F=TANF(B)**2
      REFLECT=ABS(A/B+C/D)/2.
      END
      SUBROUTINE TRNCOORD(CAMO,XT,J,FL,IPHOT)
      DIMENSION XT(3),CAMO(3,5,3)
      COMMON X(10,200)
      DO  10 K=1,3
   10 XT(K)=CAMO(IPHOT,2,K)*X(1,J)+CAMO(IPHOT,3,K)*X(2,J)+
     1 CAMO(IPHOT,4,K)*(-FL)
      XDIS=SQRT(XT(1)**2+XT(2)**2+XT(3)**2)
      DO  20 K=1,3
   20 XT(K)=XT(K)/XDIS
      RETURN
      END
      SUBROUTINE GRDCOORD (CAMO,XT,XPG,J,IPHOT)
      DIMENSION CAMO(3,5,3),XT(3),XPG(2)
      XPG(1)=CAMO(IPHOT,1,1)-XT(1)*CAMO(IPHOT,1,3)/XT(3)
      XPG(2)=CAMO(IPHOT,1,2)-XT(2)*CAMO(IPHOT,1,3)/XT(3)
      RETURN
      END
      SUBROUTINE ANGLES(XT,XS,FL,J,CAN,CCA,TAB,SUNR)
      DIMENSION XT(3),XS(9)
      DIV=SQRT(XT(1)**2+XT(2)**2)
      CAN=ABSF(DIV/XT(3))
C      ANGLE BETWEEN RAY IN AIR AND VERTICAL.
      CAN=ATANF(CAN)
      SINC=0.75*SINF(CAN)
      COSC=(1.0-SINC**2)**0.5
      TANC=SINC/COSC
C     ANGLE BETWEEN RAY TO CAMERA AND VERTICAL UNDER WATER
      CCA=ATANF(TANC)
      FT=-DIV/TANC
      XDIS=SQRT(XT(1)**2+XT(2)**2+FT**2)
      X1=XT(1)/XDIS
      X2=XT(2)/XDIS
      X3=FT/XDIS
      COSB=X1*XS(1)+X2*XS(2)+X3*XS(3)
      SINB=SQRT(1.0-COSB**2)
      TANB=SINB/ABSF(COSB)
C     ANGLE BETWEEN SUN AND CAMERA RAYS UNDERWATER.
      B=ATANF(TANB)
      B=3.14159265-B
      TAB=B-3.14159/2.
      COSB=-XS(4)*XT(1)-XS(5)*XT(2)+XS(6)*XT(3)
      SINB=SQRT(1.0-COSB**2)
      TANB=SINB/ABSF(COSB)
      SUNR=ATANF(TANB)
      IF (COSB) 260,261,261
  260 SUNR=3.14159-SUNR
  261 RETURN
      END
```

Figure B-3. Listing of subroutines (continued).

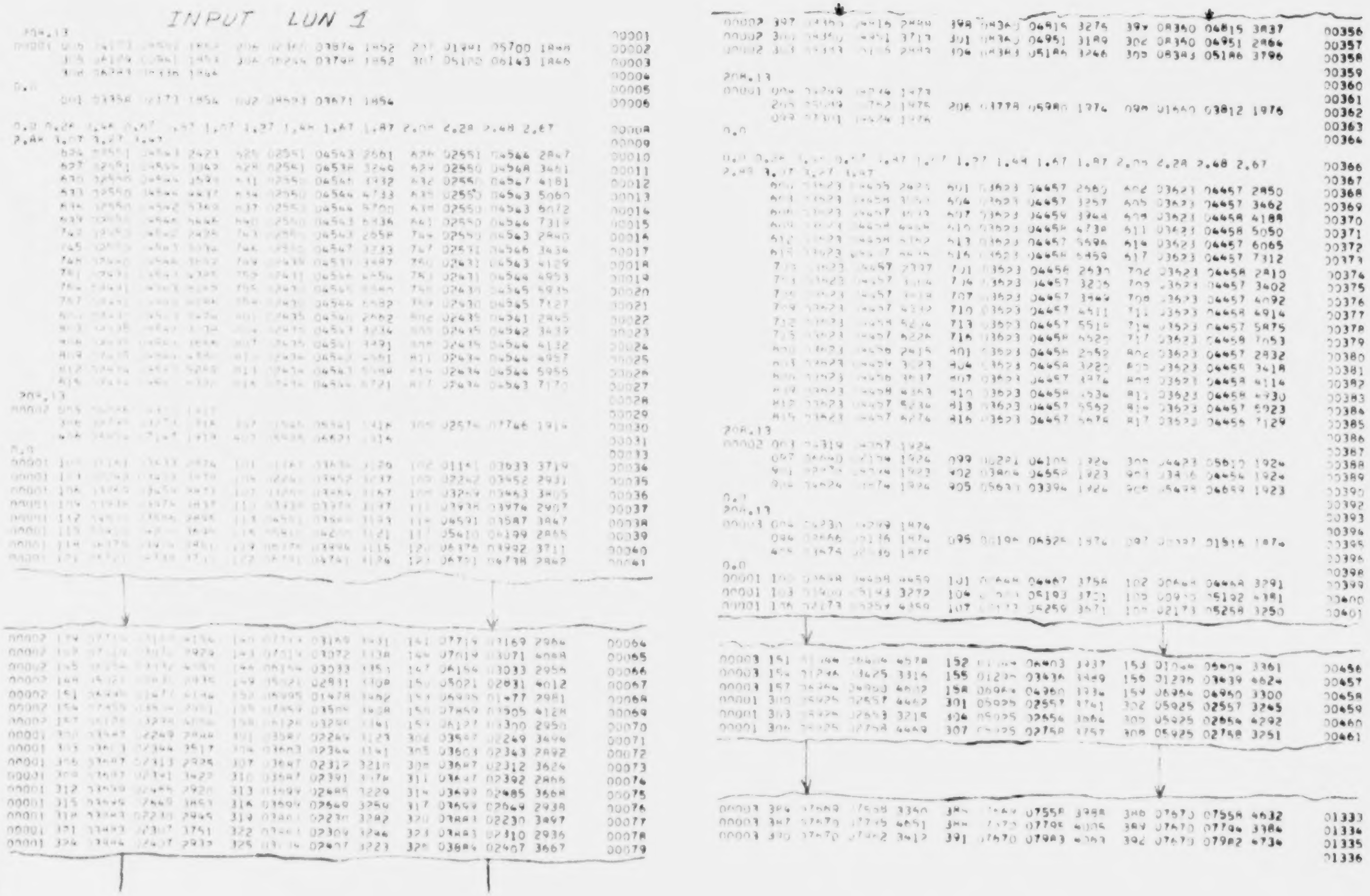

INPUT LUN 1

Figure B-4. Sample input, LUN 1.

Reproduced from best available copy.

```
206 1071096 374493 1.3
207 1072950 373906 42.3
305 1068334 378561 1.3
306 1071278 378489 1.3
307 1073606 377145 75.1
308 1075864 378167 172.1
    1071900 376300 8500
    0.0 1.0
306 1071278 378489 1.5
307 1073606 377145 75.
308 1075863 378167 172.
406 1070186 381693 1.5
407 1074821 381220 61.
    1072205 380000 8500
    0.0 1.0
205 1068382 375338 1.5
206 1071096 374493 1.5
 98 1069878 373447 1.5
 99 1070400 376350 1.5
    1070300 374700 4200
    0.0 1.0
 97 1069530 379729 1.5
 99 1070400 376350 1.5
306 1071278 378489 1.5
    1070700 378400 4200
    0.0 1.0
 96 1072026 381045 1.5
 95 1072223 379652 1.5
 97 1069530 379652 1.5
406 1070186 381693 1.5
    1071000 381800 4200
    0.0 1.0
```

INPUT LUN 3

```
  97.0      1070383      376722      3.1      5.0
  98.0      1070451      376377      3.1      5.0
  98.3      1070456      376273      3.1      5.0
  99.0      1070466      376031      7.4      5.0
  99.8      1070452      375754      6.3      5.0
 100.0      1070449      375685      4.1      5.0
 101.0      1070432      375339      4.1      5.0
 101.5      1070385      375158      4.1      5.0
 101.8      1070357      375049     13.5      5.0
 102.0      1070338      374977     13.5      5.0
 103.0      1070250      374629     12.2      5.0
 103.5      1070226      374444      8.5      5.0
 104.0      1070201      374258     12.2      5.0
 105.0      1070131      373899     11.0      5.0
 106.0      1070127      373536      8.5      5.0
 107.0      1070028      373199      8.5      5.0
 108.0      1070028      372866      8.5      5.0
 108.2      1070025      372791      8.5      5.0
 108.5      1070022      372679      3.1      5.0
 109.0      1070015      372491      3.1      5.0
 110.0      1070201      372379      3.1      5.0
 111.0      1070324      372476      2.0      5.0
 112.0      1070301      372724      3.1      5.0
 113.0      1070261      372937      4.1      5.0
 114.0      1070145      373102      8.5      5.0
 115.0      1069993      373252      7.4      5.0
 116.0      1069922      373425      4.1      5.0
 116.4      1069866      373484      5.2      5.0
 117.0      1069781      373572     14.8      5.0
 117.5      1069682      373666     16.1      5.0
 118.0      1069583      373750     13.5      5.0
 118.6      1069463      373[illegible]      9.7      5.0
```

PARTIAL INPUT LUN 19

Figure B-5. Sample input, LUNS 3 and 19.

## APPENDIX C

## PROCESSING 1969 PHOTOGRAPHIC DATA

A general description of the CDC 3300 Computer and special fortran input functions is given in the introduction of Appendix B.

Two main programs were used to process the photos taken in 1969. These were program EDIT, which used the raw data to find film density differences, and the program REMOTE, which used the differences generated by EDIT to find steady and non-steady state diffusion coefficients as well as providing data for symbolic and contour plots of waste concentrations.

### Program EDIT

A flow diagram for program EDIT is shown in figure C-1. The numbers in parentheses on the diagram refer to the line numbers on the program listing shown in figure C-2.

The input for the program is arranged on three or four LUNS, depending on the number of photographic bands available for each exposure. Each band is on a separate input file. A sample of the coordinate and voltage data is shown in figure C-3. This example shows the beginning of a file of data, with the first three lines being standardization voltages. The format is as listed below.

| Column | Data |
|---|---|
| 1 | Month photo taken |
| 2-3 | Day of month photo taken |
| 4 | Flight no. of day |
| 5 | Photo no. of flight |
| 6 | Blank |
| 7-9 | Event no. (see code below) |
| 10 | Blank |
| 11-14 | y-coordinate of photo |
| 15-18 | Voltage value from densitometer |

The lines 6-18 are repeated six times across the card. The x coordinate is interpolated across the photo by knowing the number of scan lines and the total distance covered in the x-direction.

| Event No. | Description |
|---|---|
| 40-59 | Initial red standardization. |
| 60-79 | Initial green standardization. |
| 80-99 | Initial blue standardization. |
| 100-119 | Initial gold standardization. |
| 120-139 | Final red standardization. |
| 140-159 | Final green standardization. |
| 160-179 | Final blue standardization. |
| 180-199 | Final gold standardization. |
| 200-299 | Normal red color. |
| 300-399 | Normal green color. |
| 400-499 | Normal blue color. |
| 500-599 | Infra-red red color. |
| 600-699 | Infra-red green color. |
| 700-799 | Infra-red blue color. |
| 800-899 | Infra-red black and white. |
| 900-999 | Panchromatic black and white. |

In running the program, the maximum and minimum voltages must be typed in from the teletype. The program proceeds to read the data, checking to see that it does not read data for a new photo. While reading the input, the number of scan lines are counted and the standardization data is stored. When a new photo is reached, the program backspaces the input LUN to the beginning of the photo. Subroutine LEASTFIT is called, and a least squares adjustment is made of the densitometer voltages to the standard grey scale film densities.

The photo coordinates of the principal point and scan limits are read from LUN 8. The photo coordinate and corresponding voltage are read from the data LUN which was previously backspaced. The film density and x coordinate are computed for each sample point. This process is repeated until one photographic band is completed. The program then goes to the next input LUN, and repeats the process, until all film densities are computed for a single photograph.

The differences between film densities of adjacent photographic bands are found, and the extreme differences are rejected. The remaining differences are printed in an array, from which the general shape of the plume may be found by locating abrupt changes in film density. An example of the output is shown in figure C-4, where the non-zero entries in the array are the differences between film densities of adjacent bands for a particular photo.

The program checks to see if there is another photograph to be processed and if so, the overall process is repeated.

## Program REMOTE

Program REMOTE is the second program used for processing the photographic data. A flow diagram of program REMOTE is shown in figure C-5. The numbers in parentheses correspond to the line numbers on the listing of the program in figure C-7. The subroutines are listed in figure C-8.

Differences in film densities from program EDIT are on LUNS 1, 2, or 3. The boat data is on LUN 4, general information on LUN 7, photo control coordinates on LUN 8, ground control on LUN 9, and initial orientation parameters on LUN 10. Sample input data is shown in figure C-9.

The program begins by orienting all of the photos. The current velocity and orientation of the plume are then computed. After finding the azimuth and altitude of the sun at the time the photographs were taken, sun ray vectors are computed. The waste concentrations as measured from the boat are read in, and concentration and array indices are computed at 60-ft intervals along the boat's track. These values are saved for later use on scratch LUN 5.

Subroutine PROCESS is called, which reads the photo identification, finds the atmospheric attenuation, and reads in the density difference between adjacent bands which was the output from program EDIT. Ground coordinates, array indices , light values and angles are computed, and the indices , angles, and light values written out. The equation for the light return which would be present in the open sea ($R_{pho}$) is determined. The differences between the open sea values and the values found by measuring the light return on the photograph for each sample point are computed and stored. A flow diagram of PROCESS is given in figure C-6. The subroutine then returns to the main program, which checks to see if the last band was processed. If not, the solution is repeated. When the last band is reached, the program compares the values of waste concentrations found by using various combinations of the photographic bands with those from the boat data. When a good combination is found, coefficients relating the light values to the waste concentrations are typed in, and the waste concentrations for the array are computed. The data generated is then used to form a symbolic plot (see figure 28), and can also be saved for making a contour plot of waste concentrations (see figure 29). The diffusion coefficients for each flight are computed and when the last flight has been processed, the non-steady state diffusion coefficients are determined.

## Input Data Description

The input data for program REMOTE is shown in figure C-9. The data displayed as LUN 7 is as follows:

| Line | Description |
|---|---|
| 1-2 | Approximate difference in orientation between Hasselblads and K-17 in degrees. |
| 3-5 | Times of three flights in hours and minutes, P.D.T. |
| 6 | Effluent flow rate, gpm. |
| 7-8 | Declination of sun, degrees (line 8) and minutes (line 9). |
| 10 | Change of declination of sun, minutes per hour. |
| 11-12 | Equation of time in minutes (line 11), seconds (line 12) and change in seconds per hour (line 13). |
| 13 | Longitude of outfall. |
| 14 | Latitude of outfall. |
| 15 | The difference between true north and grid north in degrees. |
| 16-23 | Each line contains the film gamma, film speed and optical thickness of the atmosphere for each of eight spectral bands. |
| 24-26 | Speed and aperture settings for K-17 for three flights. |
| 27-29 | Speed and aperture settings for Hasselblad 1 for three flights. |

| Line | Description |
|---|---|
| 30-32 | Speed and aperture settings for Hasselblad 2 for three flights. |
| 33-40 | Coefficients for determining atmospheric attenuation from the sea to the camera station. |
| 41 | Number indicating whether or not the antivignetting filter is on the K-17, 0 = yes, 1 = no. |

The input for LUN 8 contains photo coordinates as measured by the coordinatograph and digitizer. The first five digits of each line are constant data, and represent:

| Col. | Data |
|---|---|
| 1 | Month photo taken. |
| 2-3 | Day of month photo taken. |
| 4 | Flight number. |
| 5 | Photo number of flight. |

After the constant data there are three groups of data on each line, each containing an event number, x-coordinate, y-coordinate, and four zeros where the voltage is normally recorded. The event number coding is as follows:

| Event No. | Description |
|---|---|
| 000 | Principal point. |
| 001-019 | Ground control points (numbers must match those on LUN 9. See below). |
| 020-029 | Floats for computing the current velocity. |
| 030-033 | Scan limits on photograph. |
| 034 | Point near head of plume. |
| 035 | Point near tail of plume, which, together with 034 will give orientation of waste plume. |

The ground coordinate data is prepared on LUN 9. Each point listed as control on LUN 8 must have ground coordinates on LUN 9. Reading across a line are the point number, the x and y state plane coordinates, and the approximate elevation above mean sea level.

LUN 10 contains the approximate orientation parameters for the camera station relative to the state plane coordinate system. Reading across the line are the photo number, the x and y coordinates, the flying height, and the rotation angles and the x, y, and z axis. These are used in subroutine RESECT as initial conditions for a non-linear least squares solution for the camera station position and orientation.

## Subroutines for REMOTE

| Subroutine | Description |
|---|---|
| Process | Computes array indices for particular ground coordinates, light values, and sun angles. It also determines the equation for light return from the open sea, and finds the difference between the light return measured and that which would be present if waste area were open sea. |
| Resect | Determines the orientation of oblique photographs and was modified from USC and GS program RESECTION. Each time the subroutine is called, the camera station coordinates and orientation matrix are printed on LUN 20. |
| Sunlight | Computes the altitude and azimuth of the sun. Time must be given as Pacific Daylight Time, and all pertinent information dealing with the equation of time must be read in. A value for the longitude and latitude of the area being considered is also necessary. |
| Trncoord | Converts the photographic vector to a unit vector based on the state plane coordinate system. |
| Zeroarry | Sets IPHOT, X or CAMO array to zero. |
| Orimat | Determines orientation matrix. |

| Subroutine | Description |
|---|---|
| Interp | Interpolates missing values in IPHOT array. |
| Average | Averages values in IPHOT array. |
| Cull | Rejects extreme values in array. |
| Leastfit | Determines the least squares solution of the regression coefficients for a linear model with one independent and up to nine dependent variables. (See lines 351-422 of EDIT listing and omit lines 393+2, 401+1, 401+2, 405-420). |
| Matinv | Determines the inverse of a square matrix (see lines 423-490 of EDIT listing). |

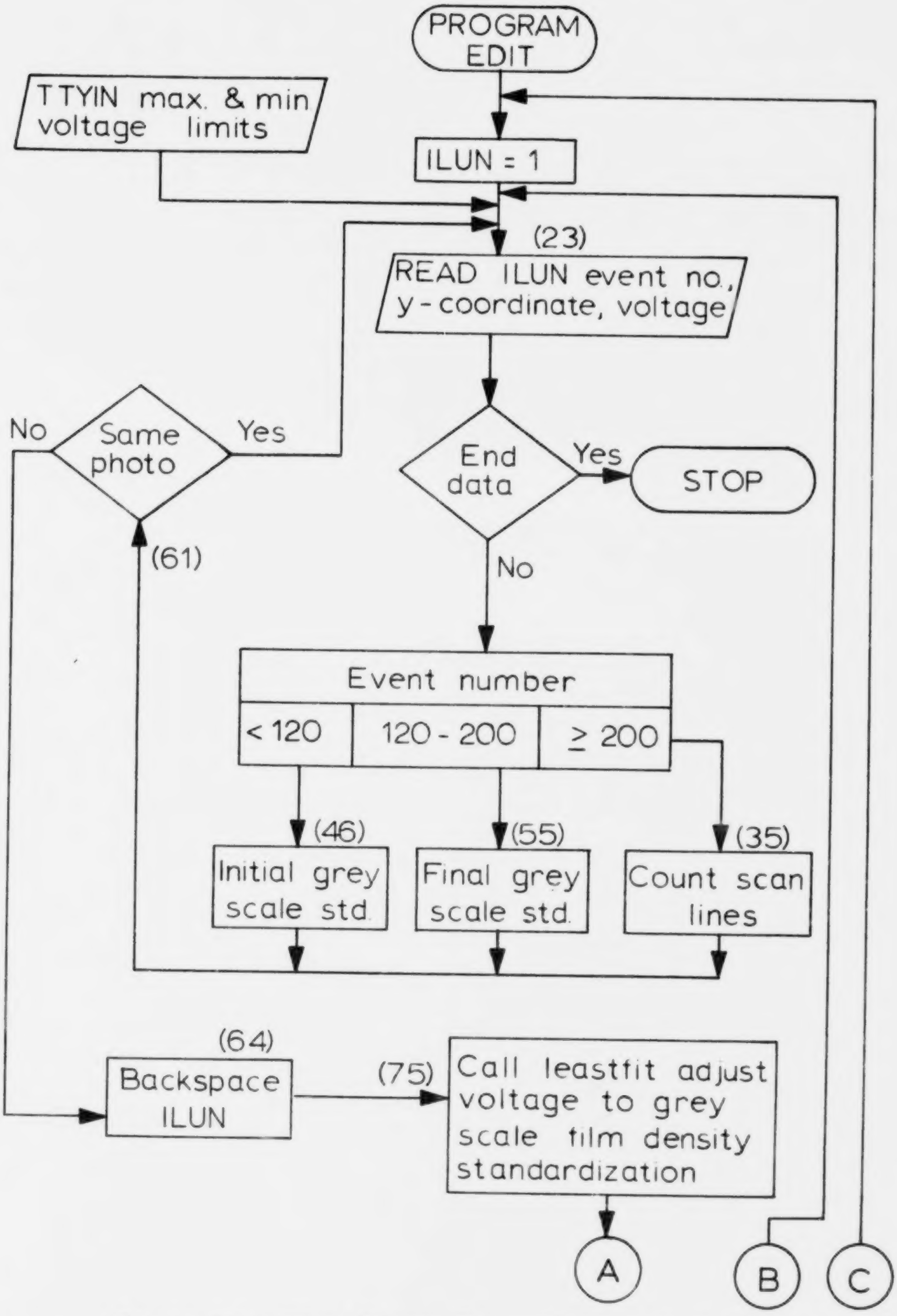

Figure C-1. Flow diagram for computer program EDIT.

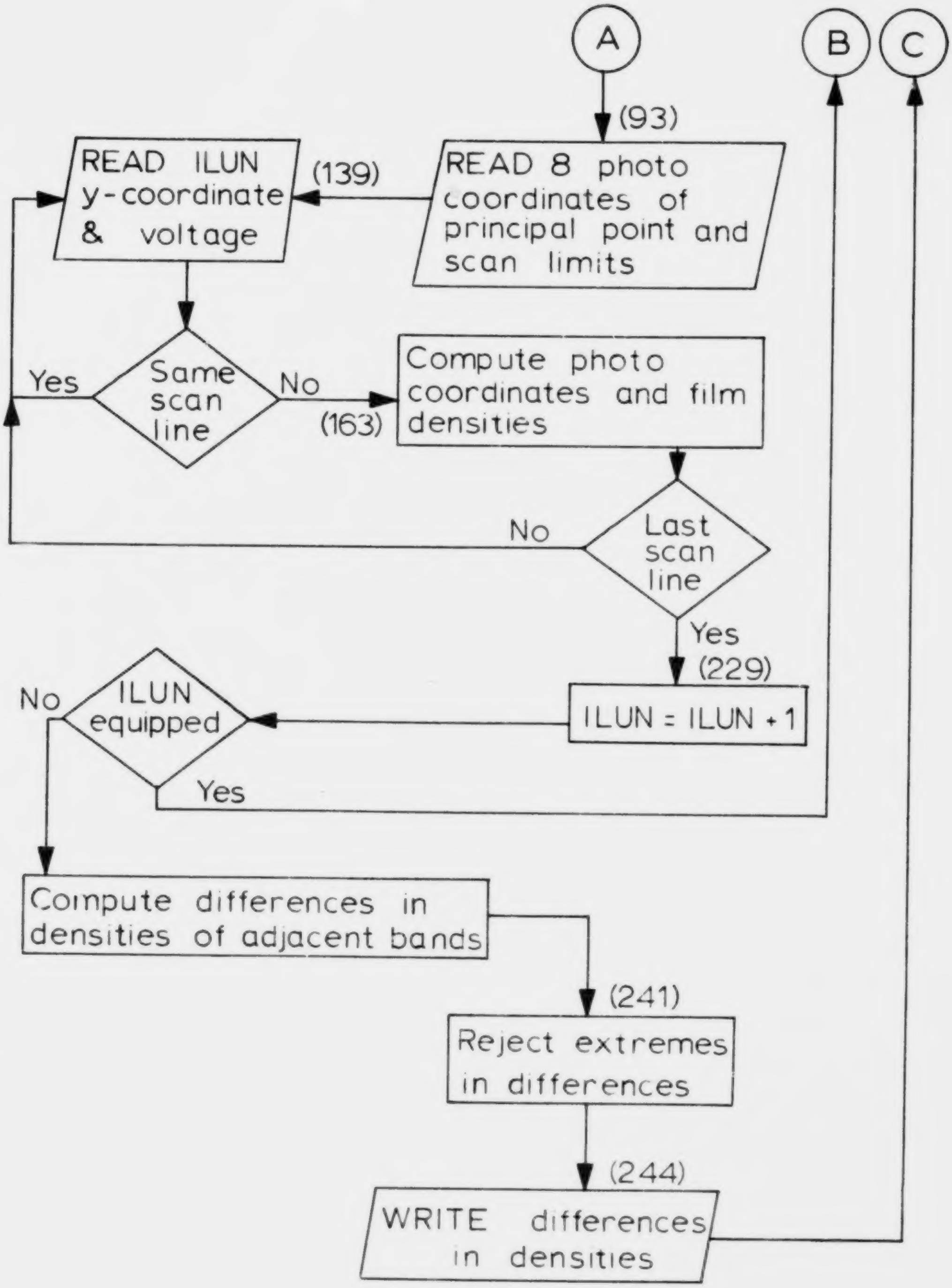

A
B
C
(93)
READ 8 photo coordinates of principal point and scan limits
(139)
READ ILUN y-coordinate & voltage
Same scan line
Yes
No
(163)
Compute photo coordinates and film densities
Last scan line
No
Yes
(229)
ILUN = ILUN + 1
ILUN equipped
No
Yes
Compute differences in densities of adjacent bands
(241)
Reject extremes in differences
(244)
WRITE differences in densities

Figure C-1. Flow diagram for computer program EDIT.

```
      PROGRAM EDIT
      COMMON IPHOT(4,60,60),X(10,60),B(15,6),IVT(6),BB(9)
      INTEGER HARDWARE
   10 ILUN=1
      DCOOR=0.07
      XPH=30.
      YPH=30.
      NXI=60
      NYI=60
      KGO=1
      DO 90 I=1,NXI
      DO 90 J=1,NYI
      DO 90 K=1,4
   90 IPHOT(K,I,J)=0
   95 NOL=0
      JNO=0
      NOS=0
      VOL1=TTYIN(4HLVOL)
      VOL2=TTYIN(4HHVOL)
      LS=0
      K=1
      KK=1
  100 READ(ILUN,1) IMO,IDATE,IFLT,IPH,(IVT(I),X(10,I),X(9,I),
     1I=1,6)
    1 FORMAT (I1,I2,2I1,X,6(I3,F5.3,F4.1))
      IF (EOF(ILUN)) GO TO 1000
      IF (IVT(1).LT.200) GO TO 120
      IF (NOL.GE. 1) GO TO 111
      IPLATE=(IFLT-1)*10+IPH
      IDENT=IFLT*10+IPH
      IBAND=IVT(1)/100-1
      IF(IPLATE .GT. 30) GO TO 111
      XPH=TTYIN(4HPHX=)
      YPH=TTYIN(4HPHY=)
  111 IF (X(10,2) .GT. X(10,1)) 112,114
  112 L=1
      GO TO 116
  114 L=2
  116 NOL=NOL+1
      IF(LS-L) 118,100,118
  118 NOS=NOS+1
      LS=L
      WRITE(61,21) LS,NOS,NOL
   21 FORMAT(3I5)
      GO TO 100
  120 IF(IVT(1).GT.119) GO TO 140
      DO 132 I=1,6
      IF (IVT(I) .EQ.0 ) GO TO 132
      X(1,K)=1.0
      X(2,K)=X(9,I)
      X(3,K)=X(9,I)*X(9,I)
      K=K+1
  132 CONTINUE
      GO TO 100
  140 NOL=NOL+1
      JNO=JNO+1
      DO 142 I=1,6
      IF (IVT(I) .EQ. 0) GO TO 142
      X(5,KK)=X(9,I)
      KK=KK+1
      IF (KK-16) 142,142,145
  142 CONTINUE
      GO TO 100
```

Figure C-2. Listing of program EDIT.

```
  145 DO 150 I=1,NOL
      BACKSPACE ILUN
  150 CONTINUE
      X(4,1)=0.0
      X(4,2)=0.27
      DO 160 I=3,16
      X(4,I)=X(4,I-1)+0.20
  160 CONTINUE
      N=4
      NO=16
      IF(K .GT. 16) 170,1000
  170 CALL LEASTFIT(N,NO,BB,RES)
      B(1,1)=BB(1)
      B(1,2)=BB(2)
      B(1,3)=BB(3)
      IF(KK .GT. 16) 180,1000
  180 DO 190 I=1,16
      X(2,I)=X(5,I)
      X(3,I)=X(2,I)*X(2,I)
  190 CONTINUE
      CALL LEASTFIT(N,NO,BB,RES)
      B(2,1)=BB(1)
      B(2,2)=BB(2)
      B(2,3)=BB(3)
      GO TO (195,250),KGO
C FIND SCAN LIMITS AND PRINCIPLE PT
  195 L=0
      K=1
      REWIND 8
  200 READ(8,2) IFC,(IVT(I),X(1,I),X(2,I),I=1,3)
    2 FORMAT(3X,I2,3(I4,2F6.3,7X))
      IF (EOF(8)) GO TO 1000
      IF (IFC-IDENT) 200,210,200
  210 DO 220 I=1,3
      IF(IVT(I).EQ.0.AND.X(1,I).GT.0.1) GO TO 212
      IF(IVT(I).GE.30.AND.IVT(I).LE.33) 216,220
  212 XP=X(1,I)
      YP=X(2,I)
      K=2
      GO TO 220
  216 J=IVT(I)-19
      B(J,1)=X(1,I)
      B(J,2)=X(2,I)
      L=L+1
  220 CONTINUE
      IF(L .GE. 4) 230,200
  230 GO TO (232,236),K
  232 SUM1=0.0
      SUM2=0.0
      DO 234 I=11,14
      SUM1=SUM1+B(I,1)
      SUM2=SUM2+B(I,2)
  234 CONTINUE
      XP=SUM1/4.
      YP=SUM2/4.
  236 DO 238 I=11,14
      B(I,1)=B(I,1)-XP
      B(I,2)=B(I,2)-YP
  238 CONTINUE
  250 AJ=NOS-1
      XADD=0.0
      IF(IFLT.LE.3) GO TO 242
      AJ=AJ+1
```

Figure C-2. Listing of program EDIT. (Continued)

```
      XADD=DELX/2.0
  242 DELX=(B(14,1)-B(11,1)+B(13,1)-B(12,1))/(AJ*2.)
      DELY1=(B(14,2)-B(11,2))/AJ
      DELY2=(B(13,2)-B(12,2))/AJ
      KNO=NCL-JNO
      WRITE(61,22) KNO,DELX,DELY1,DELY2
   22 FORMAT(I10,3F10.3)
      K=0
      KK=0
      DO 400 IK=1,KNO
      JS=K+1
      JE=K+6
C     READ AND PROCESS ONE SCAN LINE AT A TIME
      READ(ILUN,3)(X(10,I),X(9,I),I=JS,JE)
    3 FORMAT(6X,6(3X,F5.3,F4.1))
      IF(K .GT. 0) GO TO 280
      IF (X(10,1)-X(10,2)) 272,272,274
  272 L=1
      GO TO 276
  274 L=2
  276 LS=L
      K=K+6
      GO TO 400
  280 IND=K+6
      JS=K+1
      DO 290 J=JS,IND
      IF(X(10,J-1)-X(10,J)) 282,284,286
  282 L=1
      GO TO 288
  284 GO TO (286,282),L
  286 L=2
  288 IF(LS .NE. L) GO TO 300
  290 CONTINUE
      K=K+6
      GO TO 400
C     PROCESS SCAN LINE
  300 LS=L
      IST=J
      IF (J .LT. 12) GO TO 392
      ANOS=KK
      KK=KK+1
C     DENSITOMETER STD FOR LINE
      DO 310 I=1,3
      B(3,I)=B(1,I)+(B(2,I)-B(1,I))*ANOS/AJ
  310 CONTINUE
      BDIR=(X(10,3)-X(10,2))*100.
      IF (BDIR .LE. 0.) GO TO 330
C     PHOTO COORD OF START AND END OF SCAN
      XST=B(12,1)+DELX*ANOS+XADD
      YST=B(12,2)+DELY2*ANOS
      XED=B(11,1)+DELX*ANOS+XADD
      YED=B(11,2)+DELY1*ANOS
      JST=3
      J=IST-3
      KKA=2
      GO TO 340
  330 XST=B(11,1)+DELX*ANOS+XADD
      YST=B(11,2)+DELY1*ANOS
      XED=B(12,1)+DELX*ANOS+XADD
      YED=B(12,2)+DELY2*ANOS
      JST=3
      J=IST-3
      KKA=1
```

Figure C-2. Listing of program EDIT. (Continued)

```
  340 BJ=IST-1
      DELX3=(XED-XST)/BJ
      DELY3=(YED-YST)/BJ
      IF (ABS(DELY3) .GT. 0.15) GO TO 392
      DO 380 I=JST,J
      IF(ABS(X(9,I)-X(9,I+1)).GT.10..AND.ABS(X(9,I)-
     1X(9,I-1)).GT.10..AND.ABS(X(9,I+1)-X(9,I-1))
     2.LT.10.) GO TO 380
      IF(X(9,I).LT.VOL1.OR.X(9,I).GT.VOL2) GO TO 380
      AAJ=I-1
      AAJ=AAJ+0.5
      XP=XST+DELX3*AAJ
      YP=YST+(X(10,I)-X(10,1))
      LX=XP/DCOOR+XPH+0.5
      LY=YP/DCOOR+YPH+0.5
      DEN=B(3,1)+B(3,2)*X(9,I)+B(3,3)*X(9,I)*X(9,I)
      IF(IBAND.GT.6) DEN=4.0-DEN
      IF(LX.LE.0.OR.LX.GT.NXI) GO TO 380
      IF(LY.LE.0.OR.LY.GT.NYI) GO TO 380
      IPHOT(ILUN,LX,LY)=DEN*100.
  380 CONTINUE
  392 K=0
      DO 395 J=IST,IND
      K=K+1
      X(10,K)=X(10,J)
      X(9,K)=X(9,J)
  395 CONTINUE
  400 CONTINUE
      DO 410 I=1,JNO
  410 READ(ILUN,1) IMO
      B(7,ILUN)=IFLT
      B(8,ILUN)=IPLATE
      B(9,ILUN)=IBAND
      KND=4
      KDN=4
      NXS=NXI-2
      NYS=NYI-2
      CALL INTERP(NXI,NYI,NXS,NYS,KND,KDN,ILUN)
      CALL CULL(NXI,NYI,ILUN)
      ILUN=ILUN+1
      IF(HARDWARE(ILUN).EQ. 1) GO TO 95
      IK=ILUN-2
      DO 500 I=1,NXI
      DO 500 J=1,NYI
      DO 500 K=1,IK
      IF(IPHOT(K,I,J).GT.0.AND.IPHOT(K+1,I,J).GT.0) 490,495
  490 IPHOT(K,I,J)=IPHOT(K,I,J)-IPHOT(K+1,I,J)
      GO TO 500
  495 IPHOT(K,I,J)=0
  500 CONTINUE
      DO 700 K=1,IK
      CALL CULL(NXI,NYI,K)
      LUNO=30+K
      IF(HARDWARE(LUNO).NE.1) CALL EQUIP(LUNO,5HFILE )
      WRITE(LUNO,60) IMO,IDATE,B(7,1),IPH,B(8,1),B(9,K),B(9,K+1)
     1 ,XPH,YPH,DCOOR
   60 FORMAT(2I5,F5.0,I5,5F5.0,F5.3)
      IJ=NXI/2
      DO 650 J=1,NYI
  650 WRITE(LUNO,61) (IPHOT(K,I,J),I=1,IJ)
      IJ=IJ+1
      DO 660 J=1,NYI
  660 WRITE(LUNO,61) (IPHOT(K,I,J),I=IJ,NXI)
```

Figure C-2. Listing of program EDIT. (Continued)

```
   61 FORMAT(30I4)
  700 CONTINUE
      GO TO 10
 1000 STOP
      END
      FUNCTION STDDEV(SUM1,SUM2,AJ)
      STDDEV=SQRT((SUM2-SUM1*SUM1/AJ)/(AJ-1.))
      RETURN
      END
      SUBROUTINE INTERP(NXI,NYI,NXS,NYS,KND,KDN,KLUN)
      COMMON IPHOT(4,60,60),X(10,60),B(15,6),IVT(6),BB(9)
      DO 540 I=1,NYI
      DO 540 J=1,NXS
      IF (IPHOT(KLUN,J,I)) 530,540,530
  530 IF (IPHOT(KLUN,J+1,I)) 540,532,540
  532 DO 534 K=2,KND
      KJ=J+K
      IF (KJ-NXI) 533,533,540
  533 IF (IPHOT(KLUN,KJ,I)) 536,534,536
  534 CONTINUE
      GO TO 540
  536 LJ=KJ-J-1
      DJ=KJ-J
      DIF=IPHOT(KLUN,J,I)-IPHOT(KLUN,KJ,I)
      DO 538 K=1,LJ
      AJ=K
      LLJ=J+K
      IPHOT(KLUN,LLJ,I)=IPHOT(KLUN,J,I)-DIF*AJ/DJ
  538 CONTINUE
  540 CONTINUE
      DO 520 I=1,NXI
      DO 520 J=1,NYS
      IF (IPHOT(KLUN,I,J)) 510,520,510
  510 IF (IPHOT(KLUN,I,J+1)) 520,512,520
  512 DO 514 K=2,KDN
      KJ=J+K
      IF (KJ-NYI) 513,513,520
  513 IF (IPHOT(KLUN,I,KJ)) 516,514,516
  514 CONTINUE
      GO TO 520
  516 LJ=KJ-J-1
      DJ=KJ-J
      DIF=IPHOT(KLUN,I,J)-IPHOT(KLUN,I,KJ)
      DO 518 K=1,LJ
      AJ=K
      LLJ=J+K
      IPHOT(KLUN,I,LLJ)=IPHOT(KLUN,I,J)-DIF*AJ/DJ
  518 CONTINUE
  520 CONTINUE
      RETURN
      END
      SUBROUTINE AVERAGE(NXS,NYS,KLUN)
      COMMON IPHOT(4,60,60),X(10,60),B(15,6),IVT(6),BB(9)
      ITEST=1
      DO 570 I=1,NXS
      DO 560 J=2,NYS
      GO TO (562,564),ITEST
  562 X(1,J)=(IPHOT(KLUN,I,J)+IPHOT(KLUN,I,J-1)+IPHOT(KLUN,I,J+1)+
     1 IPHOT(KLUN,I+1,J))/4
  564 X(2,J)=(IPHOT(KLUN,I,J)+IPHOT(KLUN,I+1,J)+IPHOT(KLUN,I+2,J)+
     1 IPHOT(KLUN,I+1,J+1)+IPHOT(KLUN,I+1,J-1))/5
  560 CONTINUE
      ITEST=2
```

Figure C-2. Listing of program EDIT. (Continued)

```
      DO 565 J=2,NYS
      IPHOT(KLUN,I,J)=X(1,J)
      X(1,J)=X(2,J)
  565 CONTINUE
  570 CONTINUE
      RETURN
      END
      SUBROUTINE CULL(NXI,NYI,KLUN)
      COMMON IPHOT(4,60,60),X(10,60),B(15,6),IVT(6),BB(9)
      BJ=9.
      IX=NXI-2
      IY=NYI-2
      DO 100 I=1,IX
      DO 100 J=1,IY
      SUM1=0.0
      SUM2=0.0
      DO 20 IK=1,3
      DO 20 JK=1,3
      IP=I+IK-1
      JP=J+JK-1
      IF(IPHOT(KLUN,IP,JP)) 10,100,10
   10 AI=IPHOT(KLUN,IP,JP)
      SUM1=SUM1+AI
      SUM2=SUM2+AI*AI
   20 CONTINUE
      SUM2=STDDEV(SUM1,SUM2,BJ)
      AI=SUM1/BJ
      BI=IPHOT(KLUN,I+1,J+1)
      CI=(SUM1-BI)/(BJ-1.)
      SUM1=AI-SUM2
      SUM2=AI+SUM2
      IF(BI.LT.SUM1.OR.BI.GT.SUM2) IPHOT(KLUN,I+1,J+1)=CI
  100 CONTINUE
      RETURN
      END
      SUBROUTINE LEASTFIT (N,NO,BB,RES)
      COMMON IPHOT(4,60,60),X(10,60),B(15,6),IVT(6)
      DIMENSION BB(9),XX(10,10),XY(10),ZITX(10,1)
C     N=NO OF VARIABLES,NO=NO. OF DATA,B=COFF
   14 KK=N-1
      DO 15 J=1,KK
      XY(J)=0.
      DO 10 I=1,NO,1
      XY(J)=XY(J)+X(J,I)*X(N,I)
   10 CONTINUE
   15 CONTINUE
      DO 20 K=1,KK
      DO 20 J=1,KK
      XX(J,K)=0.
      DO 20 I=1,NO
      XX(J,K)=XX(J,K)+X(J,I)*X(K,I)
   20 CONTINUE
      CALL MATINV (XX,KK,ZITX,0,DETERM)
      DO 30 J=1,KK
      BB(J)=0.
      DO 30 I=1,KK
      BB(J)=BB(J)+XX(J,I)*XY(I)
   30 CONTINUE
      WRITE (20,1)
      WRITE (20,5) (BB(J),J=1,KK)
      YY=0.
      DO 40 J=1,NO
      YY=YY+X(N,J)*X(N,J)
```

Figure C-2. Listing of program EDIT. (Continued)

```
 40 CONTINUE
    BXX=0.
    DO 50 J=1,KK
    BXX=BXX+BB(J)*XY(J)
 50 CONTINUE
    IDF=NO-KK
    RES=(YY-BXX)/IDF
    WRITE (20,3) RES,IDF
  1 FORMAT (32H LEAST SQ ESTIMATE OF PARAMETERS )
  3 FORMAT (23H MEAN SQ OF RESIDUALS= ,E16.7,5X,4HDF= ,I3)
  4 FORMAT (28H VARIANCE-COVARIANCE MATRIX )
  5 FORMAT (/4E15.5)
    WRITE (20,4)
    WRITE (20,5) ((XX(I,J),I=1,KK),J=1,KK)
    WRITE (20,7)
    WRITE (61,17)
 17 FORMAT (' INDEX  Y-EST Y')
  7 FORMAT ('          Y                  EST OF Y             Y-EST Y')
    DO 70 J=1,NO
    ESTY=0.0
    DO 60 K=1,KK
    ESTY=ESTY+BB(K)*X(K,J)
 60 CONTINUE
    DIF=X(N,J)-ESTY
    WRITE (20,6) X(N,J),ESTY,DIF
    WRITE (61,13) J,DIF
 13 FORMAT (I6,F7.3)
  6 FORMAT(3F15.7)
 70 CONTINUE
    WRITE (61,8)
  8 FORMAT (' ARE THESE OK( TYPE IN 1 FOR YES,2 FOR NO')
    KTRY=TTYIN(4HTRY=)
    GO TO (100,80),KTRY
 80 WRITE (61,9)
  9 FORMAT (' WHAT IS THE INDEX OF THE X VALUE TO BE CHANGED(')
    INDX=TTYIN(4HINDX)
    WRITE (61,11)
 11 FORMAT (' WHAT IS THE VALUE(')
    X(2,INDX)=TTYIN(4H X= )
    X(3,INDX)=X(2,INDX)*X(2,INDX)
    WRITE (61,12)
 12 FORMAT (' ANYMORE CHANGES( 1 FOR YES, 2 FOR NO')
    KTRY=TTYIN(4HTRY=)
    GO TO (80,14),KTRY
100 RETURN
    END
    SUBROUTINE MATINV(A,N,B,M,DETERM)
C     MATRIX INVERSION WITH ACCOMPANYING SOLUTION OF LINEAR EQUATIONS
    DIMENSION IPIVOT(10), A(10,10), B(10,1), INDEX(10,2), PIVOT(10)
    DETERM=1.0
    DO 20 J=1,N
 20 IPIVOT(J)=0
    DO 550 I=1,N
C     SEARCH FOR PIVOT ELEMENT
    AMAX=0.0
    DO 105 J=1,N
    IF (IPIVOT(J)-1) 60, 105, 60
 60 DO 100 K=1,N
    IF (IPIVOT(K)-1) 80, 100, 740
 80 IF (ABSF(AMAX)-ABSF(A(J,K))) 85, 100, 100
 85 IROW=J
    ICOLUM=K
    AMAX=A(J,K)
```

Figure C-2. Listing of program EDIT. (Continued)

```
  100 CONTINUE
  105 CONTINUE
      IPIVOT(ICOLUM)=IPIVOT(ICOLUM)+1
C     INTERCHANGE ROWS TO PUT PIVOT ELEMENT ON DIAGONAL
      IF (IROW-ICOLUM) 140, 260, 140
  140 DETERM=-DETERM
      DO 200 L=1,N
      SWAP=A(IROW,L)
      A(IROW,L)=A(ICOLUM,L)
  200 A(ICOLUM,L)=SWAP
      IF(M) 260, 260, 210
  210 DO 250 L=1, M
      SWAP=B(IROW,L)
      B(IROW,L)=B(ICOLUM,L)
  250 B(ICOLUM,L)=SWAP
  260 INDEX(I,1)=IROW
      INDEX(I,2)=ICOLUM
      PIVOT(I)=A(ICOLUM,ICOLUM)
      DETERM=DETERM*PIVOT(I)
C     DIVIDE PIVOT ROW BY PIVOT ELEMENT
      A(ICOLUM,ICOLUM)=1.0
      DO 350 L=1,N
  350 A(ICOLUM,L)=A(ICOLUM,L)/PIVOT(I)
      IF(M) 380, 380, 360
  360 DO 370 L=1,M
  370 B(ICOLUM,L)=B(ICOLUM,L)/PIVOT(I)
C     REDUCE NON-PIVOT ROWS
  380 DO 550 L1=1,N
      IF(L1-ICOLUM) 400, 550, 400
  400 T=A(L1,ICOLUM)
      A(L1,ICOLUM)=0.0
      DO 450 L=1,N
  450 A(L1,L)=A(L1,L)-A(ICOLUM,L)*T
      IF(M) 550, 550, 460
  460 DO 500 L=1,M
  500 B(L1,L)=B(L1,L)-B(ICOLUM,L)*T
  550 CONTINUE
C     INTERCHANGE COLUMNS
      DO 710 I=1,N
      L=N+1-I
      IF (INDEX(L,1)-INDEX(L,2)) 630, 710, 630
  630 JROW=INDEX(L,1)
      JCOLUM=INDEX(L,2)
      DO 705 K=1,N
      SWAP=A(K,JROW)
      A(K,JROW)=A(K,JCOLUM)
      A(K,JCOLUM)=SWAP
  705 CONTINUE
  710 CONTINUE
  740 RETURN
      END
```

Figure C-2. Listing of program EDIT. (Continued)

```
71641  40 60592487 41 60592744 42 60592956 43 60593183 44 60593423 45 60593657
71641  46 60593912 47 60594189 48 60594469 49 60594765 50 60595085 51 60595442
71641  52 60595806 53 60596178 54 60596591 55 60597003 56 60597473  0        0  0
71641 500 41516924501 40906305502 40166308503 39286287504 38616262505 37146252
71641 506 36426258507 35626228508 34926218509 34186214510 33406209511 32676221
71641 512 31906212513 31046208514 30346194515 29616187516 28886171517 28216168
71641 518 27546147519 26786170520 26026166521 25176161522 24626202523 23846190
71641 524 23056210525 22306227526 21516252527 20776268528 20066310529 19666787
71641 530 19856256531 20566250532 21376226533 22046208534 22776186535 23576182
71641 536 24366178537 24986170538 25766167539 26416135540 27066143541 27826160
71641 542 28556177543 29246176544 29966187545 30826203546 31546214547 32336182
71641 548 33036209549 33816213550 34566233551 35366248552 36116259553 36856251
71641 554 37606275555 38346274556 39046292557 39706306558 40466296559 41157256
71641 560 41276781561 40786302562 40006293563 39306277564 38556264565 37806264
71641 566 37126253567 36336241568 35586225569 34886200570 34146186571 33376144
71641 572 32036176573 31806184574 31126172575 30276170576 29656160577 28916169
```

Reproduced from best available copy.

Figure C-3. Sample input for program EDIT.

Reproduced from best available copy.

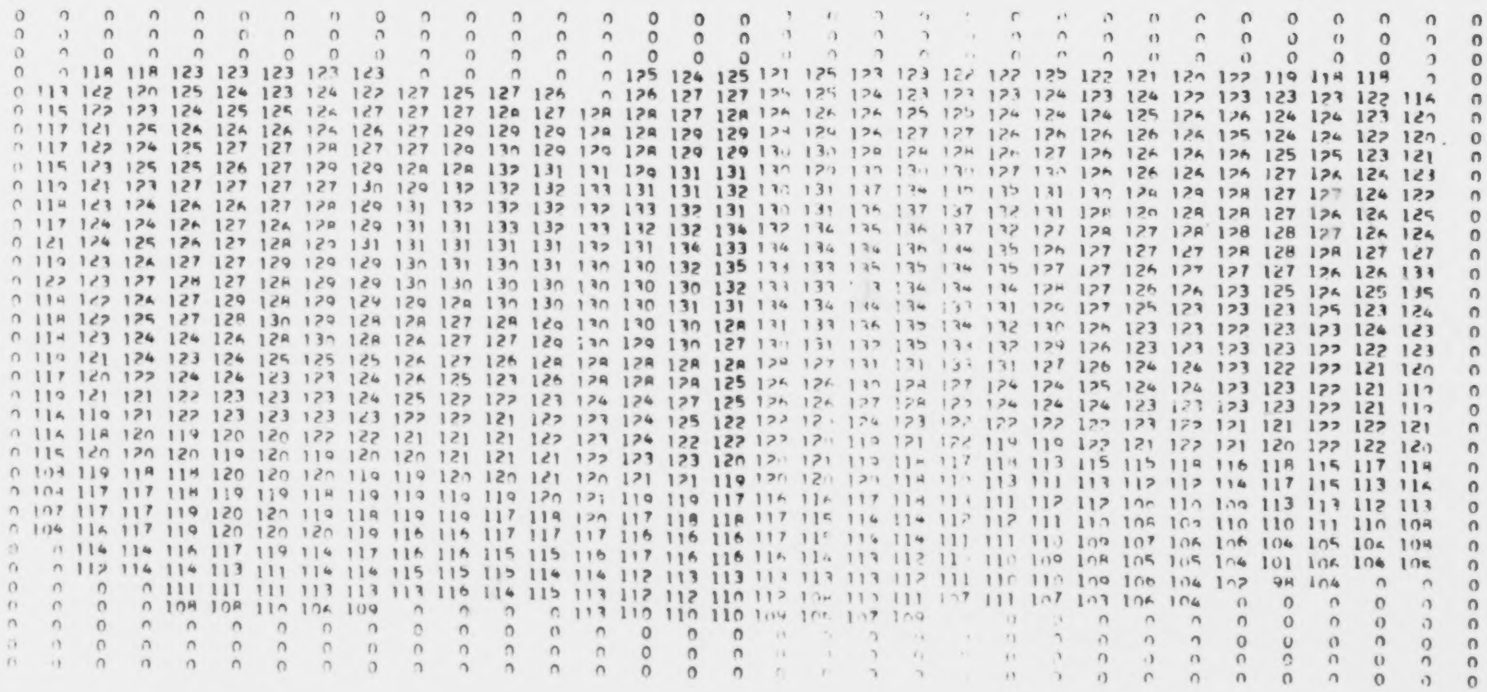

Figure C-4. Sample output from program EDIT.

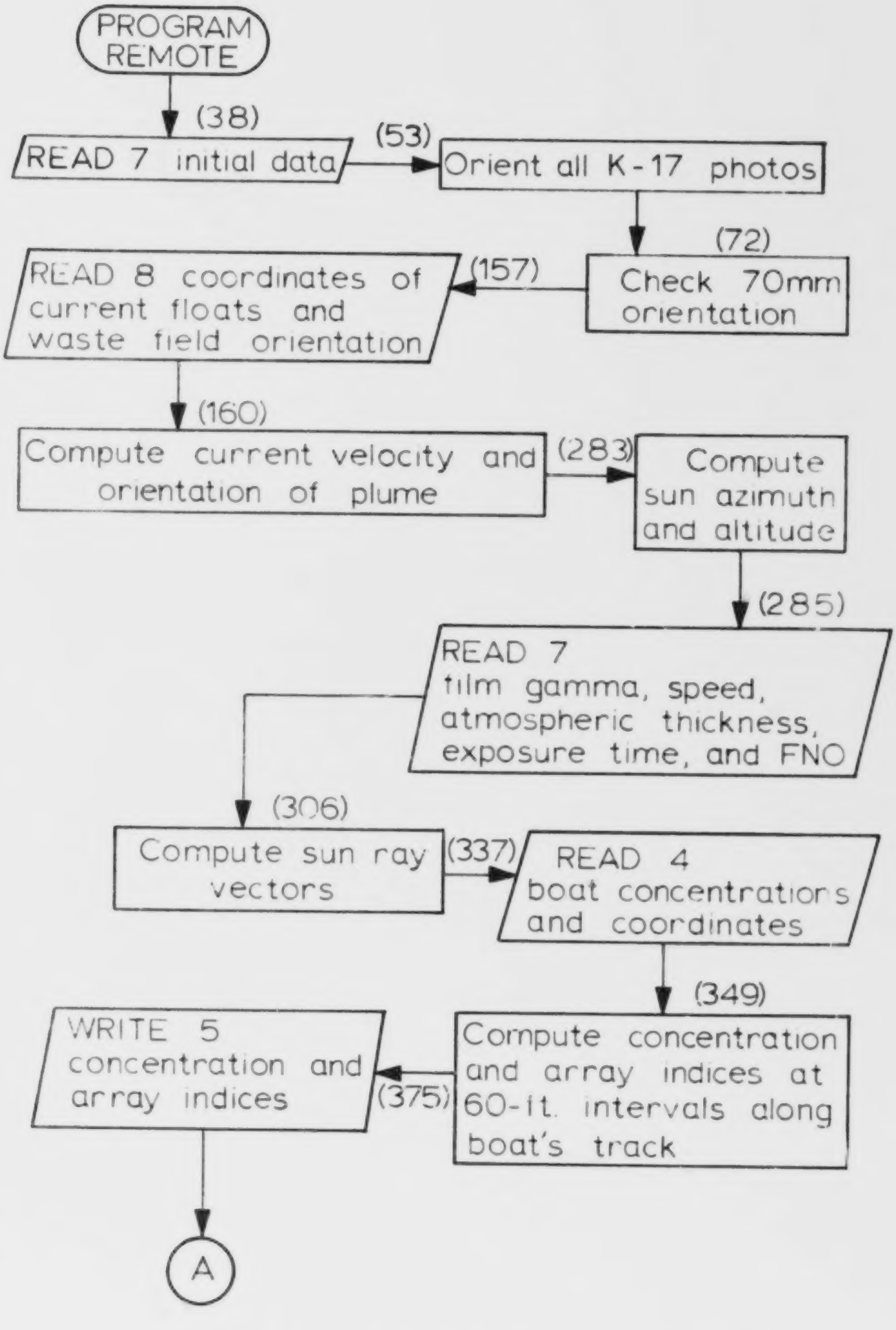
PROGRAM REMOTE
(38)
READ 7 initial data
(53)
Orient all K-17 photos
(72)
Check 70mm orientation
(157)
READ 8 coordinates of current floats and waste field orientation
(160)
Compute current velocity and orientation of plume
(283)
Compute sun azimuth and altitude
(285)
READ 7 film gamma, speed, atmospheric thickness, exposure time, and FNO
(306)
Compute sun ray vectors
(337)
READ 4 boat concentrations and coordinates
(349)
Compute concentration and array indices at 60-ft. intervals along boat's track
(375)
WRITE 5 concentration and array indices
A

Figure C-5. Flow diagram of program REMOTE.

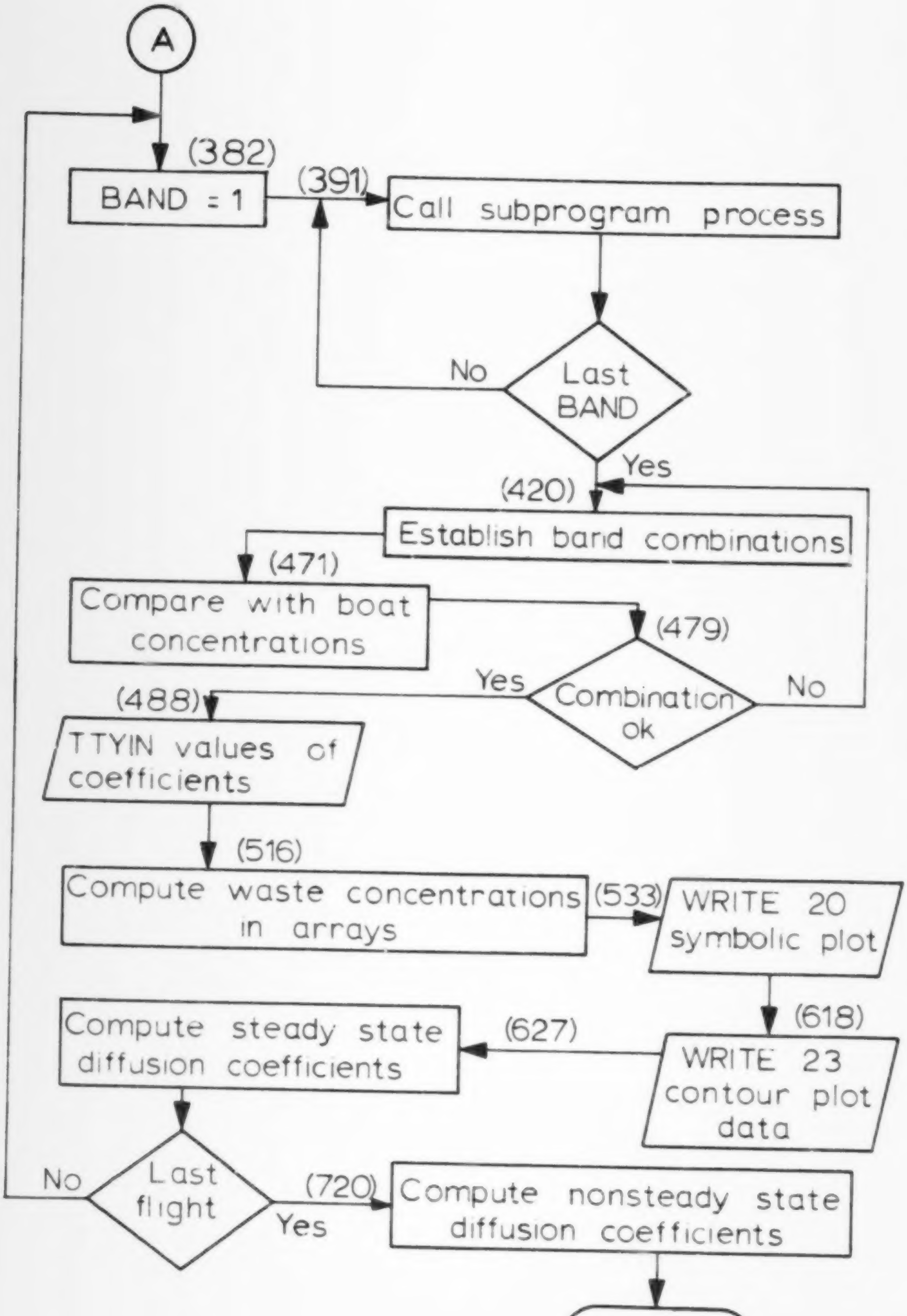
A
(382)
BAND = 1
(391)
Call subprogram process
Last BAND
No
Yes
(420)
Establish band combinations
(471)
Compare with boat concentrations
(479)
Combination ok
Yes
No
(488)
TTYIN values of coefficients
(516)
Compute waste concentrations in arrays
(533)
WRITE 20 symbolic plot
(618)
WRITE 23 contour plot data
(627)
Compute steady state diffusion coefficients
Last flight
No
Yes
(720)
Compute nonsteady state diffusion coefficients
END

Figure C-5. Flow diagram of program REMOTE.

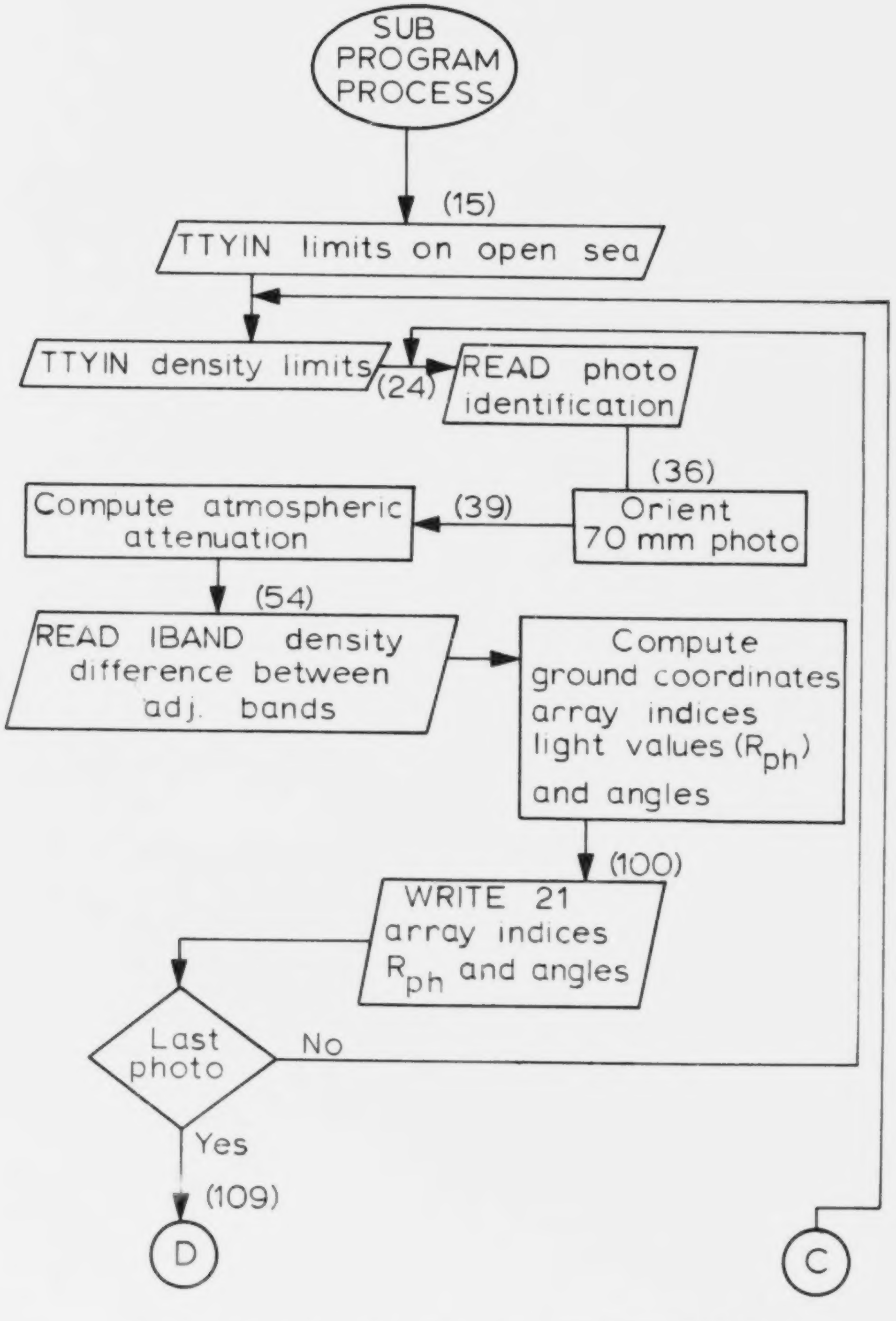
SUB PROGRAM PROCESS
(15)
TTYIN limits on open sea
TTYIN density limits
(24)
READ photo identification
(36)
Orient 70 mm photo
(39)
Compute atmospheric attenuation
(54)
READ IBAND density difference between adj. bands
Compute ground coordinates array indices light values ($R_{ph}$) and angles
(100)
WRITE 21 array indices $R_{ph}$ and angles
Last photo
No
Yes
(109)
D
C

Figure C-6. Flow diagram of subroutine PROCESS.

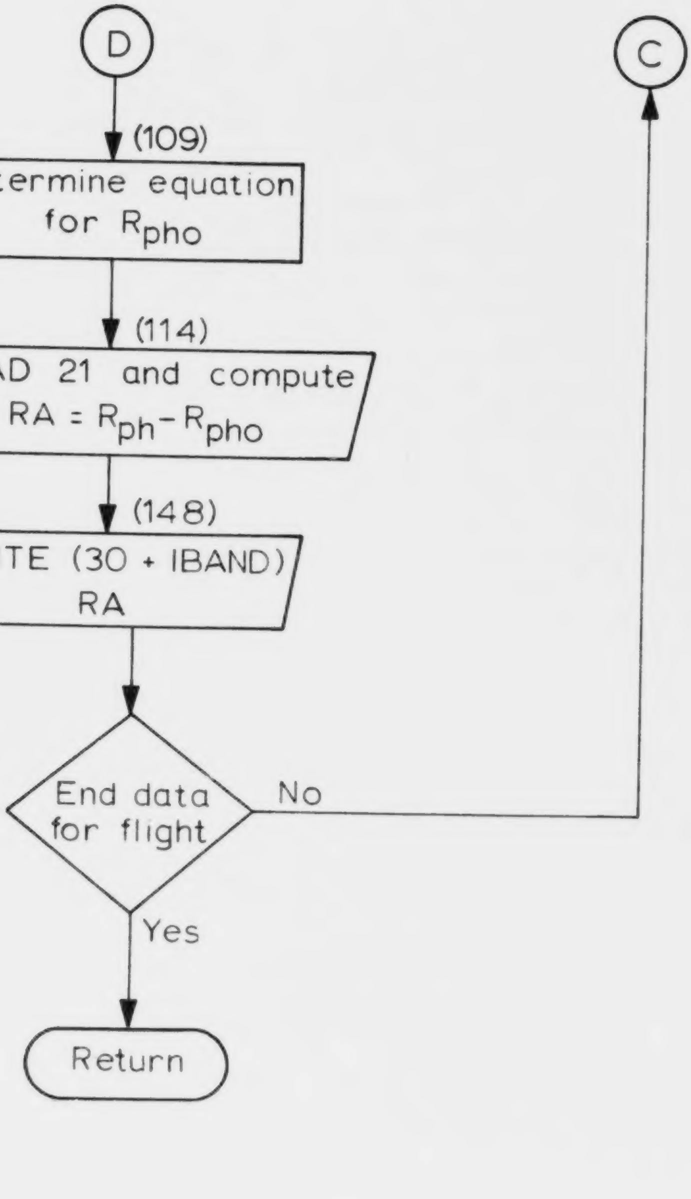
D
C
(109)
Determine equation for $R_{pho}$
(114)
READ 21 and compute $RA = R_{ph} - R_{pho}$
(148)
WRITE (30 + IBAND) RA
End data for flight
No
Yes
Return

Figure C-6. Flow diagram of subroutine PROCESS.

```
      DEFINE DECLAR
      COMMON X(10,300),IPHOT(120,80),CAMO(90,6),C(20,3)
      COMMON B(15,6),P(2,8),ANGHB(4),VOLL(2,8)
      END
      DEFINE GRDCOORD
      XG(1)=CAMO(IPLATE,1)-CAMO(IPLATE,3)*XT(1)/XT(3)
      XG(2)=CAMO(IPLATE,2)-CAMO(IPLATE,3)*XT(2)/XT(3)
      END
      PROGRAM REMOTE
C     INPUT LUNS ARE
C      1. RED-GREEN FILM DENSITIES
C      2. GREEN-BLUE FILM DENSITIES
C      3. BLUE-GOLD FILM DENSITIES
C      4. BOAT CONCENTRATIONS AND COORDINATES
C      7. GENERAL INFORMATION
C      8. PHOTO COORD. FOR CONTROL, FLOATS,SCAN LIMITS
C         AND WASTE FIELD ORIENTATION
C      9. GROUND CONTROL COORDINATES
C      10 APPROXIMATE ORIENTATION PARAMETERS
      DIMENSION TIMFLT(3),IE(3),XT(3),XG(2),H(3),AZ(3),
     1 X1(3),Y1(3),IBD(8),BB(9)
      INCLUDE DECLAR
      INTEGER HARDWARE
      IF (HARDWARE(7) .EQ. 1) 90,1000
   90 REWIND 7
      IF (HARDWARE(20) .EQ. 1) 94,92
   92 CALL EQUIP(20,5HFILE )
   94 REWIND 20
      FL=6.0
      NXX=10
      NYX=300
      NXI=TTYIN(4HNXI=)
      NYI=TTYIN(4HNYI=)
      IFRA=90
      KOR=6
C     ZERO ARRAYS
      CALL ZEROARRY(NXI,NYI,NXX,NYX,IFRA,KOR)
C     READ FROM LUN 7 HASSELBLAD ORIENTATION ANGLES, TIME
C     OF THREE FLIGHTS IN HOURS AND MIN AND EFFLUENT
C     FLOW RATE IN GPM
      DELOMG=FFIN(7)/57.2958
      DELPHI=FFIN(7)/57.2958
      DO 95 I=1,3,2
      ANGHB(I)=DELOMG
   95 ANGHB(I+1)=DELPHI
      DO 100 I=1,3
  100 TIMFLT(I)=FFIN(7)+FFIN(7)/60.
      RATE=FFIN(7)/(7.48*60.)
      IF (HARDWARE(8) .NE. 1) GO TO 1000
      IF (HARDWARE(9) .NE. 1) GO TO 1000
      IF (HARDWARE(10) .NE. 1) GO TO 1000
C     ORIENT ALL PHOTOS
      CALL RESECT(FL,DELOMG,DELPHI)
      CALL ZEROARRY(NXI,NYI,NXX,NYX,1,0)
      DO 120 I=1,30
      IF (CAMO(I,3)-1.0) 120,120,110
  110 DO 120 J=1,3
      CAMO(I+30,J)=CAMO(I,J)
      CAMO(I+60,J)=CAMO(I,J)
  120 CONTINUE
      REWIND 8
```

Figure C-7. Program listing for REMOTE.

```
      IGO=1
  105 GO TO (122,124,126,300),IGO
  122 KHBL=0
      KHBH=4
      GO TO 136
  124 KHBL=3
      KHBH=7
      GO TO 136
  126 KHBL=6
      KHBH=10
C     CHECK ONE CONTROL PT ON EACH CAMERA
  136 XP=0.
      K=0
      J=0
      SUM1=0.0
      SUM2=0.0
  140 READ(08,1) IFL,IPH,(IE(I),X1(I),Y1(I),I=1,3)
    1 FORMAT(3X,2I1,3(I4,2F6.3,7X))
      IF (EOF(8)) GO TO 250
      IF (IFL.GT.KHBL.AND.IFL.LT.KHBH) 150,140
  150 DO 180 I=1,3
      IF (IE(I) .EQ. 0 .AND.X1(I) .GT. 0.1) GO TO 155
      IF (IE(I) .GE. 1 .AND. IE(I) .LT. 20) 160,170
  155 XG(1)=X1(I)
      XG(2)=Y1(I)
      K=1
      GO TO 180
  160 IPTN=IE(I)
      XP=X1(I)
      YP=Y1(I)
      IF (K .EQ. 1) GO TO 190
      GO TO 180
  170 GO TO (180,171,171),IGO
  171 IF(IE(I) .GE. 30 .AND. IE(I) .LE. 33) 172,180
  172 J=J+1
      SUM1=SUM1+X1(I)
      SUM2=SUM2+Y1(I)
      IF (J-4) 180,190,190
  180 CONTINUE
      GO TO 140
  190 IF (XP-0.01) 136,136,192
  192 IPLATE=(IFL-1)*10+IPH
      CALL ORIMAT(IPLATE)
      GO TO (197,198,193),IGO
  197 SUM1=XG(1)*4.
      SUM2=XG(2)*4.
  198 XP=SUM1/4.-XP
      YP=SUM2/4.-YP
      CALL TRNCOORD(YP,XP,FL,XT)
      INCLUDE GRDCOORD
      REWIND 9
  194 I=FFIN(9)
      IF (EOF(9)) GO TO 250
      XP=FFIN(9)
      YP=FFIN(9)
      ZP=FFIN(9)
      IF (IPTN-I) 194,196,194
  196 DX=XP-XG(1)
      DY=YP-XG(2)
      WRITE (20,2) IPTN,XG(1),XG(2)
      WRITE (20,3) I,XP,YP
      WRITE (20,4) IPLATE,DX,DY
```

Figure C-7. Program listing for REMOTE. (Continued)

```
    2 FORMAT(≠ HB PT NO.≠,I3,≠   X=≠,F8.0,≠   Y=≠,F8.0)
    3 FORMAT(≠ GD PT NO.≠,I3,≠   X=≠,F8.0,≠   Y=≠,F8.0)
    4 FORMAT(≠ PHOTO NO.≠,I3,≠   DIFX=≠,F5.0,≠   DIFY=≠,F5.0)
      DIS=DIST(DX,DY)
      IF (DIS-20.) 136,136,200
  200 GO TO (136,210,210),IGO
  210 J=0
      K=60
      IF (IGO .EQ. 2) K=30
      K=IPLATE-K
  220 XG(1)=DY*SIN(CAMO(K,6))+DX*COS(CAMO(K,6))
      XG(2)=DY*COS(CAMO(K,6))-DX*SIN(CAMO(K,6))
      IF (J .EQ. 1) GO TO 230
      DX=XT(1)
      DY=XT(2)
      X1(1)=XG(1)
      X1(2)=XG(2)
      J=J+1
      GO TO 220
  230 SUM1=XT(3)/DIST(XG(1),XT(3))
      SUM2=XT(3)/DIST(XG(2),XT(3))
      K=3
      IF (IGO .EQ. 2) K=1
      ANGHB(K+1)=ANGHB(K+1)-X1(1)*SUM1*SUM1/CAMO(IPLATE,3)
      ANGHB(K)=ANGHB(K)+X1(2)*SUM1*SUM2/CAMO(IPLATE,3)/2.
      WRITE(20,30) ANGHB(K),ANGHB(K+1)
   30 FORMAT(≠  DELOMG≠,F7.3,/≠  DELPHI≠,F7.3)
      GO TO 136
  250 IGO=IGO+1
      REWIND 8
      GO TO 105
  300 FL=6.0
C COMPUTE CURRENTS AND ORIENTATION OF WASTE FIELD FROM K-17
  305 READ (8,1) IFL,IPH,(IE(J),X1(J),Y1(J),J=1,3)
      IF (EOF(8)) GO TO 350
      IF (IFL .LE. 3) 310,305
  310 IPLATE=(IFL-1)*10+IPH
      DO 340 I=1,3
      IF (IE(I) .EQ. 0 .AND. X1(I) .GT. 0.1) GO TO 320
      IF (IE(I) .LT. 30 .AND. IE(I) .GT. 19) GO TO 324
      IF (IE(I) .EQ. 34 ) GO TO 328
      IF (IE(I) .EQ. 35 ) GO TO 332
      GO TO 340
  320 I1=1
      I2=2
      K=IPLATE
      GO TO 338
  324 I1=IE(I)
      I2=I1
      K=IPLATE+30
      GO TO 338
  328 I1=3
      I2=4
      K=IPLATE
      GO TO 338
  332 I1=5
      I2=6
      K=IPLATE
  338 IPHOT(IPLATE,I1)=X1(I)*1000.
      IPHOT(K,I2)=Y1(I)*1000.
  340 CONTINUE
      GO TO 305
```

Figure C-7. Program listing for REMOTE. (Continued)

```
C       COMPUTE ORIENTATION OF WASTE FIELD
  350 DO 360 I=1,30
      IF (IPHOT(I,3)) 360,360,352
  352 X1(1)=IPHOT(I,2)-IPHOT(I,4)
      X1(2)=IPHOT(I,1)-IPHOT(I,3)
      Y1(1)=IPHOT(I,2)-IPHOT(I,6)
      Y1(2)=IPHOT(I,1)-IPHOT(I,5)
      XP=X1(1)/1000.
      YP=X1(2)/1000.
      CALL ORIMAT(I)
      CALL TRNCOORD(XP,YP,FL,XT)
      IPLATE=I
      INCLUDE GRDCOORD
      C(12,2)=XG(1)
      C(12,3)=XG(2)
      C(14,2)=NYI*30
      XP=Y1(1)/1000.
      YP=Y1(2)/1000.
      CALL TRNCOORD(XP,YP,FL,XT)
      INCLUDE GRDCOORD
      XP=XG(1)-C(12,2)
      YP=XG(2)-C(12,3)
      ROT=ATANF(XP/YP)
      IF (YP) 354,355,355
  354 ROT=ROT+3.14159
  355 C(13,2)=SINF(ROT)
      C(13,3)=COSF(ROT)
      WRITE(20,5) ROT,C(12,2),C(12,3)
    5 FORMAT(≠1 ROTATION ANGLE≠,F10.3,≠     RAD≠/,
     1 ≠ ORIGIN X≠,F10.0,/≠ ORIGIN Y≠,F10.0)
      GO TO 370
  360 CONTINUE
  370 K=0
      DO 380 I=1,30
      DO 380 J=20,29
      IF (IPHOT(I,J)) 380,380,375
  375 XP=IPHOT(I,2)-IPHOT(I+30,J)
      YP=IPHOT(I,1)-IPHOT(I,J)
      XP=XP/1000.
      YP=YP/1000.
      K=I/10+1
      IF (IPLATE .NE. I) CALL ORIMAT(I)
      CALL TRNCOORD(XP,YP,FL,XT)
      IPLATE=I
      INCLUDE GRDCOORD
      X(J-19,K)=XG(1)
      X(J-19,K+30)=XG(2)
      WRITE (20,6) J,I,XG(1),XG(2)
    6 FORMAT(≠  FLOAT≠,I3,≠  PLATE≠,I3,≠    X=≠,F10.0,
     1 ≠    Y=≠,F10.0)
  380 CONTINUE
      DO 385 L=1,10
      XP=X(L,1)-X(L,2)
      YP=X(L,31)-X(L,32)
      X1(1)=DIST(XP,YP)
      XP=X(L,1)-X(L,3)
      YP=X(L,31)-X(L,33)
      X(L,1)=DIST(XP,YP)
      XP=X(L,2)-X(L,3)
      YP=X(L,32)-X(L,33)
      X(L,3)=DIST(XP,YP)
      X(L,2)=X1(1)
```

Figure C-7.  Program listing for REMOTE.  (Continued)

```
  385 CONTINUE
C     COMPUTE AVERAGE CURRENT VELOCITY
      X1(1)=(TIMFLT(3)-TIMFLT(1))*3600.
      X1(2)=(TIMFLT(2)-TIMFLT(1))*3600.
      X1(3)=(TIMFLT(3)-TIMFLT(2))*3600.
      J=0
      SUM1=0.0
      SUM2=0.0
      DIF=0.0
      AI=0.0
      DO 390 L=1,10
      DO 390 I=1,3
      IF (X(L,I).LT.10..OR.X(L,I).GT.4000.) GO TO 390
      J=J+1
      VEL=X(L,I)/X1(I)
      SUM1=SUM1+VEL
      SUM2=SUM2+VEL*VEL
      K=L+19
      WRITE(20,7) K,I,VEL
    7 FORMAT(≠ FLOAT NO.≠,I3,≠   I=≠,I2,≠   VEL=≠,F5.2,≠FPS≠)
      IF (I .NE. 1) GO TO 390
      AI=AI+1
      DIF=DIF+VEL
  390 CONTINUE
      IF (J .EQ. 0) GO TO 394
      AJ=J
      VEL=SUM1/AJ
      IF (AJ .GT. 1.0) 392,400
  392 SUM2=STDDEV(SUM1,SUM2,AJ)
      WRITE(20,8) VEL,SUM2
    8 FORMAT(≠ MEAN VEL≠,F5.2,≠   STD DEV≠,F5.2)
      IF (AI .LE. 0.1) GO TO 400
      VEL=DIF/AI
      GO TO 400
  394 VEL=TTYIN(4HVEL=)
C     COMPUTE SUN ALTITUDE AND AZIMUTH
  400 CALL SUNLITE(TIMFLT,H,AZ)
C     READ FROM LUN 7 VALUES OF FILM GAMMA,FILM SPEED, ATMOS
C     OPTICAL THICKNESS FOR THE EIGHT SPECTRAL BANDS.
      DO 420 J=4,11
      DO 420 I=1,3
      C(J,I)=FFIN(7)
  420 CONTINUE
C     READ FROM 7 VALUES OF EXPOSURE TIME AND FNO
C     (NINE VALUES K-17 1,2,3;HB-1 4,5,6; HB-2 7,8,9)
      DO 430 J=12,20
      SUM1=FFIN(7)
      SUM2=FFIN(7)
      C(J,1)=SUM1*SUM2*SUM2
  430 CONTINUE
C     READ FROM 7 COEFFS FOR DETERMINING ATMOS ATTEN FROM
C     THE SEA TO THE CAMERA STATION
      DO 440 I=1,8
      DO 440 J=1,2
      P(J,I)=FFIN(7)
  440 CONTINUE
C     READ FROM 7 0 IF ANTIVIGNETTING FILTER ON K-17 1 IF NOT
      B(15,6)=FFIN(7)
C      DETERMINE SUNLIGHT VECTORS
      DO 450 I=1,3
      J=3+I
      B(1,J)=SINF(H(I))
```

Figure C-7. Program listing for REMOTE. (Continued)

```
      B(2,J)=COSF(H(I))
      B(13,J)=-SIN(AZ(I))
      B(14,J)=-COSF(AZ(I))
      B(3,J)=1.0/B(1,J)
      B(4,J)=B(2,J)*B(13,J)
      B(5,J)=B(2,J)*B(14,J)
      B(6,J)=-B(1,J)
      B(8,J)=B(2,J)/1.33
      B(7,J)=SQRT(1.0-B(8,J)*B(8,J))
      B(9,J)=1.0/B(7,J)
      B(10,J)=B(8,J)*B(13,J)
      B(11,J)=B(8,J)*B(14,J)
      B(12,J)=-B(7,J)
      SUM2=ATAN(B(8,J)/B(7,J))
      SUM1=1.5708-H(I)
      B(15,I)=REFLECT(SUM1,SUM2)
  450 CONTINUE
      B(15,4)=1.33*1.33
      IF (HARDWARE(21).EQ. 1) 460,455
  455 CALL EQUIP(21,5HFILE )
  460 IF (HARDWARE(22) .EQ. 1) 464,462
  462 CALL EQUIP(22,5HFILE )
  464 IF (HARDWARE(4) .EQ. 1) 470,1000
  470 REWIND 4
      IF (HARDWARE(5) .EQ. 1) GO TO 480
      CALL EQUIP(5,5HFILE )
  480 REWIND 5
      READ (4,9) FIX,XL,YL,CONL
  500 READ(4,9) FIX,XF,YF,CONF
      IF (EOF(4)) GO TO 600
    9 FORMAT(F7.1,2F14.0,F10.1)
      IF (FIX-0.1) 500,500,505
  505 DDEN=CONF-CONL
      DKX=XF-XL
      DKY=YF-YL
      XKX=DIST(DKX,DKY)/60.
      IF (XKX .GT. 0.5) GO TO 508
      XL=(XF+XL)/2.
      YL=(YF+YL)/2.0
      CONL=(CONF+CONL)/2.0
      GO TO 500
  508 KX=XKX
      GO TO (510,520),KX
  510 X(1,1)=(XL+XF)/2.
      X(1,2)=(YL+YF)/2.
      X(1,3)=(CONL+CONF)/2.
      KX=1
      GO TO 530
  520 DIV=KX
      IF(DIV-8.) 522,522,540
  522 DO 524 K=1,KX
      YYK=K
      X(K,1)=XL+DKX*YYK/DIV
      X(K,2)=YL+DKY*YYK/DIV
      X(K,3)=CONL+DDEN*YYK/DIV
  524 CONTINUE
  530 DO 540 K=1,KX
      X(K,1)=X(K,1)-C(12,2)
      X(K,2)=X(K,2)-C(12,3)
      XG(1)=X(K,1)*C(13,2)+X(K,2)*C(13,3)
      XG(2)=-X(K,1)*C(13,3)+X(K,2)*C(13,2)
      LX=XG(1)/60.+0.5
```

Figure C-7. Program listing for REMOTE. (Continued)

```
      IF(LX .LE. 0 .OR. LX .GT. NXI) GO TO 540
      LY=(XG(2)+C(14,2))/60.+0.5
      IF (LY .LE. 0 .OR. LY .GT. NYI) GO TO 540
      WRITE (5,10) LX,LY,X(K,3)
   10 FORMAT(2I4,F6.2)
  540 CONTINUE
      XL=XF
      YL=YF
      CONL=CONF
      GO TO 500
  600 JJFL=1
      KFLT=1
      END FILE 5
  602 K=0
      ILUN=1
  610 IF (HARDWARE(ILUN) .NE. 1) GO TO 630
      CALL ZEROARRY(NXI,NYI,1,0,1,0)
      FL=6.0
      IF (KFLT .GT. 3) FL=150./25.4
      CALL PROCESS(KFLT,JJFL,ILUN,FL,NXI,NYI)
      K=K+1
      WRITE(61,31) K,KFLT,ILUN
   31 FORMAT(3I10)
  630 ILUN=ILUN+1
      KFLT=KFLT+3
      GO TO (610,610,610,640),ILUN
  640 IF (K .EQ. 0) 642,644
  642 L=1
      GO TO 901
  644 K=0
      DO 650 I=1,8
      IBD(I)=0
      ILUN=I+30
      IF (HARDWARE(ILUN) .NE. 1) GO TO 660
      REWIND ILUN
      K=K+1
      IBD(K)=ILUN
      J=1
  655 READ(ILUN,11) X(K,J)
   11 FORMAT(F8.0)
      IF (EOF(ILUN)) GO TO 660
      J=J+1
      IF (J .LT. 300) 655,660
  660 CONTINUE
      IF (K .LE. 0) GO TO 642
      NO=J-1
      KK=K
      ITRY=1
  659 K=KK
      WRITE(61,32)(IBD(I),I=1,K)
   32 FORMAT(≠ TYPE IN 1 IF YOU WANT TO USE A PRODUCT,2 IF NOT≠/,
     1≠ THE FOLLOWING BANDS ARE USED≠≠/,9I4)
      KKGO=TTYIN(4HRAT=)
      GO TO (661,663),KKGO
  661 K=K+1
      WRITE(61,33)
   33 FORMAT(≠ TTYIN NO. OF THE TWO TERMS 1 3 ETC≠)
      KTOP=TTYIN(4H1ST=)
      KBOT=TTYIN(4H2ND=)
      DO 662 J=1,NO
      X(K,J)=X(KTOP,J)*X(KBOT,J)
  662 CONTINUE
```

Figure C-7. Program listing for REMOTE. (Continued)

```
663 WRITE(61,34) K
 34 FORMAT(≠ THERE ARE≠,I3,≠   VARIABLES USED IN THE EQ≠/,
   1≠ TTYIN 1 IF YOU WANT A SQUARED TERM 2 IF NOT≠)
    KIGO=TTYIN(4HSQU=)
    GO TO (664,666),KIGO
664 WRITE(61,35)
 35 FORMAT(≠ WHAT TERM IS TO BE SQUARED^≠)
    ISQU=TTYIN(4HSQU=)
    K=K+1
    K2=K
    DO 665 J=1,NO
665 X(K,J)=X(ISQU,J)*X(ISQU,J)
666 K=K+1
    N=K
    GO TO (672,674),ITRY
672 REWIND 5
    DO 667 J=1,NO
    READ(5,12)X(K,J)
 12 FORMAT(8X,F6.2)
667 CONTINUE
    K=0
    NKN=N-1
    DO 678 J=1,NO
    DO 676 I=1,NKN
    IF(ABS(X(I,J)).LT..001) GO TO 678
676 CONTINUE
    K=K+1
    DO 677 I=1,N
    X(I,K)=X(I,J)
677 CONTINUE
    X(9,K)=X(N,J)
678 CONTINUE
    NO=K
    GO TO 671
674 DO 675 J=1,NO
    X(N,J)=X(9,J)
675 CONTINUE
671 CALL LEASTFIT(N,NO,BB,RES)
    KCO=N-1
    WRITE(61,37) (BB(I),I=1,KCO)
    WRITE(61,36) RES
 36 FORMAT(≠ MEAN SQ≠,F10.3,/≠ IS THIS OK^  ≠/,
   1≠ TTYIN 1 FOR YES 2 FOR NO.≠)
    IGO=TTYIN(4HIGO=)
    ITRY=2
    GO TO (668,659),IGO
668 CALL ZEROARRY(NXI,NYI,1,0,1,0)
    IF(HARDWARE(24).NE.1) CALL EQUIP(24,5HFILE )
    DO 669 J=1,NO
    WRITE(24,37) (X(I,J),I=1,N)
 37 FORMAT(9E11.3)
669 CONTINUE
    N=N-1
    END FILE 24
670 WRITE(61,40)N
 40 FORMAT(≠ TTYIN VALUES OF COEFFICIENTS≠,I4,≠   REQUIRED≠)
    DO 681 I=1,N
681 BB(I)=TTYIN(4HCOEF)
    DO 680 I=1,KK
    ILUN=IBD(I)-20
    REWIND ILUN
680 CONTINUE
```

Figure C-7. Program listing for REMOTE. (Continued)

```
      LY=0
      LOWX=0
  682 DO 684 I=1,KK
      ILUN=IBD(I)-20
      READ(ILUN,13) (X(I,J),J=1,20)
   13 FORMAT(X,20F6.0)
      IF (EOF(ILUN)) GO TO 700
  684 CONTINUE
      DO 686 J=1,20
      IF(KKGO.EQ.1) X(KK+1,J)=X(KTOP,J)*X(KBOT,J)
      IF(KIGO.EQ.1) X(K2,J)=X(ISQU,J)*X(ISQU,J)
  686 CONTINUE
      LY=LY+1
      IF (LY .LE. NYI) GO TO 688
      LOWX=LOWX+20
      LY=1
  688 DO 692 J=1,20
      SUM1=0.0
      DO 690 I=1,N
      IF (ABS(X(I,J)) .LE. 0.001) GO TO 692
      SUM1=SUM1+BB(I)*X(I,J)
  690 CONTINUE
      LX=LOWX+J
      IF (SUM1 .LT. 0. .OR. SUM1 .GT. 30.) SUM1=0.
      IPLOT(LX,LY)=SUM1*10.
  692 CONTINUE
      GO TO 682
  700 DO 702 J=1,8
      X(3,J)=0.0
  702 CONTINUE
      KND=8
      KDN=5
      NXS=NXI-2
      NYS=NYI-2
      CALL INTERP(NXI,NYI,NXS,NYS,KND,KDN)
      CALL CULL(NXI,NYI)
      CALL AVERAGE(NXS,NYS)
C     WRITE SYMBOLIC PLOT
  704 REWIND 8
      READ(08,14) MO,IDATE
   14 FORMAT(I1,I2)
      WRITE (20,15) ROT,JJFL,MO,IDATE
   15 FORMAT(1H1,///42X,≠AIRPHOTO ANALYSIS OF OCEAN OUTFALL ≠
     1,≠DISPERSION≠///,45X,≠VOLUMETRIC WASTE CONCENTRATION≠
     2,≠ IN ML/LITER≠//,55X,≠SKETCH ON 60 - FT GRID≠/,49X,
     3≠DIRECTION OF PLUME ≠,F5.2,≠  RADIANS≠/,35X,
     4 ≠FLIGHT NO.≠,I4,30X,≠DATE  ≠,I2,≠/≠,I2,≠/69≠)
      WRITE(20,16)
   16 FORMAT( 48X,≠ CONCENTRATION CODE IN ML/L≠/,45X,
     1≠)       1 - 2≠,15X,≠1 1    2 - 4≠/,45X,≠  )≠,24X,≠ 1 ≠//,45X,
     2≠III     4 - 6≠,15X,≠LLL    6 - 10≠/,45X,≠III≠,24X,≠LLL≠//,45X,
     3≠PPP    10 - 15≠,14X,≠RRR   15 - 20≠/,45X,≠PPP≠,24X,≠RRR≠//,45X,
     4≠MMM    20 - 25≠,14X,≠***    GT 25 ≠/,45X,≠MMM≠,24X,≠***≠////)
      WRITE(20,17) C(12,2),C(12,3)
   17 FORMAT(60X,≠+ X=≠,F8.0,≠E, Y=≠,F7.0,≠N≠)
      NYS=NYI-10
      IKS=NYI/2
      IEKS=IKS+20
      IKS=IKS-20
      KCO=3
      DO 800 LX=2,NXI
      DO 790 LY=1,NYI
```

Figure C-7. Program listing for REMOTE. (Continued)

```
      AXZ=IPHOT(LX,LY)
      AXZ=AXZ/10.
      IF (AXZ-1.0) 710,710,705
  705 XL=AXZ/2.+1.
      IDO=XL
      GO TO (720,730,740,760),IDO
  710 X(1,LY)=8H
      X(2,LY)=8H
      GO TO 790
  720 X(1,LY)=8H)
      X(2,LY)=8H   )
      X(3,1)=X(3,1)+1.
      GO TO 790
  730 X(1,LY)=8H1 1
      X(2,LY)=8H 1
      X(3,2)=X(3,2)+1.
      GO TO 790
  740 X(1,LY)=8HIII
      X(2,LY)=8HIII
      X(3,3)=X(3,3)+1.
      GO TO 790
  750 X(1,LY)=8HLLL
      X(2,LY)=8HLLL
      X(3,4)=X(3,4)+1.
      GO TO 790
  760 IF (AXZ-10.) 750,750,770
  770 XL=AXZ/5.-1.
      IDO=XL
      GO TO (775,780,785,788),IDO
  775 X(1,LY)=8HPPP
      X(2,LY)=8HPPP
      X(3,5)=X(3,5)+1.
      GO TO 790
  780 X(1,LY)=8HRRR
      X(2,LY)=8HRRR
      X(3,6)=X(3,6)+1.
      GO TO 790
  785 X(1,LY)=8HMMM
      X(2,LY)=8HMMM
      X(3,7)=X(3,7)+1.
      GO TO 790
  788 X(1,LY)=8H***
      X(2,LY)=8H***
      X(3,8)=X(3,8)+1.
  790 CONTINUE
      KCO=KCO+1
      IF(KCO.NE.4) GO TO 795
      WRITE(61,42)(X(1,J),J=1,NYI,3)
   42 FORMAT(1X,30A1)
      KCO=0
  795 WRITE (20,18) (X(1,J),J=IKS,IEKS)
      WRITE (20,18) (X(2,J),J=IKS,IEKS)
   18 FORMAT (1HW,50A3)
  800 CONTINUE
      WRITE(61,43)
   43 FORMAT(≠ ARE THE COEFFICIENTS OK^ TTYIN 1-YES, 2-NO≠)
      KCO=TTYIN(4H GO=)
      GO TO (802,670),KCO
  802 IF(HARDWARE(23).NE.1) CALL EQUIP(23,5HFILE )
      WRITE(61,39)
   39 FORMAT(≠ TTYIN 1 IF WANT DATA FOR CONTOUR PLOT 2 NO≠)
      JGP=TTYIN(4HPLOT)
```

Figure C-7. Program listing for REMOTE. (Continued)

```
      GO TO(701,704),JGO
  701 DO 703 I=1,NXI
      K=NXI-I+1
      WRITE (23,28)(J,K,IPHOT(I,J),J=1,NYI)
   28 FORMAT(24(15I4/))
  703 CONTINUE
      END FILE 23
C     COMPUTE DIFFUSION COEFFICIENTS
      DJKK=0.
      SUM2=0.0
      DO 810 J=1,8
      X(3,J)=X(3,J)*3600.
  810 CONTINUE
      AMASS=RATE*60./VEL
      GO TO (812,820,820),JJFL
  812 DO 814 I=4,6
      DO 814 J=61,90
      CANO(J,I)=0.0
  814 CONTINUE
  820 WRITE(20,19) JJFL,MO,IDATE
   19 FORMAT(1H1,44X,*PRELIMINARY  DIFFUSION  COMPUTATIONS*/
     1,47X,*FLIGHT*,I3,12X,I2,*/*,I2,*/69*/,19X,
     2*   SEC. WIDTH  EFF DEPTH  SIGMA Y  COEFFICIENT
     3*X*,3X,*Y      DIFF. COEFF.*/,22X,*NO.   FT*,7X,
     4*FT*,20X,*PPT*,7X,*STATE PLANE COORD  FT SQ/SEC*/)
      L=1
      LOST=2.+(TIMFLT(JJFL)-TIMFLT(1))*VEL+0.5
      NXS=NXI-2
      DO 900 I=LOST,NXS,5
      JST=1
      LNY=0
      DIV=0.0
      SUM1=0.0
      DIF=0.0
      DO 880 J=JST,NYI
      AJ=J*60
      ACD=IPHOT(I,J)+IPHOT(I-1,J)+IPHOT(I-2,J)+IPHOT(I+1,J)+
     1 IPHOT(I+2,J)
      ACD=ACD/50.
      IF(ACD.LT.1.)GO TO 880
      SUM1=SUM1+ACD*AJ
      DIF=DIF+ACD
      DIV=DIV+ACD*AJ*AJ
      IF(IPHOT(I,J).GT.9) LNY=LNY+1
  880 CONTINUE
      IF(DIF.LT.1.)881,882
  881 X(10,L)=0.0
      X(5,L)=0.0
      GO TO 895
  882 XMEAN=SUM1/DIF
      X(10,L)=DIV/DIF-XMEAN*XMEAN
      X(4,L)=LNY*60
      X(5,L)=AMASS/(DIF*3.6)
      X(6,L)=SQRT(X(10,L))
      X(7,L)=DIF*60./(2.51*X(6,L))
      RGX=I*60
      RGY=XMEAN-C(14,2)
      XG(1)=+RGX*C(13,2)-RGY*C(13,3)
      XG(2)=+RGX*C(13,3)+RGY*C(13,2)
      X(8,L)=XG(1)+C(12,2)
      X(9,L)=XG(2)+C(12,3)
      IF(L .EQ. 1) 885,890
```

Figure C-7. Program listing for REMOTE. (Continued)

```
885 DJ=0.0
    GO TO 895
890 DJ=VEL*(X(10,L)-X(10,L-1))/600.
895 CAMO(L+60,JJFL+3)=X(10,L)
    IF (X(5,L).GT.0. .AND.X(5,L).LT.20.)896,897
896 WRITE(20,20) I,(X(KK,L),KK=4,9),DJ
 20 FORMAT(19X,I6,F7.0,F9.1,2E11.2,4X,2F9.0,E12.2)
    SUM2=SUM2+DJ
    DJKK=DJKK+1.
897 L=L+1
900 CONTINUE
    SUM2=SUM2/DJKK
    WRITE(20,21) RATE,VEL,AZ(JJFL),H(JJFL),SUM2
 21 FORMAT(//20X,≠FLOW    RATE≠,F5.1,≠  CFS≠/,
   120X,≠CURRENT VEL≠,F5.1,≠  FPS≠/,20X,≠SUN  AZIMUTH≠,
   2F5.1,≠  RAD≠/,20X,≠SUN ALIITUDE≠,F5.1,≠  RAD≠/,
   320X,≠AVE DIF COEF≠,F5.1,≠  FT SQ/SEC≠)
    WRITE(20,22)
 22 FORMAT(1H1,56X,≠AREA  WITHIN  EACH  CONCENTRATION≠,
   1≠  RANGE≠/,65X,≠RANGE≠,13X,≠AREA≠/,65X,
   2≠ML/L≠,13X,≠SQ FT≠)
    WRITE(20,23)(X(3,J),J=1,8)
 23 FORMAT(65X,≠0 - 2≠,8X,E11.2/,65X,≠2 - 4≠,8X,E11.2/,
   1 65X,≠4 - 6≠,8X,E11.2/,65X,≠6 -10≠,8X,E11.2/,
   2 65X,≠10-15≠,8X,E11.2/,65X,≠15-20≠,8X,E11.2/,
   3 65X,≠20-25≠,8X,E11.2/,65X,≠GT 25≠,8X,E11.2)
901 JJFL=JJFL+1
    KFLT=JJFL
    DO 910 I=11,18
    IF (HARDWARE(I).NE.1) GO TO 905
    CALL UNEQUIP(I)
905 K=I+20
    IF (HARDWARE(K).NE.1) GO TO 910
    CALL UNEQUIP(K)
910 CONTINUE
    H(JJFL-1)=L-1
    GO TO(602,602,602,920),JJFL
920 WRITE(20,24)
 24 FORMAT(1H1,///20X,≠N O N S T E A D Y   S T A T E≠,
   1≠   D I F F U S I O N   C O E F F I C I E N T S≠//)
    I=1
    KI=3
    KK=6
    K=2
    NO=1
    L=H(1)
    IF (L .LT. H(2)) L=H(2)
    IF (L .LT. H(3)) L=H(3)
926 DTIM=(TIMFLT(K)-TIMFLT(I))*120.
    DIV=0.
    SUM1=0.
    DO 930 J=1,L
    JK=J+60
    KJ=K+3
    KI=I+3
    IF(CAMO(JK,KJ) .LT.1. .AND. CAMO(JK,KI) .LT.1.)
   1 GO TO 928
    X(NO,J)=(CAMO(JK,KJ)-CAMO(JK,KI))/DTIM
    SUM1=SUM1+X(NO,J)
    DIV=DIV+1.
    X(NO+3,J)=1.0
    GO TO 930
```

Figure C-7.  Program listing for REMOTE.  (Continued)

```
 928 X(NO   ,J)=0.
 930 CONTINUE
     X(NO+4,1)=SUM1/DIV
     GO TO (932,934,940),NO
 932 NO=NO+1
     K=3
     I=1
     GO TO 926
 934 K=3
     I=2
     NO=NO+1
     GO TO 926
 940 WRITE(20,25) (TIMFLT(I),I=1,3),MO,IDATE
  25 FORMAT(20X,≠TIMES PDT -- FLIGHT 1≠,F6.1,5X,
    1≠FLIGHT 2≠,F6.1,5X,≠FLIGHT 3≠,F6.1,10X,I2,≠/≠,I2,
    2≠/69≠/,23X,≠SECTION≠,10X,≠FLIGHTS 1-2≠,10X,
    3≠FLIGHTS 1-3≠,10X,≠FLIGHTS 2-3≠/)
     DO 950 I=1,L
     K=2+5*(I-1)
     WRITE(20,26) K,(X(J,I),J=1,NO)
  26 FORMAT(25X,I3,3E22.2)
 950 CONTINUE
     WRITE(20,27) (X(I,1),I=5, 7)
  27 FORMAT(/23X,≠MEANS≠,3E22.2)
1000 STOP
     END
```

Figure C-7. Program listing for REMOTE. (Continued)

```
      DEFINE DECLAR
      COMMON X(10,300),IPHOT(120,80),CAMO(90,6),C(20,3)
      COMMON B(15,6),P(2,8),ANGHB(4),VOLL(2,8)
      END
      DEFINE GRDCOORD
      XG(1)=CAMO(IPLATE,1)-CAMO(IPLATE,3)*XT(1)/XT(3)
      XG(2)=CAMO(IPLATE,2)-CAMO(IPLATE,3)*XT(2)/XT(3)
      END
      SUBROUTINE PROCESS(KFLT,JFLT,ILUN,FL,NXI,NYI)
      DIMENSION IVT(6),BB(9),XT(3),XG(2)
      INCLUDE DECLAR
      INTEGER HARDWARE
      REWIND 21
      KGO=0
      ISEY1=TTYIN(4HSEY1)
      ISEY2=TTYIN(4HSEY2)
      ISEAX=TTYIN(4HSEAX)
      IPHX=TTYIN(4HPHOX)
   89 IPLATE=(KFLT-1)*10+1
      DENL=TTYIN(4HDNL=)
      DENH=TTYIN(4HDNH=)
      IEND=1
      INK=0
   95 READ(ILUN,1) IMO,IDATE,IFLT,IPH,IPLT2,IBD1,IBD2,
     1 XPH,YPH,DCOOR
    1 FORMAT(7I5,2F5.0,F5.3)
      IF(EOF(ILUN)) GO TO 1000
      IF(KFLT.NE.IFLT) GO TO 1000
      IF(IPLATE-IPLT2) 100,200,150
  100 BACKSPACE ILUN
  101 IEND=3
      GO TO 400
  150 IEND=2
      BACKSPACE ILUN
      GO TO 400
  200 CALL ORIMAT(IPLATE)
      IBAND=IBD1
      SUM1=CAMO(IPLATE,3)/3260.
      ATN1=P(1,IBD1)+ALOG(SUM1+1.)+P(2,IBD1)*SUM1*SUM1
      ATN2=P(1,IBD2)+ALOG(SUM1+1.)+P(2,IBD2)*SUM1*SUM1
      ATN1=ATN1-ATN2
      ATN2=(C(IBD1+3,3)-C(IBD2+3,3))*B(3,JFLT+3)
      DO 210 I=1,60
      YP=I
  210 X(9,I)=(XPH+0.5-YP)*DCOOR
      DO 300 J=1,120
      JK=J
      IST=1
      IND=30
      IF (J.LE.60) GO TO 220
      JK=J-60
      IST=31
      IND=60
  220 READ(ILUN,2) (X(10,I),I=IST,IND)
    2 FORMAT(30F4.2)
      XP=JK
      XP=(YPH+0.5-XP)*DCOOR
      KGO=1
      IF(JK.EQ.ISEY1.OR.JK.EQ.ISEY2) KGO=2
      K=0
      DO 300 I=IST,IND
      IF(X(10,I).LT.DENL.OR.X(10,I).GT.DENH) GO TO 300
      IF(K.EQ.0.AND.J.LT.60) GO TO 290
```

Figure C-8. Subroutines used with program REMOTE.

```
      YP=X(9,I)
      CALL TRNCOORD(XP,YP,FL,XT)
      INCLUDE GRDCOORD
      RGX=XG(1)-C(12,2)
      RGY=XG(2)-C(12,3)
      XG(1)=RGX*C(13,2)+RGY*C(13,3)
      XG(2)=-RGX*C(13,3)+RGY*C(13,2)
      LX=XG(1)/60.+0.5
      IF(LX .LE. 0 .OR. LX .GT. NXI) GO TO 300
      LY=(XG(2)+C(14,2))/60.+0.5
      IF (LY .LE. 0 .OR. LY .GT. NYI) GO TO 300
      CAM=ATANF(SQRT(XP*XP+YP*YP)/FL)
C ANGLE BETWEEN RAY IN AIR AND VERTICAL
      DIV=SQRT(XT(1)*XT(1)+XT(2)*XT(2))
      CAN=ATAN(-DIV/XT(3))
C ANGLE BETWEEN RAY AND VERTICAL UNDERWATE-
      SINC=0.75*SINF(CAN)
      COSC=SQRT(1.0-SINC*SINC)
C RAY VECTOR UNDERWATER
      FT=-DIV*COSC/SINC
      SINC=(XT(1)*B(10,JFLT+3)+XT(2)*B(11,JFLT+3)+FT*B(12,JFLT+3)
     1 )/1.34
      IF(SINC.GT.1.) SINC=1.
      FT=SQRT(1.0-SINC*SINC)
      TAB=ATAN(FT/SINC)
      CAN=1.0/COS(CAN)
      FT=X(10,I)/C(IBD1+3,1)+ATN2+ATN1*CAN
      DENS=EXP(FT)*1000.
      IF(I.EQ.ISEAX.AND.IPH.EQ.IPHX) GO TO 250
      GO,TO (260,250),KGO
  250 IF((INK.LT.300) INK=INK+1
      X(1,INK)=1.0
      X(2,INK)=CAM
      X(3,INK)=TAB
      X(4,INK)=CAN
      X(5,INK)=DENS
  260 WRITE(21,3)LX,LY,CAM,TAB,CAN,DENS
    3 FORMAT(2I5,5E11.3)
  290 K=K+1
  300 CONTINUE
      IPLATE=IPLATE+1
      GO TO 95
  400 IF(INK.EQ.0) GO TO 1100
      NO=INK
      N=5
      CALL LEASTFIT(N,NO,BB,RES)
      END FILE 21
      REWIND 21
  410 READ(21,3) LX,LY,CAM,TAB,CAN,DENS
      IF(EOF(21)) GO TO 500
      IPHOT(LX,LY)=DENS-(BB(1)+BB(2)*CAM+BB(3)*TAB+BB(4)
     1 *CAN)
      GO TO 410
  500 KND=4
      KDN=4
      NXS=NXI-2
      NYS=NYI-2
      CALL INTERP(NXI,NYI,NXS,NYS,KND,KDN)
      LUNO=IBAND+10
      IF (HARDWARE(LUNO).EQ. 1) GO TO 580
      CALL EQUIP(LUNO,5HFILE )
  580 REWIND LUNO
      DO 585 I=1,NXI,5
```

Figure C-8. Subroutines used with program REMOTE. (Continued)

```
      IMAX=0
      DO 583 J=1,NYI
      IF(ABS(IPHOT(I,J)).GT.ABS(IMAX)) IMAX=IPHOT(I,J)
  583 CONTINUE
      WRITE(61,10) IMAX
  585 CONTINUE
      DO 590 I=1,NXI,20
      DO 590 J=1,NYI
      KK=I+19
      WRITE(LUNO,8) (IPHOT(K,J),K=I,KK)
    8 FORMAT(X,20I6)
  590 CONTINUE
      END FILE LUNO
      LUNO=IBAND+30
      IF (HARDWARE(LUNO) .EQ. 1) GO TO 592
      CALL EQUIP(LUNO,5HFILE )
  592 REWIND LUNO
      REWIND 5
  595 READ(5,9) LX,LY
    9 FORMAT(2I4)
      IF (EOF(5)) GO TO 598
      WRITE(LUNO,10) IPHOT(LX,LY)
   10 FORMAT(I8)
      GO TO 595
  598 END FILE LUNO
      GO TO (900,900,1100),IEND
  900 CALL ZEROARRY(NXI,NYI,1,0,1,0)
      REWIND 21
      GO TO 89
 1000 BACKSPACE ILUN
      IF(KGO.GT. 0) GO TO 101
 1100 RETURN
      END
```

Figure C-8. Subroutines used with program REMOTE. (Continued)

```
      DEFINE DECLAR
      COMMON X(10,300),IPHOT(120,80),CAMO(90,6),C(20,3)
      COMMON B(15,6),P(2,8),ANGHB(4),VOLL(2,8)
      END
      DEFINE GRDCOORD
      XG(1)=CAMO(IPLATE,1)-CAMO(IPLATE,3)*XT(1)/XT(3)
      XG(2)=CAMO(IPLATE,2)-CAMO(IPLATE,3)*XT(2)/XT(3)
      END
      SUBROUTINE RESECT(FL,DELOMG,DELPHI)
      DIMENSION D(6,7)
      INCLUDE DECLAR
      IEND=1
      REWIND 8
    5 IGO=0
      I=1
C READ PHOTO CONTROL COORDINATES
   10 READ (08,1) IFL,IPH,(IPHOT(100,J),X(10,J),X(9,J),J=1,3)
    1 FORMAT(3X,2I1,3(I4,2F6.3,7X))
      IF (EOF(8)) 15,20
   15 IEND=2
      GO TO 40
   20 IPLT=(IFL-1)*10+IPH
      IF (I-1) 21,21,23
   21 IPLATE=IPLT
   23 IF(IPLT-IPLATE) 24,25,24
   24 BACKSPACE 8
      GO TO 40
   25 DO 38 J=1,3
      IF(IPHOT(100,J).EQ. 0 .AND. X(10,J).GT. 0.) GO TO 26
      IF(IPHOT(100,J).GT. 0 .AND.IPHOT(100,J).LE.19)GO TO 28
      IF(IPHOT(100,J).LE.33 .AND.IPHOT(100,J).GT.29)GO TO 30
      GO TO 38
   26 XP=X(10,J)
      YP=X(9,J)
      GO TO 38
   28 B(I,1)=IPHOT(100,J)
      B(I,2)=X(9,J)
      B(I,3)=X(10,J)
      I=I+1
      GO TO 38
   30 K=IPHOT(100,J)-29
      X(1,K)=X(10,J)
      X(2,K)=X(9,J)
   38 CONTINUE
      GO TO 10
   40 IMAGE=I-1
      IF (IMAGE-3) 1002,50,50
   50 IF (IPLATE-30) 55,55,52
   52 XP=(X(1,1)+X(1,2)+X(1,3)+X(1,4))/4.
      YP=(X(2,1)+X(2,2)+X(2,3)+X(2,4))/4.
   55 DO 57 I=1,IMAGE
      B(I,2)=YP-B(I,2)
      B(I,3)=XP-B(I,3)
   57 CONTINUE
C READ GROUND CONTROL
      DO 100 I=1,IMAGE
      REWIND 9
      K=B(I,1)
   60 J=FFIN(9)
      IF(EOF(9)) GO TO 1004
      IF (K-J) 70,80,70
   70 DO 75 J=1,3
      TRASH=FFIN(9)
```

Figure C-8. Subroutines used with program REMOTE. (Continued)

```
   75 CONTINUE
      GO TO 60
   80 DO 90 J=4,6
      B(I,J)=FFIN(9)
   90 CONTINUE
  100 CONTINUE
C READ INITIAL RARAMETERS FOR CAMERA PHOTO  NO., X,Y,Z IN FT
C AND OMEGA, PHI , KAPPA IN DEGREES
      REWIND 10
      K=(IPLATE-1)/30+1
      GO TO (102,104,106),K
  102 IPLT2=IPLATE
      DEL1=0.
      DEL2=0.
      GO TO 108
  104 IPLT2=IPLATE-30
      DEL1=DELOMG
      DEL2=DELPHI
      GO TO 108
  106 IPLT2=IPLATE-60
      DEL1=DELOMG
      DEL2=DELPHI
  108 IPLT=FFIN(10)
      IF (EOF(10)) GO TO  1006
      IF ((IPLT-IPLT2) 110,120,110
  110 DO 115 I=1,6
      TRASH=FFIN(10)
  115 CONTINUE
      GO TO 108
  120 DO 125 J=1,3
      C(1,J)=FFIN(10)
  125 CONTINUE
      C(2,1)=FFIN(10)/57.2958+DEL1
      C(2,2)=FFIN(10)/57.2958+DEL2
      C(2,3)=FFIN(10)/57.2958
      DO 130 I=1,3
      C(3,I)=COSF(C(2,I))
      C(2,I)=SINF(C(2,I))
  130 CONTINUE
C     ORIENTATION FACTORS IN C ARRAY
  610 C(4,1)=C(3,2)*C(3,3)
      C(5,1)=-C(3,2)*C(2,3)
      C(6,1)=C(2,2)
      C(10,1)=-C(2,2)*C(3,3)
      C(11,1)=C(2,2)*C(2,3)
      C(12,1)=C(3,2)
      C(10,2)=C(4,1)*C(2,1)
      C(11,2)=C(5,1)*C(2,1)
      C(12,2)=C(2,1)*C(2,2)
      C(10,3)=-C(4,1)*C(3,1)
      C(11,3)=-C(5,1)*C(3,1)
      C(12,3)=-C(3,1)*C(2,2)
      C(4,2)=C(3,1)*C(2,3)+C(12,2)*C(3,3)
      C(5,2)=C(3,1)*C(3,3)-C(12,2)*C(2,3)
      C(6,2)=-C(2,1)*C(3,2)
      C(4,3)=C(2,1)*C(2,3)+C(10,1)*C(3,1)
      C(5,3)=C(2,1)*C(3,3)+C(11,1)*C(3,1)
      C(6,3)=C(3,1)*C(3,2)
      DO 612 I=7,9
      C(I,1)=0.
      C(I,2)=-C(I-3,3)
      C(I,3)=C(I-3,2)
      C(13,I-6)=C(5,I-6)
```

Figure C-8. Subroutines used with program REMOTE. (Continued)

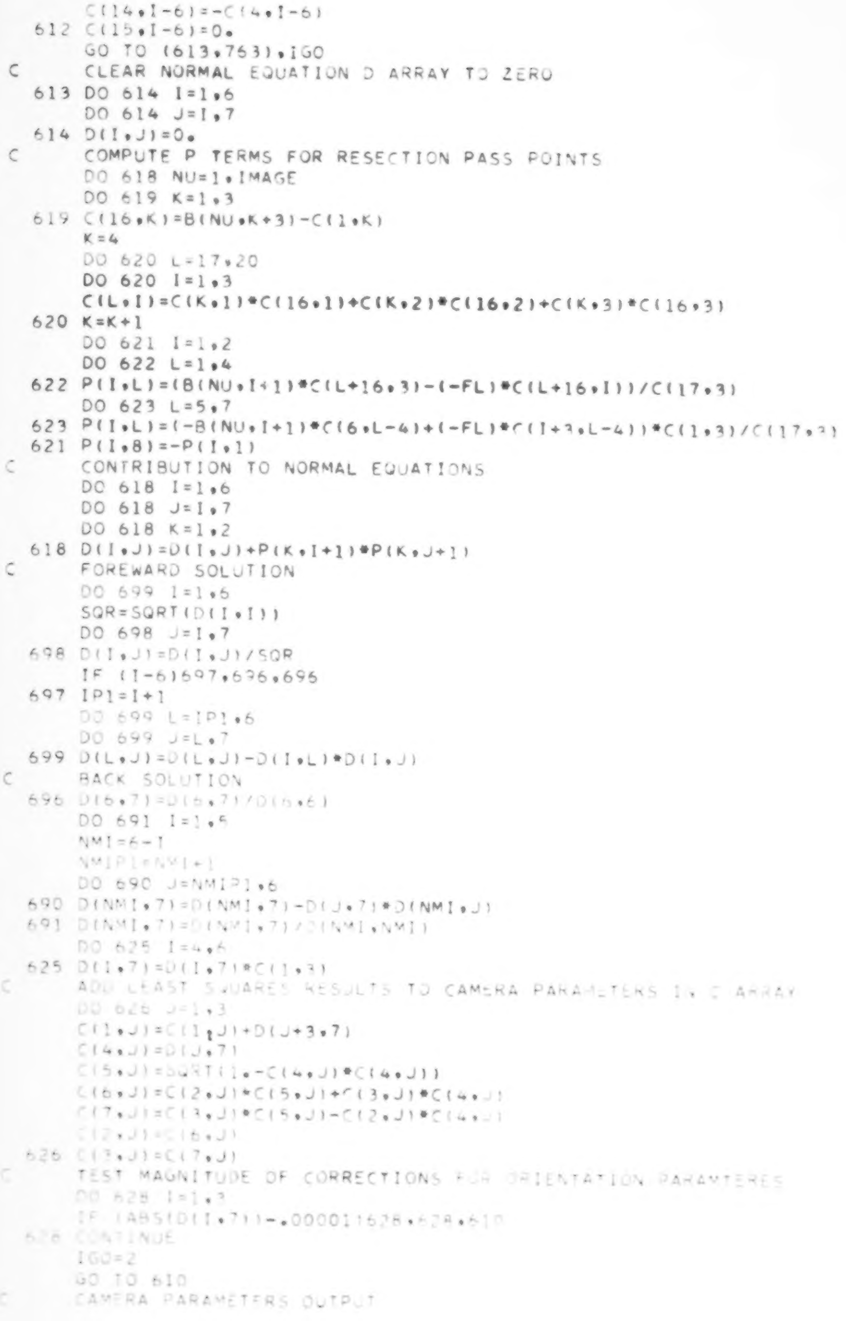

```
      C(14,I-6)=-C(4,I-6)
  612 C(15,I-6)=0.
      GO TO (613,763),IGO
C     CLEAR NORMAL EQUATION D ARRAY TO ZERO
  613 DO 614 I=1,6
      DO 614 J=I,7
  614 D(I,J)=0.
C     COMPUTE P TERMS FOR RESECTION PASS POINTS
      DO 618 NU=1,IMAGE
      DO 619 K=1,3
  619 C(16,K)=B(NU,K+3)-C(1,K)
      K=4
      DO 620 L=17,20
      DO 620 I=1,3
      C(L,I)=C(K,1)*C(16,1)+C(K,2)*C(16,2)+C(K,3)*C(16,3)
  620 K=K+1
      DO 621 I=1,2
      DO 622 L=1,4
  622 P(I,L)=(B(NU,I+1)*C(L+16,3)-(-FL)*C(L+16,I))/C(17,3)
      DO 623 L=5,7
  623 P(I,L)=(-B(NU,I+1)*C(6,L-4)+(-FL)*C(I+3,L-4))*C(1,3)/C(17,3)
  621 P(I,8)=-P(I,1)
C     CONTRIBUTION TO NORMAL EQUATIONS
      DO 618 I=1,6
      DO 618 J=I,7
      DO 618 K=1,2
  618 D(I,J)=D(I,J)+P(K,I+1)*P(K,J+1)
C     FOREWARD SOLUTION
      DO 699 I=1,6
      SQR=SQRT(D(I,I))
      DO 698 J=I,7
  698 D(I,J)=D(I,J)/SQR
      IF (I-6)697,696,696
  697 IP1=I+1
      DO 699 L=IP1,6
      DO 699 J=L,7
  699 D(L,J)=D(L,J)-D(I,L)*D(I,J)
C     BACK SOLUTION
  696 D(6,7)=D(6,7)/D(6,6)
      DO 691 I=1,5
      NMI=6-I
      NMIP1=NMI+1
      DO 690 J=NMIP1,6
  690 D(NMI,7)=D(NMI,7)-D(J,7)*D(NMI,J)
  691 D(NMI,7)=D(NMI,7)/D(NMI,NMI)
      DO 625 I=4,6
  625 D(I,7)=D(I,7)*C(1,3)
C     ADD LEAST SQUARES RESULTS TO CAMERA PARAMETERS IN C ARRAY
      DO 626 J=1,3
      C(1,J)=C(1,J)+D(J+3,7)
      C(4,J)=D(J,7)
      C(5,J)=SQRT(1.-C(4,J)*C(4,J))
      C(6,J)=C(2,J)*C(5,J)+C(3,J)*C(4,J)
      C(7,J)=C(3,J)*C(5,J)-C(2,J)*C(4,J)
      C(2,J)=C(6,J)
  626 C(3,J)=C(7,J)
C     TEST MAGNITUDE OF CORRECTIONS FOR ORIENTATION PARAMTERES
      DO 628 I=1,3
      IF (ABS(D(I,7))-.00001)628,628,610
  628 CONTINUE
      IGO=2
      GO TO 610
C     CAMERA PARAMETERS OUTPUT
```

Figure C-8. Subroutines used with program REMOTE. (Continued)

```
763 WRITE(20,532)
    WRITE(20,527)
    WRITE (20,528) IPLATE,(C(1,J),J=1,3)
    WRITE (20,529)
    WRITE (20,528) IPLATE,(C(2,J),J=1,3)
    WRITE (20,528) IPLATE,(C(3,J),J=1,3)
    WRITE (20,530) IPLATE
    WRITE (20,533) ((C(I,J),J=1,3),I=4,6)
527 FORMAT(/49H PLATE               XO              YO              ZO)
528 FORMAT(I7,3(2X,E14.7))
529 FORMAT(/50H PLATE             OMEGA            PHI             KAPPA)
530 FORMAT(/30H ORIENTATION MATRIX FOR PLATE ,I7)
532 FORMAT(/50H ORIENTATION PARAMETER CORRECTION LIMIT IS 0.00001)
533 FORMAT (1X,3(2X,E14.7))
    DO 710 I=1,3
    CAMO(IPLATE,I)=C(1,I)
    TAN=ATANF(C(2,I)/C(3,I))
    IF (C(3,I)) 702,704,704
702 TAN=3.14159+TAN
704 CAMO(IPLATE,I+3)=TAN
710 CONTINUE
    GO TO (5,1100),IEND
1002 WRITE(20,1003) IPLATE
1003 FORMAT(' INSUFFICIENT CONTROL,PLT',I6)
    GO TO (5,1100),IEND
1004 WRITE (20,1005) K
1005 FORMAT(' GRD CONTROL MISSING',I6)
    GO TO (5,1100),IEND
1006 WRITE (20,1007) IPLATE
1007 FORMAT(' INITIAL PARAMETERS NOT ON FILE',I6)
    GO TO(5,1100),IEND
1100 RETURN
    END
```

Figure C-8. Subroutines used with program REMOTE. (Continued)

```
      SUBROUTINE SUNLITE(TIMFLT,H,AZ)
      DIMENSION H(3).AZ(3),TIMFLT(3)
C      COMPUTE THF ALTITUDE AND AZIMUTH OF THE SUN
C      TIMF IS PACIFIC DAYLIGHT TIMF
C     READ IN DECLINATION OF SUN IN DEGREES (AA).AND MIN (B)
C     AND CHANGE IN MIN PER HOUR (CC). EQUATION OF TIME
C     IN MINUTES (DD). SECONDS (E). AND CHANGE PER HOUR (F)
C     LONGITUDE (WLON) AND LATITUDE (ALAT).
      AA=FFIN(7)
      B=FFIN(7)
      CC=FFIN(7)
      DD=FFIN(7)
      E=FFIN(7)
      F=FFIN(7)
      WLON=FFIN(7)
      ALAT=FFIN(7)
      ALAT=ALAT*3.14159/180.
      APANG=FFIN(7)
      DO 200 I=1.3
      GCT=TIMFLT(I)+7.
      DEC=(AA+(B+CC*GCT)/60.)*3.14159/180.
      EQT=(DD+(E+F*GCT)/60.)/60.
      GHA=(GCT+EQT)*15.0-180.
      TT=GHA-WLON
      TT=TT*3.14159/180.
      T=ABS(TT)
      Z=SINF(T)/(COSF(ALAT)*TANF(DEC)-SINF(ALAT)*COSF(T))
      AZ(I)=ATANF(Z)
      IF (TT) 120.120.123
  120 IF (AZ(I)) 121.121.126
  121 AZ(I)=3.14159+AZ(I)
      GO TO 126
  123 IF (AZ(I)) 124.124.125
  124 AZ(I)=3.14159-AZ(I)
      GO TO 126
  125 AZ(I)=6.28318-AZ(I)
  126 CONTINUE
      SINH=SINF(ALAT)*SINF(DEC)+COSF(ALAT)*COSF(DEC)*COSF(T)
      COSH=SINF(T)*COSF(DEC)/SINF(AZ(I))
      ALT=ABS(SINH/COSH)
      HH=ATANF(ALT)
      REF=((1.+25./60.)/60.)*3.14159/180.
      H(I)=HH+REF
      AZ(I)=AZ(I)-APANG/57.2958
  200 WRITE (20.1) H(I).REF.AZ(I)
    1 FORMAT(11H SUN'S ALT. .F10.6.12H REFRACTION .F10.6.
     1/16H AZIMUTH OF SUN .F10.6)
      RETURN
      END
''
      DEFINE DECLAR
      COMMON X(10.300).IPHOT(120.80).CAMO( 0.6).C(20.3)
      COMMON B(15.6).P(2.8).ANGHB(4).VOLL(2.8)
      END
      DEFINE GRDCOORD
      XG(1)=CAMO(IPLATE.1)-CAMO(IPLATE.3)*XT(1)/XT(3)
      XG(2)=CAMO(IPLATE.2)-CAMO(IPLATE.3)*XT(2)/XT(3)
      END
```

Figure C-8. Subroutines used with program REMOTE. (Continued)

```
      SUBROUTINE TRNCOORD(XP.YP.FL.XT)
      DIMENSION XT(3)
      INCLUDE DECLAR
      DO 10 K=1.3
      XT(K)=C(1.K)*XP+C(2.K)*YP+C(3.K)*(-FL)
   10 CONTINUE
      XDIS=SQRT(XT(1)*XT(1)+XT(2)*XT(2)+XT(3)*XT(3))
      DO 20 K=1.3
      XT(K)=XT(K)/XDIS
   20 CONTINUE
      RETURN
      END
      SUBROUTINE ZEROARRY(NXI.NYI.NXX.NYX.IFRA.KOR)
      INCLUDE DECLAR
      DO 100 I=1.NXI
      DO 100 J=1.NYI
      IPHOT(I.J)=0
  100 CONTINUE
      DO 200 I=1.NXX
      DO 200 J=1.NYX
      X(I.J)=0.0
  200 CONTINUE
      DO 300 I=1.IFRA
      DO 300 J=1.KOR
      CAMO(I.J)=0.0
  300 CONTINUE
      RETURN
      END
      SUBROUTINE ORIMAT(IPLATE)
      INCLUDE DECLAR
      DIMENSION AC(3.3).BC(3.3)
      IF (IPLATE.GT. 30.AND.IPLATE.LE.60) GO TO 100
      IF (IPLATE.GT. 60.AND.IPLATE.LE.90)  GO TO 200
      IGO=1
      K=IPLATE
      GO TO 300
  100 IGO=2
      K=IPLATE-30
      GO TO 300
  200 IGO=3
      K=IPLATE-60
  300 SINW=SINF(CAMO(K.4))
      COSW=COSF(CAMO(K.4))
      SINP=SINF(CAMO(K.5))
      COSP=COSF(CAMO(K.5))
      SINK=SINF(CAMO(K.6))
      COSK=COSF(CAMO(K.6))
      C(1.1)=COSP*COSK
      C(1.2)=COSW*SINK+SINW*SINP*COSK
      C(1.3)=SINW*SINK-COSW*SINP*COSK
      C(2.1)=-COSP*SINK
      C(2.2)=COSW*COSK-SINW*SINP*SINK
      C(2.3)=SINW*COSK+COSW*SINP*SINK
      C(3.1)=SINP
      C(3.2)=-SINW*COSP
      C(3.3)=COSW*COSP
      GO TO (1000.400.500.600).IGO
  400 CAMO(90.4)=ANGHB(1)
      CAMO(90.5)=ANGHB(2)
      CAMO(90.6)=0.0
  410 DO 420 I=1.3
      DO 420 J=1.3
      AC(I.J)=C(I.J)
```

Figure C-8. Subroutines used with program REMOTE. (Continued)

```
  420 CONTINUE
      K=90
      IGO=4
      GO TO 300
  500 CAMO(90,4)=ANGHB(3)
      CAMO(90,5)=ANGHB(4)
      CAMO(90,6)=0.0
      GO TO 410
  600 DO 620 I=1,3
      DO 620 J=1,3
      BC(I,J)=C(I,J)
  620 CONTINUE
      DO 700 I=1,3
      DO 700 J=1,3
      C(I,J)=0.
      DO 700 K=1,3
      C(I,J)=C(I,J)+AC(K,J)*BC(I,K)
  700 CONTINUE
 1000 RETURN
      END
      FUNCTION DIST(XP,YP)
      DIST=SQRT(XP*XP+YP*YP)
      RETURN
      END
      FUNCTION STDDEV(SUM1,SUM2,AJ)
      STDDEV=SQRT((SUM2-SUM1*SUM1/AJ)/(AJ-1.))
      RETURN
      END
      FUNCTION REFLECT(AI,AR)
      A=AI-AR
      B=AI+AR
      C=SINF(A)
      D=SINF(B)
      E=C/COSF(A)
      F=D/COSF(B)
      REFLECT=1.-((E*E)/(F*F)+(C*C)/(D*D))/2.0
      RETURN
      END
      SUBROUTINE INTERP(NXI,NYI,NXS,NYS,KND,KON)
      INCLUDE DECLAR
      DO 540 I=1,NYI
      DO 540 J=1,NXS
      IF (IPHOT(J,I)) 530,540,530
  530 IF (IPHOT(J+1,I)) 540,532,540
  532 DO 534 K=2,KND
      KJ=J+K
      IF (KJ-NXI) 533,533,540
  533 IF (IPHOT(KJ,I)) 536,534,536
  534 CONTINUE
      GO TO 540
  536 LJ=KJ-J-1
      DJ=KJ-J
      DIF=IPHOT(J,I)-IPHOT(KJ,I)
      DO 538 K=1,LJ
      AJ=K
      LLJ=J+K
      IPHOT(LLJ,I)=IPHOT(J,I)-DIF*AJ/DJ
  538 CONTINUE
  540 CONTINUE
      DO 520 I=1,NXI
      DO 520 J=1,NYS
      IF (IPHOT(I,J)) 510,520,510
  510 IF (IPHOT(I,J+1)) 520,512,520
```

Figure C-8. Subroutines used with program REMOTE. (Continued)

```
512 DO 514 K=2,KDN
    KJ=J+K
    IF (KJ-NYI) 513,513,520
513 IF (IPHOT(I,KJ)) 516,514,516
514 CONTINUE
    GO TO 520
516 LJ=KJ-J-1
    DJ=KJ-J
    DIF=IPHOT(I,J)-IPHOT(I,KJ)
    DO 518 K=1,LJ
    AJ=K
    LLJ=J+K
    IPHOT(I,LLJ)=IPHOT(I,J)-DIF*AJ/DJ
518 CONTINUE
520 CONTINUE
    RETURN
    END
    SUBROUTINE AVERAGE(NXS,NYS)
    INCLUDE DECLAR
    ITEST=1
    DO 570 I=1,NXS
    DO 560 J=2,NYS
    GO TO (562,564),ITEST
562 X(1,J)=(IPHOT(I,J)+IPHOT(I,J-1)+IPHOT(I,J+1)+
   1 IPHOT(I+1,J))/4
564 X(2,J)=(IPHOT(I,J)+IPHOT(I+1,J)+IPHOT(I+2,J)+
   1 IPHOT(I+1,J+1)+IPHOT(I+1,J-1))/5
560 CONTINUE
    ITEST=2
    DO 565 J=2,NYS
    IPHOT(I,J)=X(1,J)
    X(1,J)=X(2,J)
565 CONTINUE
570 CONTINUE
    RETURN
    END
    SUBROUTINE CULL(NXI,NYI)
    INCLUDE DECLAR
    BJ=9.
    IX=NXI-2
    IY=NYI-2
    DO 100 I=1,IX
    DO 100 J=1,IY
    SUM1=0.0
    SUM2=0.0
    DO 20 IK=1,3
    DO 20 JK=1,3
    IP=I+IK-1
    JP=J+JK-1
    AI=IPHOT(IP,JP)
    SUM1=SUM1+AI
    SUM2=SUM2+AI*AI
 20 CONTINUE
    SUM2=STDDEV(SUM1,SUM2,BJ)
    AI=SUM1/BJ
    BI=IPHOT(I+1,J+1)
    CI=(SUM1-BI)/(BJ-1.)
    SUM1=AI-SUM2
    SUM2=AI+SUM2
    IF(BI.LT.SUM1.OR.BI.GT.SUM2) IPHOT(I+1,J+1)=CI
100 CONTINUE
    RETURN
    END
```

Figure C-8. Subroutines used with program REMOTE. (Continued)

```
0
 8.8
15 15
15 21
15 50
9000

 22
31.63
-0.285
-4
-51.6
-0.39
124.0667
46.64
-2.53
-1.3 0.0 0.252
-1.3 0.0 0.331
-1.3 0.0 0.619
-1.7 1.0 0.187
-2.1 0.4 0.252
-1.3 0.4 0.331
0.82 -0.9 .252
0.91 -0.9 .187
200 6.3
200 6.3
200 6.3
250 5.6
250 5.6
250 5.6
250 5.6
250 5.6
250 5.6
0.163 -0.005
0.188 -0.005
0.272 -0.003
0.143 -0.005
0.163 -0.005
0.188 -0.005
0.163 -0.005
0.143 -0.005
1
```

LUN 7

```
80711 000 04240 03335 0000  001 03901 04321 0000  004 07136 03545 0000
80711 010 05225 01200 0000  011 02211 01241 0000  021 04219 04272 0000
80711 030 02664 04823 0000  031 02640 02882 0000  032 08031 02844 0000
80711 033 08023 06454 0000  034 03350 04044 0000  035 08030 04776 0000
80721 000 04241 03405 0000  001 03825 04424 0000  004 06331 03982 0000
80721 010 05156 01841 0000  011 02603 01699 0000  021 04513 04413 0000
80721 030 03348 04720 0000  031 03320 03101 0000  032 08246 03220 0000
80721 033 08277 06745 0000
80722 000 04205 03435 0000  001 01505 04312 0000  004 04137 03882 0000
80722 009 06913 01616 0000  010 03629 01917 0000  011 01234 01801 0000
80731 000 04241 03435 0000  001 03918 04540 0000  004 04434 03928 0000
80731 009 08528 01352 0000  010 05080 01868 0000  011 02545 01903 0000
80731 021 05631 04356 0000  030 03227 04908 0000  031 03237 03081 0000
80731 032 08065 03121 0000  033 08079 04326 0000
80732 000 04240 03392 0000  001 02314 04088 0000  004 04319 03598 0000
80732 009 07481 01214 0000  010 04071 01648 0000  011 01440 01627 0000
80733 000 04240 03403 0000  001 00940 03934 0000  004 03419 03514 0000
80733 009 04461 01291 0000  010 03149 01471 0000  011 00845 01635 0000
80751 001 01126 04512 0000  021 01785 04501 0000  030 00534 05535 0000
80751 031 00507 03368 0000  032 02647 03345 0000  033 02447 05528 0000
80752 004 01458 01455 0000  030 00512 03032 0000  031 00543 00961 0000
80752 032 02661 00840 0000  033 02642 03005 0000
80761 001 03198 06472 0000  030 02499 07411 0000  031 02472 05238 0000
80761 032 04639 05202 0000  033 04641 07385 0000
80762 004 04040 03091 0000  021 03176 03451 0000  030 02444 04930 0000
80762 031 02434 02753 0000  032 04601 02704 0000  033 04430 04868 0000
80763 004 02623 00566 0000  030 02431 02495 0000  031 02414 00321 0000
80763 032 04577 00275 0000  033 04602 02437 0000
80791 001 03241 06329 0000  030 02502 07273 0000  031 02514 05104 0000
80791 032 04679 05091 0000  033 04680 07257 0000
80792 004 04123 02991 0000  021 03239 03339 0000  030 02516 04914 0000
80792 031 02504 02640 0000  032 04649 02617 0000  033 04478 04797 0000
80793 004 02716 00381 0000  030 02507 02320 0000  031 02437 00146 0000
80793 032 04449 00133 0000  033 04642 02291 0000
```

LUN 8

```
 1 1069310 375760 0.0
 4 1069540 373540 0.0
 9 1072951 369571 130
10 1072949 373966 42
11 1073606 377145 75
```

LUN 9

```
 1 1066500 375800 3000 0 -45 0
11 1066500 375000 4000 0 -45 0
12 1066000 373500 4000 0 -45 0
21 1066500 375800 3000 0 -45 0
22 1066500 374000 3000 0 -45 0
23 1066500 372000 3000 0 -45 0
```

LUN 10

Figure C-9. Sample input data for REMOTE.

## APPENDIX D

## PROCESSING OF 1970-71 PHOTOGRAPHIC DATA

A general description of the CDC 3300 Computer and special fortran input functions is given in the introduction of Appendix B.

The program used for processing the data collected in 1970 and 1971 was program INSHORE. The program delineates the plume outline from coordinates measured from the aerial photography and determines the area of the waste field. The direction and velocity of the current and the diffusion coefficients are determined from the dye patch. In the process, state plane coordinates of the points around the plume were computed, and these were saved for later plotting on the Tektronix graphicscope. See figure D-1 for a flow diagram of program INSHORE. The numbers in parentheses on the flow diagram correspond to line numbers on the program listing in figure D-2.

### Program

Program INSHORE first orients the photo found on LUN 8 by calling RESECT2, a version of the subroutine RESECT used in processing the data in 1968 and 1969. After the orientation is completed, the coordinates of the points on the photograph are read in, and the state plane coordinates of each point are computed. As this is done, the data is sorted according to the event number so that it is known whether the point is a plume point, a point in the foam or kelp, a dye patch point, or a point representing the apparent position of the outfall.

If the point is on the plume, a code number is assigned to indicate that a continuous line is to be drawn from the previous point when the data is plotted. Therefore, IDO is set to equal 1. If the point is the first point, a line from the origin to that point is not desired, and IPEN = 0. For all other plume points, the line is required and IPEN = 1. When the last plume point is reached, the area of the plume is computed by calling subroutine SECPROP. The area is converted to acres, and is stored for later print out. As each point is assigned the proper code, the code and the coordinate are written on LUN 23.

The points indicating the foam, kelp, and the outfall are coded separately, and are also written out with their respective coordinates and codes.

The dye points are read, and as the last point is reached, section properties needed for the computation of diffusion coefficients are calculated. This is also done by subroutine SECPROP.

After the end of file has been reached on LUN 8, the time elapsed between flights is typed in. If there are two photos on file, the current velocity and direccion are computed, using section properties of the dye patch. A current vector is then generated, and the coordinates needed to plot the vector are written on LUN 23.

Diffusion coefficients are then computed and all of the general information is written on LUN 20.

Normally the data on LUN 23 is saved to be used as input for the plotting program. The data on LUN 20 is sent to the line printer and is used for reference purposes.

## Input Description

The input on LUN 8 consists of photo coordinates, with the format being the same as in the previous year (see Appendix C, figure C-8). As shown below, the event number coding differs from that listed in Appendix C.

| Event No. | Description |
|---|---|
| 000 | Principal point. |
| 001-019 | Ground control. |
| 100-498 | Plume points. |
| 499 | Last plume point (always). |
| 500-599 | Foam points. |
| 600-699 | Kelp points. |
| 700-898 | Dye patch points. |
| 899 | Last dye patch point (always). |
| 999 | Outfall. |

It should be noted that the control point numbers must correspond to the ground control numbers on LUN 9.

Data on LUNS 8 and 9 are exactly the same as listed in Appendix C. The data on LUN 9 is ground control, listing the point number, the x and y coordinates and the elevation above mean sea level. LUN 10 contains the initial orientation parameters for the camera station, and are arranged as follows: photo number, x and y coordinates, state plane coordinates, flying height, omega, phi and kappa rotation angles in degrees.

## Output Description

The major output is a listing of coordinates for each point which is to be plotted, along with a title for the plot. This is all written on LUN 23, and saved for later plotting. General information such as orientation for the photo, dye patch centroids, date, area of plume, current velocity, and diffusion coefficients are written on LUN 20, and are not saved except as hard copy. The area of the plume and date are also written on the teletype so that the operator may have a check to see if the program is operating correctly.

## Plotting of Data

The data is plotted using a program which utilizes the Tektronix T-4002 slope. A grid is drawn and the axes are labeled. The data is then plotted and the plot labeled. A polaroid photograph is taken of the plot for a permanent record. Examples of these plots are shown in Section X.

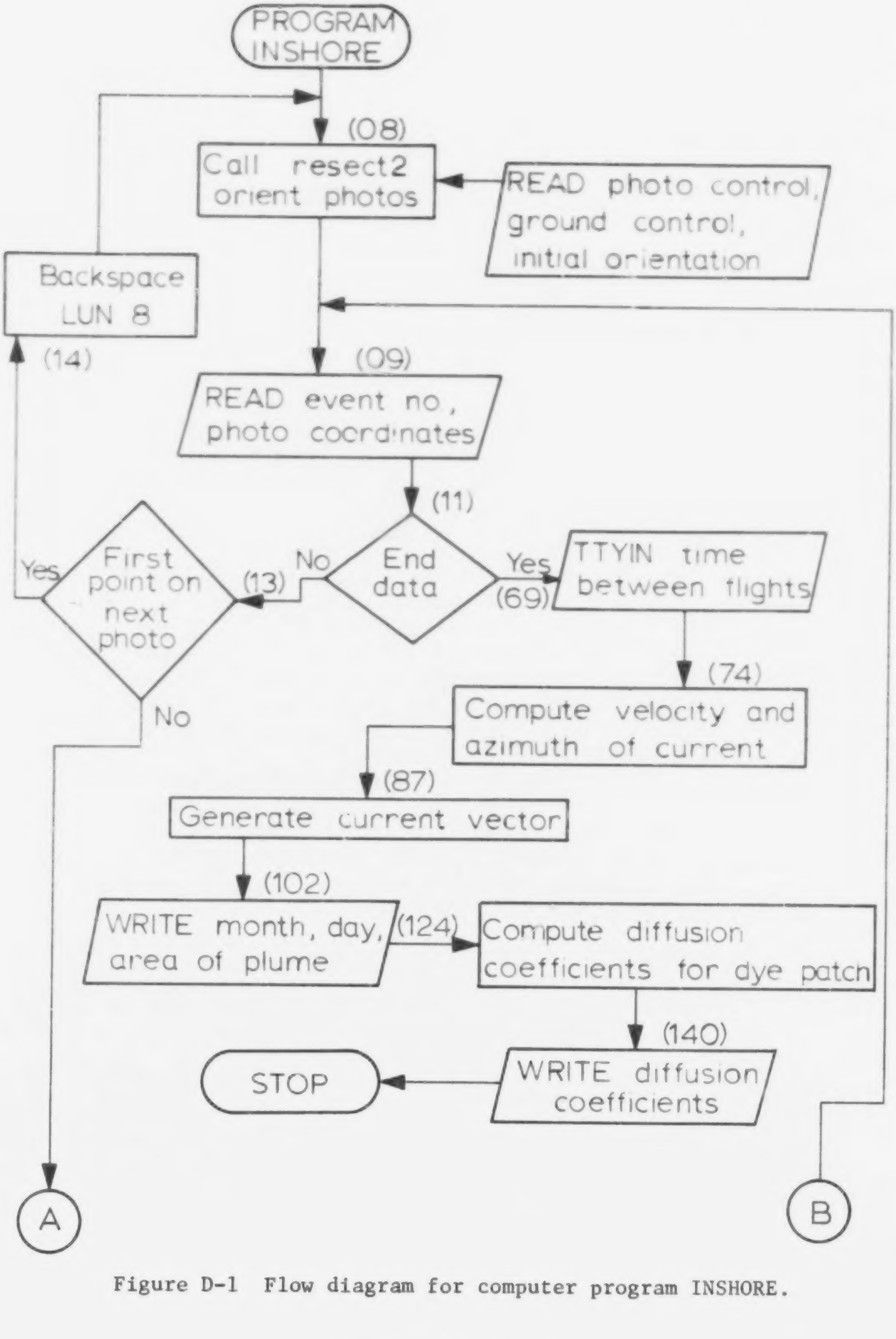
PROGRAM INSHORE
(08)
Call resect2 orient photos
READ photo control, ground control, initial orientation
Backspace LUN 8
(14)
(09)
READ event no., photo coordinates
(11)
End data
Yes
(69)
No
(13)
First point on next photo
Yes
No
TTYIN time between flights
(74)
Compute velocity and azimuth of current
(87)
Generate current vector
(102)
WRITE month, day, area of plume
(124)
Compute diffusion coefficients for dye patch
(140)
WRITE diffusion coefficients
STOP
A
B

Figure D-1 Flow diagram for computer program INSHORE.

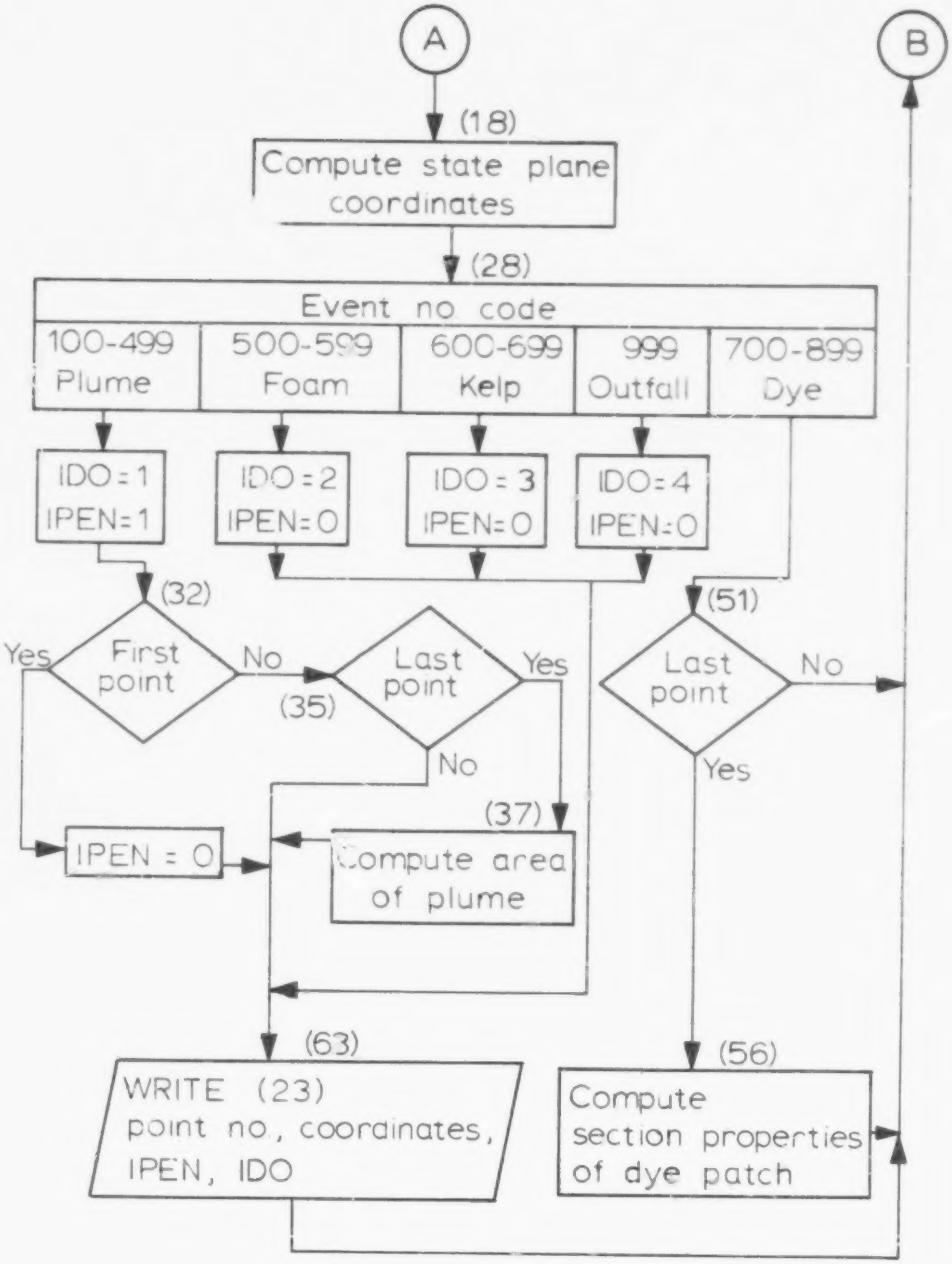

Figure D-1. Flow diagram for computer program INSHORE.

```
      PROGRAM SHORE
      COMMON C(20,3),IP(3),XF(3),YF(3)
      DIMENSION XPL(200,2),XO(200,2),XT(3),DYE(15,2,6),VEL(15),AZI(15)
      LFLT=1
      INO=1
      IFLAG=1
      ICHECK=1
  100 CALL RESECT2(FL,XP,YP)
  110 READ(9,1)IPLATE,(IP(J),XF(J),YF(J),J=1,3)
    1 FORMAT(4X,I1,3(I4,2F6.3,6X))
      IF(EOF(8)) GO TO 1000
      IF(IP(1).GT.99) GO TO 10
      IF(XF(1).LT.0.001) GO TO 110
      BACKSPACE 8
      GO TO 100
   10 DO 200 J=1,3
      IF(IP(J).EQ.0.AND.XF(J).EQ.0.) GO TO 110
      X1=YP-YF(J)
      Y1=XP-XF(J)
      DO 210 K=1,3
  210 XT(K)=C(4,K)*X1+C(5,K)*Y1+C(6,K)*(-FL)
      XDIS=SQRT(XT(1)*XT(1)+XT(2)*XT(2)+XT(3)*XT(3))
      DO 220 K=1,3
  220 XT(K)=XT(K)/XDIS
      XPG1=C(1,1)-XT(1)*C(1,3)/XT(3)
      XPG2=C(1,2)-XT(2)*C(1,3)/XT(3)
      IGO=IP(J)/100
      GO TO (20,20,20,20,30,40,50,50,60) IGO
   20 XPL(INO,1)=XPG1
      XPL(INO,2)=XPG2
      IPEN=1
      IF(INO.EQ.1) IPEN=0
      IDO=1
      INO=INO+1
      IF(IP(J).NE.499) GO TO 300
      N=INO-1
      CALL SECPROP(XPL,N,15,1,DYE)
      PAREA=DYE(15,1,3)
      AC=PAREA/43560.
      INO=1
      GO TO 300
   30 IDO=2
      IPEN=0
      GO TO 300
   40 IDO=3
      IPEN=0
      GO TO 300
   50 XO(IFLAG,1)=XPG1
      XO(IFLAG,2)=XPG2
      IFLAG=IFLAG+1
      IF(IP(J).NE.899) GO TO 200
      N=IFLAG-1
      IFLT=1
      IF(IPLATE.GT.5) IFLT=2
      IF(IFLT.NE.LFLT) ICHECK =1
      CALL SECPROP(XO,N,ICHECK,IFLT,DYE)
      LFLT=IFLT
      IFLAG=1
      ICHECK=ICHECK+1
      GO TO 200
   60 IPEN=0
```

Figure D-2. Listing of program INSHORE.

```
      IDO=4
  300 WRITE(23,2)IP(J),XPG1,XPG2,IPEN,IDO
    2 FORMAT(X,I5,2F10.0,2I5)
  200 CONTINUE
      GO TO 110
 1000 WRITE(61,3)
    3 FORMAT(* TIME ELAPSED IN MINUTES*)
      TIME=TTYIN(4HTIME)
      TIME=TIME*60.
      ICOUNT=ICHECK-1
      SUMVE=0.0
      VELNO=0.0
      DO 400 I=1,ICOUNT
      XDIST=(DYE(I,2,1)-DYE(I,1,1))
      YDIST=(DYE(I,2,2)-DYE(I,1,2))
      AZI(I)=ATAN(XDIST/YDIST)
      IF(YDIST.LT.0.) AZI(I)=AZI(I)+3.14159
      IF(AZI(I).LT.0.) AZI(I)=AZI(I)+6.28318
      XDIST=SQRT(XDIST*XDIST+YDIST*YDIST)
      IF(XDIST.GT.50.) GO TO 370
      VEL(I)=0.0
      GO TO 390
  370 IF(XDIST.LT.5000.) GO TO 380
      GO TO 400
  380 VEL(I)=XDIST/TIME
      CALL ARROW(VEL(I),DYE(I,1,1),DYE(I,1,2),AZI(I))
      SUMVE=SUMVE+VEL(I)
  390 VELNO=VELNO+1.
  400 CONTINUE
      REWIND 8
      VELM=0.0
      IF(VELNO.GT.0.1) VELM=SUMVE/VELNO
      READ(8,4) MO,IDAY
    4 FORMAT(2I2)
      WRITE(61,5)
    5 FORMAT(* TYPE IN YEAR IN WHICH PHOTO WAS TAKEN*)
      IYR=TTYIN(4HYR= )
      WRITE(61,6)
    6 FORMAT(* PLUME DATA*)
      WRITE(20,6)
      WRITE(20,7) MO,IDAY,PAREA,AC
      WRITE(61,7) MO,IDAY,PAREA,AC
    7 FORMAT(* MONTH*,I4,/* DAY*,I6,/* AREA* ,E11.3,* SQ. FT.*,/
     1* AREA*,F6.1,* ACRES*)
      IF(VELNO.GT.0.1) GO TO 410
      WRITE (23,8)AC,MO,IDAY ,IYR
    8 FORMAT(*            AREA OF PLUME*, F6.1,* ACRES*,20X,2(I2,*/*),I2)
      GO TO 420
  410 WRITE(23,14)AC,VELM,MO,IDAY,IYR
   14 FORMAT(*          AREA OF PLUME*,F6.1,* ACRES*,
     1*    VELOCITY*,F5.2,* FPS    *,   2(I2,*/*),I2)
  420 END FILE 23
      WRITE(20,9)
    9 FORMAT(* DYE PATCH DATA*)
      WRITE(20,12)(I,((DYE(I,J,K),K=1,3),J=1,2),VEL(I),AZI(I),
     5I=1,ICOUNT)
   12 FORMAT(* NO*,I2,/* XCENTROID-1*,F10.0,/* YCENTROID-1*,F10.0,/
     C* AREA-1*,F15.2,/* XCENTROID-2*,F10.0,/* YCENTROID-2*,F10.0,/
     C* AREA-2*,F15.2,/* VELOCITY*,F13.2,*FPS*,/* AZIMUTH*
     C*FROM NORTH*,F8.5,*RADIANS*)
      WRITE(20,13) TIME,VELM
   13 FORMAT(* TIME FOR VEL.*,F6.0,/* VELOCITY= *,F5.2)
```

Figure D-2. Listing of program INSHORE. (Continued)

```
      DO 430 I=1,ICOUNT
      RATIO=SQRT(DYE(I,1,4)/DYE(I,1,5))
      RAT2=DYE(I,1,3)/3.14159
      ASQ1=RAT2*RATIO
      BSQ1=RAT2/RATIO
      RATIO=SQRT(DYE(I,2,4)/DYE(I,2,5))
      RAT2=DYE(I,2,3)/3.14159
      ASQ2=RAT2*RATIO
      BSQ2=RAT2/RATIO
      RTA1=SQRT(ASQ1)
      RTA2=SQRT(ASQ2)
      RTB1=SQRT(BSQ1)
      RTB2=SQRT(BSQ2)
      DIV=1.386*TIME*2.
      DX=(ASQ2-ASQ1)/DIV
      DY=(BSQ2-BSQ1)/DIV
  430 WRITE(20,15) DX,DY,RTA1,RTA2,RTB1,RTB2
   15 FORMAT(////*    D I F F U S I O N     S T U D Y*/
     1*      DX= *,F10.2,*  FT SQ / SEC*/
     2*      DY= *,F10.2,*  FT SQ / SEC*/
     3* A1=*,F6.0,*,    A2=*,F6.0,*,      B1=*,F6.0,*,    B2=*,F6.0)
      END FILE 20
      STOP
      END
      SUBROUTINE ARROW(SCAF,XDYE,YDYE,BZI)
      COMMON/DATA/A
      DIMENSION A(10,2)
      DATA(((A(I,J),I=1,10),J=1,2)=0.,0.,30.,100.,30.,0.,-30.,
     1-100.,-30.,0.,0.,1000.,900.,800.,900.,1000.,900.,800.,900.,
     21000.)
      AZI=-BZI
      S=SIN(AZI)
      C=COS(AZI)
      IDD=1
      DO 10 J=1,2
      DO 10 I=1,10
   10 A(I,J)=A(I,J)*SCAF
      IPEN=3
      DO 20 I=1,10
      Y=YDYE+A(I,2)*C+A(I,1)*S
      X=XDYE-A(I,2)*S+A(I,1)*C
      IF(I.NE.1)IPEN=2
   20 WRITE(23,1)X,Y,IPEN,IDD
    1 FORMAT(6X,2F10.0,2I5)
      RETURN
      END
      SUBROUTINE SECPROP(X,N,NO,IFLT,DYE)
C.....PROGRAMMED MARCH 1971
C.....X&Y= COORDS OF POINTS DEFINING CLOCKWISE PATH AROUND
C.....BOUNDARY, N=NUMBER OF POINTS, CLOSURE FROM PT N TO PT 1
C.....IS AUTOMATIC (POINT 1 IS READ IN ONLY ONCE).
C.....IGX,IGY,IGXY ARE ABOUT CENTROIDAL AXES PARALLEL TO X&Y.
C.....THETA IS CLOCKWISE ANGLE FROM X AXIS TO MAJOR PRINC AXIS.
      REAL IX,IY,IXY,IGX,IGY,IGXY,IMAX,IMIN
      DIMENSION X(200,2),DYE(15,2,5)
      XLOW=X(1,1)
      YLOW=X(1,2)
      DO 10 I=1,N
      X(I,1)=X(I,1)-XLOW
      X(I,2)=X(I,2)-YLOW
   10 CONTINUE
      XI=X(N,1)
```

Figure D-2. Listing of program INSHORE. (Continued)

```
      XM=X(1,1)
      XMSQ=XM*XM
      T2X=XI+XM
      YI=X(N,2)
      YM=X(1,2)
      YMSQ=YM*YM
      T2Y=YI+YM
      A=AXBAR=AYBAR=IX=IY=IXY=0.
      DO 3 I=1,N
      IF(I.NE.N)GO TO 1
      M=1
      GO TO 2
    1 M=I+1
    2 XL=XI
      XI=XM
      XM=X(M,1)
C.....XL=X(I-1), XI=X(I), XM=X(I+1), Y'S SIMILAR.
      T1X=T2X
      T2X=XI+XM
      T3X=XM-XI
      XISQ=XMSQ
      XMSQ=XM*XM
      YL=YI
      YI=YM
      YM=X(M,2)
      T1Y=T2Y
      T2Y=YI+YM
      T3Y=YM-YI
      YISQ=YMSQ
      YMSQ=YM*YM
      A=A+XI*(YL-YM)
C.....ACCUMULATE 2*A, 6*A*XBAR, 12*IX, 72*IXY, ETC.
      AXBAR=AXBAR-YI*(XL*T1X-XM*T2X)
      AYBAR=AYBAR+XI*(YL*T1Y-YM*T2Y)
      IX=IX+T3X*(YISQ+YMSQ)*T2Y
      IY=IY-T3Y*(XISQ+XMSQ)*T2X
    3 IXY=IXY-T3Y*(18.*XISQ*T2Y+T3X*(T3X*T3Y+6.*(2.*XI+XM)*(YI+2.*YM)))
      A=A*.5
      AXBAR=AXBAR/6.
      AYBAR=AYBAR/6.
      XBAR=AXBAR/A
      YBAR=AYBAR/A
      IX=IX/12.
      IY=IY/12.
      IXY=IXY/72.
C.....TRANSFER TO CENTROIDAL AXES.
      IGX=IX-AYBAR*YBAR
      IGY=IY-AXBAR*XBAR
      IGXY=IXY-AXBAR*YBAR
      T1=(IGX-IGY)*.5
      T2=(IGX+IGY)*.5
      T3=SQRT(T1*T1+IGXY*IGXY)
C.....COMPUTE PRINC MOMENTS OF INERTIA AND ORIENTATION OF
C.....PRINC AXES.
      IF(T1.LT.0.)T3=-T3
      IMAX=T2+T3
      IMIN=T2-T3
      THETA=28.6479*ATAN(IGXY/T1)
      IF(T1.LT.0.)THETA=THETA+90.
      DYE(40,IFLT,1)=XBAR+XLOW
      DYE(40,IFLT,2)=YBAR+YLOW
      DYE(40,IFLT,3)=ABS(A)
```

Figure D-2. Listing of program INSHORE. (Continued)

```
      DYE(NO,IFLT,4)=ABS(IMAX)
      DYE(NO,IFLT,5)=ABS(IMIN)
      DYE(NO,IFLT,6)=THETA
      WRITE(20,6) IX,IY,IGX,IGY,IXY,IGXY,T1,T2,T3
    6 FORMAT(E13.4)
      WRITE(20,5)(NO,IFLT,I,DYE(NO,IFLT,I),I=1,6)
    5 FORMAT(#    DYE(#,I2,I2,I2,#)=#,F18.2)
      RETURN
      END
      SUBROUTINE RESECT2 (FL,XP,YP)
      COMMON C(20,3), IP(3), XF(3), YF(3)
      DIMENSION B(15,6), P(2,5), D(6,7)
C     INPUT LUNS ARE:
C        8  PHOTO COORDINATES
C        9  GROUND CONTROL
C       10  INITIAL ORIENTATION PARAMETERS
C     OUTPUT DATA ON LUN 20
      FL=6.0
      IGO=0
      I=1
C     READ PHOTO CONTROL COORDINATES
   10 READ(8,1)IPLATE,(IP(J), XF(J), YF(J), J=1,3)
    1 FORMAT(4X,I1,3(I4,2F6.3,6X))
      IF (IP(1) .LT. 20) GO TO 25
      BACKSPACE 8
      GO TO 40
   25 DO 38 J=1,3
      IF(IP(J) .EQ. 0 .AND. XF(J) .GT. 0.001) GO TO 26
      IF(IP(J) .EQ. 0) GO TO 38
      GO TO 28
   26 XP=XF(J)
      YP=YF(J)
      GO TO 38
   28 B(I,1)=IP(J)
      B(I,2)=YF(J)
      B(I,3)=XF(J)
      I=I+1
   38 CONTINUE
      GO TO 10
   40 IMAGE = I-1
      IF(IMAGE.LT.3)GO TO 1002
      DO 57 I=1,IMAGE
      B(I,2)=YP-B(I,2)
      B(I,3)=XP-B(I,3)
   57 CONTINUE
C READ GROUND CONTROL
      DO 100 I=1,IMAGE
      REWIND 9
      K=B(I,1)
   60 J=FFIN(9)
      IF(EOF(9)) GO TO 1004
      IF (K-J) 70,80,70
   70 DO 75 J=1,3
      TRASH=FFIN(9)
   75 CONTINUE
      GO TO 60
   80 DO 90 J=4,6
      B(I,J)=FFIN(9)
   90 CONTINUE
  100 CONTINUE
C READ INITIAL PARAMETERS FOR CAMERA PHOTO  NO., X,Y,Z IN FT
C AND OMEGA, PHI , KAPPA IN DEGREES
```

Figure D-2. Listing of program INSHORE. (Continued)

```
      REWIND 10
  108 IPLT=FFIN(10)
      IF (EOF(10)) GO TO  1006
      IF (IPLT-IPLATE) 110,120,110
  110 DO 115 I=1,6
      TRASH=FFIN(10)
  115 CONTINUE
      GO TO 108
  120 DO 125 J=1,3
      C(1,J)=FFIN(10)
  125 CONTINUE
      C(2,1)=FFIN(10)/57.2958
      C(2,2)=FFIN(10)/57.2958
      C(2,3)=FFIN(10)/57.2958
      DO 130 I=1,3
      C(3,I)=COSF(C(2,I))
      C(2,I)=SINF(C(2,I))
  130 CONTINUE
C     ORIENTATION FACTORS IN C ARRAY
  610 C(4,1)=C(3,2)*C(3,3)
      C(5,1)=-C(3,2)*C(2,3)
      C(6,1)=C(2,2)
      C(10,1)=-C(2,2)*C(3,3)
      C(11,1)=C(2,2)*C(2,3)
      C(12,1)=C(3,2)
      C(10,2)=C(4,1)*C(2,1)
      C(11,2)=C(5,1)*C(2,1)
      C(12,2)=C(2,1)*C(2,2)
      C(10,3)=-C(4,1)*C(3,1)
      C(11,3)=-C(5,1)*C(3,1)
      C(12,3)=-C(3,1)*C(2,2)
      C(4,2)=C(3,1)*C(2,3)+C(12,2)*C(3,3)
      C(5,2)=C(3,1)*C(3,3)-C(12,2)*C(2,3)
      C(6,2)=-C(2,1)*C(3,2)
      C(4,3)=C(2,1)*C(2,3)+C(10,1)*C(3,1)
      C(5,3)=C(2,1)*C(3,3)+C(11,1)*C(3,1)
      C(6,3)=C(3,1)*C(3,2)
      DO 612 I=7,9
      C(I,1)=0.
      C(I,2)=-C(I-3,3)
      C(I,3)=C(I-3,2)
      C(13,I-6)=C(5,I-6)
      C(14,I-6)=-C(4,I-6)
  612 C(15,I-6)=0.
      GO TO (613,763),IGO
C     CLEAR NORMAL EQUATION D ARRAY TO ZERO
  613 DO 614 I=1,6
      DO 614 J=I,7
  614 D(I,J)=0.
C     COMPUTE P TERMS FOR RESECTION PASS POINTS
      DO 618 NU=1,IMAGE
      DO 619 K=1,3
  619 C(16,K)=B(NU,K+3)-C(1,K)
      K=6
      DO 620 L=17,20
      DO 620 I=1,3
      C(L,I)=C(K,1)*C(16,1)+C(K,2)*C(16,2)+C(K,3)*C(16,3)
  620 K=K+1
      DO 621 I=1,2
      DO 621 L=1,4
  621 P(I,L)=(B(NU,I+1)*C(L+16,3)-(-FL)*C(L+16,I))/C(17,3)
      DO 623 L=5,7
```

Figure D-2. Listing of program INSHORE. (Continued)

```
  623 P(I,L)=(-B(NU,I+1)*C(6,L-4)+(-FL)*C(I+3,L-4))*C(1,3)/C(17,3)
  621 P(I,3)=-P(I,1)
C     CONTRIBUTION TO NORMAL EQUATIONS
      DO 618 I=1,6
      DO 618 J=I,7
      DO 618 K=1,2
  618 D(I,J)=D(I,J)+P(K,I+1)*P(K,J+1)
C     FOREWARD SOLUTION
      DO 699 I=1,6
      SQR=SQRT(D(I,I))
      DO 698 J=I,7
  698 D(I,J)=D(I,J)/SQR
      IF (I-6)697,696,696
  697 IP1=I+1
      DO 699 L=IP1,6
      DO 699 J=L,7
  699 D(L,J)=D(L,J)-D(I,L)*D(I,J)
C     BACK SOLUTION
  696 D(6,7)=D(6,7)/D(6,6)
      DO 691 I=1,5
      NMI=6-I
      NMIP1=NMI+1
      DO 690 J=NMIP1,6
  690 D(NMI,7)=D(NMI,7)-D(J,7)*D(NMI,J)
  691 D(NMI,7)=D(NMI,7)/D(NMI,NMI)
      DO 625 I=4,6
  625 D(I,7)=D(I,7)*C(1,3)
C     ADD LEAST SQUARES RESULTS TO CAMERA PARAMETERS IN C ARRAY
      DO 626 J=1,3
      C(1,J)=C(1,J)+D(J+3,7)
      C(4,J)=D(J,7)
      C(5,J)=SQRT(1.-C(4,J)*C(4,J))
      C(6,J)=C(2,J)*C(5,J)+C(3,J)*C(4,J)
      C(7,J)=C(3,J)*C(5,J)-C(2,J)*C(4,J)
      C(2,J)=C(6,J)
  626 C(3,J)=C(7,J)
C     TEST MAGNITUDE OF CORRECTIONS FOR ORIENTATION PARAMTERES
      DO 628 I=1,3
      IF (ABS(D(I,7))-.00001)628,628,610
  628 CONTINUE
      IGO=2
      GO TO 610
C     CAMERA PARAMETERS OUTPUT
  763 WRITE(20,532)
      WRITE(20,527)
      WRITE (20,528) IPLATE,(C(1,J),J=1,3)
      WRITE (20,529)
      WRITE (20,528) IPLATE,(C(2,J),J=1,3)
      WRITE (20,528) IPLATE,(C(3,J),J=1,3)
      WRITE (20,530) IPLATE
      WRITE (20,533) ((C(I,J),J=1,3),I=4,6)
  527 FORMAT(/49H PLATE                XO                YO                ZO)
  528 FORMAT(I7,3(2X,E14.7))
  529 FORMAT(/59H PLATE              OMEGA             PHI               KAPPA)
  530 FORMAT(/30H ORIENTATION MATRIX FOR PLATE ,I7)
  532 FORMAT(/59H ORIENTATION PARAMETER CORRECTION LIMIT IS 0.00001)
  533 FORMAT (1X,3(2X,E14.7))
      GO TO 1100
 1002 WRITE(20,1003) IPLATE
 1003 FORMAT(≠ INSUFFICIENT CONTROL,PLT≠,I6)
      GO TO 1100
 1004 WRITE (20,1005) K
 1005 FORMAT(≠ GRD CONTROL MISSING≠,I6)
      GO TO 1100
 1006 WRITE (20,1007) IPLATE
 1007 FORMAT(≠ INITIAL PARAMETERS NOT ON FILE≠,I6)
      GO TO 1100
 1100 RETURN
      END
```

Figure D-2. Listing of program INSHORE. (Continued)

# APPENDIX E

## Streamlines For A Source In A Uniform Flow

A general description of the CDC 3300 Computer and special fortran input functions is given in the introduction of Appendix B.

Program FLOWNET was used for generating the coordinates for plotting a flownet for a line source oriented perpendicular to a uniform stream. The program used the equation:

$$\psi = -UY + \alpha \left[ \left(Y + \frac{b}{2}\right) \theta_1 - \left(Y - \frac{b}{2}\right) \theta_2 - X \ln \frac{r_1}{r_2}) \right]$$

which was derived in Section XI as equation 112.

The variables in the equation correspond to those shown in figure 96.

A flow diagram for program FLOWNET is shown in figure E-1 and the numbers in parentheses correspond to line numbers in the program listing of figure E-2.

### Program

Program FLOWNET requires that the velocity and azimuth from the north of the uniform flow, as well as the flow rate, estimated dilution over the outfall, the depth of the waste field and the length of the diffuser section be typed in. The maximum value of $\psi$ is then computed and the y coordinate for a point 6000 ft downstream on the outermost streamline is determined. Using this as a starting point, the coordinates for successive points along one half of a stream line are computed by incrementing $\theta$ and checking the new y value against the estimated value of y. After one side of a streamline is generated, the coordinates are rotated and the mirror image is computed. These are written on LUN 2 and the process is repeated for the next streamline until three streamlines and the centerline are computed.

The data on LUN 2 is saved and used as input for a plotting program which utilizes the Tektronix T-4002 graphic-scope. Two examples of plots generated using program FLOWNET are shown in figure 97 (a and b) with uniform flow velocities of 0.1 and 0.5 ft/sec respectively.

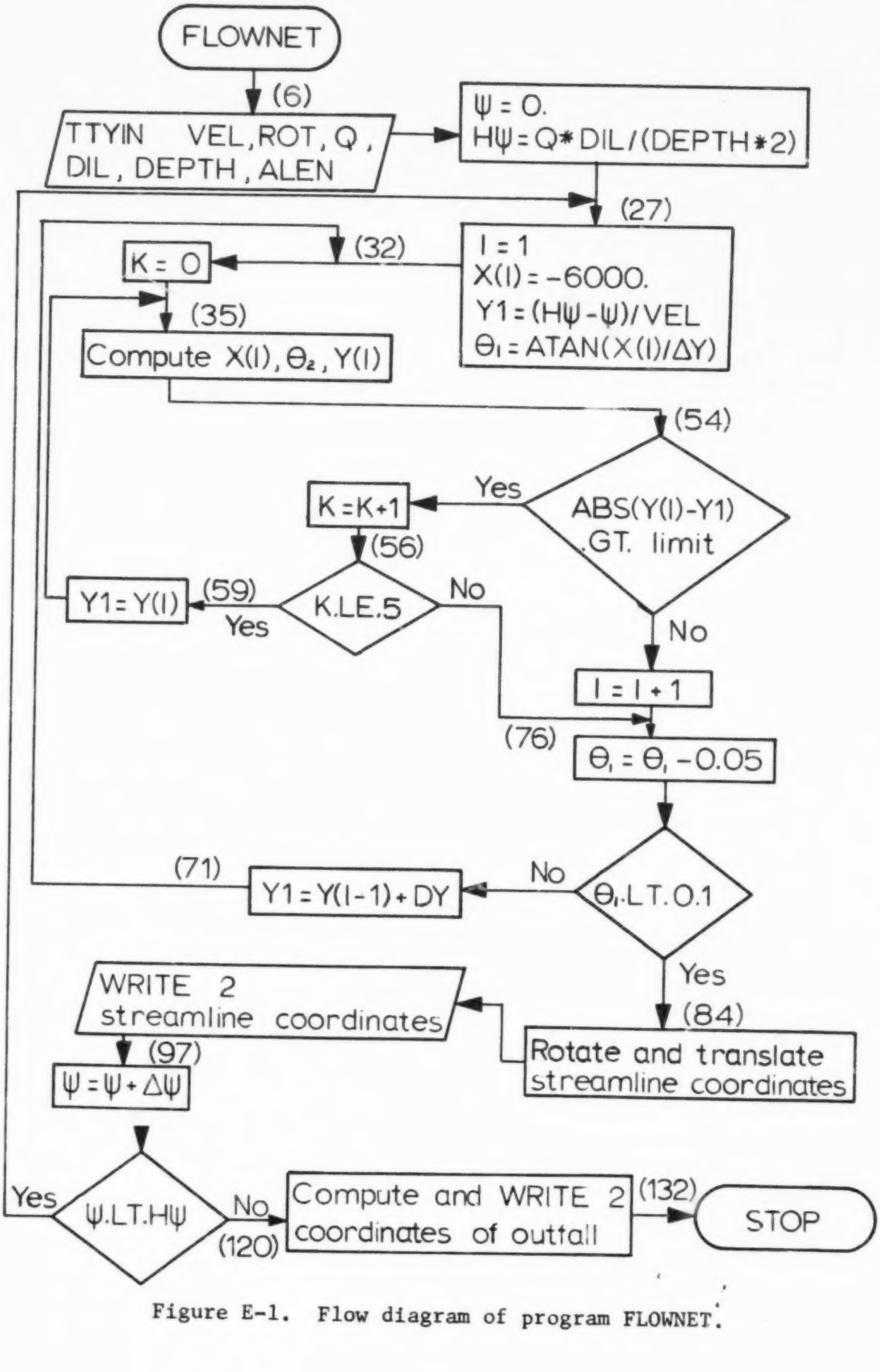

Figure E-1. Flow diagram of program FLOWNET.

```
      PROGRAM FLOWNET
      DIMENSION X(250),Y(250),IPEN(250)
 1000 KGO=0
      XOUT=1069450.
      YOUT=375770.
      U=TTYIN(4HVEL=)
      ROT=TTYIN(4HAZ= )
      ANG=ROT-1.5*3.1416
      Q=TTYIN(4HCFS=)
      DIL=TTYIN(4HDIL=)
      DEPTH=TTYIN(4HDEP=)
      QDD=Q*DIL/DEPTH
      WRITE(2,3) U,QDD
    3 FORMAT(F10.2,F10.0)
      ALEN=TTYIN(4HLEN=)
      ALPHA=QDD/ALEN
      ALEN2=ALEN/2.
      COS1=COS(ANG)
      SIN1=SIN(ANG)
      CONST=ALPHA/(3.14159*2.*U)
      HPSI=QDD/2.
      DPSI=HPSI/3.
      APSI=0.0
      XHI1=0.
      XHI=0.
      THEL=4.71
   15 X(1)=-6000.
      I=1
      Y1=(HPSI-APSI)/U
      HY=0.0
      YLIM=10.
   25 YL=Y1
      K=0
      IPEN(I)=1
   50 IF(I.GT.1) GO TO 60
      ROT=ALEN2+Y1
      THETB=-ATAN(X(I)/ROT)
      IF(ROT.GT.0) THETB=3.14159+THETB
      IF(THETB.LT.0.) THETB=6.28318+THETB
      GO TO 70
   60 X(I)=-SIN(THETB)/COS(THETB)
      X(I)=X(I)*(Y1+ALEN2)
   70 ROT=ALEN2-Y1
      THETA=ATAN(X(I)/ROT)
      IF(ROT.LT.0.) THETA=THETA+3.14159
      IF(THETA.LT.0.) THETA=THETA+6.28318
      SINA=SIN(THETA)
      SINB=SIN(THETB)
      CONST2=ABS(SINB/SINA)
      CON3=THETA+THETB-3.14159
      Y(I)=(-APSI/U+CONST*(ALEN2*CON3+X(I)*
     1 ALOG(CONST2)))/(1.+CONST*(THETA-THETB))
      YDIF=Y(I)-Y1
      IF (ABS(YDIF) .LT. YLIM) GO TO 100
      K=K+1
      GO TO (90,91,92,92,92,110) K
   90 YST=Y1
      YST1=Y(I)
      Y1=Y(I)
      GO TO 50
   91 YND=Y1
      YND2=Y(I)
      DIF1=YND2-YST1
      DIF2=YND-YST
      DIF3=YST-YST1
      DIF4=YND-YND2
```

Figure E-2. Listing of program FLOWNET.

```
      IF(ABS(DIF3).LT.ABS(DIF4)) GO TO 97
      Y1=YND+DIF2*ABS(DIF4/(DIF3-DIF4))
      GO TO 50
   97 Y1=YST-DIF2*ABS(DIF3/(DIF3-DIF4))
      GO TO 50
   92 YST=YND
      YST1=YND2
      GO TO 91
  100 IF(Y(I).GT.0..AND.X(I).LT.2000.) I=I+1
  110 THETB=THETB-0.05
      THEL=THETA
      IF(K.GT.5) GO TO 120
      DY=Y(I-1)-YL
  120 Y1=Y(I-1)+DY
      IF(THETB .GT. 1.6) GO TO 25
  130 IPEN(1)=0
      K=I-1
  210 DO 300 I=1,K
      FACT1=X(I)*COS1
      IF(X(I).GT.2000.) IPEN(I)=0
      IF(X(I).LT.-6000.) X(I)=-6000.
      FACT2=Y(I)*SIN1
      FACT3=-X(I)*SIN1
      FACT4=Y(I)*COS1
      XG1=XOUT+FACT1+FACT2
      YG1=YOUT+FACT3+FACT4
      X(I)=XOUT+FACT1-FACT2
      Y(I)=YOUT+FACT3-FACT4
      WRITE(2,1)XG1,YG1,IPEN(I)
    1 FORMAT(2F10.,I5)
  300 CONTINUE
    2 FORMAT(F5.0)
      IF(KGO.GT.0) GO TO 450
      DO 400 I=1,K
      WRITE(2,1)X(I),Y(I),IPEN(I)
  400 CONTINUE
      APSI=APSI+DPSI
      IF(APSI.LT.HPSI-0.1) GO TO 15
  450 KGO=KGO+1
      GO TO (500,700,900),KGO
  500 X(1)=0.0
      Y(1)=0.0
      K=7
      DO 600 I=2,7
      X(I)=X(I-1)-1000.
      Y(I)=0.0
  600 IPEN(I)=1
      IPEN(1)=0
      APSI=HPSI
      IPEN(K)=2
      GO TO 210
  700 CONTINUE
      WRITE(2,2) APSI
      Y(1)=-ALEN2
      Y(2)=ALEN2
      Y(3)=Y(2)
      Y(4)=Y(1)
      X(1)=20.
      X(2)=20.
      X(3)=-20.
      X(4)=-20.
      K=4
      GO TO 210
  900 END FILE 2
      GO TO 1000
      STOP
      END
```

Figure E-2. Listing of program FLOWNET. (Continued)